



TÉCNICO
LISBOA

UNIVERSIDADE DE LISBOA
INSTITUTO SUPERIOR TÉCNICO

**Deepening the role of CgHaa1- and CgPdr1- pathways in
stress resilience and pathogenesis of *Candida glabrata* to foster
new antifungal treatments**

Sara Barbosa Salazar

Supervisor: Doctor Nuno Gonçalo Pereira Mira

**Thesis approved in public session to obtain the PhD Degree in
Biotechnology and Biosciences**

Jury final classification: Pass with Distinction and Honour



UNIVERSIDADE DE LISBOA
INSTITUTO SUPERIOR TÉCNICO

**Deepening the role of CgHaa1- and CgPdr1- pathways in stress
resilience and pathogenesis of *Candida glabrata* to foster new
antifungal treatments**

Sara Barbosa Salazar

Supervisor: Doctor Nuno Gonçalo Pereira Mira

**Thesis approved in public session to obtain the PhD Degree in Biotechnology and
Biosciences**

Jury final classification: Pass with Distinction and Honour

Jury

Chairperson: Doctor Isabel Maria de Sá Correia Leite de Almeida, Instituto Superior Técnico, Universidade de Lisboa

Members of the Committee:

Doctor Frédéric Devaux, Laboratory of Computational and Quantitative Biology, Sorbonne Université, France

Doctor Isabel Maria de Sá Correia Leite de Almeida, Instituto Superior Técnico, Universidade de Lisboa

Doctor Miguel Nobre Parreira Cacho Teixeira, Instituto Superior Técnico, Universidade de Lisboa

Doctor Mariana Contente Rangel Henriques, Escola de Engenharia, Universidade do Minho

Doctor Nuno Gonçalo Pereira Mira, Instituto Superior Técnico, Universidade de Lisboa

Funding Institutions

Fundação para a Ciência e Tecnologia

Fundo Europeu de Desenvolvimento Regional

2022

Abstract

The emergence of *Candida glabrata* strains resistant to currently used antifungals is one of the more relevant factors determining the outcome of patients suffering from infections caused by this species pushing the need of identifying suitable alternative drugs and new targets different from those targeted by current antifungals. Transcription factors involved in response to environmental stress (including those that respond to the presence of antifungals in the environment) present themselves as an interesting set of possible targets considering their essential role in mounting appropriate tolerance responses. Also of importance, is the fact that the inhibition of their activity can result in a wide impact in the cell since it can affect, simultaneously, the expression of multiple genes, including those that could be required for survival in the presence of the stressor. This thesis is focused on detailing molecular aspects of two pathways controlled by two transcription factors, CgPdr1, a pivotal player in response to drugs across different Yeast species, and CgHaa1, demonstrated to serve as a determinant of tolerance to acetic acid in some species, including *C. glabrata*. It is expected that the detailing of the molecular mechanisms by which these CgPdr1- and CgHaa1- dependent pathways function, can help to foster their possible use as targets in the development of new anti-*Candida* treatments. In the specific case of CgPdr1, considering its prominent role in the acquisition of resistance to azoles in clinical strains, an aspect that is well scrutinized in this thesis, its further characterization may also pave the way for the development of tools that can facilitate the early diagnosis of resistant strains, a pressing issue since appropriate antifungal treatment according to the clinical isolate resistance profile has been found to play an important role in determining mortality rates of patients suffering from invasive candidiasis.

A lot of knowledge has been gathered concerning molecular mechanisms underlying tolerance to azoles in *C. glabrata*, but most of it was gathered in laboratory strains without scrutinizing involvement in the acquisition of the resistance phenotype in clinical strains. In this sense, one of the objectives of this thesis was to focus on clinical strains, not only those retrieved from sterile sites (usually more focused by being implied in invasive infections) but also commensal strains, retrieved from non-sterile sites where *C. glabrata* can thrive as part of the commensal micro(myco)biome. Using comparative transcriptomic and genomic analyses of azole susceptible and resistant strains, it was possible to demonstrate that the acquisition of mutations in the coding sequence of CgPDR1 resulting in hyper-activation of this regulator is the most commonly found resistance mechanism, being possible to identify new variants that were not previously described: CgPdr1^{K274Q}, CgPdr1^{I392M} and CgPdr1^{I803T}. To further understand how the impact of these three novel hyper-activating mutations affect the biochemical activity of CgPdr1, their impact in the tridimensional structure of the protein was studied (using *in silico* modelling) along with possible changes in the set of promoters and interactors directly bound *in vivo*. Altogether the results obtained in this thesis confirm that hyper-active CgPdr1^{K274Q} variant recognizes *in vivo* the same set of promoters recognized by the wild-type CgPdr1, although they show enhanced capacity to induce expression of a set of target genes. It was possible to identify a set of proteins interacting with wild-type and with the K274Q variant of CgPdr1, but further studies will be required to understand whether these differences in the interaction to both variants are responsible for the detected different capabilities of the two proteins to induce target gene expression.

Following the demonstration that CgHaa1 is required for maximal tolerance and response to acetic acid in *C. glabrata*, in this thesis, it was addressed the dissection of the regulatory network controlled by this transcription factor and a possible involvement of this system in biofilm formation and pathogenesis of this species. Using ChIP-Seq it was possible to demonstrate that CgHaa1 directly binds to at least 22 genes *in vivo*, a few of them (e.g. *CgTPO3*, *CgYRO2*, *CgYGP1*) with orthologs in *S. cerevisiae* being previously shown to confer protection against acetic acid. Only 20% of the direct regulon of CgHaa1 identified is conserved from that of *S. cerevisiae*, which indicates a noteworthy divergence of this transcriptional networks in both species. The evolution of the direct Haa1 network in *C. glabrata* may be the result of the recognition of a new *cis*-element identified *in silico*, that binding by the transcription factor requires further confirmation. The results obtained also demonstrate that CgHaa1 is required for maximal adherence and biofilm formation of *C. glabrata* on both biotic and abiotic surfaces. The expression of CgHaa1 and of its target genes, *CgAWP12*, *CgAWP13*, *CAGL0K10164g*, *CAGL0I07249g*, *CAGL0E03740g* and *CAGL0G05632g*, was also found to maximize virulence against the model wax *Galleria mellonella*, this being of particular interest since it augments the biological functions for this systems beyond response to acetic acid at a low pH.

Keywords: *Candida glabrata*, azole resistance, CgPdr1- and CgHaa1- transcriptional regulation, response to environmental stress, comparative transcriptomics and genomics

Resumo

O aparecimento de isolados clínicos de *Candida glabrata* resistentes aos antifúngicos atualmente disponíveis é um dos fatores mais relevantes na determinação do sucesso do tratamento dos doentes com infeções causadas por esta espécie, tal leva à necessidade de identificar medicamentos alternativos adequados e novos alvos terapêuticos diferentes dos visados pelos antifúngicos existentes. Os fatores de transcrição envolvidos na resposta ao stress ambiental (incluindo stress causado pela presença de antifúngicos) apresentam-se como um conjunto interessante de possíveis alvos considerando o seu papel essencial na regulação das respostas de tolerância adequadas. Igualmente importante, é o facto de a inibição da sua atividade poder resultar num amplo impacto na célula, uma vez que pode afectar em simultâneo a expressão de múltiplos genes, incluindo os que poderiam ser necessários para a sobrevivência na presença do agente de stress. Esta tese foca-se em detalhar aspetos moleculares de duas vias transcriptómicas controladas por dois fatores de transcrição, o CgPdr1, um fator central na resposta a múltiplas drogas em diferentes espécies de leveduras, e o CgHaa1, identificado como um fator determinante na tolerância ao ácido acético em algumas espécies, incluindo em *C. glabrata*. É espectável que ao detalhar ao pormenor os mecanismos moleculares que regulam o funcionamento das vias de transcrição CgPdr1 e CgHaa1 seja possível clarificar a possível utilização de ambas vias regulatórias como alvos no desenvolvimento de novos tratamentos anti-*Candida*. No caso específico do CgPdr1, considerando o seu papel proeminente na aquisição de resistência aos azóis em estirpes clínicas, aspeto bem escrutinado nesta tese, a sua posterior caracterização pode também abrir caminho para o desenvolvimento de ferramentas que possam facilitar o diagnóstico precoce de estirpes resistentes, uma questão importante uma vez que se verificou que a terapia apropriada consoante a resistência do isolado clínico desempenha um papel importante na determinação das taxas de mortalidade de pacientes que sofrem de candidíase invasiva.

Até à data, foram detalhados vários mecanismos moleculares subjacentes à tolerância aos azóis em *C. glabrata*, incluindo o papel proeminente desempenhado pelo CgPdr1, no entanto, a maioria deste conhecimento foi obtido através do uso de estirpes laboratoriais sem escrutinar o envolvimento na aquisição do fenótipo de resistência em estirpes clínicas. Neste sentido, um dos objetivos desta tese é o foco do estudo de resistência em estirpes clínicas, não só aquelas recuperadas de locais estéreis (geralmente implicadas em infeções invasivas) mas também em estirpes comensais, isoladas de locais não estéreis onde a *C. glabrata* pode prosperar como parte do micro(mico)bioma comensal. Utilizando análises comparativas transcriptómicas e genómicas de estirpes suscetíveis e resistentes a azóis, foi possível demonstrar que a aquisição de mutações na sequência de codificação de CgPDR1 resultando na hiperativação deste regulador é o mecanismo de resistência mais comumente encontrado, tendo sido possível identificar novas variantes que não foram previamente descritas: CgPdr1^{K274Q}, CgPdr1^{I392M} e CgPdr1^{I803T}. Para compreender melhor como o impacto destas três novas mutações hiper-activadoras na atividade bioquímica do CgPdr1, foi estudado o seu impacto na estrutura tridimensional da proteína (utilizando modelação *in silico*) juntamente com a análise de possíveis alterações da ligação direta ao conjunto de promotores e interactoma *in vivo*. No conjunto, os resultados obtidos nesta tese confirmam que a variante hiper-ativa do CgPdr1^{K274Q} reconhece *in vivo* o mesmo conjunto de promotores CgPdr1 do tipo selvagem, embora mostre uma maior capacidade de induzir a expressão de um conjunto de genes alvo. Foi também possível identificar um conjunto de proteínas que interagem com o tipo selvagem e com a variante K274Q do CgPdr1, mas serão

necessários mais estudos para compreender se possíveis diferenças de interação com ambas as variantes são responsáveis pelas diferentes capacidades demonstradas das duas proteínas induzirem a expressão dos genes alvo.

Após ter sido demonstrado que CgHaa1 é necessário para a máxima tolerância e resposta a ácido acético em *C. glabrata*, nesta tese foi abordada a clarificação da rede transcriptômica controlada por este factor de transcrição e um possível envolvimento deste sistema na formação de biofilme e da patogénese desta espécie. Usando a metodologia de ChIP-seq foi possível demonstrar que o CgHaa1 se liga diretamente a 22 genes *in vivo*, alguns deles (por exemplo, CgTPO3, CgHRK1, CgYGP1) com ortólogos em *S. cerevisiae* que foram previamente demonstrados ser importantes para conferir proteção contra o ácido acético. Apenas 20% do regulão direto de CgHaa1 identificado é conservado quando comparado ao de *S. cerevisiae*, o que indica uma divergência notável destas redes transcripcionais em ambas as espécies. A evolução da rede direta de Haa1 em *C. glabrata* pode ser o resultado do reconhecimento de um novo elemento *cis* identificado *in silico*, cuja ligação pelo fator de transcrição requer confirmação adicional. Os resultados obtidos demonstram também que o CgHaa1 é necessário para a máxima aderência e formação de biofilme de *C. glabrata* tanto em superfícies bióticas como abióticas. A expressão de CgHaa1 e dos seus genes alvo, CgAWP12, CgAWP13, CAGL0K10164g, CAGL0I07249g, CAGL0E03740g e CAGL0G05632g, foi também demonstrada ser importante para maximizar a virulência de *C. glabrata* no modelo de lagarta da traça-de-cera *Galleria mellonella*, o que é de particular interesse uma vez que aumenta as funções biológicas deste sistema para além da resposta ao ácido acético a pH baixo.

Palavras-chaves: *Candida glabrata*, resistência a azóis, CgPdr1- e CgHaa1 - rede de transcrição, resposta a stress ambiental, transcriptômica e genómica comparativa

Acknowledgments

First of all, I would like to acknowledge my supervisor, Professor Nuno Mira, for his guidance, shared scientific discussions, for fostering a feeling of group support, and for the many given opportunities to constantly learn new techniques and visit different laboratories, all fundamental for the realization of this work and that has contributed much to my personal and professional growth.

The second acknowledgment goes to Professor Isabel Sá-Correia as the head of the Biological Sciences Research Group (BSRG) and the director of the BIOTECnico program, for the opportunity to enroll in such a prestigious doctoral program in a group that provided the fundamental conditions for the work here developed, and constant support throughout the PhD, especially relevant during the limitations caused by the COVID pandemic.

A special acknowledgment goes to all the collaborators of the work presented in this thesis. Of most importance, a special thanks go to Professor Frédéric Devaux for receiving me at LCBQ, allowing me to have an abroad experience during this PhD, to which I am very grateful. Furthermore, I would like to extend the gratitude for the ChIP-seq results obtained during this period that added great value to this thesis. Professor Frédéric Devaux is also thanked for sharing the pYR29-MycHis plasmid and for the support in engineering the pYR29-MycHis_CgPdr1-derived plasmids and CgHaa1-Myc strain construct, and for sharing the design of the DNA microarrays used in Chapter V and VII. This acknowledgment is extended to Dr. Thierry Delaveau and Médine Benchouaia for their contribution, and for the guidance offered during my time at LCBQ. Lasse van Wijlick from the Institute Pasteur is further acknowledged for the collaboration in the ChIP-SICAP experiments. GenomePT – National Laboratory for Genome Sequencing and Analysis (POCI-01-0145-FEDER-022184) and the iBiMED-UAVR Genome Medicine Laboratory are acknowledged for providing access to the required infrastructures to perform the gene expression microarray profiling experiments presented in Chapter IV with the guidance of Dr. Ana Raquel Soares. Professor Geraldine Butler from the University College of Dublin is acknowledged for sharing the design of the DNA microarrays used in Chapter III and Chapter IV. I would also like to thank Professor Arsénio Fialho and its group of the BSRG, especially Dr. Dalila Mil-Homens and Dr. Andreia Pimenta, for the collaboration in the works with *Galleria mellonella* infection model assays. Dr. Hiroji Chibana from Chiba University is acknowledged for kindly providing the *Candida glabrata* mutant strains and Dr. Jane Usher from the University of Exeter is acknowledged for kindly providing a large-scale *C. glabrata* deletion mutants collection. Professor Moye-Rowley from the University of Iowa is kindly acknowledged for providing the *C. glabrata* SKY107 and LYS2 strains and the pSP76 plasmid. Dr. Cecília Arraiano from ITQB and Dr. Rute Matos are acknowledged for their collaboration in the SPR experiments. Dr. Sónia Silva is acknowledged for the assays of *C. glabrata* adhesion to the reconstructed epithelium cell assays. A final thanks is directed to Dr. Vitória Rodrigues from SYNLAB and Professor Maria Manuel Lopes from the Faculdade of the Farmácia da Universidade de Lisboa for the extensive clinical isolates collections provided. Increased gratitude must also be expressed towards the Dr. Nuno Mira group, specially the MsC students, including Maria Joana Pinheiro, Noémi Velez, Rui Carvalho, Catarina Mendonça, Rita Simões, Daniella Sotti, João Lucas and Dr. José António Souza, whose contributions were crucial for the work herein developed. I would further like to extend a personal thanks for their patience in teaching me how to pass my experience to others.

This work was financially supported by FCT in the scope of the project UIDB/04565/2020 and UIDP/04565/2020 of the Research Unit Institute for Bioengineering and Biosciences - iBB and the project LA/P/0140/2020 of the Associate Laboratory Institute for Health and Bioeconomy - i4HB. Programa Operacional Regional de Lisboa 2020 are acknowledged for its financial support to iBB (project no. 007317). Financial support Ireland science foundation (grant number 12IA1343) is also acknowledged. Finally, the doctoral program BIOTECnico is acknowledged for supporting the PhD grant (grant PD/BD/135139/2017).

I would like to continue my personal acknowledgments by extending my thanks to Méline, Salomé, Hussam, and Thierry for making me feel very much welcome in LCBQ. Further thanks go to Ilaria and Sam for their friendship during this period. The following personal acknowledgments will be addressed in Portuguese. Começo por agradecer aos meus colegas do grupo BSRG-iBB que permitiram que ao longo dos anos sempre se preservasse um sentimento de apoio e de amizade, começando pelo grupo de alunos do Professor Nuno Mira, com especial agradecimento aos meus colegas Maria João Tavares, Ana Vila-Santa, Nuno Pedro, Andreia Lourenço e João Santos. Um especial agradecimento é estendido à Mafalda Cavalheiro, Mónica Galocha, Catarina Costa, Ricardo Ribeiro, Sara Rosa e Marta Mota pela entajuda e acima de tudo amizade. Um especial agradecimento vai para a amizade do Tiago Pedreira e da Andreia Pimenta que me acompanharam desde a Licenciatura até ao meu início do doutoramento. Gostaria também de agradecer aos amigos que preservei durante o mestrado no BSRG e que torceram por mim neste processo, Diana Cunha, Nicole Rodrigues e José Rodrigues e aos meus colegas da MDU-IMM pelo apoio na reta final, incluindo a Sandra, o Gerson, Maggie e Mariana e não esquecendo um agradecimento especial à Dr. Patrícia Napoleão pelo extraordinário apoio e ajuda. Queria também deixar um especial reconhecimento aos amigos de longa data que me apoiaram nesta fase em especial a Fara, o André e o Rolando, o Pedro e em especial à Cristina. Por fim, agradeço à minha família que tanto foi um apoio para mim nos últimos anos, em especial aos meus avós pelo carinho, à minha tia Luísa pela companhia e aos meus primos Barbosa, com especial apreço ao Rui e à Daniela pela força dada nesta fase, e à nova geração iniciada pelo Tiago Maria e pela felicidade que consigo traz. Por fim, um agradecimento especial aos meus pais, nem que seja pelo facto de terem investido tanto na educação da filha para no fim escolher a vida de bolseira. Nesse sentido, gostaria de agradecer em especial o sentimento de suporte que sempre me deram que permitiu que tomasse as escolhas que fiz, tendo como base que o tempo deve ser reservado para fazer algo que nos motive. Por último, esta tese é dedicada à minha mãe e aos seus ensinamentos que na vida, tal como no trabalho, o mais importante é a empatia pelo outro e com isso a preservação do sentido de comunidade, de apoio e de amizade. Dedico esta tese também ao seu pai e ao meu avô, Joaquim.

List of Acronyms

ABC	<u>A</u> TP-binding cassette	MDR	<u>M</u> ultidrug resistance
ADP	<u>A</u> denosine diphosphate	MFS	<u>M</u> ajor <u>F</u> acilitator <u>S</u> uperfamily
AGC	<u>A</u> utomatic gain control	MIC	<u>M</u> inimum inhibitory concentration
ANOVA	<u>A</u> nalysis of variance	MHR	<u>M</u> iddle <u>h</u> omology region
ATP	<u>A</u> denosine triphosphate	MM	<u>M</u> inimal growth <u>m</u> edium
BAM	<u>B</u> inary <u>A</u> lignment <u>M</u> ap files	MMS	<u>M</u> ethyl <u>M</u> ethanesulfonate
BSA	<u>B</u> ovine <u>s</u> erum <u>a</u> lbumin	MOCK	Control sample IP
BED	Browser Extensible Data files	MOPS	<u>M</u> orpholinepropanesulfonic acid
CDS	<u>C</u> o <u>D</u> ing <u>S</u> equence	MS	<u>M</u> ass <u>s</u> pectrometry
CFU	<u>C</u> olony forming units	OD	<u>O</u> ptical <u>d</u> ensity
CGD	<u>C</u> andida <u>G</u> enome <u>D</u> atabase	ORF	<u>O</u> pen reading frame
CRD	<u>C</u> entral <u>R</u> egulatory <u>D</u> omain	PBS	<u>P</u> hosphate-buffered <u>S</u> aline
ChIP	<u>C</u> hromatin <u>I</u> mmunoprecipitation	PCR	<u>P</u> olymerase <u>C</u> hain <u>R</u> eaction
ChIP-Seq	<u>C</u> hromatin <u>I</u> mmunoprecipitation - sequencing	PDR	<u>P</u> leiotropic <u>d</u> rug resistance
DBD	<u>D</u> NA-binding domain	PDRE	<u>P</u> leiotropic <u>d</u> rug resistance element
DD	<u>D</u> imerization domain	pH	<u>P</u> otential of <u>H</u> ydrogen
DTT	<u>D</u> ithiothreitol	pKa	$-\log(K_a)$, where K_a is the dissociation constant
DNA	<u>D</u> eoxyribonucleic acid	RHVE	<u>R</u> econstituted <u>H</u> uman <u>V</u> aginal <u>E</u> pithelium
DMSO	<u>D</u> imethyl sulfoxide	RD	<u>R</u> egulatory domain
ECOFF	<u>E</u> pidemiological cut-off	RNA	<u>R</u> ibonucleic acid
EDTA	<u>E</u> thylenediaminetetraacetic acid	RPMI	<u>R</u> oswell <u>P</u> ark <u>M</u> emorial Institute
EUCAST	<u>E</u> uropean <u>C</u> ommittee on <u>A</u> ntimicrobial <u>S</u> usceptibility <u>T</u> esting	RT-PCR	<u>R</u> everse transcriptase polymerase chain reaction
FACT	<u>F</u> acilitates chromatin transcription	SAGA	<u>S</u> pt- <u>A</u> da- <u>G</u> cn5 acetyltransferase
FBD	<u>F</u> luconazole binding domain	SAM	<u>S</u> equence <u>A</u> lignment <u>M</u> ap files
GIM	<u>G</u> race's insect medium	S-DD	<u>S</u> usceptible - <u>D</u> ose <u>D</u> ependent
GO	<u>G</u> ene ontology	SDS	<u>S</u> odium dodecyl sulfate
GOF	<u>G</u> ain-of-function	SICAP	<u>S</u> elective <u>I</u> solation of <u>C</u> hromatin-associated <u>P</u> roteins
HCL	<u>H</u> ydrochloric <u>A</u> cid	SNP	<u>S</u> ingle <u>N</u> ucleotide <u>P</u> olymorphism
HPLC	<u>H</u> igh-pressure <u>L</u> iquid <u>C</u> hromatography	SEM	<u>S</u> canning <u>E</u> lectron <u>M</u> icroscopy
HRE	<u>H</u> aa1-responsive element	SWI/SNF	<u>S</u> W <u>I</u> tch/ <u>S</u> ucrose <u>N</u> on- <u>F</u> ermentable
ID	<u>I</u> nhibitory <u>D</u> omain	TAD	<u>T</u> ransactivation <u>D</u> omain
IP	<u>I</u> mmunoprecipitated DNA	TBP	<u>T</u> ATA-binding protein
IPTG	<u>I</u> sopropyl β -D-1-thiogalactopyranoside	TBS	<u>T</u> ris-buffered saline
KIX	<u>K</u> inase-inducible domain <u>I</u> nteracting <u>D</u> omain	TE	<u>T</u> ris- <u>E</u> DTA buffer
NACS	<u>N</u> on- <u>a</u> lbicans <u>C</u> andida species	YEASTRACT+	<u>Y</u> east search for transcriptional regulators and consensus tracking
NAD(H)	<u>N</u> icotinamide <u>A</u> denine <u>D</u> inucleotide (+ <u>H</u> ydrogen)	YPD	<u>Y</u> east peptone dextrose growth medium
NLS	<u>N</u> uclear localization signal	YRE	<u>Y</u> rr1-responsive element
MALDI	<u>M</u> atrix-assisted laser	XBD	<u>X</u> enobiotic <u>B</u> inding <u>D</u> omain
-TOF	<u>d</u> esorption/ionization – <u>t</u> ime-of- <u>f</u> light		

List of Contents

Abstract.....	i
Resumo	iii
Acknowledgments.....	v
List of Acronyms	vii
List of Tables	xiii
List of Figures.....	xvi
I. Thesis Outline	1
II. Introduction.....	5
1. The human opportunistic pathogen <i>Candida glabrata</i> and its high resilience to azole antifungal drugs	6
1.1 Mechanisms underlying the innate resilience to azoles in <i>Candida glabrata</i> and consequences for resistance	7
2. The Pleiotropic Drug Resistance transcription factor, CgPdr1, in <i>Candida glabrata</i>	11
2.1. The Pleiotropic Drug Resistance network: from <i>Saccharomyces cerevisiae</i> to <i>Candida glabrata</i>	11
2.3. The complex and intertwined interactions established between the Pleiotropic Drug Resistance regulatory network and other stress-responsive regulators.....	14
2.4 A molecular view on the transcription of Pdr-target genes	17
2.5. Mechanistic insights underlying regulation and regulators of the activity of PDR transcription factors	24
2.5.1 Ligand Binding	24
2.5.2 Chaperones and Ubiquitin proteases that regulate the Pdr transcription factors activity	26
2.5.3 Activity of upstream signalling pathways.....	27
2.5.4 Regulation of the activity PDR transcription factor through protein structural changes.....	29
2.5.5 The impact of gain-of-function mutations in the activation of CgPdr1 in <i>Candida glabrata</i>	31
3. The acetic acid-responsive transcription factor CgHaa1 and its dependent regulatory network	34
III. Comparative genomic and transcriptomic analyses unveil novel features of azole resistance and adaptation to the human host in <i>Candida glabrata</i>	39
1. Abstract.....	40
2. Introduction	41
3. Methods	42
3.1. Strains and growth media	42
3.2. Assessment of resistance to antifungals of <i>Candida glabrata</i> clinical isolates	42
3.3. FFUL887 genomic DNA extraction and whole-genome sequencing.....	43
3.4. Comparative transcriptomic analysis of <i>C. glabrata</i> CBS138 and FFUL887 strains.....	44

3.5. Cg <i>PDR1</i> gene disruption in the FFUL887 clinical strain.....	44
3.6. Effect of the CgPdr1 ^{K274Q} variant in expression of Cg <i>CDR1</i> , Cg <i>PDH1</i> , Cg <i>QDR2</i> and Cg <i>PDR1</i> genes.	44
3.7. Effect of the CgPdr1 ^{K274Q} variant in tolerance to environmental stressors.....	45
4. Results	46
4.1. Identification of FFUL887 as a fluconazole- and voriconazole- resistant strain.....	46
4.2. FFUL887 genome sequencing and annotation	48
4.3. Comparative genomic analysis between FFUL887 and CBS138 focused on azole-resistance genes: emphasis on Cg <i>PDR1</i>	49
4.4. The deletion of Cg <i>PDR1</i> ^{A820C} allele affects tolerance to environmental stress of the FFUL887 isolate.	51
4.5. Comparative transcriptomic analysis between FFUL887 and CBS138 show dramatic alterations in the expression of genes involved in carbohydrate, nitrogen and sulphur metabolism.	52
5. Discussion.....	56
IV. Disclosing azole resistance mechanisms in resistant <i>Candida glabrata</i> strains encoding wild-type or gain-of- function Cg <i>PDR1</i> alleles through comparative genomics and transcriptomics	61
1. Abstract.....	62
2. Introduction	63
3. Methods	65
3.1. Strains, clinical isolate collections and growth media used.....	65
3.2. Plasmids	65
3.3. Azole susceptibility testing of the clinical isolates collected in this study	65
3.4. Sequencing of Cg <i>PDR1</i> allele encoded by the azole-resistant <i>Candida glabrata</i> isolates.....	66
3.5. Assessment of Cg <i>CDR1</i> and Cg <i>PUP1</i> expression in azole-resistant strains.....	66
3.6. Comparative transcriptomics of azole resistant isolates FFUL443, FFUL674 and ISTB218 with laboratory strain CBS138	67
3.7. Genomic profiling of isolates ISTB218 (azole-resistant) and ISTA29 (azole-susceptible).....	67
3.7. Susceptibility assays to fluconazole of Δ Cg <i>pdr1</i> and Δ Cg <i>pdr1</i> Δ Cg <i>gal11a</i> <i>Candida glabrata</i> cells expressing different Cg <i>PDR1</i> alleles.....	68
4. Results	70
4.1. Distribution of <i>Candida</i> species among a cohort of isolates recovered across epidemiological surveys undertaken in Portugal.....	70
4.2. Profile of resistance to fluconazole and voriconazole among the <i>Candida albicans</i> and <i>Candida glabrata</i> strains	70

4.3. Sequencing of the <i>CgPDR1</i> allele encoded by the azole-resistant <i>Candida glabrata</i> isolates.	71
4.4. The I803T and I392M substitutions are new gain-of-function CgPdr1 variants.	72
4.5. The I392M and K274Q CgPdr1 gain-of-function variants rely on the mediator subunit CgGal11A to enhance tolerance to fluconazole in <i>Candida glabrata</i> , while only a partial dependence for CgGal11A is observed for cells encoding the I803T variant.	74
4.6. OMICS profiling of the azole-resistant isolate <i>Candida glabrata</i> ISTB218, encoding a “wild-type” <i>CgPDR1</i> allele.....	75
5. Discussion.....	80
V. Impact of gain-of-function mutations in different biochemical aspects of the activity of the transcription factor Pdr1 from <i>Candida glabrata</i>	83
1. Abstract.....	84
2. Introduction	85
3. Material and methods.	88
3.1. Modelling of CgPdr1 tridimensional structure and visualization	88
3.2. Growth media, strains and plasmids used	88
3.3. Fluconazole susceptibility testing of $\Delta Cgpdrl$ <i>Candida glabrata</i> cells expressing different <i>CgPDR1</i> alleles.....	89
3.4 Transcriptomic analysis of <i>C. glabrata</i> cells expressing the CgPdr1 ^{WT} and the CgPdr1 ^{K274Q}	89
3.4. Chromatin immunoprecipitation sequencing assay	90
3.5. Peak calling and network construction.....	91
3.6. Chromatin immunoprecipitation selective isolation of chromatin-associated proteins (ChIP-SICAP). 91	
3.7. High pH fractionation and mass spectrometry	92
3.8. MS data analysis.....	93
4. Results and Discussion	94
4.1 General overview of the predicted structure of the zinc finger transcription factor and nuclear receptor CgPdr1.....	94
4.2. Distribution of gain-of-function mutations across the different structural features predicted for CgPdr1	102
4.2. Overview of the insights brought by the <i>in silico</i> structural analysis over CgPdr1 activity	108
4.5 Effect of the CgPdr1 ^{K274Q} variant in <i>Candida glabrata</i> genomic expression	110
4.7. Comparison of the interactomes of wild-type CgPdr1 and of K274Q GOF mutant.....	117
VI. Effect of CgHaa1 and of CgHaa1-regulon in <i>Candida glabrata</i> ability to form biofilms and in virulence against the infection model <i>Galleria mellonella</i>	123
1. Abstract.....	124

2. Introduction	125
3. Materials and Methods	128
3.1. Strains and growth medium.....	128
3.2. Gene disruption	128
3.3. Assessment of the deletion of <i>CgHAA1</i> gene and of the target adhesins <i>CgAWP12</i> , <i>CgAWP13</i> , <i>CAGL0H07469g</i> , and <i>CAGL0K10164g</i> genes in <i>Candida glabrata</i> ability form biofilms in the presence of acetic acid.....	128
3.4. Assessment of the expression of <i>CgHAA1</i> , <i>CgAWP12</i> , <i>CgAWP13</i> , <i>CAGL0H07469g</i> , and <i>CAGL0K10164g</i> genes during biofilm formation in the presence or absence of acetic acid.....	130
3.5. Effect of CgHaa1 and CgHaa1-regulated adhesin genes <i>CgAWP12</i> , <i>CgAWP13</i> , <i>CAGL0H07469g</i> , and <i>CAGL0K10164g</i> in adherence of <i>Candida glabrata</i> to the reconstituted human vaginal epithelium	130
3.6. Effect of <i>CgHAA1</i> and of CgHaa1-regulated genes in virulence of <i>Candida glabrata</i> against <i>Galleria mellonella</i>	131
3.7. Effect of <i>CgHAA1</i> and of CgHaa1-regulated genes in the ability of <i>Candida glabrata</i> to proliferate inside <i>Galleria mellonella</i> hemocytes.....	132
3.9. Effect of the deletion of <i>CgHAA1</i> and of CgHaa1-regulated genes <i>CAGL0L00649g</i> , <i>CgICL1</i> , and <i>CgMLS1</i> in <i>Candida glabrata</i> tolerance to acetic acid at a low pH and in co-consumption of acetate and glucose.....	132
4. Results	134
4.1. In the presence of acetic acid, the expression of <i>CgHAA1</i> and of the CgHaa1-regulated genes <i>CgAWP12</i> , <i>CgAWP13</i> , <i>CAGL0H07469g</i> , and <i>CAGL0K10164g</i> is necessary for the proper formation of <i>Candida glabrata</i> biofilms in biotic and abiotic surfaces.....	134
4.2. Effect of CgHaa1 and of CgHaa1-regulated genes in virulence of <i>Candida glabrata</i> against the infection model <i>Galleria mellonella</i>	136
4.3. Role of CgHaa1 in co-consumption of glucose and acetate by <i>C. glabrata</i>	138
5. Discussion.....	141
VII. Elucidation of the CgHaa1-regulatory network by ChIP-seq analysis	145
1. Abstract.....	146
2. Introduction	147
3. Material and methods	149
3.1. Strains and growth medium.....	149
3.2. Chromatin immunoprecipitation of CgHaa1 and sequencing of the interacting DNA	149
3.4. Transcriptomic analyses of the CgHaa1 influence during 30 mM acetic acid stress.....	150

3.5. Heterologous expression in <i>E. coli</i> of CgHaa1-DBD peptide and subsequent purification by affinity chromatography.....	151
4. Results and Discussion	153
4.1. Identification of promoter regions recognized <i>in vivo</i> by CgHaa1 in acetic acid-stressed <i>Candida glabrata</i> cells and prediction of the set of directly regulated genes	153
4.2. <i>In silico</i> identification of a putative CgHaa1 DNA-binding site	162
4.3. Heterologous expression of the CgHaa1 DNA binding domain and study of its interaction with the candidate DNA motifs.....	164
5. Final Remarks	167
VIII. Final Discussion	169
IX. List of Publications and Communications	179
X. References	183
Appendix – Supplementary Data	201

List of Tables

Table II. 1. <i>General susceptibility patterns of Candida species to antifungal drugs used in the treatment of candidiasis</i> (adapted from [15] and [34]). S-susceptible; S-DD – susceptible dose-dependent; I – intermediate; R – resistant.	8
Table II. 2. <i>Summary of the determinants of resistance identified in azole-resistant Candida glabrata isolates</i> ..	9
Table II. 3. (Part 1) <i>Transcription initiation co-activators described to influence the expression of PDR-dependent genes in Saccharomyces cerevisiae and in Candida glabrata</i> . The influence of the genes encoding the different transcriptional co-activators or subunit of chromatin modifying complexes in the activity of Pdr1 regulator and in the transcription of target genes or in tolerance to PDR xenobiotics response in <i>S. cerevisiae</i> and <i>C. glabrata</i> is summarized in this table. The negative effect of transcriptional co-activators gene deletion in xenobiotic resistance is highlighted in red, and a positive effect is highlighted in green. Proteins/genes whose deletion were found to result in opposite effects in different studies concerning tolerance to drugs responded by Pdr1 are written in red; n.i. indicates that no information was found; FLZ - fluconazole; KTZ - ketoconazole; CTZ - clotrimazole; VZ - voriconazole; ECZ - econazole; PCZ - posaconazole; MCZ - miconazole; CHX - cycloheximide; OM - oligomycin; AVT - Atorvastatin.	21
Table III 1. <i>List of laboratory strains used in this study</i>	42
Table III. 2. <i>List of primers used in this study</i>	45
Table III 3. <i>Subset of proteins previously described to be involved in fluconazole and/or voriconazole resistance in Candida glabrata that were found to harbour non-synonymous SNPs in the FFUL887 strain, when compared with their CBS138 counter-partners</i> . Functions were derived from CGD database [140].	50
Table IV. 1. <i>List plasmids and primers used in this study</i> . In the case of the plasmids it is also provided their origin while in the case of the primers it is indicated for which their application was used for.	69
Table IV. 2. <i>Results obtained upon sequencing of the CgPDR1 gene from the seven azole-resistant Candida glabrata strains examined in this study</i> . The non-synonymous modifications found in the coding sequencing of the CgPDR1 gene encoded by the strains are compared with the one of the azole-susceptible reference strain CBS138. Those modifications demonstrated before as CgPdr1 GOF variants are marked in black boxes, while those previously reported in azole-resistant strains but not in susceptible ones are indicated in grey boxes. SNPs described in azole susceptible and resistant strains are underlined. The herein described I392M and I803T substitution is indicated in the orange box.	72
Table IV. 3. <i>Results from the comparative transcriptomic analysis between the azole-resistant Candida glabrata strain ISTB218 and the azole-susceptible strain CBS138 during growth in RPMI medium until mid-exponential phase, as suggested by DNA microarray analyses</i> . A selected set of genes found to be differently transcribed (above or below 2-fold) in the two strains (the full list is available in Annex Table IV. 5) is shown in this table, along with the description of their function and the reported outcome of gene deletion in tolerance to azoles in <i>C. glabrata</i> (green denotes a gene whose deletion results in improved tolerance to azoles; in red denotes a gene whose deletion results in decreased susceptibility to azoles).	77
Table IV. 4. <i>SNPs identified in the gene sequences encoded by the azole-resistant ISTB218 strain but not by the azole susceptible strains ISTA29, as suggested upon whole-genome sequencing of the clinical strains and subsequent comparison with the available genomic sequence of CBS138</i> . It is indicated the alteration found in the	

coding sequence of the gene encoded by the ISTB218 strain and the effect that deletion of genes have on azole tolerance. In green denotes a gene whose deletion results in improved tolerance to azoles; in red denotes a gene whose deletion results in decreased susceptibility to azoles. Fs, denote changes exhibiting frame-shifts resulting in premature truncation. 79

Table V. 1. *Primers and plasmids used in this study.* In the case of the plasmids, it is also provided their origin while in the case of the primers it is indicated for which their application was used for. 89

Table V. 2. *Minimum inhibitory concentration values of fluconazole obtained for SKY107 cells ($\Delta pdr1$) transformed with plasmid pSP76 and pYR29-MycHis which drives expression of CgPDR1 from its natural promoter and terminator and in the derived plasmids that encode the CgPDR1 allele with the individual substitutions K274Q. 110*

Table V. 3. *Comparative transcriptomic analysis of C. glabrata SKY107 cells ($\Delta pdr1$) transformed with pYR29_Myc-HIS_CgPDR1^{WT} or pYR29_Myc-HIS_CgPDR1^{A820C} plasmids, which drive the production of the wild-type or K274Q hyperactive variant, during growth in RPMI medium. Mid-exponential phase cells cultured in an RPMI medium were collected at a DO~1. A gene was considered differentially expressed if its mean absolute Log2 fold change value of two independent biological experiments was higher than 0.5 or lower than -0.5, with a cut-off p-value of 0.05. The PathoYeast database [141] was used to identify which of the differentially expressed genes are direct (in bold) or indirect targets of CgPdr1 (in underline). The information regarding the protein encoded function was summarized from the CGD database. 112*

Table V. 4. *Genes identified to be directly regulated by the CgPdr1^{K274Q} and CgPdr1^{WT} variants in this study using ChIP-seq analysis.* Information regarding the protein encoded function was summarized from the CGD database [140]. 113

Table V. 5. *Adapted table from Paul, S. et al. 2014 summarizing the direct CgPdr1 direct targets in rho⁰ cells predicted by the interaction of CgPdr1 with the promoter with PDRE motifs.* Gray lines indicated the genes defined as possible targets only in ChIP-seq results in rho⁰ cells but not in this work. The PDRE motifs identified in the promoters of the gene targets are summarized. A central sequence highlighted in blue is conserved in most PDRE detected. Change of at least one of the two initial thymine is highlighted in red. 117

Table V. 6. (Part 1) *Interactome of the CgPdr1^{WT} and CgPdr1^{K274Q} analyzed by mass-spectrometry of the immunoprecipitated CgPdr1 variants with interacting proteins through ChIP-SICAP technique.* Only proteins identified in the MS of CgPdr1^{WT} or CgPdr1^{K274Q} immunoprecipitated samples but not in the MOCK sample were considered. Two biological replicates were used for each condition in the study. Furthermore, the usual contaminants peptides of IP-MS such as ribosomal proteins and core histones were discarded from the analysis. Information herein detailed regarding the protein function summarized from the CGD and SGD databases. In bold are marked encoding genes that deletion was demonstrated to influence azole resistance and protein was demonstrated to interact with CgPdr1. 120

Table VII. 1. *List of strains, plasmids and primers used in this work. 152*

Table VII. 2. (Part I) *Genes to which CgHaa1 was found to be bound to the promoter in acetic acid-stressed C. glabrata cells, as indicated by ChIP-seq analysis.* The table describes the list of genes presumed to be directly regulated by CgHaa1 *in vivo* under acetic acid stress (30 mM, pH 4), using the experimental setting detailed in materials and methods. The effect of CgHaa1 in the expression of these genes is also indicated, based on the results of the transcriptomic analysis herein carried out, as well as the predicted *S. cerevisiae* orthologue and the existence

of an eventual regulatory association with ScHaa1. Encoded protein function was retrieved from CGD or SGD databases [140, 407]. The second set of genes, in grey lines, represents a set of possible direct targets that interaction of CgHaa1 to the promotor needs to be confirmed since the peaks observed in the CHIP-seq experiments have often low intensities and were not detected by bPeaks, at least not in all replicates. 155

Table VII. 3. *Listing of the sequences of the different motifs identified by RSAT tools within the peaks sequence identified by bPeaks software.* The sequences of high reads peaks identified by the bPeaks software, located at gene promoters regions, that result from the sequencing of DNA immunoprecipitated with the Myc tagged CgHaa1 *in vivo* in response to acetic acid stress (30 mM, pH 4), were used to find the HRE motif recognized by ScHaa1 using RSAT tools. *De novo* search for the most represented motifs identified two main motifs denominated HRE-like motif - due to the similarity to HRE, and RSAT motif 1 – the motif with higher incidence identified by the RSAT tools. The HRE-like motifs that were identified by RSAT tools *in novo* motif search that corresponds to the previously identified ScHaa1 HRE motif are underlined. Bold RSAT motif 1's have a stretch of CG nucleotides that resemble the HRE motif. The motifs found in the reverse strand of the DNA are highlighted in italic. 164

List of Figures

Figure II. 1. Schematic representation of the known mechanisms of action of the different classes of antifungals available for the treatment of candidiasis. 5-FU – 5-fluorouracil; 5-FUMP- 5-fluorouridine monophosphate; FdUMP -5-fluorodeoxyuridine monophosphate; FUTP- 5-fluorouridine triphosphate. Figure retrieved from Salazar, S.B. *et al.* 2020 [7]. 7

Figure II. 2. Comparison of the genes directly regulated by *Pdr1* in *Saccharomyces cerevisiae* and *Candida glabrata*. Networks detailed in this figure [70, 71, 84] were defined by the *Pdr1* interaction with the promoter region of targets by DNA-footprinting, ChIP-chip and ChIP-seq technologies plus monitorization of gene transcription. Only genes with PDRE motif in the promoter are herein detailed..... 14

Figure II. 3. Schematic representation illustrating the interactions established between the pleiotropic drug resistance transcription factors with other regulatory networks in *Saccharomyces cerevisiae* and in *Candida glabrata*. A schematic view of the complexity of the regulatory associations established between PDR transcription factors (represented in grey) with other transcription factors involved in response to oxidative stress (represented in blue), in protein degradation (represented in yellow), in ergosterol biosynthesis (represented in red) in *S. cerevisiae* and in *C. glabrata* [60, 70, 71, 75, 78, 88, 101, 119-126]. The represented models distinguish the direct effect (backed by evidence of regulatory element presence in the promoter and/or direct binding to the promoter, accompanied by the demonstration that the transcription factor influences gene expression. Dimerization of ScStb5 with ScPdr1 is also represented as it influences PDR transcription. The stressor stimuli in which the transcription is influence by the different transcription factors is also indicated (Ergosterol pathway defects (EPD); fluconazole (FLZ); gain-of-function mutation (GOF); methyl methanesulfonate (MMS); azetidine-2-carboxylic acid (ACZ), a proline analog that miss-incorporates into proteins and leads to proteotoxic stress; mitochondrial defects (MitD)). 15

Figure II. 4. Physiologically relevant stimuli that result in activation of *Pdr1* and consequent phenotypic traits resulting from such activation..... 26

Figure II. 5. Described regulators of the pleiotropic drug resistance transcription factors protein activity in *Saccharomyces cerevisiae* and *Candida glabrata*. Representation of the identified positive and negative regulators, represented in green and red respectively, of the activity regulation of the PDR transcription factors in blue. The main component of the mediator complex involved in the PDR transcription activation, if known, is represented in light blue. When characterized, the stimulus resulting in a specific regulation pathway is highlighted. 29

Figure II. 6. Different functional domains in the Pleiotropic Drug Resistance transcription factor of *Candida glabrata*, *CgPdr1*. The DBD (1 to 254 a.a.), CRD (255 to 968 a.a.), and TAD (969 to 1107 a.a.) domains were defined in Simonicova, L. and Moye-Rowley, W.S. 2020 [181]. The ID (322-372), the minimum XDB (417 to 608 a.a.), and NLS (793 to 819 a.a.) were defined by sequence homology to these domains identified in *S. cerevisiae* [105, 225, 227]...... 31

Figure II. 7. Distribution of reported gain-of-function mutations in *CgPdr1* structure. Non-synonymous mutations summarized in this picture were only found in resistant clinical isolates or strains. These point mutations were further defined as gain-of-function mutation if, when introduced in a susceptible background, the strain becomes resistant and/or induces *CgPdr1* target genes upregulation (black). Highly potential GOF mutations that were identified in strains after *in vitro* evolution during azole exposure or during *in vivo* evolution in a patient

undergoing azole treatment are also represented in grey. The full list of non-synonymous mutations identified till today and the references that reported them are summarized in Annex Table II. 1..... 32

Figure II. 8. Schematic representation of the biological functions of genes belonging to the *CgHaa1*-regulon in *Candida glabrata*. 36

Figure II. 9. Comparison of the *CgHaa1*- and *ScHaa1*-regulons active in response to acetic acid stress. The dataset of genes found to be activated by *CgHaa1* or by *ScHaa1* during the response of *C. glabrata* or *S. cerevisiae* to acetic acid (at pH 4) were compared [252, 262]. The intersection of the two datasets revealed a modest overlap between the two networks. The functional classes most represented within the dataset of genes specifically regulated by *CgHaa1* are indicated in the figure, alongside the names of some of the genes clustered in these functional classes. The homologs genes regulated by *ZbHaa1* during acetic acid stress are also highlighted underlined [260, 265]. The image was adapted from Bernardo, R. *et al.* 2017 [262]. 37

Figure III. 1. Distribution of minimum inhibitory concentration values of fluconazole, voriconazole (panel A) caspofungin and anidulafungin (panel B) obtained for the cohort of *Candida glabrata* clinical isolates tested in this work. The dashed line indicates the resistance breakpoints defined by EUCAST (as detailed in materials and methods). These results were obtained based on the assessment of MIC₅₀ value by the microdilution method recommended by EUCAST and that gave rise to the results shown in Annex Figure III. 1. 47

Figure III. 2. Number of non-synonymous single nucleotide polymorphisms present in FFUL887 predicted proteins, when compared with their CBS138 counter-partners. The reads obtained after whole-genome sequencing of the FFUL887 strain were mapped against the genome of the reference strain CBS138, as detailed in materials and methods. Those genes exhibiting a higher number of non-synonymous SNPs in the FFUL887 strain are highlighted in the figure. Adhesin-encoding genes are evidenced in light blue. 49

Figure III. 3. Deletion of the *CgPDR1*^{A820C} allele from FFUL887 genome abrogated azole resistance and reduced expression of *CgPdr1* target genes. (A) MIC for fluconazole and voriconazole was obtained for the CBS138, FFUL887 and the FFUL887_Δ*Cgpd1* strains, as determined by the microdilution method recommended by EUCAST. For the statistical analysis, the results obtained for the mutant strain devoid of *CgPDR1* gene were compared with those gathered for the wild-type FFUL887 strain using one-way ANOVA. (B) Comparison of the transcript levels of *CgPDR1*, *CgCDR1*, *CgPDH1* and *CgQDR2* genes in CBS138, FFUL887 and the FFUL887_Δ*Cgpd1* strains. Cells of the different strains were cultivated in RPMI growth medium until mid-exponential phase after which the expression of *CgPDR1*, *CgCDR1*, *CgPDH1* and *CgQDR2* genes was compared by RT-qPCR. The values represented for the FFUL887 and FFUL887_Δ*Cgpd1* strains are relative to the value obtained for the CBS138 strain, which was considered to be equal to 1. For the statistical analysis, the results obtained for the FFUL887 strain were compared with those gathered for CBS138 (black), while the results obtained for the FFUL887_Δ*Cgpd1* mutant were compared with those obtained for FFUL887 (grey) using one-way ANOVA. * *p*-value below 0.05, **** *p*-value below 0.0001..... 51

Figure III. 4. Comparison of the susceptibility of CBS138, FFUL887 and the FFUL887Δ*Cgpd1*, *KUE_chr606* and *KUE100ΔCgpd1* strains to environmental stressors based on spot assays. Mid-exponential phase cells of the different strains were cultivated in solid MM growth medium or in this same medium supplemented with inhibitory concentrations of H₂O₂ or of acetic acid, propionic acid and butyric acid. Final cell suspension was prepared with an OD_{600nm} of 0.05 ± 0.005 and dilutions of the cell suspension are spotted. Growth was compared after two to

three days of incubation at 30°C, depending on the severity of growth inhibition. The same experimental setup was used to compare the tolerance of the strains to different temperatures. 52

Figure III. 5. Schematic representation of the metabolic pathways related with carbon and nitrogen metabolism including genes up-regulated in the FFUL887 strain, when compared to CBS138. The reactions allocated to metabolism and transport of carbohydrates are shown in green while those associated with nitrogen metabolism are shown in blue. 54

Figure III. 6. Schematic representation of the genes involved in trans-sulfurylation pathway in *Candida glabrata*, those being up-regulated in the FFUL887 strain being highlighted in blue. Association between genes and metabolic pathways was performed using the KEGG database. 55

Figure III. 7. Schematic representation highlights the modest overlap existing between genes that are under the regulation of different *CgPdr1* gain-of-function mutants. Venn diagram comparing the set of genes regulated by the *CgPdr1* gain-of-function mutants K274Q, K274N, P927L and L946S, as revealed by transcriptomic analyses. The set of genes herein identified as being up-regulated in the FFUL887 isolate that were previously described to be *CgPdr1* dependently transcribed was compared with the set of genes previously described to be under the regulation of K274N, P927L and L946S *CgPdr1* gain-of-function mutations [27, 56]. 58

Figure IV. 1. Species distribution of the collection of *Candida* isolates examined in this work according to the product they were retrieved from. Species of the *Candida* genus were identified on MALDI-TOF profiling. 71

Figure IV. 2. Comparative gene and genomic expression between the azole-susceptible strain *Candida glabrata* CBS138 and the azole-resistant isolates FFUL443 and FFUL674, encoding a *CgPDR1* allele that harbors the not previously described non-synonymous substitution I392M and I803T. (A) The expression of *CgCDR1* and of *CgPUP1* was compared in CBS138, FFUL443 and FFUL674 cells during cultivation in drug-free RPMI medium until mid-exponential phase. The level of expression registered in the CBS138 was set at 1 and the other values compared with that. The transcript levels of *CgRDN25* were used as an internal control. The expression level of these two described *CgPdr1*-target genes was also monitored in isolates, FFUL830 and ISTA56 encoding, respectively, E555K and G558C, also found in azole-resistant isolates. As a positive control, the expression of *CgPUP1* and *CgCDR1* genes in ISTB607 strain was also monitored, encoding the demonstrated *CgPdr1* GOF variant R376W. (B) Venn diagram showing the number of *CgPdr1* documented activated genes (according to the information available in the PathoYeast database) found to be over-expressed in the transcriptome of isolates FFUL443 and FFUL674 cultivated in the same growth conditions (compared with transcript levels registered in the azole-susceptible strain CBS138). (C) MIC for fluconazole assessed by the recommended EUCAST microdilution method obtained for SKY107 cells transformed with plasmid pYR29-MycHis which drives expression of *CgPDR1* from its natural promoter and terminator and in the derived plasmids that encode the *CgPDR1* allele with the individual substitutions I392M and I803T. As a control, the described *CgPdr1* GOF variant K274Q was also used. 73

Figure IV. 3. Influence of the *CgGal11A* mediator subunit in tolerance to fluconazole of *Candida glabrata* cells producing the wild-type or the gain-of-function K274Q, I392M and I803T *CgPdr1* variants. $\Delta Cgpd1$ (SKY107) or $\Delta Cgpd1\Delta Cggal11a$ (LYS2) cells were transformed with the pYR29-MycHis_*CgPDR1* plasmid (which drives expression of *CgPDR1* from its natural terminator and promoter) or with the derived plasmids pYR29-MycHis_*CgPDR1*^{A820C}, pYR29-MycHis_*CgPDR1*^{T1176G} or pYR29-MycHis_*CgPDR1*^{T2408C}, encode the corresponding K274Q, I392M and I803T variants, and were used to compare susceptibility to fluconazole by spot

assay in MM or in YPD rich medium. Final cell suspension of mid-exponential phase cells was prepared with an OD_{600nm} of 0.05 and dilutions of the cell suspension are spotted. Growth was compared after two to three days of incubation at 30°C, depending on the severity of growth inhibition. 75

Figure IV. 4. *Number of non-synonymous single-nucleotide polymorphisms found upon the comparison of gene sequences encoded by the azole-resistant strain ISTB218 and the azole-susceptible strains CBS138 and ISTA29.* The names of adhesin-encoding genes are depicted in the figure to denote the high number of SNPs found in these sequences encoded by the azole-resistant strain ISTB218. Those adhesins that are described to provide protection against azoles in *C. glabrata* are highlighted in blue. 77

Figure V. 1. *The modelling of the CgPDR1 protein structure allows the characterization of the conserved structural domains of zinc-finger nuclear receptor transcription factors.* (A) Structural modelling of *C. glabrata* Pdr1 according to AlphaFold Protein Structure Database with confidence modelling representation. (B) The CgPdr1 protein structure is composed of four different structural features: the DNA-binding domain (DBD, yellow), the linker sequence (light grey) the dimerization domain (DD, dark grey), the core structure central regulatory domain (CRD, beige), and the transactivation domain (TAD, green). (C) Representation of two sides of the CgPdr1 protein in surface view (a) and backbone view (b), respectively. (D) Representation of the CgPdr1 hydrophobic properties of the dimerization domain and (E) of the hydrophobic and electrostatic properties of the individualized CgPdr1 TAD domain. The hydrophobicity potential is represented from blue for the most hydrophilic residues, to white if neutral, and to yellow if hydrophobic, while the electrostatic charged surface is represented from red for the most negative potential, to white if neutral, and to blue if positive. 95

Figure V. 2. *Prediction of the secondary structure of CgPdr1 and of the residue's propensity for DNA and protein binding.* (A) Secondary structure prediction along the CgPdr1 amino acid sequence was obtained in PSIPRED workbench. (B) DisoRDPbind was used to predict the propensity for the different residues of CgPdr1 to bind to DNA and Proteins. 96

Figure V. 3. *Analysis of the properties of the CgPdr1 structures involved in the interaction between the transactivation domain and the central regulatory domain.* (A) The 3D structures of the TAD and CRD interacting were individualized from the rest of the CgPdr1 structure for further analysis. Further individualization of the TAD region (C and D) from the CRD domain (B) was obtained to characterize the hydrophobic (b) and electrostatic (b) properties of the interacting surfaces. The hydrophobicity potential is represented in blue for most hydrophilic surfaces, in white, for neutral residues, and in yellow for hydrophobic ones. The electrostatic charged surface interaction is represented in red for the most negative potential, in white if neutral, and in blue if positive. The backbone view is also represented in (a), marking in cyan the CDR structures predicted to interact with TAD, which is itself highlighted in green. The region of the TAD docking in the CRD structure is further marked in a black box. 97

Figure V. 4. *In silico prediction of CgPdr1 3D structure helps to detail the sequestration of the transactivation domain by the internal core of the protein.* (A and B) Using the *in silico* prediction of the CgPdr1 structure by Alphafold it was possible to identify (using Chimera Integrated Find Contact tools) the core structural features (represented in cyan) of the protein such as α -helixes in the central regulatory domain (CRD) as well the residues of this domain (identified in dark blue) involved in contacts (represented as light yellow) with the transactivation domain (represented in green). (C) The amino acids that interact with the residues of the TAD domain are highlighted in green in the amino acid sequence of CgPdr1. (D) The undertaken prediction allowed an

identification of three predicted inhibitory domains (ID) marked as three stretches along the central regulatory domain of CgPdr1 (grey). The tridimensional structures of ID I are highlighted in red, ID II in green, and ID III in black in panels A and B. 99

Figure V. 5. *Modelling of fluconazole docking in the CgPdr1 nuclear receptor transcription factor structure.* The Chimera software integrated AutoDock Vina tool was used to simulate the most probable docking regions for fluconazole molecule in CgPdr1. (A) For the simulation, the minimum XBD was defined as the receptor (defined in Thakur, J. K. *et al.* 2008, represented in red), predicting only one probable region of docking. The different scores of qualities in prediction are summarized in the table. (B) The predicted fluconazole (represented in blue and signal by an orange arrow) docking site occurs in a channel that crosses the core structure of the CgPdr1. The DBD and linker domain were removed for better visualization. (C) The Chimera Find Contact tool was used to predict the residues capable of interacting with the best scored simulated fluconazole (-7.8) binding modes and are marked in green in the amino acid sequence..... 101

Figure V. 6. *Definition of the CgPdr1 protein structural features that interact with fluconazole antifungal molecule.* (A) The predicted structural features of CgPdr1 that are predicted to be involved in the interaction and possibly modified by the binding of the fluconazole molecule (red) are marked in dark blue, with amino acid residue stretch circled in black, with the specific residues predicted to interact with fluconazole marked in yellow. The structures previously predicted to contact with the docked TAD domain are also represented in cyan and residues circled in red (B) The contacts formed by the different functional structures were further analyzed and are marked in green. D) The undertaken prediction allowed the identification of three predicted fluconazole binding domains (FBD, blue) marked as three stretches along the central regulatory domain of CgPdr1 (grey). 102

Figure V. 7. *Gain-of-function mutations are distributed in the central regulatory domain of the CgPdr1 transcription factor protein.* The Chimera visualization software was used to inspect closely the distribution of residues affected by GOF mutations (red) along with the structure of CgPdr1. (A) The influence that the change of these residues of the core structure of CgPdr1 can have on the fluconazole docking structure (dark blue), with residues that interact with fluconazole (highlighted in yellow), the TAD domain (green) and the structural features that interact with the TAD (cyan) were carefully analyzed. (B) Analyses of the effect that the residues (red) changes P822L and I803T in the core of CgPdr1, reported resulting in CgGal11A partially independent CgPdr1 hyperactivation, might have on CgPdr1 protein structure. (a) Influence of the mentioned GOFs and the connected (represented with green lines) α -helix structures where they are located might have on the CgPdr1 structure and specifically the nuclear localization signal region (dark grey) (b) The surface region of this CgPdr1 structure region is specially enriched in negative charges (red). (C) The 392 residue (red) is buried in the CgPdr1 structure and located in an α -helix structure involved in TAD domain sequestration (cyan) that is also located near the fluconazole (yellow) predicted docking site. The modification to a Met amino acid generates clashes (red lines) to the near T520 residue (green). 104

Figure V. 8. *Gain-of-function mutations distributed in the transactivation domain of the CgPdr1 transcription factor protein.* The Chimera visualization software was used to inspect closely the distribution of residues affected by GOF mutations (red) along with the structure of CgPdr1. (A) The influence that the change of these residues in the TAD (green) was carefully analyzed. (B) Analysis of the distinct effect of the modifications LWG1097AAA and D1082G, different dependencies on CgGal11A for hyperactivation of CgPdr1, have on the TAD domain overall negative electrostatic charge (red) and hydrophobic surface (yellow). 105

Figure V. 9. *Gain-of-function mutations distributed in the exposed region of the middle homology domain of the CgPdr1 transcription factor protein.* The Chimera visualization software was used to inspect closely the distribution of residues affected by GOF mutations (red) along with the structure of CgPdr1. (A) Several residues of the middle homology region (MHR) were also identified to be affected by GOF mutations; specifically, aromatic amino acids enriched in this region. (B) This zinc transcription factor conserved region is a structural part of the channel where fluconazole docks (highlighted in blue). The predicted fluconazole molecule (yellow) docking channel structure is signaled in surface representation with a red arrow. 106

Figure V. 10. *Gain-of-function mutations distributed in exposed regions in CgPdr1 transcription factor protein.* (A) The Chimera visualization software was used to inspect the disordered region that connects the dimerization domain (dark grey) and the predicted TAD docking domain (cyan) that is enriched with residues affected by GOF (red) (B) The localization of the residues affected by the G346D and L280F GOF mutations, with opposing effects in CgEPA1 expression, in the of CgPdr1 protein structure was analyzed. The effect of the L280P GOF mutation in the destabilization of the α -helix secondary structure is also analyzed. (C) The K274 residue (red) interacts with the amino acids of a nearby loop structure (yellow), which in its turn has residues that have a connection with those of the TAD domain (green) or the TAD docking region (cyan). Change of the lysine by glutamate or asparagine reduces the number of interactions of the 274 residues. 107

Figure V. 11. *Redefinition of the regulatory domains of CgPdr1 based on the predicted structure features, the effect of gain-of-function mutations in CgPdr1 activity, and literature information.* (A) The different regulatory domains of CgPdr1 identified include the DNA-binding domain (DBD), the linker region, the dimerization domain (DD), the regulatory domain (RD), three inhibitory domains (ID), three domains involved in fluconazole binding signalling (FBD), the middle homology region (MHR) the nuclear localization signalling (NLS) and the transactivation domain (TAD). The distribution of the gain-of-function mutations found in the literature in the amino acid sequence of CgPdr1 is also represented, including in green the GOFs characterized in this thesis. The structural representation of the different domains is represented with the same color in (B) backbone and (C) surface structural representation. 109

Figure V. 12. *Representation of the CgPdr1^{K274Q} and CgPdr1^{WT} interaction with the promoter of some CgPdr1 identified direct targets.* Three examples of peaks of reads obtained in ChIP-seq analysis in the promoters of found upregulated genes by CgPdr1^{K274Q} vs CgPdr1^{WT} (green) and without change (black). Images were obtained in IGV viewer using ChIP-seq sequence files of three different replicates of each CgPdr1 variant. The MOCK IP reads used as the control for peak calling using bPeaks software are also represented. 114

Figure V. 13. *The K274Q gain-of-function mutation does not affect the CgPdr1 promotor binding preference.* ChIP-seq analyses of the CgPdr1 Myc-tagged versions expressed in the SKY107 strain and immunoprecipitated in mid-exponential growth in RPMI pH7. ChIP-seq analyses identified the same direct regulated genes for CgPdr1^{K274Q} and CgPdr1^{WT}. Genes represented in bold have increased expression in a strain expressing CgPdr1^{K274Q} variant compared CgPdr1^{WT}. This set of genes was previously confirmed in Paul S. *et al.* 2014 directly regulated targets of CgPdr1 activated in a petite strain. From those, only identified direct targets with a PDRE found in the promotor were considered in the present comparative analysis. 116

Figure V. 14. *Mass spectrometry identification of the nuclear proteins immunoprecipitated with the Myc-tag CgPDR1 wild-type variant and K274Q gain-of-function variant using ChIP-SICAP methodology.* Gene ontology (GO) categories in the proteins identified were defined using the CGD database “GO term finder” tool [345]. 122

Figure VI. 1. Assessment of the effect and expression of *CgHAA1* and *CgHaa1*-regulated adhesion genes *CgAWP12*, *CgAWP13*, *CAGL0H07469g*, and *CAGL0K10164g* in biofilm formation in biotic and abiotic surfaces. (A) Cell viability in biofilm was measured using PrestoBlue after 6 h and 24 h growth in RPMI at pH4, with or without acetic acid. Results represent the means of ten independent experiments. (B) Comparison, measured by real-time PCR, of transcription levels of the *CgHaa1*-regulated adhesion genes in the control KUE100_chr606 and $\Delta CgHaa1$ strain in control or acetic growth conditions, after 6 h in RPMI growth at pH 4. (C) Effect in RHVE cells in adhesion of *C. glabrata* of the deletion of the *CgHAA1*, *CgAWP12*, *CgAWP13*, *CAGL0H07469g*, and *CAGL0K10164g* when compared to the KUE100_chr606 control strain, after 12 hours growth in RPMI at pH 4, with or without 30 mM acetic acid. Significant differences in adhesion of the deletion mutants with the wild-type strain are signaled in black, while significant differences in adherence of the same strain when grown in control or acetic acid stressed conditions are marked in grey. Results represent the means of a minimum of three independent experiments. Statistical significance of the data shown was assessed using ANOVA considering different replicas performed (* $p > 0.05$, ** $p \leq 0.01$, *** $p \leq 0.01$, **** $p \leq 0.0001$). 135

Figure VI. 2. Importance of *CgHaa1* and *CgHaa1* regulated adhesins genes for virulence in *Candida glabrata* of the *Galleria mellonella* infection model (A) *G. mellonella* survival after injection with *C. glabrata* control KUE100_chr606 strain, and the deletion mutants $\Delta CgHaa1$, $\Delta Cgawp12$, $\Delta Cgawp13$, $\Delta CAGL0K10164g$, $\Delta CgCAGL0I07249g$, $\Delta CAGL0E03740g$ and $\Delta CAGL0G05632g$. Differences in survival rates were calculated by using a log-rank (Mantel-Cox) statistical test ($P < 0.01$, for comparison of the wild-type and the mutant). (B) *In vitro* infection of hemocytes with *C. glabrata* control KUE100_chr606 strain, and the mutants of $\Delta CgHaa1$, $\Delta Cgawp12$, $\Delta Cgawp13$, $\Delta CAGL0K10164g$, $\Delta CgCAGL0I07249g$, $\Delta CAGL0E03740g$ and $\Delta CAGL0G05632g$. *Candida* load in the hemocytes was assessed upon 1 and 8 h of internalization by the *G. mellonella* hemocytes, using a MOI of 1:5. The displayed results are relative to the concentration of viable cells inoculated at time zero. Statistical significance differences shown comparing the KUE100_chr606 with the mutant strains were assessed using one-way ANOVA considering the different replicas performed (** $p \leq 0.01$, **** $p \leq 0.0001$). All the results represent the means of a minimum of three independent experiments. 137

Figure VI. 3. Importance of *CgHaa1* and *CgHaa1* regulated acetate metabolism genes for the co-consumption of acetic acid with glucose and the role in virulence. (A) *G. mellonella* survival after injection with *C. glabrata* control KUE100_chr606 strain, and the deletion mutants $\Delta CAGL0L00649g$ and $\Delta Cgic11$. Differences in survival rates were calculated by using a log-rank (Mantel-Cox) statistical test ($P < 0.01$, for comparison of the wild-type and the mutant). (B) Comparison of the susceptibility of control *C. glabrata* KUE100_chr606 and deletion mutants $\Delta CAGL0L00649g$ and $\Delta Cgic11$ to inhibitory concentrations of acetic acid. Cells used to prepare the spots in MM at pH 4.5 were cultivated until the mid-exponential phase, harvested by centrifugation. The final cell suspension was prepared with an OD_{600nm} of 0.05 and dilutions of the cell suspension were spotted. (C) For evaluating the consumption of acetic acid and glucose, the control KUE100_chr606 strain, and the deletion mutant strains $\Delta CAGL0L00649g$ and $\Delta Cgic11$ were cultivated in liquid MM medium at pH 4.0 either or not supplemented with acetic acid. Growth was followed for approximately 72 h during which samples of culture supernatants were harvested and used for the quantification of acetic acid and glucose concentrations by HPLC. The results shown are means of the results obtained in three independent experiments. 140

Figure VII. 1. (Part II) Representation of the *CgHaa1* interaction with the promoter of potential direct targets genes. Images were obtained in IGV and represent visually the alignment to the *C. glabrata* genome of the

sequenced reads obtained by the three biological replicates of CgHaa1 ChIP-seq, specifically in the promotor regions where high intensity of reads (peaks) were identified by bPeaks software (black boxes) when compared to the MOCK control. 158

Figure VII. 2. Representation in IGV of possible CgHaa1 interaction with the promoters of upregulated genes.

These interactions require further confirmation, since they are low in intensity and not always identified by bPeaks, at least consistently in all replicates (black), were found in the promoters of chipable genes (blue, possible peaks in promoters highlighted in dashed boxes) or found in up-regulated genes (green, possible peaks in promoters highlighted in dashed boxes)..... 159

Figure VII. 3. Representation of the two most significant consensus binding motifs for CgHaa1 during acetic acid stress predicted from the ChIP-seq peaks sequences using the RSAT tools.

The sequences of high reads peaks identified by the bPeaks software, located at gene promoters regions, that result from the sequencing of DNA immunoprecipitated with the Myc tagged CgHaa1 *in vivo* in response to acetic acid stress (30 mM, pH 4), were used to find the most represented motifs using the RSAT tools. 163

Figure VII. 4. Amino acid alignment of the N-terminal regions of ScHaa1 and CgHaa1 presumed to include the DNA-binding domains of these regulators. (A) The existence of a non-conserved region in CgHaa1 lead to the identification of two candidate regions to be the CgHaa1 DBD, between residues 1-104 (highlighted in blue) and the other between residues 1-153 (highlighted in green). (B) DisoRDPbind prediction of the amino acids in CgHaa1 involved in DNA interaction. The plot shows the propensity score calculated for each residue to interact with DNA. If the propensity score is above the threshold of 0,245 the amino acid is predicted to interact with DNA and is scored with 1, if not it's scored with 0. The non-conserved CgHaa1 DBD sequence is highlighted in pink.

..... 165

Figure VII. 5. Heterologous expression of the CgHaa1-153DBD. The CgHaa1-153DBD His tagged peptide was heterologous expressed in *E. coli* BL21-CodonPlus(DE3)-RIL cells from the pET23a+ plasmid. The peptide was afterwards purified by the sonicated cell pellet using a His-trap column and further concentrated and through fast protein liquid chromatography. Confirmation of the expression and purification of the two peptides was performed by SDS (A) and detection of the His-tag by western blot (B)..... 166

Figure VII. 6. Representation of the preliminary regulatory network of CgHaa1 during acetic acid stress. The network constructed has two levels of confidence: 1) interaction of CgHaa1 transcription factor with the promoter of the gene confirmed by ChIP-seq analysis during acetic acid growth conditions; 2) Using the same growth conditions, confirmation of CgHaa1 dependence for gene expression using microarray assay (marked in green arrows). A dashed arrow represents the lack of a predicted DNA binding site in the promoter ChIP-seq peaks. Genes circled in dashed lines require further confirmation of CgHaa1 interaction to the promotor. Gene name was defined by the orthologue in *S. cerevisiae*. 167

Figure VIII. 1. Different effects of gain-of-function mutations identified in the course of this thesis in the CgPdr1-direct regulon. The upregulated known direct CgPdr1 target genes of the clinical isolates with distinct CgPdr1 gain-of-function variants when compared to de CBS138 azole sensitive laboratorial strain show little overlap. 171

Figure VIII. 2. Genome and transcriptome-wide studies results were used to identify changes in resistance factors in azole-resistant clinical isolates. During the current thesis, a total of ten clinical isolates were found to have an azole resistance phenotype. Azole resistance of seven clinical isolates was associated with non-synonymous

mutations in CgPdr1, including K274Q, I392M and I803T demonstrated herein for the first time to be gain-of-function mutations. One azole resistance clinical isolate was found to encode a CgPdr1 “wild-type” allele. OMICs studies helped identified several non-synonymous mutations (grey) or changes in transcription (green if upregulated and red if downregulated) of known azole resistance genes that can be in the future scrutinized as important mechanisms of resistance. 173

Figure VIII. 3. *Different effects of gain-of-function mutations identified in the course of this thesis in the CgPdr1 protein structure and activity.* (A) The GOFs K274Q and I392M that are dependent on CgGal11A for CgPdr1 hyperactivity are located in the regulatory domain (RD) and inhibitory domain (IDI), while the I803T GOF, that CgPdr1 hyperactivity is less dependent on CgGal11A, is located in the nuclear localization signalling domain (NLS). (B) ChIP-seq analysis revealed that CgPdr1^{K274Q} variant (blue) as the same distribution has the wild-type variant (orange) in the promotor region of its target genes despite having a different influence on their expression. The genes upregulated using transcriptomic analysis by the CgPdr1^{K274Q} variant compared to the CgPdr1^{WT} variant are marked in blue. 175

Figure VIII. 4. *Comparison of the CgHaa1 and ScHaa1 predicted direct regulatory network during acetic acid stress.* The CgHaa1 regulatory network was defined in this thesis for the first time based on the ChIP-seq analysis explored in Chapter VII. CgHaa1 dependence for gene expression was confirmed by microarray assay to predict if CgHaa1 interaction with a gene promotor could result in gene upregulation (when that is found not to be the case, the gene is underlined). Genes marked with * required further validation by ChIP-qPCR since a low-intensity profile of the reads in the regions where CgHaa1 is presumably bound was observed. The ScHaa1 regulatory network was predicted by Mira, NP. *et al.* 2011 [253], based on the presence of the identified binding motif HRE in the promotor of genes that expression is dependent of ScHaa1 during acetic acid stress. The effect in transcription on the target genes by CgHaa1 and ScHaa1 were accessed under similar growth conditions, mid-exponential phase cells grown in minimal medium at pH4 after 30 min acetic acid exposure. 178

I. Thesis Outline

The increase in the incidence of isolation of resistant *Candida glabrata* clinical isolates, together with the shortage of new antifungal molecules introduced in the market, brings a serious Public Health issue, considering the high relevance of these species as causative agents of fungal infections. In this context, it is essential to scrutinize the molecular mechanisms by which *C. glabrata* cells acquire resistance to antifungals *in vivo* with the aim of identifying what could be novel therapeutic targets. This knowledge may also pave the way for the development of new tools that could be used for the rapid diagnosis of resistant strains, a particularly important aspect since delays in diagnosis and treatment of *Candida* infections greatly determine the outcome of infected patients, specially in the case of those caused by *C. glabrata*, a species that distinguishes among *Candida* spp. for its higher resilience to azoles and a more rapid capability of acquiring resistance *in vitro*. This thesis starts with an introductory chapter (Chapter II) that focus on what is known in the field of azole-resistance in *Candida* species, with a particular emphasis on the knowledge gathered in *C. glabrata*. From this survey of the literature available, it was evident that the relevance of most tolerance mechanisms described in laboratory strains in the azole resistance phenotype in clinical strains remains to be studied. This aspect renders particularly important the focus herein put on the study of resistant clinical *C. glabrata* strains, as a way to provide more knowledge about the genomics and physiology of these strains that can be used in the future to better address these still yet elusive questions concerning underneath molecular players.

Chapter III of the thesis describes the whole-genome sequencing of a fluconazole and voriconazole-resistant clinical *C. glabrata* isolate (named FFUL887) that was identified after a phenotypic screening of a collection of strains recovered not only from sterile niches but also from other niches in which *C. glabrata* exists as a commensal (such as vaginal or oral swabs, for example). This is a distinguishable aspect of this study since the azole-resistance phenotype in commensal populations is likely to play a very important role considering the growing body of knowledge that demonstrates the potential of these populations in disseminating from their original niches to the bloodstream. The genome of the FFUL887 strain was compared with the genome of the susceptible strain CBS138, which revealed prominent differences in several genes documented to promote azole resistance in *C. glabrata*. Of many differences that were found in the coding sequence of genes described to confer protection against azoles in *C. glabrata*, focus was put on the *CgPDR1* allele encoded by this strain since this encoded a K274Q non-synonymous modification that was not described before. Through transcriptomic analysis coupled with more detailed molecular analysis, it was possible to demonstrate that this modification represents a new gain-of-function mutation of CgPdr1. The genomic and transcriptomic analyses also provided insights into what can be adaptive responses evolved by *C. glabrata* during adaptation to the host environment.

Chapter IV continues the efforts in disclosing azole-resistance phenotype of clinical *C. glabrata* strains. In this study, a large collection of clinical isolates belonging to different *Candida* species, encompassing strains retrieved from sterile infection sites and commensal ones, resulted in the identification of 11 *C. glabrata* strains resistant to fluconazole and to voriconazole. Ten out of these eleven azole-resistant strains were found to encode *CgPDR1* GOF alleles, with two of them, being herein characterized for the first time, I392M and I803T. The sole resistant isolate, ISTB218, which was found to encode a wild-type *CgPDR1* allele, was subjected to comparative genomic and transcriptomic profiling to shed light into what can be resistance mechanisms independent of CgPdr1. Comparison of the transcriptomic expression of the several azole-resistant strains identified in the course of chapters III and IV encoding the CgPdr1 GOF variants K274Q, I392M and I803T appears to suggest that different gain-of-function modifications have a different impact in the biochemical activity of CgPdr1 and, consequently,

in the genomic expression of the strains. Although the great differences in the genetic background of different clinical strains is an essential issue that needs to be accounted in the interpretation of these results, other results published in the literature (and also obtained in Chapter IV) reinforce this idea by demonstrating that different CgPdr1 variants have different requirements for the mediator subunit complex CgGal11A. In Chapter V, it is addressed a more molecular perspective of how the different GOF mutations affect the overall biochemical activity of CgPdr1 including its impact in the regulatory network governed by wild-type or GOF variants of this regulator, and also in the tridimensional structure of the protein. For this last aspect, *in silico* analysis was performed using the recently predicted structure of CgPdr1. Using a laboratory strain of *C. glabrata* expressing the alleles of the wild-type or a CgPdr1^{K274Q} variant and exploring chromatin immunoprecipitation approaches, it was examined how this GOF modification impacted the set of promoters recognized *in vivo*, the ability to induce target gene expression and the set of interactors.

Chapters VI and VII of the thesis also address a transcriptional regulatory network in *C. glabrata*, but this time the one that depends on the transcription factor CgHaa1. This novel regulator was identified in our laboratory as mediating *C. glabrata* response and tolerance to high concentrations of acetic acid, a relevant trait to assure that these cells are not excluded from the vaginal tract when the concentrations of this organic acid increase prominently during bacterial vaginosis. Taking into consideration the observation that CgHaa1 was demonstrated to be required for maximal adhesion of *C. glabrata* to vaginal epithelial cells and was identified as a positive regulator of several adhesin-encoding genes, in Chapter VI it was addressed the involvement of this regulon in the ability of *C. glabrata* cells to form biofilms and also in virulence of this species against the infection model *Galleria mellonella*. In a second step, in Chapter VII, it is detailed the elucidation of the CgHaa1-dependent regulatory network active in *C. glabrata* cells and the way it might have evolved from the network described in the budding yeast *Saccharomyces cerevisiae* that is controlled by ScHaa1, orthologue of CgHaa1. A particular emphasis was put on the identification of genes that were found to be under the regulation of CgHaa1, but not of ScHaa1, suggesting that some functional expansion of the network could have worked aiming to encompass new genes that bring new physiological functions into the network.

In Chapter VIII, a final discussion provides an integrated perspective of the findings of the presented work and explores future perspectives of the results obtained.

II. Introduction

Part of the results shown in this chapter were published in:

Salazar SB, Simões RS, Pedro NA, Pinheiro MJ, Carvalho NFNN, Mira NP, “An overview on conventional and non-conventional therapeutic approaches for the treatment of candidiasis and underlying resistance mechanisms in clinical strains”, *J Fungi*. 10;6(1), 2020. doi: 10.3390/jof6010023

1. The human opportunistic pathogen *Candida glabrata* and its high resilience to azole antifungal drugs

Candida species are commensal organisms of the human gastrointestinal and genitourinary tracts, however, under certain conditions, such as the decreased activity of the immune system, this commensal colonization can progress to infections that can range from mucocutaneous candidiasis to disseminated mycosis [1]. Although *C. albicans* remains the leading agent of invasive candidiasis, an alarming increase in the incidence of infections caused by non-*Candida albicans* species occurred in the past decades, this being worrisome as these species are often more resilient to antifungal drugs [2, 3]. Specifically, *C. glabrata* is today the second most common causative agent of candidiasis, this emergence being associated with its innately higher resilience to azoles, the frontline antifungal therapy used today in the clinical setting [2-4]. A higher emergence of *C. glabrata* clinical isolates resistant to azoles and/or echinocandins is also being increasingly reported [2, 3, 5], this being of concern as it may result in therapeutic failure and, consequently, in increased mortality and morbidity rates [6].

The development of antifungal drugs is limited by the similarity between fungal and human cells, which difficulties the identification of molecules that specifically target the microbial cell while not damaging the host. Only four different classes of antifungals are available to treat infection caused by *Candida* species: azoles, polyenes, fluoropyrimidines, and echinocandins (reviewed in [7]). The mechanism of action of the different classes of antifungals is schematized in Figure II. 1. Briefly, while azoles and polyenes target the biosynthesis of ergosterol [8, 9], echinocandins affect the cell wall [10]; two cellular traits that are absent in mammalian cells and are therefore largely explored as therapeutic targets. Fluoropyrimidines, like 5-fluorocytosine enters fungal cells through cytosine transporter(s) being afterward metabolized via the pyrimidine salvage pathway to 5-fluorouracil (5-FU), considered the active form of 5-FC. 5-FU incorporates in RNA, causing premature chain termination, and inhibiting the activity of thymidylate synthase, an enzyme essential for DNA synthesis [11]. This thesis focuses on the mechanisms of tolerance to azoles in *C. glabrata*, as such, there will be an emphasis on the known molecular responses to these antifungals.

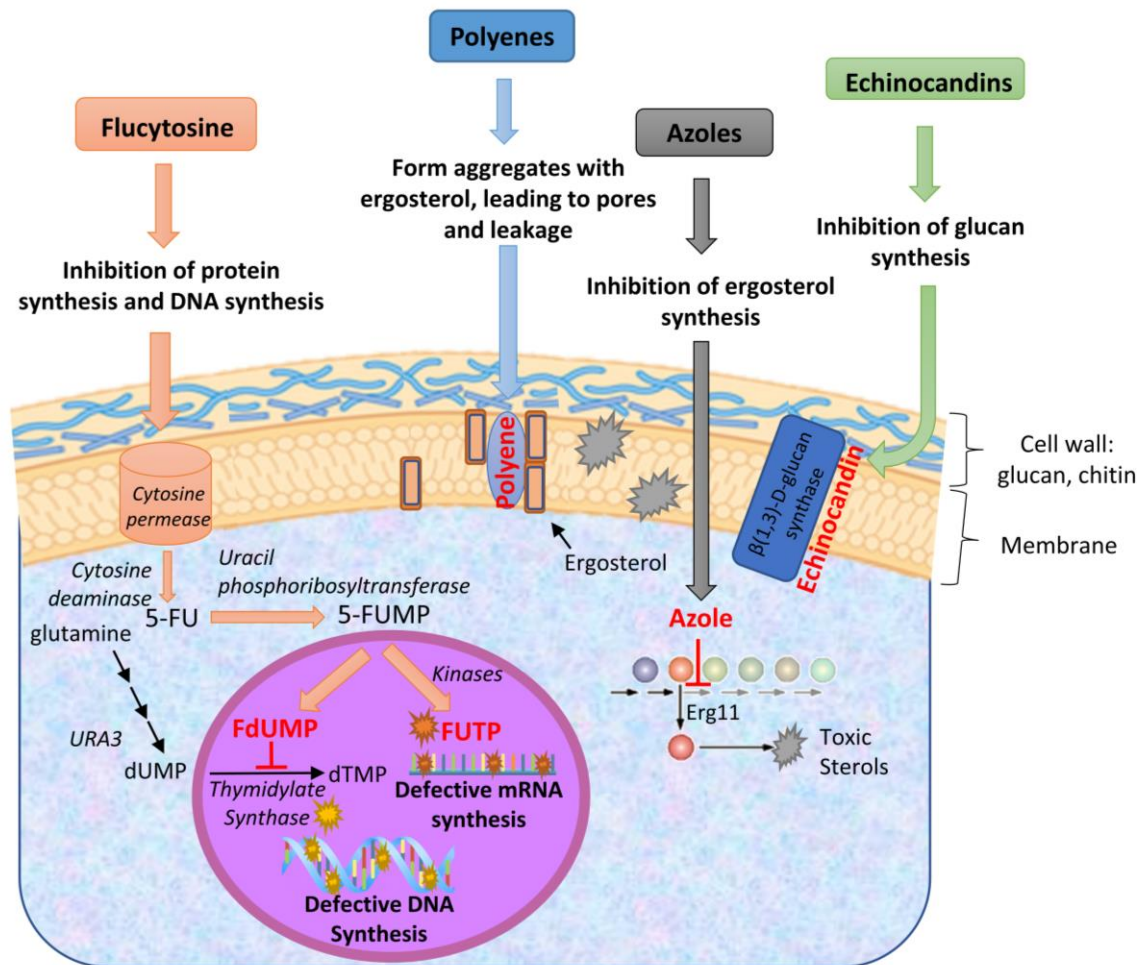


Figure II. 1. Schematic representation of the known mechanisms of action of the different classes of antifungals available for the treatment of candidiasis. 5-FU – 5-fluorouracil; 5-FUMP- 5-fluorouridine monophosphate; FdUMP -5-fluorodeoxyuridine monophosphate; FUTP- 5-fluorouridine triphosphate. Figure retrieved from Salazar, S.B. *et al.* 2020 [7].

1.1 Mechanisms underlying the innate resilience to azoles in *Candida glabrata* and consequences for resistance

Azoles act by inhibiting the activity of the lanosterol-14 α -demethylase enzyme (encoded by the *ERG11* gene) that is involved in ergosterol biosynthesis [12]. As a result of this inhibition, azole-exposed fungal cells accumulate toxic sterols in the plasma membrane dramatically affecting its permeability, among other effects (Figure II. 1)[7]. Azole antifungals have a fungistatic activity against *Candida*, meaning that after removal of the antifungal, *in vitro* exposed cells are able to resume growth, contrary to what is observed upon exposure to amphotericin B or echinocandins that are fungicidal [13]. The benefit of using fungicidal agents during patient treatment remains elusive since the outcome of invasive infections is often the same, even though several reports highlight a significant increase in therapeutic success using fungicidal agents in the early treatment of *Candida* infections [13, 14]. *C. glabrata* and *C. krusei* show less susceptibility to azoles than the remaining *Candida* spp. (Table II. 1) and thus higher doses are recommended to treat infections caused by this species [3, 15] (Table II. 1). The mechanisms underlying this increased resilience of *C. glabrata* towards azoles are not totally

clear, being suggested that this species could have evolved responses to handle changes in sterol content distinct from those verified *S. cerevisiae* or of other *Candida* species. Specifically, the inactivity of CgErg11 appears to result in the accumulation of sterols that compensate for the lack of ergosterol instead of having a toxic effect [16-19]. While the emergence of resistance to azoles in *C. albicans*, *C. krusei*, *C. parapsilosis*, or *C. tropicalis* has been largely associated with changes in the ergosterol pathway, including modifications in sequence or overexpression of *ERG11* [20-26], the allele encoded by *C. glabrata* azole-resistant clinical isolates is, in the vast majority of the cases, identical to the one encoded by susceptible strains [16, 27-29]. No link between expression of this gene and increased resistance to azoles could also be established in *C. glabrata* [27, 29, 30] and disruption of Cg*ERG11* gene results in the cross-resistance to amphotericin B and azoles [17, 31, 32]. Another striking difference observed is the report that in *C. albicans* deletion of *ERG3* [33], involved in the conversion of sterol intermediates into toxic sterols, results in enhanced resistance to azoles, a phenotype that is not observed in *C. glabrata* [31, 32]. Interestingly, non-synonymous mutations in CgErg3 that are thought to increase protein activity appeared with high frequency during *in vitro* evolution of echinocandin resistance, but not during evolution towards increased azole resistance [32], even though these observed modifications in CgErg3 were found to enhance tolerance to azoles.

Table II. 1. General susceptibility patterns of *Candida* species to antifungal drugs used in the treatment of candidiasis (adapted from [15] and [34]). S-susceptible; S-DD – susceptible dose-dependent; I – intermediate; R – resistant.

Species	Imidazole	Triazoles
<i>C. albicans</i>	S to R	S
<i>C. tropicalis</i>	S	S
<i>C. parapsilosis</i>	S	S
<i>C. glabrata</i>	S-DD to R	S-DD to R
<i>C. krusei</i>	S to R	S-DD to R

The induction of the activity of drug-efflux pumps has also been observed as an almost transversal mechanism of resistance to azoles across different *Candida* species. In this context, the more studied drug efflux pumps linked to azole resistance are those belonging to the ATP-binding cassette (ABC) superfamily out of which CgCdr1 stands out as having the more prominent role [35](Table II. 2). The expression of Cg*PDH1*, Cg*YOR1* and Cg*SNQ2* genes, also encoding ABC-transporters, was found to be increased in azole resistant clinical strains [28, 36], however, the deletion Cg*PDH1* and of Cg*YOR1* only resulted in enhanced susceptibility to azoles in a Δ *cdr1* mutant strain [36, 37]. This observation highlights the overwhelming role of CgCdr1 in enhancing tolerance to azoles, a feature that may mask the importance of other MDR transporters in this phenotype. Despite this, CgYor1 was found to protect *C. glabrata* cells from azole stress under nitrogen depletion conditions [37] while the expression of CgAus1 favored tolerance to azoles when exogenous sterols were present in the medium [38]. Although the influence of MDR transporters belonging to the Major Facilitator Superfamily (MFS) in mediating tolerance to azoles in *C. glabrata* has not been studied at the same extent as those belonging to the ABC superfamily, promising results had been obtained in a recent study showing a positive correlation between the expression of the *C. glabrata* Cg*AQR1*, Cg*TPO1_1*, Cg*TPO3*, and Cg*QDR2* MFS-MDR transporters genes in resistance to clotrimazole [39](Table II. 2). In this study, it was also shown that the deletion of Cg*TPO3* abolishes resistance to clotrimazole in one of the identified resistant clinical isolates [39]. CgPdr16, CgPdr17, CgTpo1_2, and CgFlr2 were also found to be required for maximum tolerance to ketoconazole and/or fluconazole in laboratory

strains [40-42]. The model that is generally accepted to explain the positive effect of ABC and MFS transporters in drug resistance is their role in directly mediating the extrusion of the drugs, however, from the biochemical point of view, this model is difficult to accept considering the wide structural divergence of the hypothesized substrates [as reviewed in 43]. Indeed, more recent studies performed in the eukaryotic model yeast *S. cerevisiae* show that ABC and MFS-MDR transporters have physiological substrates whose transport may affect the partition of the drugs between the intra- and the extracellular environment [as reviewed in 43, 44]. In specific, some MDR transporters have been shown to influence the lipid composition of the plasma membrane, by promoting the transport of phospholipids and/or ergosterol, which thereby may affect the diffusion rate of the drugs across the membrane [as reviewed in 44]. In this context, it was recently shown that deletion of the poorly characterized *C. albicans* ABC transporter CaRoa1 results in increased membrane rigidity and, consequently, in a reduced intracellular concentration of azoles [45]. In *C. glabrata* the transcriptional regulation of MDR efflux pumps is under the tight control of the pleiotropic drug resistance network (or PDR) that is dependent on the CgPdr1 regulator [46](Table II. 2). The involvement of the PDR network, and of CgPdr1 in particular, in tolerance of *C. glabrata* to azoles will be scrutinized in a dedicated section in this introduction.

Genomic analyses have unveiled an important role in the inactivation of the *CgMSH2* gene as a driver of resistance to antifungals (including azoles, echinocandins and amphotericin B) in *C. glabrata* while colonizing the host [47]. The *CgMSH2* gene encodes a protein involved in DNA repair and its inactivation (promoted by frameshift mutations in the coding sequence) leads to increased genetic diversity in the *C. glabrata* population. As such, isolates harboring inactive *CgMSH2* alleles rapidly acquired resistance to antifungals resulting from the rapid acquisition of beneficial mutations [47]. The genomic plasticity exhibited by *C. glabrata* has also been found to contribute to increased drug resistance in these species. In specific, in azole-resistant clinical *C. glabrata* isolates it has been described the increase of *CgCDR1*, *CgPDH1* or *CgERG11* gene copy number, which may be correlated to interchromosomal duplication or the formation of mini-chromosomes harboring several copies of the same genes [48, 49].

Table II. 2. Summary of the determinants of resistance identified in azole-resistant *Candida glabrata* isolates

Modification of drug target (protein or pathway)	Increased activity of drug-efflux pumps	Increased activity of PDR transcription factors
Missense mutation <i>CgERG11</i> bypassing inactivation of ergosterol biosynthesis by azoles [17]	Over-expression of <i>CgAQR1</i> , <i>CgCDR1</i> , <i>CgPDH1</i> , <i>CgQDR2</i> , <i>CgSNQ2</i> , <i>CgTPO1_1</i> , <i>CgTPO3</i> [28, 35, 36, 39]	Increased activity of CgPdr1 [27, 29, 50-56]

In recent years, global phenotypic studies, first using collections of laboratory mutant strains and more recently resorting to transposon gene disruption approaches, expanded (in some cases by a lot) the set of genes and biological processes conferring protection against azoles in *C. glabrata* [40, 57-59]. These studies confirmed the important role of CgPdr1 and its target MDR transporters for tolerance to azoles, while also implicating other regulators in the transcriptional regulation of drug-efflux pumps or ergosterol metabolism under azole stress including CgStb5 [60] or CgUpc2A [61]. It was also highlighted the role of several genes encoding transcription coactivators of the mediator complex, proteins involved in calcium-dependent signaling pathway or in Rho1-mediated signaling, as well as proteins involved in cell wall homeostasis [40, 57-59]. Furthermore, deletion of genes involved in ribosomal biogenesis and mitochondrial translation, the activity of the Krebs cycle and respiration, were found to exert protection against azoles [40, 58]. Nevertheless, a very modest overlap of those

genetic elements identified were confirmed to underlie azole resistance in clinical strains (none of these genes/functions being indicated in Table II. 2). This lack of correspondence might reflect that the occurrence of factors conditioning azole resistance *in vivo* may not be reflected in those found *in vitro*. Furthermore, the cellular functions identified to be relevant for the response to azole antifungals might not necessarily be involved in the development of azole resistance. Despite this, the dissimilarities in the findings obtained in the laboratory and clinical strains also reflect the lower amount of work that has been undertaken in clinical strains, compared to laboratory strains [as reviewed in 7]. In the vast majority of the cases, azole resistance in *C. glabrata* clinical strains derives from them acquiring gain-of-function (GOF) mutations in the transcription regulator CgPdr1 [as reviewed in 62]. In line with these results, a recent study using a transcriptomic approach to unveil the mechanisms of *in vitro* evolution of fluconazole resistance in *C. glabrata*, reported that the population transcriptomic profile appeared to select in the end the acquisition of CgPdr1 GOF mutations and consequently the upregulation of MDR efflux pumps, possibly reflecting a minimum cost of this resistance mechanism [63]. However, the development of resistance reported in clinical isolates [64, 65] and *in vitro* evolved strains [32, 63] is often gradual, reflecting transient resistance mechanisms by modifications in distinct genes and changes in the transcriptome-wide remodeling. Furthermore, secondary mutations often arise to balance the loss of fitness of resistance mechanisms [64-66]. Also relevant, is the fact that *in vivo*, there is a genetic heterogeneity that should not be neglected in the clonal population, in which different mutations in resistance and pathogenic genes might appear dominant during different times of infections in response to different stresses and can provide an advantage to the changing environment. These mutations, therefore, do not necessarily reflect an evolution of the isolate, but rather a selection within the host of the prevalent clonal genotype [66, 67].

2. The Pleiotropic Drug Resistance transcription factor, CgPdr1, in *Candida glabrata*

As said above, the major contributor to the multidrug resistance (MDR) phenotype in Yeasts is the pleiotropic drug-resistant (PDR) network, which has been shown to respond to a diverse range of xenobiotics [68-70]. The impacts of MDR are varied but in the specific context of *Candida* species, its impact in the tolerance and resistance of clinical isolates to azoles stands out. In the following chapter, an overview of the organization of this network is provided, starting first with its description in the non-pathogenic yeast species *Saccharomyces cerevisiae* and how it changes when compared to the network active in *C. glabrata*. Detailed analysis on the molecular mechanisms underlying the control of the activity of this regulatory network, in particular, of the Pdr1 transcription factor, will also be provided.

2.1. The Pleiotropic Drug Resistance network: from *Saccharomyces cerevisiae* to *Candida glabrata*

The PDR transcription factors in both *S. cerevisiae* and *C. glabrata* are found constitutively bound to the highly conserved pleiotropic drug response element sequences (PDRE; 5'- TCCRYGSR -3' and 5'- YCCRKGGGR - 3', respectively [71, 72]) present in the promoter of target genes [70, 73, 74]. Without further stimulus, the interaction of the PDR transcription factors with the PDRE motifs happens at low activity, resulting in the maintenance of a basal level of expression for target genes [70, 73, 74]. Pdr-dependent genes transcription is further activated upon stimulus [70]. The network of target genes directly regulated by ScPdr1, as evaluated by the interaction of the transcription factor with gene promoters [70, 75](Figure II. 2), identified several MDR transporters including *ScPDR5*, *ScPDR10*, *ScPDR15*, *ScSNQ2*, and *ScYOR1*. These MDR-transporters genes were found to be induced in an ScPdr1-dependent manner upon xenobiotic stimulation, including fluphenazine, selenite, progesterone, or benomyl [76-78]. However, the induction of genes may depend not only of the binding of ScPdr1 to the PDRE motif but also of additional factors [70]. A good demonstration of this is the observation that ScPdr1 plays an important role in the induction of *ScSNQ2* during exposure of the cells to fluphenazine, but the same does not happen in response to benomyl stress [70, 76]. Therefore, a combination of transcription inputs upon stress will help define the PDR-dependent transcriptional response and determine the final impact in gene transcription [70]. Lipid plasma membrane homeostasis is another major function regulated by the ScPdr1-network (Figure II. 2) including genes involved in biosynthesis and transport of phospholipids (*ScPDR16* and *ScICT1* [79, 80]), in the synthesis of sphingolipids (*ScIPT1* and *ScRSB1* [81, 82]) and in transport of sterols (*ScLAF1* [83]) [70, 84]. The ScPdr1-dependent network also includes *ScGRE2*, encoding a reductase responsive to osmotic and oxidative stress and that has an important, yet unclear, role in ergosterol metabolism [85]. Demonstrating the complexity of the network, ScPdr1 was confirmed to directly regulate other transcriptional activators (Figure II. 2) including the biotin regulator *ScVHR1* [86], *ScYRR1* and *ScPDR3* both regulators of drug-response, and Pdr1 itself [70, 86, 87]. ScPdr1 and ScPdr3 are paralogues

and share most of the directly regulated target genes and thus the basal expression of ScPdr1-dependent genes can be maintained in a $\Delta pdr1$ mutant due to compensation by ScPdr3 [70, 88-90]. However, it has been demonstrated that despite their homology, ScPdr1 and ScPdr3 diverged and specialized in response to different physiological signaling events and regulatory mechanisms [77, 88, 91-97]. ScPdr1 is the main responsible for response to xenobiotic stimulus, while ScPdr3 plays only a minor role in this although it has been shown to bind xenobiotics as well [70, 91]. In turn, ScPdr3 alone is responsible for the activation of the PDR-dependent genes in response to mitochondrial defects [92-95]. The expression of ScPDR3 is maintained at low levels in ρ^+ cells and is strongly induced in ρ^0 mutants, this induction being dependent of the ScPdr3 transcriptional auto-regulation, since deletion of the two PDRE motifs found in SPDR3 promotor abolishes PDR transcription activation in ρ^0 cells [94, 98, 99]. This autoregulatory circuit is not verified for ScPDR1 since PDRE motifs are not found in its promotor [100, 101]. Despite this ScPDR3 induction, ScPdr3 protein levels are still underrepresented when compared to those of ScPdr1, and therefore, other mechanisms must be involved in the increased binding of ScPdr3 to PDRE of target genes [102]. Also highlighting this specialization of ScPdr1 and ScPdr3, in response to the same stress these transcription factors can exert a different effect in the transcription of a specific group of genes [77]. For instance, in response of *S. cerevisiae* cells to progesterone, both transcription factors have identical and overlapping activity on the expression of several PDR transporter genes (including *ScPDR5*, *ScPDR15*, *ScSNQ2*, and *ScTPO1*), while ScPdr1 has a dominant effect in the transcription of lipid metabolism gene transcription [77]. ScPdr3 further diverges from ScPdr1 by having a broader spectrum of induced genes, including *ScRTG3* gene from the retrograde system and genes induced in response to DNA damage or to salt-induced stress [88, 96]. These differences in transcription specificity between ScPdr1 and ScPdr3 were correlated to specific variations in the PDRE sequence and the number of PDRE motifs present in the promoter region of target genes, suggesting differences in the DNA binding affinity of the two regulators [77, 97]. Another striking example of the difference in the impact of both transcription factors in the expression of the same genes is the observation that while ScPdr3 is the main activator of the PDR genes in response to retrograde mitochondrial dysfunction, the same signaling results in ScPdr1 being a negative regulator of the expression of *ScPDR5*, *ScSNQ2* and *ScYOR1* [94, 95, 102, 103]. In opposition, in normal growth conditions, ScPdr3 inhibits the expression of these same genes and further inhibits expression of *ScPDR5* and *ScPDR15* in response to mycotoxin, while under this same stress ScPdr1 positively regulates them [90, 91].

In *C. glabrata*, the single copy of the PDR transcription factor CgPdr1 regulates transcription of target genes after activating stimuli (that can be exposure to a xenobiotic or response to a mitochondrial defect, as detailed below) thus congregating functions that are attributed to ScPdr1 or ScPdr3 [104, 105]. Another noticeable difference between the Pdr1-dependent genes in *S. cerevisiae* and in *C. glabrata* is the auto-regulation of CgPDR1 from two PDRE motifs found in the promotor gene in *C. glabrata*, while in *S. cerevisiae* this is only observed in the promoter region of ScPDR3 but not of ScPDR1 [71, 73, 94, 100]. Elimination of the two PDRE motifs from CgPDR1 promoter results in the significant reduction of CgPdr1 protein levels and, consequently, reduced azole tolerance, thus highlighting the crucial role of the CgPdr1 autoregulatory circuit for the normal function of the PDR network in this pathogenic species [73]. Notably, upon fluconazole stimulus, CgPdr1 protein is still over-produced (compared to the levels attained in the

absence of the antifungal) even when both PDRE motifs are deleted, demonstrating that CgPDR1 transcription is under the regulation of other transcription factors as well [73].

Using ChIP-seq Paul, S. *et al.* 2014 [71] defined 25 genes as those more likely to be direct targets of CgPdr1, based on the enrichment of CgPdr1 binding observed in the corresponding promoter of target genes in rho⁰ cells, compared to the same binding observed in rho⁺ cells (Figure II. 2). These results showed a substantial overlap of target genes directly regulated by Pdr1 in *S. cerevisiae* and in *C. glabrata* [71, 72, 95], including those encoding MDR transporters (e.g. ScPDR5/CgCDR1, ScPDR15/CgPDH1, and YOR2) or involved in plasma membrane homeostasis (ScIPT1/CAGL0G05313g, RSB1 and YMR102C/CAGL0K03377g) [71](see Figure II. 2). Another relevant direct target of Pdr1 in both *S. cerevisiae* and *C. glabrata* is the Rpn4 transcription factor, a major regulator of proteasome and ubiquitination machinery genes [106-108]. In *C. glabrata* Rpn4 is also a positive contributor to maintaining intracellular ergosterol levels and membrane permeability through the up-regulation of genes encoding enzymes of the ergosterol biosynthetic pathway and heme biosynthesis [78, 108]. Despite the convergence in functions regulated by the Pdr network in both species, specific target genes were also identified as detailed in Figure II. 2. In specific, CgPdr1 regulates the MDR transporters genes CgQDR2, with a putative physiological role in the export of amino acids and copper in *S. cerevisiae* [109, 110], while a similar connection was not observed for ScPdr1-ScQdr2. CgPdr1 was also found to specifically regulate CgYBT1, a putative vacuole ABC transporter presumed to promote vacuolar sequestration of azole [111]; CgRTA1, a predicted member of the fungal lipid translocating exporters with a suggested role in the export of aberrant sterol intermediates [112]; and CAGL0J05852g, predicted to encode an oxidoreductase that regulates the morphology of lipid droplets [113]. CgPdr1 was also found to exclusively interact with the promoter of CgATF2, a putative alcohol acetyltransferase suggested to be involved in sterol detoxification [114], and of CgNCE103 encoding a carbonic anhydrase activator necessary for growth in aerobic conditions [115, 116]. Another specific direct target in *C. glabrata* is CgPUP1, which encodes a mitochondrial protein with an unknown function, but whose deletion reduces the virulence of this species against mice [117].

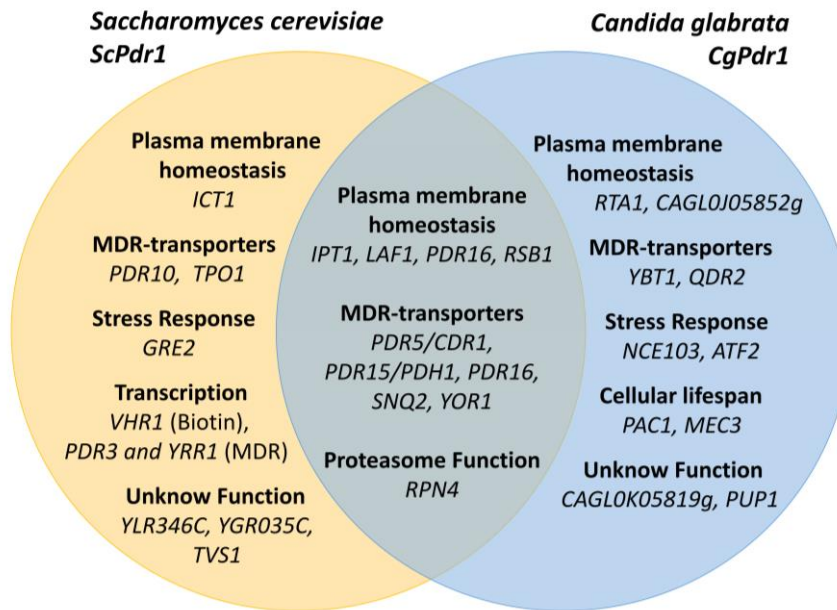


Figure II. 2. Comparison of the genes directly regulated by *Pdr1* in *Saccharomyces cerevisiae* and *Candida glabrata*. Networks detailed in this figure [70, 71, 84] were defined by the *Pdr1* interaction with the promoter region of targets by DNA-footprinting, ChIP-chip and ChIP-seq technologies plus monitorization of gene transcription. Only genes with PDRE motif in the promoter are herein detailed.

2.3. The complex and intertwined interactions established between the Pleiotropic Drug Resistance regulatory network and other stress-responsive regulators

The PDR regulatory network becomes more complex as the central regulator *Pdr1* directly regulates other genes encoding transcription factors, including, as mentioned, *CgRPN4* in *C. glabrata* or *ScRPN4*, *ScYRR1* and *ScVHR1* in *S. cerevisiae* [70, 71, 75]. In *C. glabrata*, disruption of *Rpn4* transcription factor-encoding gene results in increased susceptibility to azoles, consistent with its *Pdr*-dependent regulation being relevant to favor azole tolerance [108, 118]. Other transcription factors such as *CgUpc2A* or *CgStb5* were also found to directly affect *CgPDR1* transcription and *CgPdr1* function, respectively [60, 119]. In *S. cerevisiae*, close contacts between the *Pdr* network with other networks involved in response to oxidative stress-mediated by *Yap1* and in response to protein degradation mediated by *Rpn4*, have also been described [78, 120-124] (Figure II. 3).

Saccharomyces cerevisiae

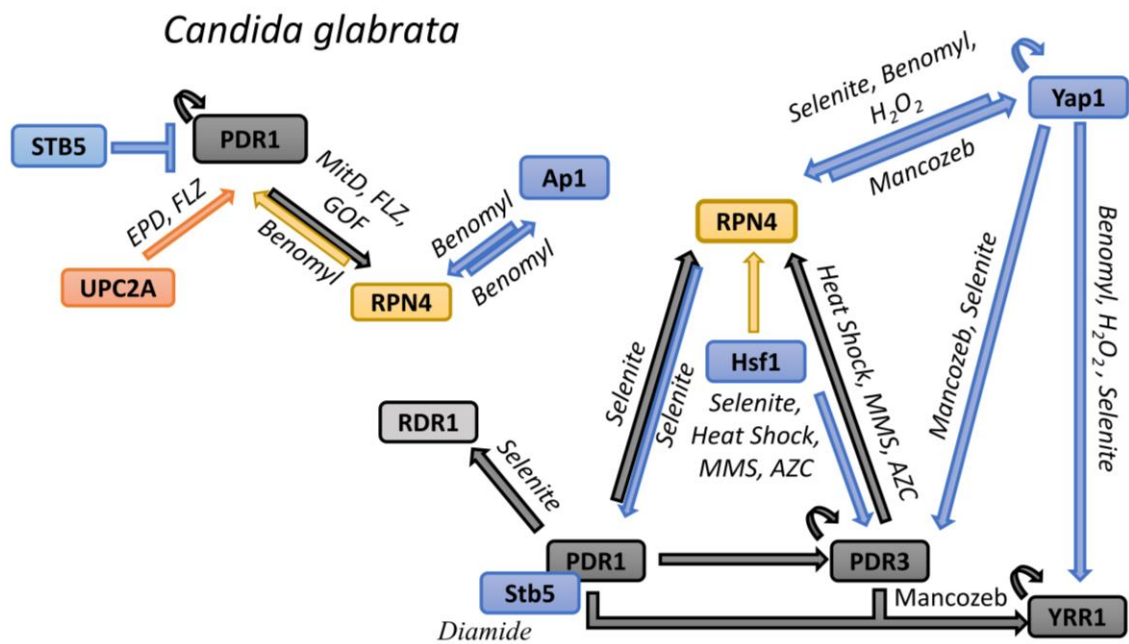


Figure II. 3. Schematic representation illustrating the interactions established between the pleiotropic drug resistance transcription factors with other regulatory networks in *Saccharomyces cerevisiae* and in *Candida glabrata*. A schematic view of the complexity of the regulatory associations established between PDR transcription factors (represented in grey) with other transcription factors involved in response to oxidative stress (represented in blue), in protein degradation (represented in yellow), in ergosterol biosynthesis (represented in red) in *S. cerevisiae* and in *C. glabrata* [60, 70, 71, 75, 78, 88, 101, 119-126]. The represented models distinguish the direct effect (backed by evidence of regulatory element presence in the promotor and/or direct binding to the promotor), accompanied by the demonstration that the transcription factor influences gene expression. Dimerization of ScStb5 with ScPdr1 is also represented as it influences PDR transcription. The stressor stimuli in which the transcription is influenced by the different transcription factors is also indicated (Ergosterol pathway defects (EPD); fluconazole (FLZ); gain-of-function mutation (GOF); methyl methanesulphonate (MMS); azetidine-2-carboxylic acid (ACZ), a proline analog that misincorporates into proteins and leads to proteotoxic stress; mitochondrial defects (MitD)).

In *S. cerevisiae*, in response to mancozeb and selenite the major oxidative transcription regulator ScYap1 regulates ScPDR3 expression [78, 124] by directly binding to the corresponding promoter region, even in control conditions [123]. ScYap1 can also regulate ScPDR1, albeit indirectly, via ScRPN4 (confirmed to be directly regulated by ScYap1 during H₂O₂, selenite and benomyl stress [78, 121]), while ScPdr1 also regulates ScRPN4 during selenite stress [78]. Concordantly, a complete ScYap1-dependent response to benomyl, acetaminophen and diazaborine, is reduced in the absence of a downstream functional ScPdr1 and/or ScPdr3 [127-129]. ScRpn4 was further reported to bind to Yap1 promoter in highthroughput chromatin immunoprecipitation assays [120] and positively influence ScYAP1 gene expression in response to mancozeb stress [124]. Notably, during selenite stress ScRpn4 negatively influences ScYap1 expression [78, 120]. Interestingly, the influence of ScPdr1 or ScYap1 on ScRPN4 transcription was found to depend on the other being absent in the promoter, increasing the complexity of the cross-regulation of these transcription factors [107]. Another direct target of ScYap1 during benomyl, H₂O₂ and selenite stress is the transcription factor ScYrr1 [78], which has been shown to influence expression of some of the Pdr-

dependent genes like *ScSNQ2* both under non-stressful conditions and also in response to 4-nitroquinoline n-oxide stress [130-132]). Notably, *ScYrr1* was found to negatively regulate other Pdr genes like *ScPDR5*, as it was observed to occur in response to vanillin stress [133]. This influence of *ScYrr1* in the expression of the above-mentioned genes was found to be direct since it was demonstrated the direct interaction of the regulator with the corresponding promoter regions [134]. Altogether this data suggests that *ScYrr1* may play a role in fine-tuning the PDR response [88](Figure II. 3). *ScYrr1* was further identified to be a direct target of *ScPdr1* and *ScPdr3*, where higher expression was found to be regulated during mancozeb stress [88, 101](Figure II. 3). *ScHsf1* heat-shock responsive transcription factor provides another network crossing paths with *S. cerevisiae* PDR transcriptional network being involved in the direct regulation of *ScPDR3* and *ScRPN4* in response to heat shock, methyl methanesulfonate or to the proline analog azetidine-2-carboxylic acid [121] and possibly indirectly by *ScPdr1* during selenite stress as well [78] (Figure II. 3). In response to these stressors, *ScPdr3* exerted a minor role in the direct regulation of *ScRpn4* upregulation, as well [121]. The *ScStb5* transcriptional regulator is also activated in response to oxidative stress caused by diamide and H_2O_2 and regulates genes involved the pentose phosphate pathway (presumably to increase the supply of NADPH) and also genes of the PDR network like *ScSNQ2*, *ScPDR5* or *ScIPT1* [132, 135, 136]. *ScStb5* is found predominantly in the cell as a heterodimer with *ScPdr1* (but not with *ScPdr3*) able to interact with the PDRE motif (Figure II. 3)[125]. Expression of *ScSTB5* is dependent of *ScYap1* after long selenite exposure, during H_2O_2 or in response to arsenite stress; thus showing the dense nature of the transcriptional regulatory networks involving the PDR system [78, 137, 138]. Interaction of *ScYap1* to *ScSTB5* promoter was also reported in a high throughput assay [139]. In *S. cerevisiae* the PDR-dependent transcriptional response was also found to rely on transcriptional repressors and not only transcriptional activators, being of notice the involvement of *ScRdr1*, a described repressor of *ScPDR5*, *ScPDR15*, *ScPDR16* or *ScRSB1* genes [126]. The negative regulation of these genes is dependent on the presence of PDRE in the promoters although, the interaction of *ScRdr1* with this DNA motif was not further confirmed [126]. Up-regulation of *ScRdr1* expression was found to be dependent of *ScPdr1* in response to selenite stress and further interaction in the promoter in high throughput assay was reported, this being suggestive of a negative transcriptional regulation loop between both transcription factors [78, 120, 126].

In *C. glabrata*, no information is available on the potential role of the *HSF1* orthologue in the regulation of *CgPDR1* transcription. Also, an extensive remodeling in the chromosomal region encoding *Rdr1* has occurred along with the evolution between *S. cerevisiae* and *C. glabrata* that has resulted in the loss of this orthologue [140]. A *CgPdr1*-*CgAp1*-*CgRpn4* orthologue co-transcriptional network appears to have been conserved [78]. In specific, benomyl stress was found to induce the expression of the three transcription factors and since the DNA motifs recognized by those are conserved in the promoter regions of the corresponding encoding genes, it is likely that the transcriptional loops described in *S. cerevisiae* could still be active in this pathogenic yeast [78]. A PDRE motif is also found conserved in the promoter of *CgYRR1* and this transcription factor was also found to play a role in conferring protection against azoles in *C. glabrata* [118, 141]. In *C. glabrata*, *CgRpn4* protein is relocated to the nucleus upon cell exposure to azoles suggesting an activation of the regulator in these conditions [108]. Interestingly, during growth in azole-unsupplemented medium, the expression of *CgRpn4* was found to negatively affect

the expression of several direct targets of CgPdr1 (including Cg*CDR1*, Cg*QDR2*, Cg*EPA1*, or Cg*PUP1*) [108] which indicates that even under these non-activating conditions there might be some cross-talk between the CgPdr1- and CgRpn4- regulatory pathways. Contrary to *S. cerevisiae*, the transcription factor CgStb5 was found to negatively regulate Pdr-regulated target genes like Cg*CDR1*, Cg*PDH1* or Cg*YORI* and this was consistent with the Δ Cg*stb5* mutant exhibiting decreased susceptibility to azoles, while Cg*STB5* overexpression results in increased resilience [60]. The ability of CgStb5 to form heterodimers with CgPdr1 and to interact with PDRE, similar to what was reported in *S. cerevisiae*, was not further demonstrated [60]. A specific feature observed in *C. glabrata* is that CgUpc2A directly regulates Cg*PDR1* gene expression in response to inhibition of the ergosterol pathway (even if this takes place at different steps) [119]. In specific, it was observed that the deletion of genes involved in the ergosterol biosynthetic pathway results in CgUpc2A re-localization from the cytoplasm to the nucleus indicating that this regulator responds to perturbations in sterol composition of the membrane [119]. Indeed, ScUpc2 was found to directly bind to ergosterol and dehydroergosterol also relocating to the nucleus upon changes that lead to alterations in plasma membrane sterol content [119, 142]. In response to azoles, ergosterol biosynthesis genes are positively regulated by CgUpc2A expectedly to counteract the deleterious effects exerted by these drugs on the membrane sterol content [143, 144]. Recently, CgUpc2A was reported to directly regulate a large number of genes, to which the *ERG* genes account only for a small part [61] with many overlapping with those regulated by CgPdr1, including Cg*PDR1* itself [61, 71, 119]. In agreement with CgUpc2A having an independent role in the activation of PDR genes, the deletion of CgUpc2A affects azole susceptibility even in the presence of a hyperactive form of CgPdr1 [144]. Until today, there is no evidence linking the activity of ScUpc2 to ScPdr1 or ScPdr3 activity [61]. Recently two putative negative transcriptional regulators of Cg*PDR1* were reported, specifically CgGln3 and CgZap1 [145, 146]. CgGln3 was reported to repress Cg*PDR1*, Cg*CDR1*, and Cg*PDH1* transcription during *C. glabrata* growth in ammonium sulphate, the preferred nitrogen source of this species [145]. However, since Gln3 is generally described to exert a positive role in transcription, this effect should not result from direct regulation, and further studies are required to elucidate the CgGln3 role in PDR regulation [146]. CgZap1, responds to zinc nutrient limitation and was found to inhibit the expression of Cg*PDR1*, but also of the MDR-transporter Cg*CDR1* and the ergosterol metabolism genes Cg*ERG3* and Cg*ERG5* [146]. The direct/indirect nature of the regulation of Cg*PDR1* was not yet further inferred. However, deletion of Cg*ZAP1* renders *C. glabrata* cells more susceptible to azole antifungals by affecting the membrane properties including the depletion of ergosterol and decrease phosphatidylinositides levels [146].

2.4 A molecular view on the transcription of Pdr-target genes

Transcription activation triggered by nuclear receptors such as Pdr1 appears to happen in a multistep cascade of events (as reviewed in [147, 148]). In the absence of the activating ligand, the nuclear receptor interacts with negative regulators (such as chromatin regulators that repress transcription) thus maintaining the expression of target genes at low levels. Upon binding to the ligand, the nuclear receptors release the co-repressors allowing the recruitment of co-activators that facilitate chromatin remodeling and subsequent contacts with the transcriptional machinery. ScPdr1 constitutively recruits transcriptional

machinery to the *ScPDR5* promoter to assure a basal expression level. In specific, ScPdr1 was found to recruit the TBP general transcription factor (TATA-binding protein); the mediator complex, that will subsequently interact with the polymerase [149, 150]; and components of the SAGA (Spt-Ada-Gcn5 acetyltransferase), FACT (facilitates chromatin transcription), or SWI/SNF (SWItch/Sucrose Non-Fermentable) complexes, all involved in chromatin remodeling [149, 150] (Table II. 3). Although these interactions were observed to occur during growth in drug-free medium, they are further enhanced by the xenobiotics-induced activation of ScPdr1 [105, 150, 151]. As a consequence, the transcription of ScPdr1-target genes is up-regulated in response to the activating xenobiotic, this increase in expression happening at the same extent as the enhanced recruitment of co-activators [105, 150, 151]. It is, however, essential to note that most of the studies undertaken thus far addressing this issue have focused only a few genes, with emphasis on *ScPDR5*, leaving unclear whether these mechanisms would also be observed for all genes of the Pdr1-regulon. After being recruited to the promoter, the mediator complex prompts the recruitment of Pol II to target promoters, stimulating the formation of the pre-initiation complex and the subsequent transition to the transcription elongation step, while promoting chromatin remodeling as a mean of facilitating access to DNA (reviewed in [152]). In response to azoles, the component of the tail module ScGal11 in *S. cerevisiae* (as well as its orthologue CgGal11A in *C. glabrata*) is responsible for the interaction of Pdr1 with the mediator complex [105, 150]. Consequently, deletion of *CgGAL11A* severely reduces the activation of CgPdr1-dependent transcription, while also contributing for significantly enhanced susceptibility of *C. glabrata* cells to azoles [105]. Besides CgGal11A, the disruption of the mediator complex components *CgMED2*, *CgMED3* and *CgMED14* from the tail module, *CgMED5* from the middle module and *CgMED12* of the CDK8 complex, were also found to be required for *C. glabrata* maximum tolerance to azoles [58, 59, 153](Table II. 3). Despite this tight interaction between CgPdr1 and the CgGal11A mediator complex subunit, there are evidences suggesting that other mechanisms are in place to assure expression of CgPdr1-target genes including the observation that some expression of CgPdr1 target genes is observed upon deletion of *CgGAL11A* [105] or the fact that CgGal11A (and also ScGal11) is dispensable for the induction of PDR-dependent genes in response to retrograde signaling in rho⁰ mutants [71, 99].

As said above, several complexes mediating chromatin remodeling through the modification of histones have been found to be required for the full induction of PDR-dependent genes. These include several components of the SAGA complex that were found to be recruited to *ScPDR5* promoter and were found to be co-immunoprecipitated with ScPdr1 [149, 154, 155] (Table II. 3), although the ScGcn5 nucleosome acetyltransferase was found to be dispensable for transcription, even if recruited to the promoter [149, 156]. Consistently, *ScPDR5* xenobiotics-induced transcription is not correlated with a change in histone acetylation levels in the corresponding promoter region [149]. In *C. glabrata*, cells devoid of genes belonging to the SAGA complex were found to be susceptible to azoles, however, this effect could not be attributed to different expression levels of CgPdr1 target genes [58, 157, 158](Table II. 3). Strikingly, disruption of *CgGCN5* was synthetically lethal with CgPdr1 hyperactivation during fluconazole stress [159]. Overall, these results show divergences in the way the SAGA complex connects with Pdr1 in *C. glabrata* and in *S. cerevisiae*. Another histone acetylation complex that was found to play an important role in the regulation of *ScPDR5* expression in *S. cerevisiae* is ScRdp3L (Table II. 3). This

complex was found to be required for basal expression of *ScPDR5* and also for the drug-induced up-regulation of this gene in response to xenobiotics or to retroactive signaling [160, 161]. Noteworthy, the overexpression of *ScPDR3* or the expression of an *ScPDR3* GOF variant did not suppress hypersensitivity of the *S. cerevisiae* mutant strain $\Delta rpd3$ [161]. ScUme6, the DNA binding component of the Rpd3L complex, was also found to be required for *ScPDR3* and *ScPDR5* expression during retroactive signalling in ρ^0 cells, possibly by direct binding to these genes promoters [162] (Table II. 3). However, in ρ^+ cells, ScUme6 suppresses the basal transcription levels of *ScPDR1*, *ScPDR3*, *ScPDR5*, consequently affecting fluconazole resistance, while ScRdp3 appears to not interfere with *ScPDR5* expression in this same cells [163]. Regardless of its importance in *S. cerevisiae*, in *C. glabrata* the Rdp3 complex does not appear to influence azole tolerance [40, 57] (Table II. 3).

Besides acetylation, methylation of histones was also associated with the CgPdr1-dependent transcriptional response of *C. glabrata* to azoles. In specific, in response to azoles, it has been observed that there is a decrease in histone H3 and H4 methylation and consequent stabilization of higher histone H3 and H4 protein levels in the cell [164]. As a result a concomitant increase in the expression of PDR genes is observed, including *CgPDR1*, *CgCDR1*, *CgPDH1* and *CgSNQ2*, as a possible consequence of an open chromatin state at the CgPdr1 promotor targets [164]. In line with these results, several proteins involved in histone methylation were found to be positive regulators of the expression of known CgPdr1-targets, while demethyltransferases exert a negative effect [164] (Table II. 3). Of note, histone methylation further promotes histone acetylation [164-167] and therefore, a combination of histone modifications is likely to determine the final level of expression of PDR-target genes in azole-challenged *C. glabrata* cells [164]. In *S. cerevisiae* this mechanism may not be conserved, since the deletion of the same identified effectors appear to have a contrary impact in tolerance to xenobiotics that Pdr-transcription factors respond to [168-170] (Table II. 3). Inhibition of the chromatin silencing complex CgHst1-CgRfm1-CgSum1 induced by niacin limitation was found to prompt the upregulation of *CgPDR1* and target genes *CgCDR1* and *CgEPA1* [171], this mechanism being relevant for colonization of the urinary tract by *C. glabrata* [172]. In specific, in the niacin-limited environment of the urinary tract, the NAD⁺-dependent CgHst1 sirtuin deacetylase is inactive, alleviating transcription repression through allowing histone acetylation and consequently the transcription of genes required for the uptake of niacin, oxidative stress, adhesion, and those dependent of CgPdr1 [171, 173]. This regulatory association between sirtuins and Pdr1 appears unique to *C. glabrata*, since Rfm1 and Sum1 proteins are absent in the CTG clade of *C. albicans* and in *S. cerevisiae* the ScHst1-ScRfm1-ScSum1 complex only regulates sporulation [174] and results in improved tolerance to azoles when deleted [170] (Table II. 3). A recent study demonstrated that this specialization in *C. glabrata* might have derived from the evolution of Sum1, the sequence-specific DNA binding component of the complex, from the remaining *Saccharomycetaceae* family [175].

The FACT (complex, which removes nucleosomes to allow the transcription elongation by Pol II but also facilitates nucleosome re-assembly after the Pol II transcription (reviewed in [176]), also plays an essential role in *ScPDR5* transcription [150] (Table II. 3). In specific, recruitment of FACT (components ScSpt16-ScPob3) to the *ScPDR5* promoter coincides with the loss of the nucleosome during transcriptional activation of this gene induced by azoles and afterward repopulation of the chromatin with nucleosomes

[150]. Up to now the influence of FACT complex in tolerance to azoles or in determining the transcription of PDR-dependent genes has not been studied in *C. glabrata*.

Table II. 3. (Part 1) *Transcription initiation co-activators described to influence the expression of PDR-dependent genes in Saccharomyces cerevisiae and in Candida glabrata.* The influence of the genes encoding the different transcriptional co-activators or subunit of chromatin modifying complexes in the activity of Pdr1 regulator and in the transcription of target genes or in tolerance to PDR xenobiotics response in *S. cerevisiae* and *C. glabrata* is summarized in this table. The negative effect of transcriptional co-activators gene deletion in xenobiotic resistance is highlighted in red, and a positive effect is highlighted in green. Proteins/genes whose deletion were found to result in opposite effects in different studies concerning tolerance to drugs responded by Pdr1 are written in red; n.i. indicates that no information was found; FLZ - fluconazole; KTZ - ketoconazole; CTZ - clotrimazole; VZ - voriconazole; ECZ - econazole; PCZ - posaconazole; MCZ - miconazole; CHX - cycloheximide; OM - oligomycin; AVT - Atorvastatin.

Complex Component	Effects of gene disruption in the expression of CgPdr1-regulated genes	Effect of gene disruption in tolerance to drugs	REFs	Effects of gene disruption in the expression of ScPdr1/3-regulated genes	Effect of disruption in tolerance to drugs	REFs
<i>Mediator complex</i>						
<i>Med2</i>	Reduces the capacity of CgPdr1 ^{L280F} to induce Cg <i>CDR1</i> and Cg <i>PDR1</i>	Increased susceptibility to FLZ, KTZ, CTZ and CHX, including in a strain producing CgPdr1 ^{L280F} GOF variant	[59, 153]	n.i	n.i	-
<i>Med3</i>	n.i	Increased susceptibility to FLZ, <u>but not</u> in a strain producing CgPdr1 ^{L280F} GOF variant	[59, 153]	n.i	Increased susceptibility to CTZ and CHX	[177, 178]
<i>Med5</i>	n.i	Increased susceptibility to FLZ, including in a strain producing CgPdr1 ^{L280F} GOF variant	[58, 153]	n.i	Increased susceptibility to FLZ	[170, 179, 180]
<i>Med12</i>	n.i	Increased susceptibility to FLZ, including in a strain producing CgPdr1 ^{L280F} GOF variant	[58, 153]	Reduces the basal expression of Sc <i>PDR5</i> and the increased expression of Sc <i>PDR5</i> and Sc <i>PDR3</i> in rho ⁰ cells (correlated to the increased recruitment to gene promoter in rho ⁰ cells and coimmunoprecipitation with Sc <i>PDR3</i>)	Increased susceptibility to FLZ, CHX, OM and AVT	[99, 156, 170]
<i>Med14</i>	n.i	Increased susceptibility to FLZ, <u>but not</u> in a strain producing CgPdr1 ^{L280F} GOF variant	[58, 153]	n.i	n.i	-
<i>Gal11 (A)</i>	Reduces the expression of Cg <i>CDR1</i> , Cg <i>PDR1</i> and Cg <i>PDH1</i> during KTZ and/or FLZ stimulus (<u>but not</u> in a rho ⁰ strain).	Increased susceptibility to FLZ, KTZ and CHX.	[60, 73, 104, 105, 181]	Reduces the expression of Sc <i>PDR5</i> and Sc <i>SNQ2</i> during FLZ, KTZ and CHX exposure (correlated to the recruitment to gene promoter, increased in GOF variants and KTZ stimulus) Deletion does not affect PDR transcription activation in rho ⁰ cells	Increased susceptibility to FLZ, KTZ and CHX	[99, 105, 149, 150, 170, 177, 179, 182]
	Reduces the expression of Cg <i>CDR1</i> , Cg <i>PDH1</i> , Cg <i>SNQ2</i> and Cg <i>YBT1</i> in strains producing CgPdr1 ^{R376W} and CgPdr1 ^{Y584C} , CgPdr1 ^{P822L} and CgPdr1 ^{D1082G} (less pronounced in the two later variants)	Increase susceptibility to fluconazole in a strain producing CgPdr1 ^{R376W} , CgPdr1 ^{Y584C} , CgPdr1 ^{P822L} and CgPdr1 ^{D1082G} (less pronounced in the two later variants)				
<i>Med17</i>	n.i.	No effect in tolerance to FLZ	[40]	Reduces the basal expression of Sc <i>PDR5</i> (correlated to the recruitment to gene promoter, increased in GOF variants)	Increased susceptibility to CTZ	[149, 177]

Table II. 3 (Part 2)

Complex Component	Effects of gene disruption in the expression of CgPdr1-regulated genes	Effect of gene disruption in tolerance to drugs	REFs	Effects of gene disruption in the expression of ScPdr1/3-regulated genes	Effect of disruption in tolerance to drugs	REFs
<i>Histone methyltransferases</i>						
<i>Fpr3</i>	Increases <i>CgPDR1</i> , <i>CgPDR5</i> , <i>CgPDH1</i> and <i>CgSNQ2</i> basal expression	Increased resistance to FLZ	[164]	n.i.	Increased susceptibility to CHX	[169]
<i>Fpr4</i>	Increases <i>CgPDR1</i> , <i>CgPDR5</i> , <i>CgPDH1</i> and <i>CgSNQ2</i> basal expression	Increased resistance to FLZ	[164]	n.i.	n.i.	n.i.
<i>Set2</i>	Increases <i>CgPDR1</i> , <i>CgPDR5</i> and <i>CgPDH1</i> basal expression	Increased resistance to FLZ	[164]	n.i.	Increased susceptibility to CHX Increased resistance to CHX	[170] [183]
<i>Rph1</i>	Reduces <i>CgPDR1</i> , <i>CgPDR5</i> and <i>CgPDH1</i> basal expression	Increased susceptibility to FLZ	[164]	n.i.	Increased susceptibility to FLZ	[168]
<i>SAGA (Histone acetylation)</i>						
<i>Ada2</i>	Deletion does not affect CgPdr1 target genes expression, with the exception of <i>CgEPA1</i> that is more transcribed in a mutant strain	Increased susceptibility to FLZ, VZ, PCZ	[157, 158]	Reduces the basal expression of <i>ScPDR5</i> (correlated to the recruitment to gene promotor, increased in GOF variants)	n.i	[149, 155]
<i>Ada3</i>	n.i	No effect in tolerance to FLZ	[40, 57]	Reduces the basal expression of <i>ScPDR5</i> (correlated to the recruitment to gene promotor and coimmunoprecipitation with ScPdr1)	Increased susceptibility to MCZ and CHX	[155, 178, 184, 185]
<i>Spt3</i>	n.i	No effect in tolerance to FLZ	[57]	Reduces the basal expression of <i>ScPDR5</i> (correlated to the recruitment to gene promotor, increased in GOF variants)	Increased susceptibility to FLZ and CHX	[149, 178, 179]
<i>Spt7</i>	n.i	No effect in tolerance to FLZ	[40]	Reduces the basal expression of <i>ScPDR5</i>	Increased susceptibility to FLZ, CTZ, KTZ and OM	[149, 156, 182]
<i>Spt8</i>				Reduces the basal expression of <i>ScPDR5</i>	Increased susceptibility to FLZ	[149, 156, 170]
<i>Spt20</i>	n.i	Increased susceptibility to FLZ	[58]	Reduces the basal expression of <i>ScPDR5</i> (correlated to the recruitment to gene promotor, increased in GOF variants)	Increased susceptibility to FLZ, MCZ and CHX	[149, 178, 179, 184]
<i>Gcn5</i>	n.i	No effect in tolerance to FLZ	[57, 159]	Deletion does not affect <i>ScPDR5</i> basal expression (even if recruited to the promotor)	Increased susceptibility to MCZ and CHX	[149, 156, 178, 185, 186]

Table II. 3 (Part 3)

Complex Component	Effects of gene disruption in the expression of CgPdr1-regulated genes	Effect of gene disruption in tolerance to drugs	REFs	Effects of gene disruption in the expression of ScPdr1/3-regulated genes	Effect of disruption in PDR resistance ^a	REFs
<i>Rpd3L (Histone deacetylase)</i>						
<i>Rdp3</i>	n.i	No effect in tolerance to FLZ	[40, 57]	Reduces the expression of <i>ScPDR5</i> during CHX stimulus, in rho ⁰ cells and during basal expression in rho ⁺	Increased susceptibility to FLZ and CHX	[160, 161, 187]
<i>Sin3</i>	n.i	Increased resistance to FLZ	[58]	Reduces the expression of <i>ScPDR5</i> during CHX stimulus and basal expression	Increased susceptibility to MCZ and CHX	[161, 179, 184, 187]
<i>Ume6</i>	n.i	n.i	-	Reduces the expression of <i>ScPDR3</i> and <i>ScPDR5</i> in rho ⁰ cells being enhanced by exposure to CHX (correlated to the recruitment to gene promotor)	Increased susceptibility to FLZ and CHX in rho ⁰ cells	[160]
				Represses basal expression of <i>ScPDR1</i> , <i>ScPDR3</i> , <i>ScPDR5</i> in rho ⁺	Increased resistance to FLZ and CHX in rho ⁺ cells	[163]
<i>Hst1-Rfm1-Sum1 (Histone deacetylase)</i>						
<i>Hst1</i>	Negatively regulates the Cg <i>CDR1</i> (correlated to the recruitment to gene promotor) and Cg <i>PDR1</i> basal expression	Increased resistance to FLZ	[171]	n.i.	Increased susceptibility to FLZ	[170]
<i>Sum1</i>	Negatively regulates the Cg <i>CDR1</i> (correlated to the recruitment to gene promotor) and Cg <i>PDR1</i> basal expression	Increased resistance to FLZ	[171]	n.i.	Increased susceptibility to FLZ and CHX	[179]
<i>FACT (nucleosome assembly)</i>						
<i>Spt16</i>	n.i	n.i	-	Recruitment to <i>ScPDR5</i> promotor is increased during xenobiotic stimulus, affects nucleosome depletion and re-deposition across <i>ScPDR5</i> open reading frame	Increased susceptibility to KTZ	[149, 150]
<i>Pob3</i>	n.i	n.i	-	Recruitment to <i>ScPDR5</i> promotor	Increased susceptibility to KTZ	[149, 150]

2.5. Mechanistic insights underlying regulation and regulators of the activity of PDR transcription factors

2.5.1 Ligand Binding

The PDR transcription factors are nuclear receptors whose activity is modulated by direct binding of xenobiotics. The work of Thakur, J.K. *et al.* 2008 [105] pioneered this knowledge by demonstrating that ScPdr1, ScPdr3, or CgPdr1 immunopurified (using sepharose beads) could directly bound to radiolabeled ketoconazole. Using cold competition assays this work further demonstrated that other xenobiotics like the antibiotic rifampicin or cycloheximide compete with ketoconazole for binding to ScPdr1 and ScPdr3 proteins, while the same was not detected for ethanol or for the glucocorticoid dexamethasone. A second study, undertaken by Vanacloig-Pedros, E. *et al.* 2019 [91], used a binary vector system in which the Gal4 DNA binding domain (DBD) was fused with the various *S. cerevisiae* pleiotropic transcription factors, including ScPdr1, ScPdr3, ScYrr1, ScStb5, and ScPdr8. The activity of these hybrid proteins was measured using luciferase as a reporter gene put under the control of *GALI_{UAS}* sequences. This system allowed the evaluation of the transcription factors' response to xenobiotics in a quantitative and time-elapsing manner [91]. The results demonstrated that ScPdr1 has the lowest specificity of all the transcription factors tested since it was able to trigger the higher levels of activation of the reporter gene in response to distinct xenobiotics, including the mycotoxins citrinin and ochratoxin, and the hydrophobic membrane oxidant menadione [91]. This decreased specificity in ligand binding is suggested to allow Pdr transcription factors to be economic effectors for the survey of the accumulation of excess levels of diverse toxicants [147]. Differently, ScPdr3 was found to play a minor contribution in inducing expression of the reporter gene, in agreement with its reported minor role in prompting activation of target genes in response to xenobiotics [91]. After xenobiotic activation, ScPdr1p protein was found to undergo rapid degradation, this being dependent on the xenobiotic itself, while ScPdr3 protein levels remain constant [91]. Since most of the after-mentioned compounds are not naturally occurring molecules found by *C. glabrata* in their life as a commensal organism, other unidentified molecules found in the host environment are likely to interact with CgPdr1 thereby promoting its activation. Indeed, progesterone is a metabolite that has been described to result in a long-term activation of ScPdr1 in *S. cerevisiae* [77]. Recently, hormone exposure was reported to reduce azole susceptibility in *C. glabrata* as well, but further studies are required to correlate this phenotype with the activity of CgPdr1 [188]. Another recent study identified the glycolytic side-product methylglyoxal as capable of triggering activation of CIMrr1, the transcription regulator of azole resistance genes in *C. lusitaniae* [189]. More recently, the same phenotype was demonstrated for *C. auris* Mrr1 orthologue [190]. Factors leading to an internal accumulation of methylglyoxal in humans coincide with those increasing risk for the development of candidiasis including diabetes or uremia and is further generated during inflammation by neutrophils [189, 191, 192]. Thus, persistent exposure of *Candida* cells to this molecule during colonization is likely to serve as an inducer factor for the appearance of gain-of-function mutants and, consequently, in the emergence of azole-resistant strains [190]. Further studies are required to understand if methylglyoxal is a general activator of the MDR transcription in other commensal and/or pathogenic yeasts, however, it is interesting to note that ScGRE2, a direct target of ScPdr1, has an NADPH-dependent methylglyoxal reductase activity [85, 192, 193]. The demonstration that mitochondrial

defects resulting in the petite mutant phenotype trigger activation of the PDR network, either in *S. cerevisiae* and in *C. glabrata* [194-196], is also consistent with this idea that “internal stimuli” are relevant inducers of Pdr regulators. The defects resulting in the petite mutant phenotype include deletions in the mtDNA, defects in the activity of the mitochondrial F₀ATPase, disruption of the mitochondrial protein import, and/or the destabilization of the mitochondrial membrane [71, 92-94, 197]. The mechanisms underlying the activation of the Pdr network in response to mitochondrial defects fall outside the model of ligand binding and are still elusive. Despite this link between mitochondrial dysfunction and increased Pdr1 activity, only a few clinical azole-resistant *C. glabrata* strains were found to display the petite phenotype [51, 195, 196, 198]. It has been suggested that the petite phenotype could be a transient strategy to face certain stressful conditions being reverted when the stress is removed [199, 200]. In favor of this hypothesis, *in vitro* petite variants selected upon exposure of *C. glabrata* cells to macrophages reverted back to the wild-type phenotype when the cells were cultivated in the absence of the macrophage cells, possibly since they were found to exhibit a reduced growth rate (and also reduced virulence against the murine model of systemic infection) [199, 200]. Interestingly, *C. glabrata* cells engulfed by neutrophils were also found to over-express genes of the CgPDR1 regulon [201]. Notably, clinical strains displaying the petite phenotype did not show any significant growth defects, which suggests a more complex layer of regulation rather than restoration of fitness alone [196].

Other environmental stimuli besides the accumulation of methylglyoxal and compromised mitochondrial function have also been found to result in up-regulation of genes of the CgPdr1 regulon in *C. glabrata*, including glucose depletion or niacin limitation [171, 201]. Differently, growth in the presence of ammonium (the preferred nitrogen source) resulted in prominent down-regulation of PDR target genes [145]. More recently, a clear link between the activity of CgPdr1 and ergosterol biosynthesis has been established clearly [119]. A similar connection is observed in *S. cerevisiae*, since exposure to different plasma membrane-destabilizing compounds were found to result in a rapid up-regulation of PDR-target genes [202]. Altogether this data demonstrates that although direct binding by ligands explains well the underlying activating mechanism of Pdr1 in response to azoles, it is likely that other environmental stressors, more physiologically relevant, can also play a role in modulating the activity of this regulator and, indirectly, contribute for azole resistance.

Several studies surveying azole resistance in *C. glabrata* clinical strains found that most of these encode CgPDR1 alleles harboring specific non-synonymous mutations not observed in the corresponding allele encoded by susceptible isolates [27, 50, 51, 53, 55, 194, 203-208]. These mutations were found to result in hyper-active gain-of-function (GOF) CgPdr1 mutants able to up-regulate target genes of the PDR network, even in the absence of a stimuli. This issue will be analyzed in detail in the following section but is worthwhile mentioning that up to now no significant cost in fitness has been reported associated with the encoding of CgPdr1 GOF mutants, something that has been observed in *C. albicans* and in *C. parapsilosis* strains encoding hyper-active Tac1, Upc2A and Mrr1 (MDR transcription factors in these species) mutants [209-211]. In fact, strains expressing CgPdr1 GOF variants exhibited increased fitness *in vitro* and also enhanced virulence towards murine models [51]. Notwithstanding that, the study of Vermitsky, J.P. *et al.* 2006 [56], showed that a strain encoding the GOF CgPdr1^{P927L} variant exhibited increased sensitivity to H₂O₂ and ethanol, a phenotype that was no longer observed upon deletion of the CgPDR1 GOF allele.

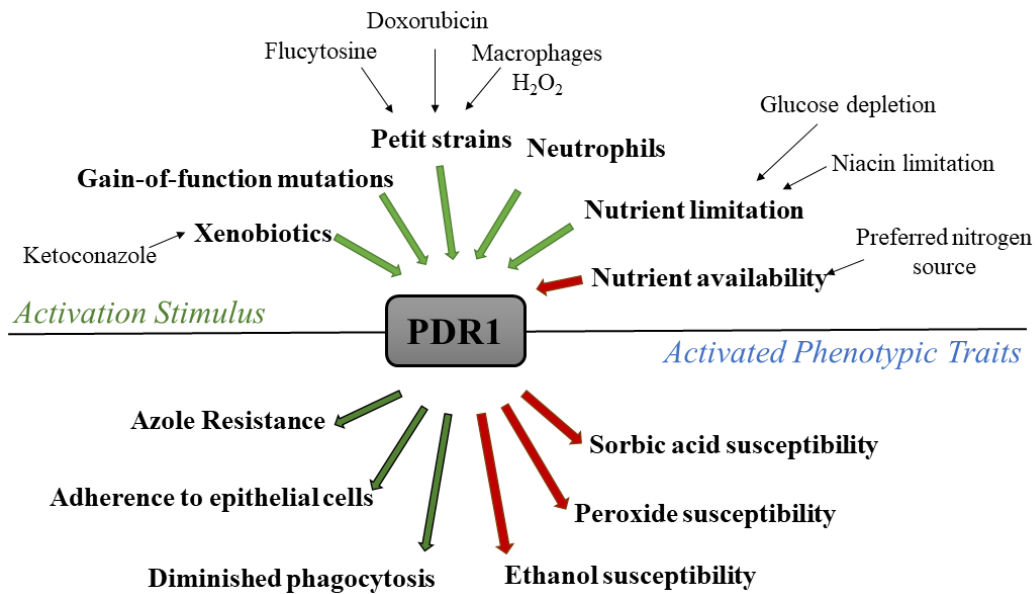


Figure II. 4. Physiologically relevant stimuli that result in activation of *Pdr1* and consequent phenotypic traits resulting from such activation

2.5.2 Chaperones and ubiquitin proteases that regulate the *Pdr* transcription factors activity

As mentioned before, during growth in non-stressful conditions, the PDR transcription factors have a low activity regulating only the basal expression of its target genes [70, 73, 74]. Increased activation is dependent on the alleviation of the interaction established with negative regulators while promoting the interaction with positive cofactors (Figure II. 5). As mentioned before, ScPdr3 and CgPdr1 both respond to mitochondrial defects and therefore their negative regulation is fundamental to ensure that the activity of the transcription factor is kept low and only specifically activated in response to retrograde signaling [89, 98]. The ScSsa1/ScSsa2 chaperones of the Hsp70 family directly interact with ScPdr3 in rho⁺ cells, exerting a negative regulation on its activity [89, 212]. In rho⁰ cells, the negative regulation of ScSsa1/2 is alleviated presumably as a consequence of excess misfolded proteins in these cells that will compete for the chaperone function and release ScPdr3 [89]. In line with this model, the ScFes1 exchange factor, which triggers ADP release and consequent inactivation of ScSsa1, is a positive regulator of ScPDR5 expression [89]. In *C. glabrata*, neither CgFES1 nor CgSSA1 disruption affects azole resistance suggesting that regulation of CgPdr1 activity via these chaperones may not be conserved [40]. Despite this, it was shown that the ubiquitin protease cofactor CgBre5 inhibits the transcription of CgPDR1, CgCDR1, CgPDH1 and CgSNQ2 genes in rho⁺ cells and this is dependent of the existence of direct interaction between CgBre5 and CgPdr1 [213]. In response to defects in mitochondrial function, the inhibitory activity of CgBre5 over CgPdr1 is released showing some degree of similarity to the regulatory mechanism involving ScSsa1/2-ScFes1 and ScPdr3 in *S. cerevisiae* [213, 214]. Notably, this regulatory role of Bre5 over the activity of Pdr1 was not observed in *S. cerevisiae*, suggesting that independent mechanisms were developed in both species to control the activity of Pdr transcription factors in the absence of retroactive signaling [213]. Chaperones that positively regulate of the activity of Pdr1/Pdr3 have also been identified including ScSsz1, from the Hsp70 chaperone protein family, and ScZuo1, a J-protein cochaperone [215, 216]. Like other Hsp70

chaperones, ScSsz1 and ScZuo1 are ribosome-associated co-chaperones usually found in the cytoplasm that under certain physiological conditions re-localize to the nucleus to interact with nuclear proteins [74]. For instance, the over-expression of ScSsz1 alone increases the proportion of protein not attached to the ribosome and that is thus free to bind other proteins, including ScPdr1 [215, 216]. ScSsz1 is unable to up-regulate PDR-dependent genes in an ScPdr1 mutant devoid of the central regulatory domain, suggesting that this region should be the regulatory target [74]. In its turn, ScZuo1 is released from the ribosome after conformational changes and in this “free-form” the C-terminal domain of the protein becomes free and is sufficient for ScPdr1 activation [217]. These two chaperones have been found to physically interact with ScPdr1 at the promoter of PDR-dependent genes contributing to maximize the activity of this regulator [216-218]. Consistently, gain-of-function mutants in both ScSsz1 and ScZuo1 were found to over-express genes of the PDR regulon [215, 216]. Although ScSsz1 and ScZuo proteins can independently regulate ScPdr1, they form a very stable heterodimer and thus both are believed to act in a complex in the regulation of ScPdr1 [216-218]. Overall, the evidences obtained until thus far point to the existence of a communication signal that transmits changes in the translation apparatus to the PDR regulon, however, the trigger of these molecular events has not yet been identified [217]. A notable aspect was the observation that the role of these chaperones was only observed for ScPdr1 but not for ScPdr3 [215]. The importance of CgSsz1 or CgZuo1 in the regulation of CgPdr1 in *C. glabrata* was not studied in detail although disruption of ScZuo1 orthologue did not enhance susceptibility to azoles [40]. In *C. glabrata*, the activity of CgJjj1, a predicted chaperone of the Hsp40 family that plays a role in stimulating ATP hydrolysis prompted by Hsp70 ATPase domains [219], was demonstrated to be a negative regulator of CgPdr1-dependent targets and consequently of fluconazole tolerance in *C. glabrata* [220]. A more detailed analysis revealed that the deletion of the CgJJJ1 gene increases the expression of CgPDR1 and consequently increases the corresponding protein levels and enhances transcription of about 25% of the described direct targets of CgPdr1 [71, 220]. Interestingly, the deletion of CgJJJ1 also resulted in the up-regulation of several adhesins regulated by CgPdr1, including CgEPA1, which is usually under sub-telomeric silencing [173, 220]. Contrarily, in *S. cerevisiae* deletion of the ScJJI gene decreases tolerance to fluconazole [221].

2.5.3 Activity of upstream signalling pathways

The rapid induction of the PDR network upon stress was also suggested to involve upstream signalling pathways [70, 156], although the exact players that could underlie these responses remain to be identified both in *S. cerevisiae* and in *C. glabrata*. The mitotic signalling protein kinase ScElm1 was found to influence modifications in the nucleosome structure upstream of the PDRE motif in the ScPDR5 promoter, this being an essential feature for ScPdr1 to promote the up-regulation of this gene [222]. In line with this observation, the expression of ScPDR5 peaks during mitosis [222]. Disruption of ScELM1 (as well as of other mitotic progression genes) reduces expression of ScPDR5 even in strains encoding a hyper-active ScPdr1 markedly showing a connection between cellular cycle progression and the PDR network [222]. Although it has been hypothesized that this influence of ScElm1 over ScPDR5 transcription can occur due to an effect of this kinase in phosphorylation of ScPdr1, this remains to be demonstrated [222]. In *C. glabrata* the orthologues of those *S. cerevisiae* mitotic progression genes shown to influence ScPDR5 transcription [222] were found not to play a relevant role in tolerance to azoles [40,

57]. In its turn, the disruption of *CgBEM2*, *CgSLT2*, and *CgBNR1* genes encoding kinases and Rho GTPase proteins that regulate the PKC pathway, that responds to cell wall damage, were found to affect the azole resilience [57, 59]. Intriguingly, *CgBem2* which negatively regulates the PKC signalling, was found to regulate PDR-dependent genes expression, including of *CgPDR1* and *CgCDR1*, albeit the underneath molecular mechanism remains to be disclosed [57, 59]. In *S. cerevisiae*, *ScBem2* and *ScRom2* are required for proper expression of the *ScPDR5* gene as well [156, 161].

Regulatory mechanisms linking mitochondrial dysfunction and PDR pathway activation remain far from fully understood. Two independent retroactive signaling pathways were identified linking mitochondrial defects to the activation of the PDR transcriptional network in *S. cerevisiae* [92, 93, 223]. Activation of Pdr transcription through the loss of mitochondrial genome involves the retroactive signaling pathway component *ScRtg2* and *ScRtg1* [92]. The PDR transcription activation through this retrograde signaling may be conserved in *C. glabrata* since the disruption of *CgRTG2* also influences azole resistance [58]. The second signalling mechanism identified, but not fully understood, is dependent on the cytoplasmic localization of the protein *ScPsd1* observed in ρ^0 cells, a mitochondrial intermembrane space protein [93, 223]. This signaling pathway also involves the increased activity of *ScLge1* nuclear protein, which is thought to induce the recruitment of *ScPdr3* to its promotor. However, the mechanisms connecting *ScPsd1* presence in the cytoplasm to the *ScLge1* nuclear protein activity remain to be clarified [98]. In *C. glabrata*, the overproduction of *CgPsd1* also increases *CgCDR1* gene expression and consequent drug resistance, even in ρ^+ cells [104].

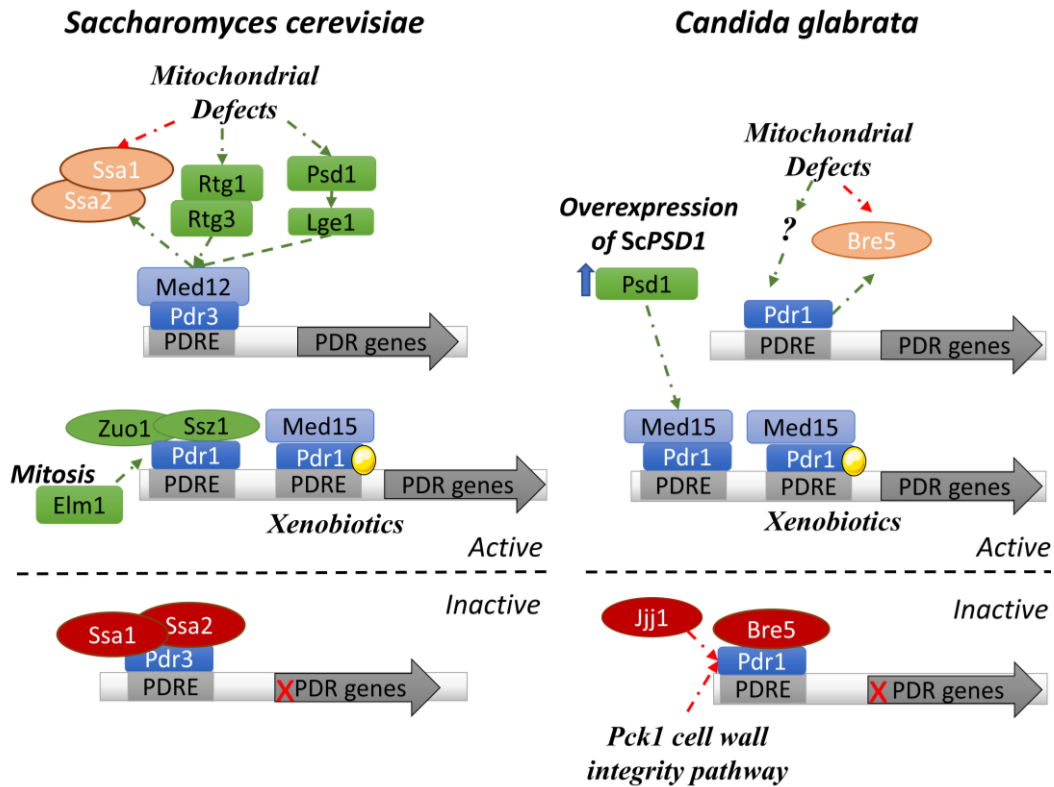


Figure II. 5. Described regulators of the pleiotropic drug resistance transcription factors protein activity in *Saccharomyces cerevisiae* and *Candida glabrata*. Representation of the identified positive and negative regulators, represented in green and red respectively, of the activity regulation of the PDR transcription factors in blue. The main component of the mediator complex involved in the PDR transcription activation, if known, is represented in light blue. When characterized, the stimulus resulting in a specific regulation pathway is highlighted.

2.5.4 Regulation of the activity PDR transcription factor through protein structural changes

As said above PDR regulators belong to the zinc-finger family of transcription factors [73, 147], being the zinc finger DNA binding domain (DBD) located at the N-terminal region (in specific, between amino acids 1 and 205/258 in the case of ScPdr1/CgPdr1 (Annex Figure II. 1) and including three structural regions: the Zn₂Cys₆ motif followed by a linker sequence and a coiled-coil motif involved in dimerization to other zinc transcription factors [97, 147] (Figure II. 6). The Zn₂Cys₆ zinc cluster motif recognizes the CG triplets half-sites in the DNA, while the configuration of the coiled-coil structure and of the linker sequence will then guide the dimer contact to the preferred DNA sequence (in the case of ScPdr1/CgPdr1, the PDRE motif), specifying the inter-base pair separation between DNA half-sites [97, 147, 224]. ScPdr1 and ScPdr3 can form both homo- and hetero- dimers [97], being still elusive whether the different forms bind to the DNA with different specificity [97]. As mentioned before, ScPdr1 (but not ScPdr3) also forms heterodimers with ScStb5, an association that might be conserved in *C. glabrata*, since CgStb5 also affects Pdr-regulated genes expression [60, 125, 132]. A central regulatory domain (CRD) is usually located after the dimerization domain in nuclear receptors [73, 147]. In ScPdr1 a short sequence located at the N-terminal of the CRD (residues 238-276) was identified as being essential to restrict ScPdr1 activity and, due to that

phenotype, was defined as an inhibitory domain (ID)(Figure II. 6)[225]. However, this inhibitory effect of the CRD domain does not fully abrogate Pdr1 activity since, without further stimulus, basal levels of expression of target genes are still observed [70, 73, 74]. Upon interaction of Pdr1 with xenobiotics, through the xenobiotic binding domain (XBD) located within CRD, the inhibitory effect is relieved (Figure II. 6)[105]. Despite the strong homology established between ScPdr1 and ScPdr3, the XBD only shares ~40% similarity, in agreement with the reported different responses of these proteins to xenobiotics [91] (Annex Figure II. 1). Similarly, the XBD of ScPdr1 is not similar to that of CgPdr1, which may suggest different binding specificity of the two proteins to xenobiotics (Annex Figure II. 1). Also localized in the CRD is the middle homology region (MHR) (Figure II. 6) [226] that is present in most yeast zinc transcription factors. This domain is located within the XBD, which might suggest a potential role in the sensing/binding of xenobiotics to the protein [105, 147] and it was further suggested to assist in the discrimination of target DNA by facilitating direct interaction between the DBD and the linker DNA [224]. The nuclear localization signal of ScPdr1 is located within the CDR as well and is enriched with serine and tyrosine residues, most of these also being found conserved in CgPdr1 (Annex Figure II. 1)[227]. The nuclear import of ScPdr1 involves the nuclear importer ScPse1, however indirectly through the possible interaction of another uncharacterized factor [227]. The NLS motif is not conserved in ScPdr3 and its import to the nucleus was shown to be independent of ScPse1 [227]. This observation reinforces the idea of ScPdr1 and ScPdr3 have significant differences in the way their CRD is regulated [227]. Both ScPdr1 and ScPdr3 are assumed to be immediately transported to the nucleus after translation since both proteins are constitutively located in the nucleus [74, 97, 222, 227]. Differently, and although CgPdr1 is constitutively bound to the PDRE motifs [71], *C. glabrata* CgPdr1 when in a complex with CgGal11A was found to be located in the nucleus or the cytoplasm [207]. Nevertheless, changes in CgPdr1 activity regulated through subcellular localization have not been described.

In *C. glabrata* removal of CRD from CgPdr1 results in hyper-activation of the regulator to a degree so high that becomes toxic for the cells, possibly due to extreme sequestration of the transcriptional machinery [73]. This observation highlights the necessity of maintaining some degree of negative regulation over the activity of CgPdr1. In *S. cerevisiae* the deletion of the CRD also yields a hyperactive ScPdr1, however, without the toxic effects observed in *C. glabrata* [73, 74, 100]. From the molecular point of view, it is believed that the CRD controls the activity of the C-terminal transactivation domain by sequestering it thus preventing a subsequent interaction with the transcriptional machinery [181]. Upon activation, the transactivation domain is released from the core structure of the protein being free to engage in multivalent interactions with the transcriptional machinery [62]. In zinc finger transcription factors the structure of transactivation domains includes conserved short helix structures enriched with negatively charged residues, this enrichment in negative charges being suggested to serve as a repellent to the DNA and serving to facilitate in engagement with positively charged patches of transcriptional regulatory proteins (Figure II. 6) [228]. The TAD structure is also enriched in hydrophobic residues (preferable aromatic) to allows this structure to be buried and locked in binding pockets through an aromatic anchor [228]. This domain is further reported to interact with the positively charged histones and hydrophobic pocket of nucleosomes, promoting chromatin remodeling and thus facilitating transcription [228]. The transactivation domain of ScPdr1 was found to interact with the hydrophobic patch present on the surface

of the kinase-inducible domain interacting domain (KIX) of ScGal11 upon transcriptional activation [105]. Due to the importance of this domain in the regulation of PDR transcription factors, any modifications in the C-terminal can result in changes in azole resistance phenotype [51, 54, 56, 117, 196, 207].

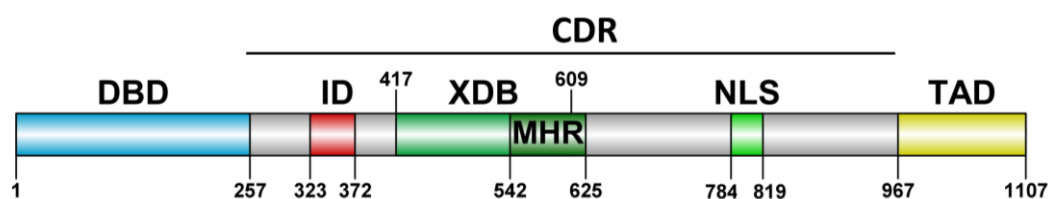


Figure II. 6. Different functional domains in the Pleiotropic Drug Resistance transcription factor of *Candida glabrata*, CgPdr1. The DBD (1 to 254 a.a.), CRD (255 to 968 a.a.), and TAD (969 to 1107 a.a.) domains were defined in Simoncova, L. and Moye-Rowley, W.S. 2020 [181]. The ID (322-372), the minimum XDB (417 to 608 a.a.), and NLS (793 to 819 a.a.) were defined by sequence homology to these domains identified in *S. cerevisiae* [105, 225, 227].

2.5.5 The impact of gain-of-function mutations in the activation of CgPdr1 in *Candida glabrata*

As said above, in *C. glabrata* the more common mechanism described to underlie resistance to azoles in clinical strains results from these encoding hyper-active alleles of CgPDR1, the so-called gain-of-function mutants (or GOF) [7]. As such, in the past decade, there has been a noteworthy increase in the identification of these CgPDR1 GOF mutations (Figure II. 7, Annex Table II. 1) [27, 50, 51, 53, 55, 194, 203-208]. Notably, a recent study by Won, E. J. *et al.* 2021 [6] highlighted the correlation of azole resistance in *C. glabrata* clinical isolates, with non-synonymous mutations in CgPdr1 uniquely to resistant isolates, to the increased mortality of almost 90% of patients that receive inappropriate azole monotherapy. The sole factor leading to a reduction of mortality was an appropriate antifungal treatment, either by the treatment with combinatory antifungal therapy or with an antifungal to which the clinical isolate was found susceptible [6]. In line with these results, CgPdr1 GOF mutations reduce the efficacy of fluconazole treatment in a murine model of *C. glabrata* disseminated infection [196].

Most of the GOFs identified in the sequence of CgPDR1 affect the CRD or the TAD domain. Notably, some regions of the CRD of CgPdr1 appear more prone to accumulate non-synonymous mutations in *C. glabrata* azole-resistant strains including the terminal region of the minimum XDB, the surrounding of the predicted NLS region and a region before the predicted TAD domain (Figure II. 7).

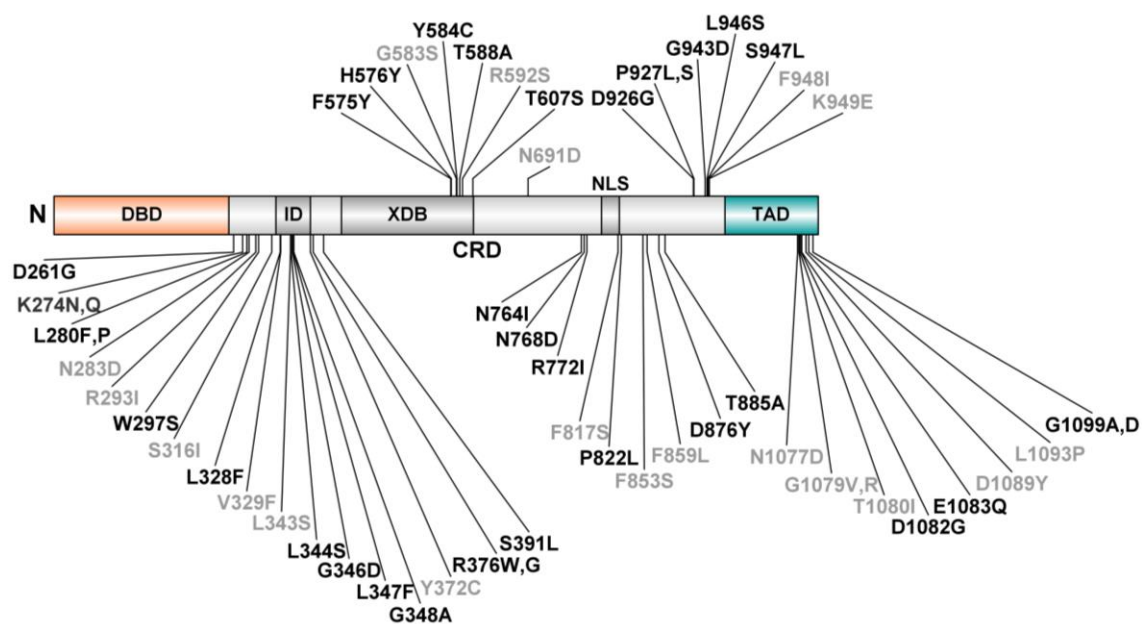


Figure II. 7. Distribution of reported gain-of-function mutations in *CgPdr1* structure. Non-synonymous mutations summarized in this picture were only found in resistant clinical isolates or strains. These point mutations were further defined as gain-of-function mutation if, when introduced in a susceptible background, the strain becomes resistant and/or induces *CgPdr1* target genes upregulation (black). Highly potential GOF mutations that were identified in strains after *in vitro* evolution during azole exposure or during *in vivo* evolution in a patient undergoing azole treatment are also represented in grey. The full list of non-synonymous mutations identified till today and the references that reported them are summarized in Annex Table II. 1.

Although the detailed effect of how these modifications affect the biochemical activity of the protein is not well understood, it is believed that these alterations may cause structural changes that relieve the negative role of the CRD over TAD, thereby enabling interactions with the transcriptional machinery [62]. In line with this, higher activity of GOF *CgPdr1* variants correlates with increased recruitment of the transcriptional machinery to the promoter region of *CgPdr1* target genes. In *S. cerevisiae*, an *ScPdr1* GOF variant was found to occupy more the promotor of the target gene *ScPDR5* (compared to a corresponding wild-type), further enhancing the recruitment of the components of the mediator complex, the SAGA and SWI/SNF complexes, and the TATA-binding protein [149]. Furthermore, a significant loss of histones linked to the promoter and coding sequence DNA of *ScPDR5* was reported in the strain overexpressing the *ScPDR1* GOF allele [149]. Interestingly, all these modifications in transcription co-factors and chromatin remodeling are not clear in cells expressing a wild-type *ScPdr1* activated upon exposure to xenobiotics, only being observed slight changes in the structure of the nucleosome surrounding the PDRE motif in the promoter region of target genes, suggesting different underlying activation mechanisms when compared to *CgPdr1* GOF variants [149]. In *C. glabrata*, this detailed analysis of the differences obtained in the promoter region of *CgPdr1*-target genes has not been performed to the same extent, however, the notable remark is the fact that induction of PDR-dependent genes in strains encoding hyperactive *CgPdr1* can reach five times the level that is attained upon xenobiotic-induced activation of *CgPdr1*, this being observed also for the *CgPDR1* gene itself [46, 50, 62]. Consequently, *CgPdr1* GOF mutants overproduce *CgPdr1p* [73] although this increase does not appear to constitute the main driver of tolerance to azoles [73, 74, 181]. It is

noteworthy that strains over-expressing CgPdr1 variants do not show fitness defects considering that these modifications are believed to restrict the inhibitory effect of the CRD over the transactivation domain, something that when it is performed at the full extent (that is upon full abrogation of CRD) results in high toxicity for *C. glabrata* cells [51, 73]. One possible mechanism by which the cells expressing CgPDR1 GOF variants control the hyper-activation may be the degradation rate of the protein that, in some cases, has been shown to be twice the one observed for wild-type CgPdr1 [73]. It is also possible that GOF mutations affect only mildly the CRD (and thus its inhibition over the TAD would still be active in these cells, albeit less intense) or that it has a limited effect in alleviating negative regulatory mechanisms of CgPdr1. Consistent with the idea that the interactome of CgPdr1 may differ between wild-type and GOF variants, recent studies have reported that specific GOFs have different dependencies of the mediator subunit CgGal11A [153, 181, 212]. Furthermore, different GOF mutants affect differently the transcriptome, this being observed even when the modifications occur in the same genetic background [54, 117]. No apparent correlation between the structural region of CgPdr1 affected by GOF mutations and the generated genomic expression could be established [50, 194]. In fact, only two genes were found to be commonly activated in isolates expressing different GOF variants: CgCDR1, that as said above encodes a multidrug efflux pump of the ABC Superfamily, and CgPUP1, encoding a mitochondrial protein with unknown function whose deletion reduces *C. glabrata* virulence against mice [27, 50, 55, 56, 117]. Concordant to the different transcription profiles, when reconstituted in the same genetic background, different Pdr1 GOF mutations led to different degrees of tolerance to azoles [51, 54], different adherence capabilities to epithelial cells [54, 229], different degrees of virulence against the murine infection model [51] and different protein degradation rates [118]. Furthermore, the effects of hyperactivation of CgPdr1 in virulence and fitness are not transversal to all GOFs and a specific GOF loss of fitness traits can be attenuated in different genetic backgrounds [56, 196]. Altogether these observations show that the consequences of the different modifications in biochemical activity of CgPdr1 are complex to understand and are likely multi-factorial.

3. The acetic acid-responsive transcription factor CgHaa1 and its dependent regulatory network

To successfully colonize the vaginal tract *Candida* cells, including those of *C. glabrata*, must cope with several stressful conditions that may restrain growth. These include fluctuations of nutrients, changing hormones, the activity of the immune system, or competing microbiota. Concerning this last aspect, the vaginal microbiota is largely composed of lactic acid bacteria [230, 231] that are believed to play an instrumental role in maintaining vaginal health by maintaining an acidic pH (~4.5)[137, 232]. This acidification is prompted by the production of significant amounts of lactic acid produced mainly by the commensal *Lactobacillus*, but also by epithelial cells [233]. Acetic acid has also been found in vaginal fluid [137, 232, 234] resulting from metabolic activity of colonizing bacteria, specially the species associated with bacterial vaginosis (reviewed in Aldunate, M. *et al.* 2015 [235]). In conditions of dysbiosis, an over-proliferation of anaerobic bacteria occurs and the concentration of acetic acid increases prominently (up to a maximum of 120mM mM) [233, 236]. To avoid exclusion from the vaginal tract, *Candida* cells are expected to have evolved adaptive mechanisms that allow them to thrive in this environment, being among these the capacity to tolerate acetic acid at a low pH. Notably, while lactic acid at physiological conditions found in the vaginal environment exerted no significant inhibitory effect against *C. glabrata*, concentrations of acetic acid in the range of those found upon dysbiosis were found to affect significantly the growth of this pathogenic yeast [237]. At the vaginal pH of 4.5, acetic acid (pKa 4.7) is found mainly in its undissociated form that can permeate the plasma membrane by passive diffusion [232, 233, 235]. Once inside *C. glabrata* cell, where the cytosolic pH is close to neutrality, acetic acid dissociates leading to the accumulation of protons and of the negatively charged counter-ion [238-241]. In *C. glabrata* the effects of stress-induced by acetic acid or by other carboxylic acids have been relatively poorly studied, however, a lot of knowledge has already been gathered in *S. cerevisiae* (reviewed in Mira, N. *et al.* 2010 [242]). Among other effects, it has been suggested that the consequences of acetic acid/acetate accumulation include oxidative stress [243, 244], with repercussions in lipid peroxidation and inhibition of membrane sensors and transporters [245]; severe depletion of energy, likely resulting from the great demand for ATP due to the activation of many energy-consuming defense mechanisms (out of which the plasma membrane H⁺-ATPase proton pumps stand out); and inhibition of glucan synthase enzyme [246, 247]. Recently, our group has also demonstrated that acetic acid at physiological vaginal pH has a high synergic effect with azoles in inhibiting the growth of *C. glabrata* [237]. Similarly, the presence of acetic acid was found to render fluconazole cidal against *Candida albicans* but not against *C. glabrata*, although the concentrations of acid tested were only those found under eubiosis conditions [248]. Interestingly, it has been shown that vaginal *C. glabrata* strains are highly tolerant to acetic acid at a low pH, this being attributed to a lower internal accumulation of the acid [249], this reduction correlating, at least in part, with structural changes of the cell wall architecture of these cells, compared to susceptible strains [249]. Recently, remodeling of the cell wall structure was found to play an instrumental role in tolerance of *S. cerevisiae* to acetic acid [250]. Another factor that appears to contribute to this higher tolerance of vaginal strains to acetic acid

includes a capacity to consume acetic acid even when glucose is present in the medium [249]. This metabolic flexibility is an essential advantage for human colonizing microbiota to cope with the nutrient deprivation that characterizes the different infection sites [251]. Strains exhibiting higher tolerance to acetic acid were also found to exhibit higher levels of CgPma1 activity when facing acetic acid stress suggesting better control of internal pH homeostasis in these vaginal strains as well [249].

In *S. cerevisiae* tolerance to acetic acid has been found to be largely dependent on the transcription factor ScHaa1 where this regulator was found to regulate, directly or indirectly, the expression of more than 80% of the acetic acid-responsive genes, including several genes involved in multidrug resistance transport, encoding regulators and effectors of the carbohydrate metabolism, genes involved cell wall homeostasis and lipid metabolism, or several transcription factor genes [252, 253]. The expression of *ScHAA1* significantly increased tolerance of *S. cerevisiae* to acetic acid and, consistently, the expression of some of the ScHaa1-regulated genes has also found to exert protection against the acid [254, 255]. Specific ScHaa1-regulated genes [252] contributing for tolerance to acetic acid included the multidrug resistance transporter ScTpo3 [256], which was implicated in the reduction of the internal accumulation of acetic acid in acid-challenged cells; or the protein kinase Hrk1 [252], which was proposed to be involved in the post-translational regulation of other acetate exporters, based on the demonstration that deletion of this gene also caused increased accumulation of acetate in acid-challenged cells [252, 256]. A homologue of ScHaa1 has been identified in the species *Zygosaccharomyces bailii*, known by its very high tolerance to acetic acid, and its corresponding regulon was characterized [257]. The results obtained revealed that ZbHaa1 regulates genes encoding several heat-shock proteins during acetic acid stress [257], responding to the acid-induced protein denaturation and misfolding [258, 259]. ZbHaa1 was also found to induce *ZbMDH1* that encodes mitochondrial malate dehydrogenase protein, presumed to be involved in the metabolization of the acid in the presence or absence of glucose [260, 261]. More recently, a study disclosed the involvement of a Haa1-regulon in *C. glabrata* tolerance to acetic acid [262] (Figure II. 8). In particular, it was demonstrated that deletion of *CgHAA1* (ORF *CAGL0L09339g*) significantly increased tolerance of *C. glabrata* to acetic acid at a low pH, also reducing the expression of around 70% of the acid-induced genes. The CgHaa1 targets genes included genes encoding enzymes involved in the main pathways of central carbon metabolism and the generation of energy such as glycolysis, glyoxylate cycle, pentose phosphate pathway, Krebs cycle, and catabolism of trehalose and glycogen [262]. The transcription of several genes encoding stress chaperones or enzymes of the antioxidant response was also dependent of a functional CgHaa1 [262], as well as a set of genes involved in the control of internal pH homeostasis: *CgPMA1*, encoding the plasma membrane proton pump; *CgPMP2* and *CgHSP30*, two predicted regulators of CgPma1p activity; and *CgVMA1*, encoding a subunit of the vacuolar proton pump [262]. Concordantly, under acetic acid stress, CgHaa1 expression increases the amount in the plasma membrane and the activity of the proton pump CgPma1 [262]. Among the set of CgHaa1-regulated genes was also the drug-efflux pump CgTpo3, confirmed to be involved in the reduction of the internal accumulation of the acid in *C. glabrata* [262], similarly to what was observed in *S. cerevisiae* [252]. Under acetic acid stress, CgHaa1 was also found to activate the expression of *CgYPS2*, *CgYPS4*, and *CgYPS10* genes [262], which belong to a family of yapsins required for control of *C. glabrata* internal pH homeostasis [263], as well as several adhesin-encoding genes [262]. Consistent with this positive role in inducing expression of genes related with adhesion, the expression of

CgHaa1 was demonstrated to be necessary for maximal adherence of *C. glabrata* to vaginal epithelial cells in the presence of 30 mM acetic acid, a concentration that is in the range of those observed under eubiosis conditions [262].

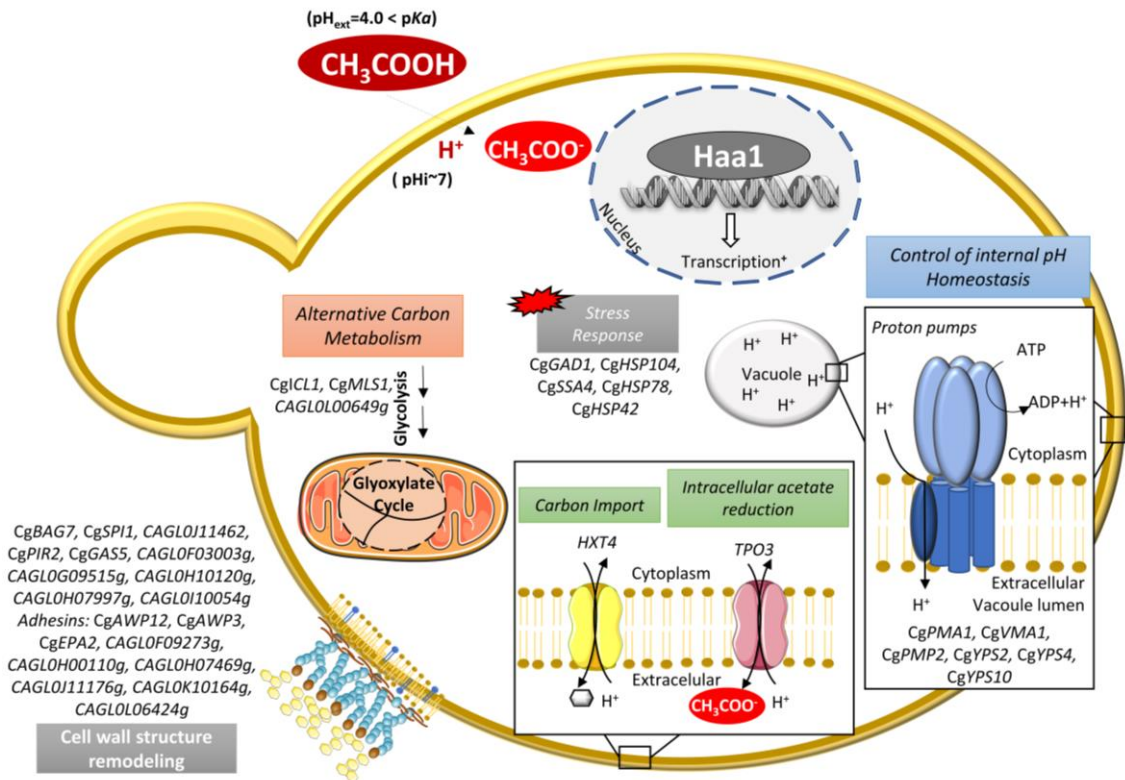


Figure II. 8. Schematic representation of the biological functions of genes belonging to the *CgHaa1*-regulon in *Candida glabrata*.

A comparison of the dataset of genes regulated by ScHaa1 and CgHaa1 revealed some similarities, but also significant disparities, which is interesting considering that the experiments were performed using similar experimental settings (same growth medium and pH and using comparable inhibitory concentrations of acetic acid), a condition that is essential for accurate comparison of transcriptional regulatory networks across yeasts [264](Figure II. 9).

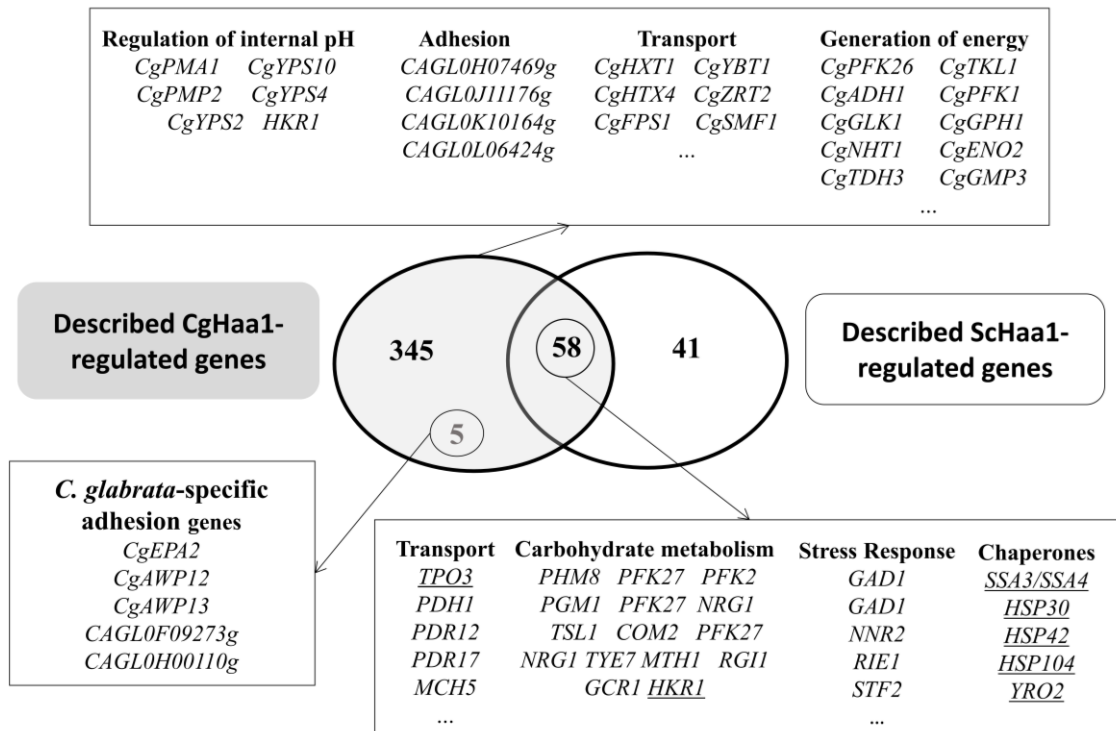


Figure II. 9. Comparison of the CgHaa1- and ScHaa1-regulons active in response to acetic acid stress. The dataset of genes found to be activated by CgHaa1 or by ScHaa1 during the response of *C. glabrata* or *S. cerevisiae* to acetic acid (at pH 4) were compared [252, 262]. The intersection of the two datasets revealed a modest overlap between the two networks. The functional classes most represented within the dataset of genes specifically regulated by CgHaa1 are indicated in the figure, alongside the names of some of the genes clustered in these functional classes. The homologs genes regulated by ZbHaa1 during acetic acid stress are also highlighted underlined [260, 265]. The image was adapted from Bernardo, R. *et al.* 2017 [262].

The Haa1 transcription network active during the response of *S. cerevisiae* or *C. glabrata* to acetic acid stress was found to commonly regulate the expression of some genes such as the glycoprotein *YGP1*; the MFS-MDR transporters *TPO3/TPO2*, or the kinase *HRK1*, all described to play a role in conferring protection against the acid [256, 262, 266-271]. Several chaperone-encoding genes also appear to be under the regulation of Haa1 in both species [252, 262]. Notably, all these genes were also found to be under the regulation of ZbHaa1 in *Z. balli* [257, 260](Figure II. 9). Both ScHaa1- and CgHaa1- regulon also regulate genes responsive to oxidative and dissection stress response, membrane transport and carbohydrate metabolism genes [252, 262](Figure II. 9). ScHaa1 recognizes the responsive element 5' - (G/C)(A/C)GG(G/C)G - 3' motif [253], a motif similar to the one predicted for ZbHaa1, 5' - (A/C)GGG(A/C)G(A/G)(C/T)(G/T)- 3'[260]. Despite these similarities, the number of genes under the regulation of CgHaa1 was considerably larger and included genes and biological functions that were not found to be under the regulation of ScHaa1 (and here it is important to again refer that the experiments resulting in the elucidation of these regulons in the two species were performed under similar experimental conditions)(Figure II. 9). Among these functions that stood out from the “specific” set of CgHaa1-regulated genes emerged those involved in adhesion, including a set of adhesins that are present in *C. glabrata* genome but not in *S. cerevisiae* (Figure II. 9); *CgTIR3*, involved in the uptake of sterols; several genes involved in the synthesis of β -1,3 and β -1,6-glucans; and the genes involved in the regulation of internal

pH homeostasis [262]. This last aspect was particularly relevant since in *S. cerevisiae* the regulation of the activity of the plasma membrane protein pump was found not to occur at the transcriptional level but post-translationally, via multiple post-translation modifications [252, 268, 272]. Several genes found to be regulated exclusively by CgHaa1 have an HRE-like motif that is not found in the ortholog promoter of *S. cerevisiae*, suggesting the addition of new genes to the regulon through the addition of the Haa1 regulatory element during promoter evolution [262]. Further and more detailed studies will be required in order to scrutinize how this regulatory network evolved from *S. cerevisiae* to *C. glabrata*.

III. Comparative genomic and transcriptomic analyses unveil novel features of azole resistance and adaptation to the human host in *Candida glabrata*

Part of the results shown in this chapter was published in:

Salazar SB, Wang C, Münsterkötter M, Okamoto M, Takahashi-Nakaguchi A, Chibana H, Lopes MM, Güldener U, Butler G and Mira NP, “Comparative genomic and transcriptomic analyses unveil novel features of azole resistance and adaptation to the human host in *Candida glabrata*”, FEMS Yeast Res, 18(1), 2018. doi: 10.1093/femsyr/fox079

1. Abstract

The frequent emergence of azole resistance among *Candida glabrata* strains contributes to the increase in the incidence of infections caused by this species. Whole-genome sequencing of a fluconazole and voriconazole-resistant clinical isolate (FFUL887) and subsequent comparison with the genome of the susceptible strain CBS138 revealed prominent differences in several genes documented to promote azole resistance in *C. glabrata*. Among these was the transcriptional regulator CgPdr1. The CgPdr1 FFUL887 variant included a K274Q modification not documented in other azole-resistant strains. Transcriptomic profiling evidenced the up-regulation of 92 documented targets of CgPdr1 in the FFUL887 strain, supporting the idea that the K274Q substitution originates a CgPdr1 gain-of-function mutant. Notably, the production of CgPdr1^{K274Q} variant in the background of FFUL887 cells was associated with a higher susceptibility of the cells against organic acids at a low pH (4.5), but had no detectable effect in tolerance towards other environmental stressors. Comparison of the genome of the FFUL887 and CBS138 also revealed prominent differences in the sequence of adhesin-encoding genes, while the comparison of the transcriptome of the two strains showed a significant remodelling of the expression of genes involved in the metabolism of carbohydrates, nitrogen and sulphur in the FFUL887 strain; these differences likely reflecting adaptive responses evolved by the clinical strain during colonization of the host.

2. Introduction

An alarming increase in the incidence of infections caused by *C. glabrata* has been reported in the last years [2, 3]. As such, in most epidemiological surveys this species ranks as the second major causative agent of invasive fungal infections worldwide, behind *C. albicans* [2, 3]. This increase in the incidence of infections caused by *C. glabrata* is believed to result from its naturally high resilience to azoles, the frontline antifungal therapy used to treat candidiasis [273]. The remarkably high rate at which *C. glabrata* strains acquire resistance to azoles, higher than the one registered for any other *Candida spp.*, is another key factor contributing to the emergence of resistant strains [274-276]. Mutations in Erg11, the enzyme targeted by azoles, is not a primary mechanism of resistance in *C. glabrata*, in contrast with what is observed to occur for other *Candida* species [27, 29, 30]. This observation suggests that *C. glabrata* clinical strains rely on other mechanisms to cope with azole stress. In line with this, several reports have underlined the important role of the ABC drug-efflux pumps such as CgCdr1 and CgPdh1 in contributing for azole resistance in clinical strains [28, 35, 36]. More recently, the involvement of MDR transporters belonging to the MFS in azole resistance of *C. glabrata* has also been described [39].

The transcriptional regulation of drug-efflux pumps in *C. glabrata*, as in other yeasts, relies on the activity of the well-organized PDR regulatory network [276]. In *C. glabrata* the key regulator of the PDR network is the transcription factor CgPdr1 and, concomitantly, this has been demonstrated to play an essential role in conferring tolerance to azoles [46, 56], including in resistant clinical isolates [27, 28, 35, 50, 51, 194]. CgPdr1 has been implicated in the regulation of the drug-efflux pumps CgCDR1, CgPDH1, CgQDR2 and CgYORI [27, 56, 117]. Other azole-responsive genes regulated by CgPdr1 have biological functions related to stress response, metabolism of fatty acids and sterols, transcriptional regulation and adhesion [27, 50, 51, 56, 117]. Analysis of the coding sequence of the CgPDR1 gene in susceptible and in resistant clinical isolates identified a panoply of GOF mutations that are believed to constitutively activate the transcription factor resulting in enhanced *C. glabrata* azole resistance (reviewed in Annex Table II. 1).

In this work, the genome and transcriptome of the azole-susceptible reference strain *C. glabrata* CBS138 were compared with the those of an azole-resistant clinical isolate (named FFUL887) recovered along the course of an epidemiological survey undertaken in hospitals of the Lisbon area. Besides providing clues to the mechanisms underlying the acquisition of azole resistance in the host, the results may also contribute for a better understanding of the different responses evolved by *C. glabrata* in the colonization of the human host.

3. Methods

3.1. Strains and growth media

The laboratory strains used in this work are listed in Table III 1 while the 58 *C. glabrata* clinical isolates (recovered from patients attending three major Hospitals of the Lisbon area between 2000 and 2008) are detailed in supplementary materials (Annex Table III. 1). The strains were cultivated in rich growth media Yeast Peptone Dextrose (YPD), in RPMI (Roswell Park Memorial Institute Medium), or Minimal Medium (MM). YPD contains, per liter, 20 g glucose (Merck Millipore), 10 g yeast extract (HiMedia Laboratories, Mumbai, India) and 20 g Peptone (HiMedia Laboratories). RPMI, contains, per liter, 20.8 g RPMI-1640 synthetic medium (Sigma), 36 g glucose (Merck Millipore), 0.3g of L-glutamine (Sigma) and 0.165 mol/L of MOPS (3-(N-morpholino) propanesulfonic acid, Sigma). MM contains, per liter, 20 g glucose (Merck Millipore), 2.65 g (NH₄)₂SO₄ (Merck Millipore) and 1.7 g of yeast nitrogen base without amino acids and without ammonium sulphate (Difco). YPD and MM medium were sterilized by autoclaving for 15 minutes at 121°C and 1 atm, while RPMI medium was filtered with a 0.22-µm pore size filter and preserved at 4°C until further use. Solid media was prepared supplementing the corresponding liquid media with 2% agar.

Table III 1. List of laboratory strains used in this study.

Strain	Parental Strain	Description	Reference
KUE100	2001H	Parent strain; histidine auxotroph; the recipient enables high efficient gene targeting in which <i>yku80</i> is repressed with a <i>SAT1</i> flipper	Ueno <i>et al.</i> , 2011 [277]
KUE100_chr606	KUE100	Control strain derived from KUE100 parental strain in which the <i>CgHIS3</i> marker was ectopically integrated at a non-coding locus	Ueno <i>et al.</i> , 2011 [277]
KUE100_Δ <i>Cgpd1</i>	KUE100	Δ <i>Cgpd1</i> strain, <i>CgPDR1</i> (<i>CAGLOA00451g</i>) was replaced with the <i>CgHIS3</i> marker	This study
CBS138	-	Reference strain	CBS-KNAW Fungal Biodiversity Centre

3.2. Assessment of resistance to antifungals of *Candida glabrata* clinical isolates

To assess the resistance of the *C. glabrata* clinical isolates and of the reference strain CBS138 to voriconazole, fluconazole, anidulafungin and caspofungin the MIC₅₀ (minimum inhibitory concentration) of each of the antifungals was estimated using the micro-dilution method recommended by the European Committee on Antimicrobial Susceptibility Testing (EUCAST) [278]. The concentrations of fluconazole tested ranged from 0.125 mg/L to 64 mg/L and for the remaining antifungals ranged from 0.015 mg/L to 8 mg/L. MIC₅₀ value was taken as being the first concentration of antifungal that reduced growth of the strains to half that registered in drug-free medium, as defined by EUCAST [278]. The MIC₅₀ of each antifungal determined for the strain was compared with the clinical breakpoints recommended by EUCAST (32 mg/L

for fluconazole, 0.06 mg/L for anidulafungin) to classify the strains as resistant (the MIC₅₀ is above the defined breakpoint), susceptible (MIC₅₀ equal or above the breakpoint) or intermediate (MIC₅₀ shows a susceptible dose-dependence (SDD)). Since a breakpoint value is not yet established for voriconazole in *C. glabrata* the epidemiological cut-off value (ECOFF) (1 mg/L) was used to detect non-wild type isolates, as recommended [279]. The stock solutions of the antifungals were prepared from the powder and using DMSO (Dimethyl sulfoxide, Sigma) as the solvent. Fluconazole was purchased from Sigma; voriconazole and anidulafungin were kindly provided by Pfizer; and caspofungin was provided by Merck Sharp Dohme. Growth curves of the *C. glabrata* reference strain CBS138 and of the FFUL887 isolate in the presence of fluconazole and voriconazole were performed using the same experimental setup described above for the microdilution assays, with the difference that instead of measuring OD of the culture only after 24h this was measured every 30 minutes during 42h.

3.3. FFUL887 genomic DNA extraction and whole-genome sequencing

FFUL887 cells were cultivated in YPD growth medium (up to an OD_{600nm} of approximately 3.0) and then centrifuged at 5000 rpm, for 5 min at 4°C. The pellet was resuspended in 1 ml solution A (1 M Sorbitol (Sigma); 0.1 M EDTA (ethylenediaminetetraacetic acid) at pH 7.5). Afterwards, 10 mg/mL zymolyase (Zymo research) was added to the cellular suspension and the solution was incubated at 37°C until protoplast formation. The suspension was centrifuged at 5000 rpm for 5 min and the pellet was resuspended in 1 mL solution B (50 mM Tris-HCL at pH 7.4 (Sigma-Aldrich), 20 mM EDTA). After this step, 30 µL of sodium dodecyl sulfate (SDS) 10% were added to the mixture and this was left for 30 min at 65 °C. 250 µL of potassium acetate (5 M, Merck) were subsequently added and the mixture was left for 1h on ice. The suspension was clarified by centrifugation (10000 rpm, 10 min) and the supernatant was transferred to two fresh microfuge tubes. 1 volume of cold isopropanol was used to precipitate the pellet followed by centrifugation at 5000 rpm for 15 min. Supernatant was discarded and the resulting pellet was incubated in 1 mL ethanol 70 % during 5 min, and washed twice with ethanol 70 %. The pellet was then dried in speed vacuum and resuspended in 200 µl Tris-EDTA buffer (TE) at pH 7.4. 0.5 µl of RNase (10 mg/ml) was added followed by 1 h incubation at 37 °C. The mixture was centrifuged at 10000 rpm for 15 min and the supernatant was preserved at 4 °C till further use. FFUL887 genome sequencing was based on Ion Torrent and was performed by Stab Vida (Portugal) as a paid service. Two rounds of paired-end sequencing were performed which resulted in approximately 6 million reads with an average size of 199 bp. The reads were trimmed based on quality and for SNP calling the trimmed reads were mapped against the reference genome of CBS138 (available on Candida Genome Database (CGD)) using CLC Genomics Workbench. Variant detection was performed from the mapped reads using both the probabilistic and quality-based variant detection tools embedded on CLC to increase confidence on the results obtained. To annotate the genome of the FFUL887 strain the reads were de novo assembled into 799 contigs yielding a total of assembled bases of 12.29 Mb and genome coverage of around 96x. *Ab initio* gene detection was performed using PEDANT genome database, using different algorithms followed by manual curation to select the more appropriate gene models [280]. The sequence and annotation of the genome of the FFUL887

clinical strain has been deposited in ENA (<http://www.ebi.ac.uk/ena/data/view/FWDN01000001-FWDN01000799>).

3.4. Comparative transcriptomic analysis of *C. glabrata* CBS138 and FFUL887 strains.

The transcriptomes of FFUL887 and CBS138 strains was compared using DNA microarrays specifically designed for *C. glabrata* (design ID 064590)[281]. Both strains were cultivated over-night in 25 mL of YPD at 30°C with orbital agitation (250 rpm) and then re-inoculated (at an OD_{600nm} of 0.2±0.05) in 150 mL of fresh RPMI. The cells were harvested by centrifugation (8000 x g, 7min, 4 °C – Beckman J2.21 Centrifuge, rotor JA.10) in mid-exponential phase (OD_{600nm}~2±0.05) and immediately frozen at -80 °C until further use. RNA extraction was performed as described in Bernardo *et al.* 2017 [262] and in Rossignol *et al.* 2007 [281].

3.5. *CgPDR1* gene disruption in the FFUL887 clinical strain

The deletion of the *C. glabrata PDR1* (*CAGL0A00451g*) in strain KUE100 (parental to the $\Delta Cgpdrl$ mutant used in spot assays) was carried out using the method described by Ueno *et al.* 2011 [277]. The target gene *CgPDR1* was replaced by a DNA cassette including the *CgHIS3* gene, through homologous recombination. The replacement cassette was prepared by PCR. Recombination locus and gene deletion were verified by PCR. Deletion of the same gene in the background of the clinical isolate strain FFUL887 was carried out using a little modified method from the one above described for the KUE100 strain. In specific, *CgPDR1* was replaced by a DNA cassette containing the zeocin resistant marker by homologous recombination. Transformants were isolated on YPD supplemented with 100µg/ml zeocin. Correct insertion of the zeocine resistance cassette and corresponding deletion of *CgPDR1* were verified by PCR and by confirming the absence of *CgPDR1* expression in the mutant strains by real-time RT-PCR (primers available in Table III. 2).

3.6. Effect of the *CgPdr1*^{K274Q} variant in expression of *CgCDR1*, *CgPDH1*, *CgQDR2* and *CgPDR1* genes.

The expression of *CgCDR1*, *CgPDH1*, *CgQDR2* and *CgPDR1* genes was compared in CBS138, FFUL887 and FFUL887_ $\Delta Cgpdrl$ strains by RT-PCR. Cells of the different strains were cultivated in identical conditions to those used for the microarray analysis. Conversion of total RNA into cDNA was performed using 1µg of RNA. The reverse-transcription step was performed in a C1000 Thermal Cycler (Bio-Rad, Hercules, USA). The subsequent quantitative PCR step was performed using 2.5µL of the cDNA. Gene expression was calculated using *CgRDN5.8* as an internal control.

Table III. 2. *List of primers used in this study.*

Primer identification	Primer sequence
CgRDN5.8	Forward 5'-AACAACTCACCGGCCGAAT-3' Reverse 5'-CTTGGTTCTCGCATCGATGA-3'
CgPDR1	Forward 5'-CGATTGCCAACCCGTTAGA-3' Reverse 5'-GACGACCTTGGTGTAGGAGTCAT-3'
CgCDR1	Forward 5'-GCTTGCCCGCACATTGA-3' 5'- CCTCAGGCAGAGTGTGTTCTTTC-3'
CgPDH1	Forward 5'-GCCATGGTACCTGCATCGAT-3' 5'-CCGAGGAATAGCAAAACCAGTATAC-3'
CgQDR2	Forward 5'-TCACTGCATAGTTTCATATCGGACTA-3' Reverse 5'-TGCCGATATGTTCCCAAGTGA-3'

3.7. Effect of the CgPdr1^{K274Q} variant in tolerance to environmental stressors.

Comparison of susceptibility of CBS138, KUE100_chr606, KUE100_ΔCgpdrl, FFUL887 and FFUL887_ΔCgpdrl cells to inhibitory concentrations of H₂O₂ and of the organic acids acetic, propionic and butyric acids was based on spot assays. Cells of the different strains were cultivated in MM growth medium until mid-exponential phase (OD_{600nm}~0.8) and then diluted in 1 mL of sterile PBS to obtain a cell suspension having an OD_{600nm} of 0.05. 4 μL of this cell suspension and of two subsequent dilutions (1:5 and 1:10) were applied onto the surface of MM agarised plates supplemented or not with inhibitory concentrations of H₂O₂ (5-18 mM), of acetic acid (50-60 mM), of propionic acid (17-20 mM) and of butyric acids (15-17 mM). The plates were incubated at 30°C for two to three days depending on the severity of growth inhibition. The same experimental setup was used to assess the susceptibility of the strains to heat stress with the difference that instead of incubating the inoculated plates at 30°C, these were incubated at 37°C, 40°C or 42°C.

4. Results

4.1. Identification of FFUL887 as a fluconazole- and voriconazole- resistant strain

To characterize the incidence of resistance to fluconazole, voriconazole, caspofungin and anidulafungin in a cohort of 58 *C. glabrata* clinical isolates the concentration of each of these antifungals leading to a 50% growth inhibition (generally designated as MIC₅₀), compared with growth registered in drug-free medium, was determined. This phenotypic screening was performed using the highly standardized microdilution method recommended by EUCAST. As a control, we have also included the reference strain CBS138 in the screening. The MIC value obtained for each drug and each isolate is shown in Annex Figure III. 1 and the distribution of MIC values across all isolates is shown in Figure III. 1. The MIC values obtained were compared with the clinical resistance breakpoints defined by EUCAST (32 mg/L for fluconazole and 0.06 mg/L for anidulafungin) to classify the strains as resistant, intermediate or susceptible. To identify voriconazole-resistant strains the MIC value obtained was compared with the ECOFF (epidemiological cut-off) value (1 mg/mL) which can be used to distinguish wild-type from non wild-type isolates [279]. For caspofungin no breakpoint has been defined by EUCAST and therefore the strains were not classified. Under the experimental conditions used, the MIC value of the reference strain CBS138 was 16 mg/L for fluconazole and 0.25 mg/L for voriconazole, indicating that the reference strain is susceptible to these two azoles. Seven isolates (FFUL412, FFUL443, FFUL674, FFUL830, FFUL866, FFUL878, FFUL887) were resistant to fluconazole and voriconazole, two only resistant to fluconazole (FFUL98 and FFUL4012) and one only resistant to voriconazole (FFUL677) (Annex Table II. 1). Notably, three of the cross-resistant isolates (FFUL412, FFUL443 and FFUL674) were retrieved from patients undergoing fluconazole-based therapy (Annex Table III. 1). Despite the small number of isolates examined in this study, the percentage of resistance obtained for fluconazole and voriconazole (16% for fluconazole and 14% for voriconazole) are close to the values reported (10-15%) in antifungal surveillance tests undertaken with much larger cohorts of strains (e.g.[2]). None of the *C. glabrata* isolates tested could be considered susceptible to fluconazole as the MIC values were always above 0,002 mg/L (Figure III. 1), consistent with the described increased resilience of *C. glabrata* to this azole drug [273, 276]. All the isolates tested exhibited high susceptibility to anidulafungin, none of them exhibiting growth when cultivated in the presence of 0.06 mg/L, the defined resistance breakpoint (Figure III. 1 panel B; Annex Figure III. 1). For caspofungin only one isolate, FFUL887, exhibited a MIC value of 0.25, while for the remaining isolates this MIC value was of 0.125 or below (Figure III. 1 panel B; Annex Figure III. 1).

The FFUL887 strain was selected for further analysis since it was demonstrated to be resistant to fluconazole and voriconazole and also exhibited higher resilience to caspofungin, compared to the other clinical isolates compared in this study. To assess how the presence of the fluconazole and voriconazole affected growth kinetics of the FFUL887 and CBS138 strains, growth curves in liquid medium were performed using the same experimental setup that was used for the estimation of the MIC₅₀ value (Annex Figure III. 2). Three concentrations of voriconazole and fluconazole were tested: one corresponding to the resistance breakpoint, one below and one above that value (Annex Figure III. 2). The results obtained show that the two strains exhibited a similar fitness when cultivated in drug-free medium, with only a slight

decrease in the final biomass produced by the FFUL887 strain (Annex Figure III. 2). Supplementation of the RPMI medium with the two azole drugs led to a drastic growth inhibition of the CBS138 strain, whereas growth of the FFUL887 strain was almost identical to the control conditions, with only a small detectable decrease of the growth rate (e.g. 0.033 h^{-1} in the presence of 64 mg/L fluconazole and 0.044 h^{-1} in control conditions) (Annex Figure III. 2) and a slight increase in the lag phase that was observed upon inoculation in the drug-supplemented medium (Annex Figure III. 2).

To assess if the resistant phenotype exhibited by the FFUL887 strain towards fluconazole and voriconazole was generalized for azoles or was limited to azoles of the triazole family (including fluconazole or voriconazole), growth of this strain in the presence of the imidazoles ketoconazole and clotrimazole was examined (Annex Figure III. 3). Cells were cultivated for 24h in 96-multiwell plates containing RPMI or in the same growth medium supplemented with 4 mg/L ketoconazole and 1 mg/mL of clotrimazole, the defined resistance breakpoints for these two drugs. Annex Figure III. 3 shows that FFUL887 cells are more tolerant to the tested concentrations of ketoconazole and clotrimazole than the CBS138 strain; however, the FFUL887 strain is still considered susceptible to the two imidazoles since the concentrations tested reduced growth by more than 50% the one registered in control conditions (Annex Figure III. 3).

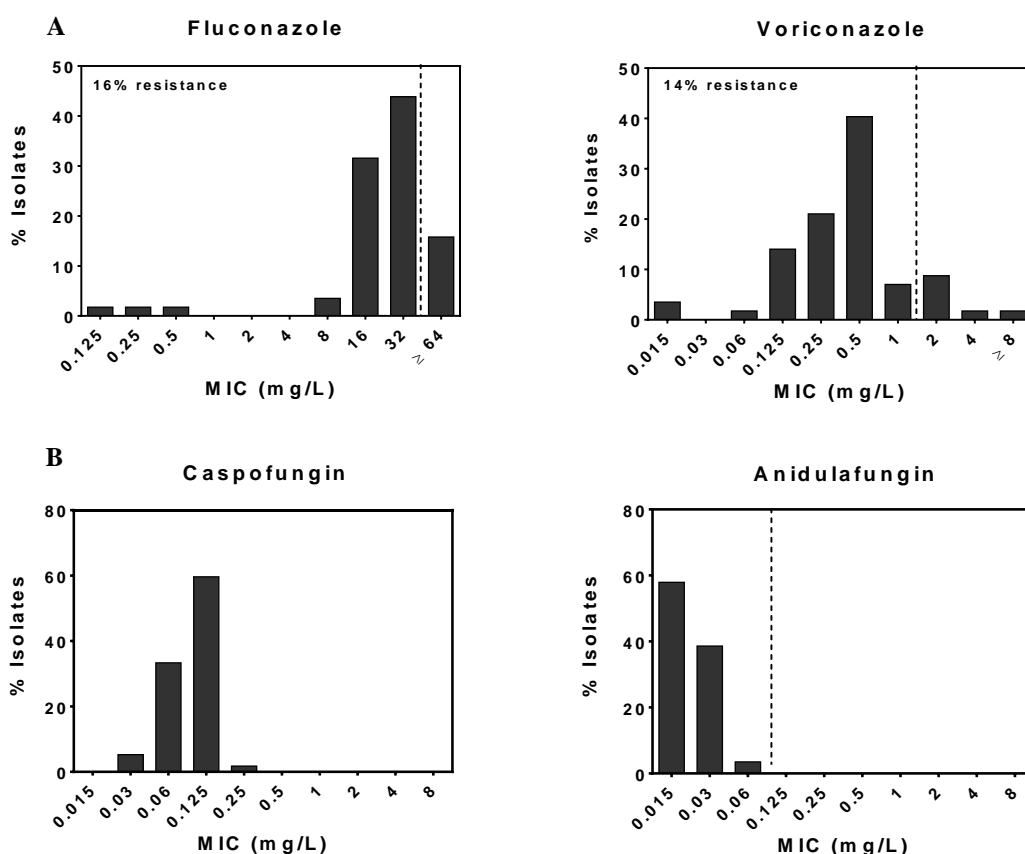


Figure III. 1. Distribution of minimum inhibitory concentration values of fluconazole, voriconazole (panel A) caspofungin and anidulafungin (panel B) obtained for the cohort of *Candida glabrata* clinical isolates tested in this work. The dashed line indicates the resistance breakpoints defined by EUCAST (as detailed in materials and methods). These results were obtained based on the assessment of MIC₅₀ value by the microdilution method recommended by EUCAST and that gave rise to the results shown in Annex Figure III. 1.

4.2. FFUL887 genome sequencing and annotation

The fluconazole- and voriconazole- resistance phenotype exhibited by the FFUL887 strain prompted us to obtain the genome sequence of this isolate. The assembled contig sequences were used for automatic *ab initio* gene detection that was subsequently manually curated to select the more appropriate gene models. This analysis allowed us to predict that the ORFeome of the FFUL887 strain includes 5079 genes, which corresponds to 96% of the total number of genes annotated for the CBS138 strain [282]. The number of ORFs obtained for the FFUL887 strain is also in line with those recently reported for other *C. glabrata* clinical isolates (in the range of 5300 coding sequences (CDS)) [283, 284]. The vast majority (5039) of the protein pairs present in CBS138 and FFUL887 shared more than 90% identity at the amino acid level indicating that the proteins encoded by the two strains are fairly similar. For the identification of single nucleotide polymorphism (SNP) that could underlie the observed resistance to fluconazole and voriconazole of the FFUL887 strain the reads obtained were mapped against the genome sequence of the CBS138 strain, as detailed in materials and methods. This comparison yielded 77749 SNPs between the genomes of FFUL887 and CBS138 (Annex Figure III. 4). A similar high number of SNPs was also reported in a recent comparative genomic analysis between two *C. glabrata* clinical isolates and the reference strain CBS138 [283]. About 45% of the SNPs identified between CBS138 and FFUL887 were located in coding regions, affecting 3194 of the gene sequences predicted for the FFUL887 strain. The percentage of genes harboring non-synonymous SNPs in the FFUL887 strain was similar throughout the nine *C. glabrata* nuclear chromosomes (~60%) but considerably smaller (~18%) in the mitochondrial chromosome (Annex Figure III. 4). On average FFUL887 and CBS138 orthologous genes harbored 5 non-synonymous SNPs; however, in some cases this number increased up to more than 30 non-synonymous SNPs including in *CAGL0K12078g* (>50 non-synonymous SNPs), encoding a putative transcription factor similar to ScNrg1; *CAGL0C00231g* (42 non-synonymous SNPs), encoding a presumed plasma membrane nucleobase transporter, and the adhesin *CgPWP4* (52 non-synonymous SNPs)(Figure III. 2). Other adhesin-encoding genes were also observed to harbor a high number of non-synonymous SNPs between FFUL887 and CBS138 including *CgEPA8*, *CgPWP5*, *CAGL0C03575g* and *CAGL0L10092g* (Figure III. 2).

No non-synonymous SNPs were found in the sequence of *CgERG11* gene encoded by FFUL887, consistent with the idea that azole resistance of this strain is not driven by alterations in the drug target as shown for most *C. glabrata* azole-resistant isolates [27, 29, 30]. No SNPs were also found in FFUL887 *CgMSH2*, a DNA repair protein whose mutations had been linked to the development of azole resistance in *C. glabrata* resistant clinical strains [47]. Concerning *CgFKS1* and *CgFKS2*, the two enzymes targeted by echinocandins, the FFUL887 alleles harbour one non-synonymous SNP each (Gly14Ser in *CgFks1* and Thr926Pro in *CgFks2*), compared to CBS138 orthologues; however, these polymorphisms are outside of the hot-spots regions commonly found to be altered in echinocandin-resistant isolates [285]. It thus remains to be examined whether the higher tolerance of the FFUL887 strain to caspofungin comes from these polymorphisms or if it results from other genetic traits.

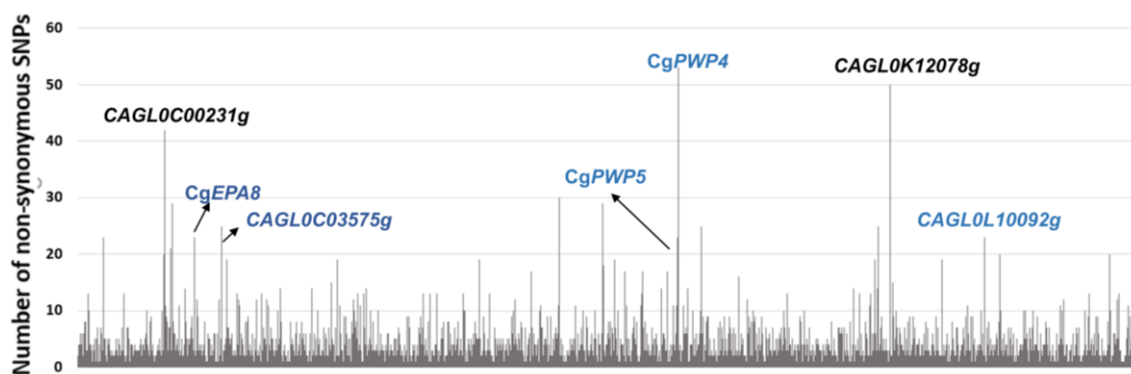


Figure III. 2. Number of non-synonymous single nucleotide polymorphisms present in FFUL887 predicted proteins, when compared with their CBS138 counter-partners. The reads obtained after whole-genome sequencing of the FFUL887 strain were mapped against the genome of the reference strain CBS138, as detailed in materials and methods. Those genes exhibiting a higher number of non-synonymous SNPs in the FFUL887 strain are highlighted in the figure. Adhesin-encoding genes are evidenced in light blue.

4.3. Comparative genomic analysis between FFUL887 and CBS138 focused on azole-resistance genes: emphasis on *CgPDR1*

To gather insights into the differential levels of resistance to fluconazole and voriconazole of the CBS138 and FFUL887 strains, the set of proteins found to harbour non-synonymous SNPs in the resistant strain were compared with a comprehensive list of genes previously implicated in *C. glabrata* resistance to fluconazole and voriconazole. 214 genes (listed in Annex Table III. 2) associated with resistance to these two azoles differed in FFUL887 and in CBS138, a subset of these being shown in Table III 3.

One of the proteins that differed between FFUL887 and CBS138 is CgPdr1, which exhibited 4 non-synonymous SNPs (G271A, T293C, G727A and A820C, resulting in the aminoacid changes V91I, L98S, D243N and K274Q, respectively), when compared with the corresponding CBS138 orthologue. Three of these modifications (V91I, L98S and D243N) were found to be present simultaneously in the CgPdr1 variants encoded by isolates resistant and susceptible to azoles (Annex Table II. 1), while the K274Q was not previously described. Based on this observation, it was hypothesized that the substitution K274Q could represent a gain-of-function substitution of *C. glabrata* CgPdr1. To test this hypothesis, the transcriptomes of the FFUL887 and CBS138 strains were compared in drug-free RPMI medium using species-specific DNA microarrays. Out of the 409 genes found to be over-expressed in the FFUL887 strain (above 1.5-fold, *p*-value below 0.001; listed in Annex Table III. 3) 92 genes are documented targets of CgPdr1, according to the information available in the PathoYeast database [141] (highlighted in grey in the Annex Table III. 3). Among these were the well-characterized CgPdr1 targets *CgPDH1* and *CgCDR1*, as well as *CgPDR1* itself (Annex Table III. 3). Deletion of *CgPDR1* from the FFUL887 genome abrogated the increase in transcription of *CgPDH1*, *CgCDR1*, *CgPDR1* and *CgQDR2* genes registered (Figure III. 3 panel A). As expected, elimination of the production of the CgPdr1^{K274Q} variant also resulted in sensitization of the FFUL887 strain to fluconazole and voriconazole (Figure III. 3 panel B). Overall, the results of the transcriptomic profiling of the CBS138 and FFUL887 strains strongly support the idea that FFUL887 encodes a CgPdr1 gain-of-function allele, resulting from the K274Q modification.

Table III 3. Subset of proteins previously described to be involved in fluconazole and/or voriconazole resistance in *Candida glabrata* that were found to harbour non-synonymous SNPs in the FFUL887 strain, when compared with their CBS138 counter-partners. Functions were derived from CGD database [140].

	ORF/Standard Name	Function	FFUL887 amino acid modification
PDR1 and regulators	<i>CAGL0A00451g/CgPDR1</i>	Zinc finger transcription factor activator of drug resistance genes	Val91Ile; Leu98Ser; Asp243Asn; Lys274Gln
	<i>CAGL0J07370g/CgJJI1</i>	Co-chaperone that negatively regulates fluconazole resistance; deletion causes elevated expression of Cg <i>CDR1</i> and Cg <i>PDR1</i>	Thr77Ala; Tyr479Phe
Mediator Complex	<i>CAGL0H06215g/CgGAL11A</i>	Component of the transcriptional Mediator complex that provides interfaces between RNA polymerase II and upstream activator proteins; essential for CgPdr1-dependent activation of azole-resistance genes	Ser134Asn; Ser965Gly; Ser1084Asn
	<i>CAGL0E00627g/CgSRB8</i>	Subunit of the RNA polymerase II mediator complex	Tyr399Cys; His1051Asn; Gln1322His
MDR-transporters	<i>CAGL0F02717g/CgPDH1</i>	Multidrug transporter of the ABC Superfamily	Lys438Gln; Glu839Asp
	<i>CAGL0G08624g/CgQDR2</i>	Drug:H ⁺ antiporter of the Major Facilitator Superfamily that confers imidazole drug resistance	Asn417Asp; Leu309Ile; Leu307Ile; Arg304His; Ile255Phe; Ser212Ala; Ala69Thr; Asn38Ile
Transcription Factors	<i>CAGL0C01199g/CgUPC2A</i>	Zinc finger transcription factor required for transcriptional regulation of genes involved in uptake and biosynthesis of ergosterol	Arg92Lys; Asn304Ser; Glu822Val
	<i>CAGL0L04400g</i>	Zinc finger transcription factor involved in the transcriptional regulation of MDR genes. Orthologue of <i>S. cerevisiae</i> ScYRR1	Cys24Gly; Ala58Val; Ile137Leu; Asp229Glu; Ile346Val; Glu574Lys; Ile593Leu; Glu710Asp; Ala933Val
	<i>CAGL0B03421g/CgMARI</i>	Predicted zinc-finger transcription factor, regulator of genes involved in plasma membrane lipid biosynthesis	Asn321Asp; Ala306Thr; Ala274Thr; Met139Val
	<i>CAGL0K05841g/CgHAP1</i>	Predicted zinc finger transcription factor that regulates genes involved in the transcriptional response to levels of heme and oxygen	Ala364Val; Asn378Thr; Ala676Gly; Ser743Ala; Ser894Ala; Gly1219Val
	<i>CAGL0K01727g/CgRPN4</i>	Transcription factor that regulates proteasome genes	Asn335Thr; Asp334Glu; Val160Asp; Ala98delinsAlaGlnAla
	<i>CAGL0I05170g/CgCST6</i>	bZIP domain-containing protein involved in the regulation of biofilm formation	Ser39Pro; Ser321Pro; Ser462Asn
	<i>CAGL0L03377g</i>	Predicted zinc finger transcription factor, orthologue of <i>S. cerevisiae</i> ScSIP4 involved in positive regulation of gluconeogenesis	Gly134Asp; Gly172Ser; Lys252Arg; Ile347Met; Ala695Gly; Lys813Arg; Asp819Glu; Thr867Met
	<i>CAGL0L09383g</i>	Predicted zinc finger transcription factor. Orthologue of <i>S. cerevisiae</i> ScSUT2 that positively regulates sterol uptake under anaerobic condition	Ser116Asn; Ile185Val; Met202Val
Chromatin Regulators	<i>CAGL0C05357g/CgHST1</i>	Histone deacetylase that regulates gene expression in niacin-limiting condition	Met70Lys
	<i>CAGL0E02475g/CgSIN3</i>	Component of the Rpd3S and Rpd3L histone deacetylase complexes	Asn50Lys; Lys288Thr

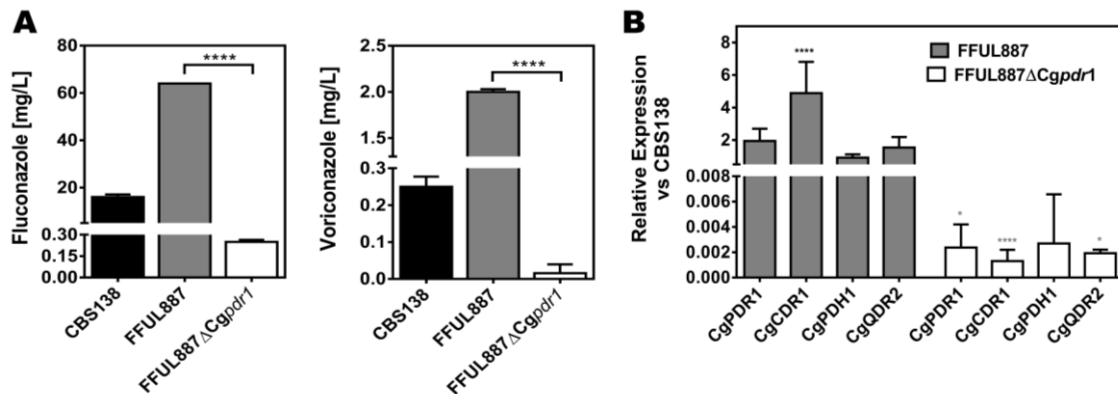


Figure III. 3. Deletion of the *CgPDR1*^{A820C} allele from FFUL887 genome abrogated azole resistance and reduced expression of *CgPdr1* target genes. (A) MIC for fluconazole and voriconazole was obtained for the CBS138, FFUL887 and the FFUL887_ Δ Cgpd1 strains, as determined by the microdilution method recommended by EUCAST. For the statistical analysis, the results obtained for the mutant strain devoid of *CgPDR1* gene were compared with those gathered for the wild-type FFUL887 strain using one-way ANOVA. (B) Comparison of the transcript levels of *CgPDR1*, *CgCDR1*, *CgPDH1* and *CgQDR2* genes in CBS138, FFUL887 and the FFUL887_ Δ Cgpd1 strains. Cells of the different strains were cultivated in RPMI growth medium until mid-exponential phase after which the expression of *CgPDR1*, *CgCDR1*, *CgPDH1* and *CgQDR2* genes was compared by RT-qPCR. The values represented for the FFUL887 and FFUL887_ Δ Cgpd1 strains are relative to the value obtained for the CBS138 strain, which was considered to be equal to 1. For the statistical analysis, the results obtained for the FFUL887 strain were compared with those gathered for CBS138 (black), while the results obtained for the FFUL887_ Δ Cgpd1 mutant were compared with those obtained for FFUL887 (grey) using one-way ANOVA. * *p*-value below 0.05, **** *p*-value below 0.0001.

4.4. The deletion of *CgPDR1*^{A820C} allele affects tolerance to environmental stress of the FFUL887 isolate.

Previous studies have shown that deletion of gain-of-function *CgPdr1* alleles results in altered stress resilience of azole-resistant *C. glabrata* strains [56]. We, therefore, compared the growth of CBS138, FFUL887 and FFUL887_ Δ Cgpd1 in the presence of various environmental stressors including H₂O₂, acetic acid, propionic acid, butyric acid and at different temperatures (30°C, 37°C, 40°C or 42°C). Under the experimental conditions used the deletion of *CgPDR1* in the FFUL887 background led to a mild decrease in growth of the strains when cultivated at all the temperatures tested (Figure III. 4). No significant differences were observed upon *CgPDR1* deletion in the FFUL887 background concerning tolerance to H₂O₂ but, surprisingly, during cultivation in the presence of inhibitory concentrations of the organic acids acetic, propionic and butyric acids (at pH 4.5) the deletion of *CgPDR1*^{A820C} was beneficial (Figure III. 4). These experiments were also performed in the genetic background of the laboratory strain KUE100 that encodes a wild-type *CgPdr1* allele. The results obtained confirmed a slight protective effect exerted by *CgPDR1* expression against high temperatures, while in the presence of acetic, propionic or butyric acids there were no significant differences in growth of the wild-type or of the Δ Cgpd1 mutant (Figure III. 4).

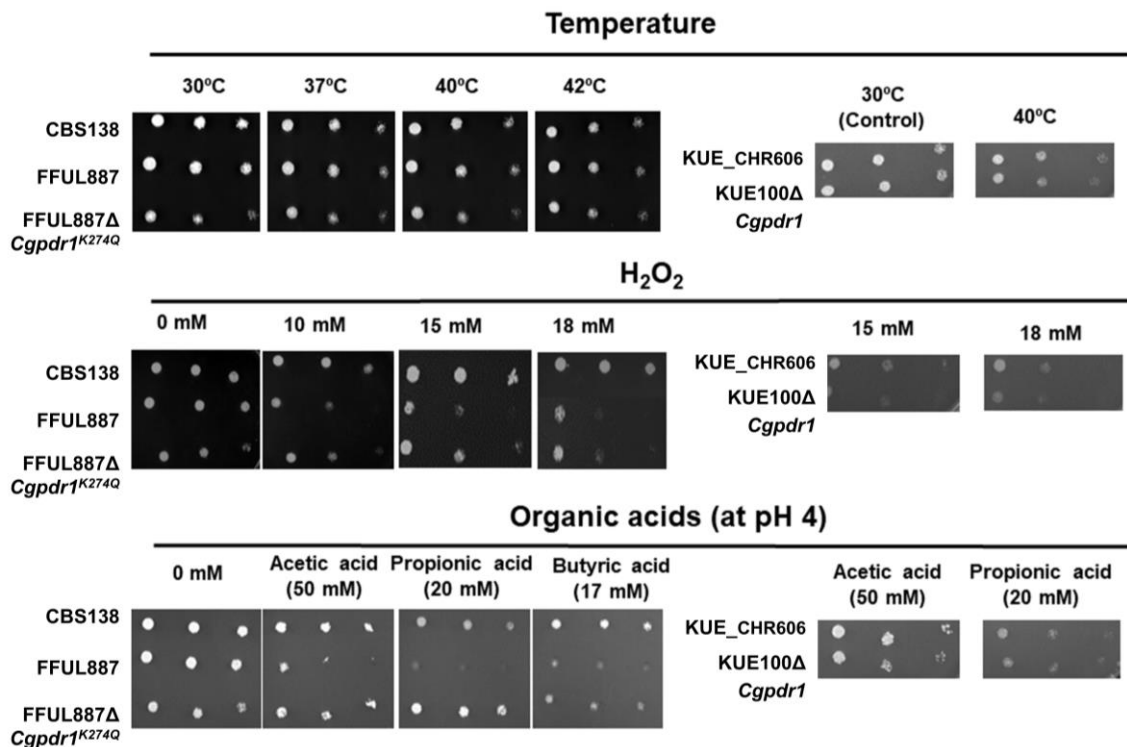


Figure III. 4. Comparison of the susceptibility of CBS138, FFUL887 and the FFUL887ΔCgpd1, KUE_chr606 and KUE100ΔCgpd1 strains to environmental stressors based on spot assays. Mid-exponential phase cells of the different strains were cultivated in solid MM growth medium or in this same medium supplemented with inhibitory concentrations of H₂O₂ or of acetic acid, propionic acid and butyric acid. Final cell suspension was prepared with an OD_{600nm} of 0.05 ± 0.005 and dilutions of the cell suspension are spotted. Growth was compared after two to three days of incubation at 30°C, depending on the severity of growth inhibition. The same experimental setup was used to compare the tolerance of the strains to different temperatures.

4.5. Comparative transcriptomic analysis between FFUL887 and CBS138 show dramatic alterations in the expression of genes involved in carbohydrate, nitrogen and sulphur metabolism.

We have further explored our results concerning the comparison of the transcriptome of the FFUL887 and CBS138 strains during growth in RPMI medium aiming to gain further insights into the responses evolved by *C. glabrata* during colonization of the human urinary tract considering that this was the niche where FFUL887 isolate was retrieved from. The CBS138 strain has an intestinal origin, however, its extensive utilization in the laboratory has likely resulted in its domestication leading to large phenotypic differences compared to those observed in *C. glabrata* clinical isolates including those of intestinal origin [249, 286]. The genes over-expressed (above 1.5-fold and having a *p*-value below 0.001) in the FFUL887 isolate were clustered according to their biological function using the MIPS functional catalogue (Annex Figure III. 5). Results revealed a significant enrichment (*p*-value below 0.001) of genes involved in “metabolism of amino acids”, “metabolism of carbohydrates”, “nitrogen, sulphur, and selenium metabolism”, “lipid, fatty acid and isoprenoid metabolism”, “generation of energy”, “vacuolar protein degradation”, “transport” and “oxidative stress response” (Annex Figure III. 5). Similarly, the set of genes

up-regulated in CBS138 (and consequently down-regulated in FFUL887) was enriched (p -value below 0.001) in genes related to “protein synthesis” (Annex Figure III. 5 and Annex Table III. 3).

The genes up-regulated in the FFUL887 strain related with carbohydrate and lipid metabolism included enzymes involved in fatty acid β -oxidation, in the catabolism of acetate, of propionate and of glycogen, as well as genes encoding neoglucogenic and Krebs cycle enzymes (Figure III. 5). This observation was surprising considering that at the time point where FFUL887 and CBS138 cells were harvested for the microarray analysis (after 6 hours of cultivation in the rich RPMI medium supplemented with 20 g/L glucose) there was still a considerable amount of glucose present in the culture supernatant of the two cultures (~18.5 g/L, based on high-pressure liquid chromatography (HPLC) analysis of the supernatants). The genes up-regulated in the FFUL887 strain related with amino acid and sulphur metabolism classes were essentially those involved in the metabolism of various amino acids and genes of the trans-sulfuration pathway that allows transport and incorporation of sulphate in methionine and cysteine (Figure III. 6). Consistently, several transporters involved in the uptake of amino acids, small peptides and of inorganic sulphur were also found to be up-regulated in the FFUL887 strain (Figure III. 5).

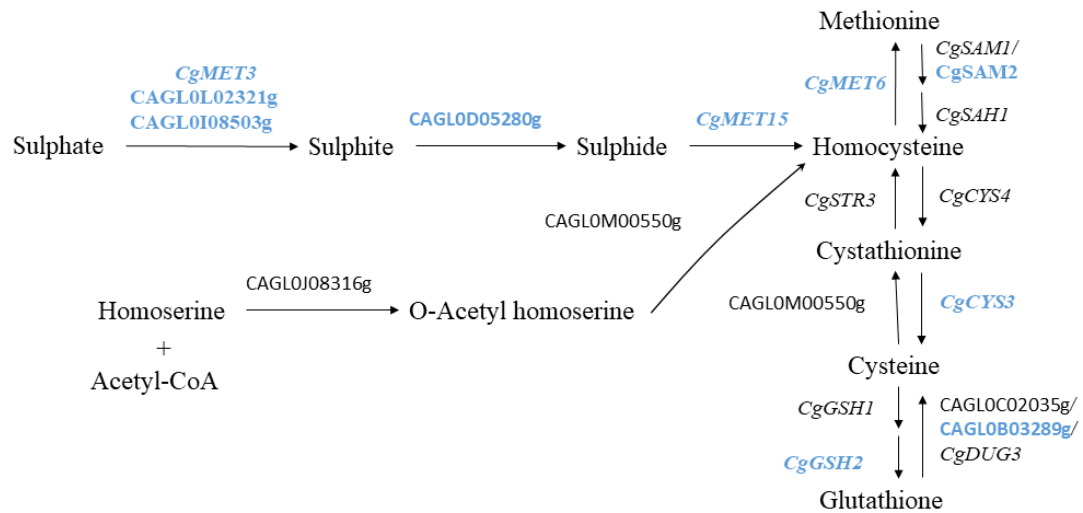


Figure III. 6. Schematic representation of the genes involved in trans-sulfurylation pathway in *Candida glabrata*, those being up-regulated in the FFUL887 strain being highlighted in blue. Association between genes and metabolic pathways was performed using the KEGG database.

5. Discussion

In this work we have disclosed the genome sequence of a *C. glabrata* clinical isolate, FFUL887, resistant to voriconazole and fluconazole and also exhibiting enhanced tolerance to caspofungin. The higher resistance of the FFUL887 strain to these two types of antifungals is striking considering that they have different modes of action. Resistance to voriconazole and fluconazole in FFUL887 was largely dependent on the expression of CgPdr1; however, this is not likely to underlie the higher tolerance of this strain to caspofungin since CgPdr1 expression is dispensable for *C. glabrata* tolerance to echinocandins [57].

A very high number of SNPs was obtained when comparing the genomic sequences of CBS138 and FFUL887, probably reflecting the different genetic background of these two strains. Nevertheless, the vast majority of the proteins encoded by the two strains were still very similar with >90% of these proteins sharing a degree of homology above 90%. Recent comparative genomic analysis between *C. glabrata* clinical isolates and the CBS138 strain also revealed very prominent differences, within the range of those reported in our study [283, 284], while a strain used for carboxylic acids production was much more similar to CBS138 [286]. Interestingly, even the comparison of cohorts of related clinical isolates shows very prominent differences, similar to those that are observed when the isolates are compared with the CBS138 strain [283, 287]. These observations reflect the described genomic plasticity of *C. glabrata* species which gives rise to a large genetic and phenotypic diversity among isolated strains [288]. While in our study we have focused on the comparison between the transcriptome and genome of an azole-resistant strain with the susceptible CBS138 strain, others have performed similar analyses but using related isolates (for example, strains retrieved from patients obtained before and after application of azole-therapy (e.g. [46, 56, 283])). In our case, a similar approach was not possible since we could not identify among the sensitive strains tested one that could be related with FFUL887. Necessarily, the option of comparing the genomes of CBS138 vs FFUL887 difficults the establishment of genotype-phenotype associations; however, it has the advantage of allowing the identification of new SNPs that could be relevant for azole resistance and that wouldn't be detected when comparing two already adapted clinical strains such as modifications occurring early during the process of colonization of the human host. Besides CgPdr1, several other well-characterized determinants of *C. glabrata* resistance to azoles were found to harbour SNPs in the resistant strain FFUL887 including the multidrug resistance transporters CgPDH1 and CgQDR2, the transcriptional regulators CgUPC2A, CgYRR1, CgSTB5 or CgRPN4 and the CgGAL111A of the mediator complex and CgJJI both regulators of CgPdr1 activity (Annex Table III. 2). It is difficult to understand whether these polymorphisms contribute to the higher resistance exhibited by FFUL887 cells towards fluconazole and voriconazole because the biochemical activity of these proteins is not well studied, and therefore it is hard to predict the consequences for protein activity of the identified SNPs. Nevertheless, these indicatives deserve further exploration since azole-resistance genes are surely under selective pressure, as occurs with CgPdr1.

The extensive up-regulation of about 90 documented targets of CgPdr1 that was observed in the FFUL887 strain during cultivation in drug-free growth medium strongly supports the idea that the K274Q substitution is, indeed, a new gain-of-function mutation of this protein. Interestingly, a K274N substitution has been previously reported, however, while this results in mild increase in fluconazole tolerance (MIC of

16 mg/L)[50], the herein reported K274Q substitution results in a much higher resistance (MIC of 64 mg/L). The K274 residue lies within a region of CgPdr1 where several other mutations have been described (as detailed in Figure II. 7) and is located near a predicted inhibitory regulatory domain of CgPdr1 (residues 322-465)(Figure II. 7). In *Saccharomyces cerevisiae* this regulatory domain inhibits the activity of ScPdr1 [225], for which it can be hypothesized that the K274Q modification could compromise the function of the inhibitory domain resulting in a hyper-activation of CgPdr1. Further studies are required to better understand how the K274Q and other GOF mutations modulate the activity of CgPdr1.

The genes that are under the regulation of different CgPdr1 gain-of-function mutants have a modest overlap [27, 50, 51, 117]. In order to determine the effect of the CgPdr1 K274Q substitution in *C. glabrata* genomic expression, the 92 genes up-regulated in the FFUL887 strain that were found to be dependently regulated by CgPdr1 according to PathoYeasttrack[141], were compared with the set of genes regulated by three other gain-of-function variants, P927L and L946S and K274N (Figure III. 7). Only 5 genes were in common in the three datasets: CgCDR1, CgYOR1, CgPDR1, CgPUP1 and CAGL0M09713g (Figure III. 7). Consistently, CgCDR1 and CgPUP1 genes were recently shown to be up-regulated among a cohort of CgPdr1 gain-of-function mutants different from those used to build Figure III. 7 [117]. The pattern of expression of other drug-efflux pumps varied according to the gain-of-function mutation: while K274Q, L946S, P927L led to the up-regulation of CgQDR2 and CgPHD1, K274N was the only mutation causing up-regulation of CgTPO1_1 (Figure III. 7). The expression of adhesin-encoding genes was also found to vary according to the CgPdr1 gain-of-function mutation (Figure III. 7). This observation is particularly interesting in light of the described effect of CgPdr1 in contributing for *C. glabrata* adhesion to epithelial cells [289]. Surprisingly, the overlap between the genes regulated by the CgPdr1 GOF mutants K274N and K274Q was very limited (Figure III. 7) demonstrating that even polymorphisms in the same CgPdr1 residue have a very different impact on the control of gene expression. One of the mechanisms that have been hypothesized to explain this divergence in the set of genes regulated by different CgPdr1 mutants is that they might be differently activated thereby resulting in a different interaction with the transcriptional machinery [62]. The different genetic backgrounds of the strains used in the different transcriptomic profilings may also contribute for some of the observed divergences.

As well as contributing to maximal resistance to voriconazole and fluconazole, we also showed that the CgPdr1^{K274Q} variant is detrimental for growth of FFUL887 cells when cultivated in the presence of organic acids at a low pH. Similarly, cells producing the CgPdr1^{P927L} gain-of-function variant was also found to be susceptible to organic acids at a low pH [56]. On the background of the KUE100 strain (derived from CBS138) which encodes a wild-type CgPdr1 allele, this phenotype towards organic acids was not observed indicating that it could be a feature of CgPdr1 gain-of-function mutants, or at least of a sub-set of them. It is not possible with the data available until so far to clarify the reasons why the presence of organic acids seems to sensitize FFUL887 cells, although this is certainly a feature that deserves further exploration as it could be used to improve the treatment of infections caused by isolates harboring CgPdr1 gain-of-function alleles. In line with this idea, our group has demonstrated that acetic acid at low pH has a synergic effect with azoles even against the azole resistant isolates identified in the current study, including FFUL887 [237].

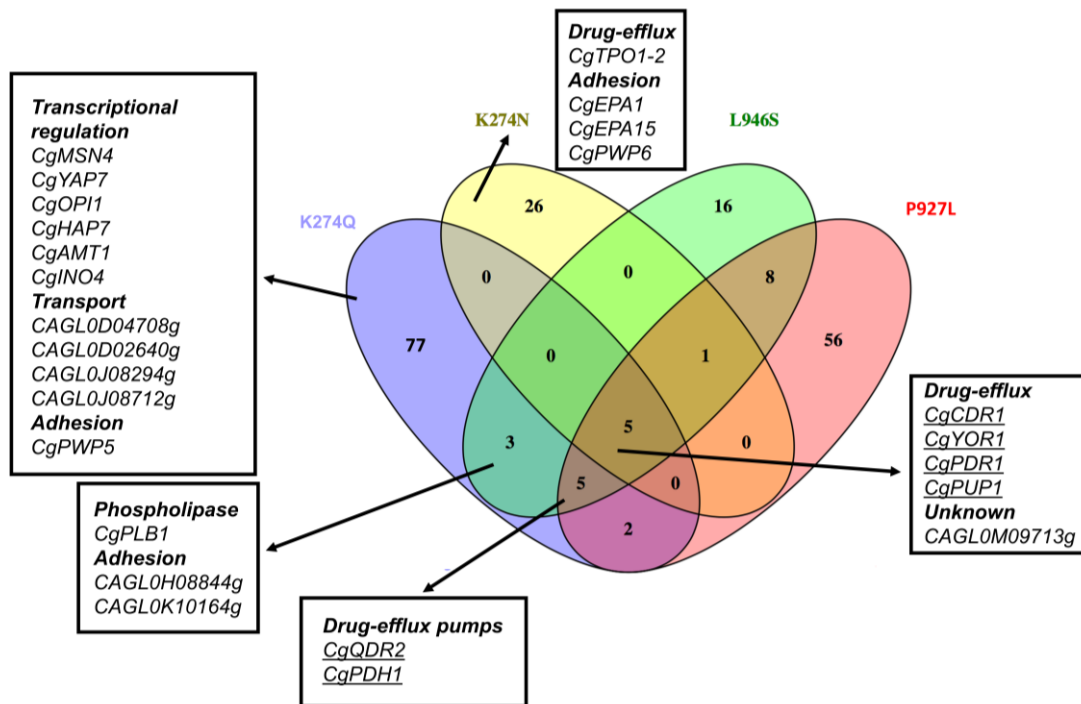


Figure III. 7. Schematic representation highlights the modest overlap existing between genes that are under the regulation of different *CgPdr1* gain-of-function mutants. Venn diagram comparing the set of genes regulated by the *CgPdr1* gain-of-function mutants K274Q, K274N, P927L and L946S, as revealed by transcriptomic analyses. The set of genes herein identified as being up-regulated in the FFUL887 isolate that were previously described to be *CgPdr1* dependently transcribed was compared with the set of genes previously described to be under the regulation of K274N, P927L and L946S *CgPdr1* gain-of-function mutations [27, 56].

Besides contributing to a better understanding of the acquisition of azole resistance, the comparative analyses of the genome and transcriptome of the CBS138 and FFUL887 strains also had the potential to elucidate some aspects underlying *C. glabrata* colonization of the human urinary tract (the site where FFUL887 was retrieved from). In this sense, one of the observations that emerged from the comparative genomic analysis performed was the identification of several genes encoding adhesins as among those that had the higher number of non-synonymous SNPs in the FFUL887 strain. Adhesion is a fundamental step for *C. glabrata* ability to successfully colonize infection sites and as such adhesin-encoding genes are subjected to a tight selective pressure demonstrated to occur both at the transcriptional and genomic level [283, 287, 290, 291]. The microarray analysis performed revealed only two adhesin-encoding genes, *CAGL0K10164g* and *CAGL0H08844g*, as being up-regulated in the FFUL887 strain; however, this analysis was performed using planktonic cells and thereby adhesion was not being favored. The herein observed prominent differences in the primary sequence of the adhesins encoded by FFUL887 and CBS138, with emphasis for *CgPwp4* which was the protein that differed the most in the two strains (Figure III. 2), shows that these genes are also subjected to a strong selective pressure probably to select those variants contributing more to improve adherence to the available surfaces. Another observation that emerged from the comparative transcriptomic analysis performed was the significant up-regulation in the FFUL887 strain of genes involved in the metabolism of amino acids and of sulphur as well as a large number of genes involved in metabolization of fatty acids, glycogen and other carbon sources. Since the

RPMI growth medium where the strains were cultivated for the transcriptomic analysis contains glucose (20 g/L) and sulphate (50 mg/L), the higher expression of these genes in the FFUL887 strain is more likely to reflect a higher basal level of expression, compared to the one observed in the CBS138 strain. In *C. glabrata* the presence of glucose in the medium does not appear to repress metabolization of other carbon sources nor of the genes involved in those processes, as observed in *S. cerevisiae* [249, 262]. A similar alleviation of glucose repression over metabolism of alternative carbon sources was observed in *C. albicans* [251]. We have searched the genome sequence of the CBS138 and of the FFUL887 strains for genes homologous to those that mediate glucose repression in *S. cerevisiae* (Annex Table III. 4). With the exception of the *ScMTH1* gene, all the other genes mediating glucose repression in *S. cerevisiae* have robust homologues in CBS138 and in FFUL887; however, in some cases, there were marked differences between the *S. cerevisiae* and the *C. glabrata* proteins those more prominent being the Mig1, Mig2 and Mig3 transcriptional regulators (Annex Table III. 4). Further studies are required to understand the molecular players underlying the alleviation of glucose repression in *C. glabrata* and how their activity is modified by selective pressure during colonization.

The increased resilience of *C. glabrata* to antifungal therapy and the persistent emergence of resistant strains is highly problematic considering the high rates of morbidity and mortality associated with infections caused by this pathogenic yeast. The results presented in this study provide a further contribution for a better understanding of the key players contributing for the acquisition of resistance in the host, with special emphasis on CgPdr1 transcription factor; a knowledge that can be used to guide the development of more efficient therapeutical strategies. In specific, it was shown for the first time that the K274Q substitution results in a gain-of-function CgPdr1 mutant and, consequently, in enhanced azole resistance. An observation of remark from our study and others was that the expression of the K274Q and of P927L CgPdr1 variants increases susceptibility to organic acids at a low pH, suggesting that these molecules could be used to sensitize azole-resistant strains dependent on CgPdr1 gain-of-function alleles. The herein reported whole-genome analysis of the FFUL887 strain and subsequent comparison with CBS138 strain reinforced the extreme genetic diversity among *C. glabrata* strains providing clues into the adaptive responses evolved during colonization of the human host and advancing current knowledge on the biology and physiology of this yeast species.

IV. Disclosing azole resistance mechanisms in resistant *Candida glabrata* strains encoding wild-type or gain-of-function CgPDR1 alleles through comparative genomics and transcriptomics

Part of the results shown in this chapter was published in:

Salazar SB, Pinheiro MJF, Sotti-Novais D, Soares AR, Lopes MM, Ferreira T, Rodrigues V, Fernandes F and Mira NP, “Disclosing azole resistance mechanisms in resistant *C. glabrata* strains encoding wild-type or gain-of-function CgPDR1 alleles through comparative genomics and transcriptomics” (in press at G3)

1. Abstract

The relevance of *C. glabrata* as a human pathogen is linked with its poor susceptibility to azoles as well as its extreme genomic plasticity that allows the rapid acquisition of resistance. Extensive characterization of azole-resistant *C. glabrata* strains unveiled the central role of the transcriptional regulator CgPdr1 in the resistance phenotype, with many strains encoding hyperactive (or gain-of-function; GOF) CgPDR1 alleles. Large-scale profiling of a collection of clinical *C. glabrata* isolates recovered in hospitals of the Lisbon area, in Portugal, led to the identification of eleven strains exhibiting resistance to fluconazole and/or voriconazole. Among these strains, ten were found to encode alleles of the CgPDR1 gene harbouring multiple non-synonymous SNPs that were not found in the alleles encoded by susceptible strains, including those resulting in the amino acid changes K274Q, I392M and I803T not previously described as GOF mutations. The isolates encoding these alleles were found to over-express several CgPdr1 target genes including the azole efflux pump CgCDR1 sustaining the idea that these represent new gain-of-function CgPdr1 alleles. Only one of the identified azole-resistant strains was found to encode a CgPDR1 allele fully identical to the one encoded by susceptible strains. To better understand the resistance phenotype of this strain, its transcriptome was compared with the one of a susceptible strain and of strains encoding CgPdr1 GOF alleles. The results of this comparative transcriptomic analysis will be discussed shedding light into the different azole-resistance mechanisms evolved by *C. glabrata*, including those independent of CgPdr1 GOF strains.

2. Introduction

Compared to *C. albicans*, non-*albicans Candida* species (NCAS) are generally more tolerant to antifungals [7] and can acquire resistance at a higher rate, specially *C. glabrata* [2, 3]. The increase in azole resistance among *Candida* strains threatens the successful therapeutic utilization of azoles, as confirmed by the prolonged hospital stays and poorer outcomes of patients colonized with azole-resistant strains [4]. The low susceptibility of *C. glabrata* to azoles is attributed to its capability of bypassing the accumulation of toxic sterols in the plasma membrane caused by the azole-induced inhibition of Erg11, an essential enzyme for ergosterol biosynthesis [16, 18, 19, 292, 293]. While in *C. albicans* azole resistance is largely determined by the occurrence of point modifications in Erg11 coding sequence, in *C. glabrata* this mechanism is very rare [16, 27-29]. The formation of mini-chromosomes harboring multiple copies of essential azole-resistance genes or the inactivation of the DNA repair enzyme *CgMSH2* as a mean to increase genetic diversity are mechanisms described to mediate azole resistance in *C. glabrata* clinical isolates [48, 49, 294]. Although these mechanisms reflect the highly plastic nature of the *C. glabrata* genome, which favors the rapid acquisition of resistance to azoles *in vivo* and *in vitro*, they are not observed to underlie the azole resistance-phenotype of many clinical strains [as reviewed in 7]. In fact, a recent overview of the genes described to influence azole resistance in laboratory strains and those confirmed to underlie azole resistance in clinical strains shows a very modest overlap reflecting the lower amount of work that has been undertaken in clinical strains, compared to laboratory strains [as reviewed in 7]. Also, the occurrence of factors conditioning azole resistance *in vivo* that may not be mimicked to the studies conducted *in vitro* also contributes for some dissimilarities in the findings obtained in laboratory and in clinical strains. In most cases, azole resistance in *C. glabrata* clinical strains derives from them acquiring GOF mutations in the transcription regulator *CgPdr1*, a central player in control of response and tolerance to xenobiotics in yeasts [as reviewed in 62]. GOF mutations render *CgPdr1* constitutively active resulting in a potent up-regulation of target genes even when drugs are not present. The more prominent *CgPdr1* target that is up-regulated upon *CgPdr1* activation are the drug-efflux pumps *CgCdr1* and *CgPdh1* [7, 62] that are believed to play an essential role in promoting the active efflux of azoles thereby alleviating the deleterious effects prompted by their internal accumulation. Notably, although the outcome of the occurrence of *CgPdr1* GOF mutations appears to be the same (constitutive activation of *CgPdr1* and azole resistance) the molecular mechanisms underneath are apparently different since it has been observed that GOFs have a very different impact in *C. glabrata* genomic expression, probably due to different interactions with the transcriptional machinery [55, 117, 181].

Despite the prevalence of *CgPdr1* gain-of-function mutants among azole-resistant *C. glabrata* strains, resistant strains encoding wild-type *CgPDR1* alleles have also been isolated [46, 47, 51, 205, 206, 295, 296], however, these were not further investigated and therefore the underlying resistance mechanisms remain unknown. In the present work, we scrutinized the azole-resistance phenotype of eleven *C. glabrata* resistant strains that we have identified in the course of epidemiological surveys undertaken in Portugal. Ten of these strains were found to encode *CgPdr1* variants, with two of them, I392M and I803T, being herein characterized for the first time. One strain (ISTB218) was found to encode a wild-type *CgPDR1* allele and was therefore subjected to comparative transcriptomic and genomic analyses (using two

susceptible strains as references) to shed light into genes and pathways that could mediate azole resistance *in vivo*, beyond CgPdr1.

3. Methods

3.1. Strains, clinical isolate collections and growth media used

The different clinical isolates and laboratorial strains (CBS138, SKY107 and LYS2) are detailed in Annex Table IV. 1. This work resorted to 1269 clinical isolates identified as belonging to the *Candida* genus by MALDI-TOF and retrieved from samples obtained from patients attending hospitals of the Lisbon area during the period of 2015-2017. Besides these, another cohort of resistant clinical isolates gathered during the previous epidemiological survey presented in Chapter III were also used (FFUL412, FFUL443, FFUL674, FFUL830, FFUL866, FFUL878 and FFUL887)[55]. The full list of isolates is presented in Annex Table IV. 1. Strains were cultivated in YPD [20g/L of glucose (Merck), 20 g/L bactopectone (Difco) and 10 g/L yeast extract (Difco)], in RPMI media [20.8 g/L RPMI-1640 synthetic medium (Sigma), 36 g/L glucose (Merck Millipore), 0.3 g/L of L-glutamine (Sigma) and 0.165 mol/L of MOPS (Sigma)] or in MM media [20 g/L of glucose or N-acetylglucosamine (Sigma), 1.7 g/L yeast nitrogen base without amino acids and ammonium (Difco) and 2.65 g/L ammonium sulphate (Merck)].

3.2. Plasmids

Plasmid pYR29-MycHis_CgPDR1, which expresses CgPDR1 from its natural promoter and terminator, was used to complement the deletion of CgPDR1 in SKY107 ($\Delta pdr1$) and LSY2 ($\Delta pdr1\Delta gal11a$) backgrounds (detailed in Table IV. 1). To obtain the pYR29-MycHis_CgPDR1 plasmid the coding sequence of the CgPDR1 gene, along with promoter and terminator, were amplified from plasmid pSP76 and inserted in the NotI/BamHI sites of the pYR29-MycHis_CgAFTI plasmid [297]. Using pYR29-MycHis_CgPDR1 as a template, three derivative plasmids were generated to allow expression of the CgPDR1 mutants A820C (yielding the K274Q substitution), T1176G (yielding the I392M substitution) and T2408C (yielding the I803T substitution). Codon substitution was obtained by amplification of the plasmid pYR29-MycHis_CgPDR1 plasmid with PfuUltra High-Fidelity DNA polymerase (Agilent) using the mutagenic primers detailed in Table IV. 1. The PCR product was treated with 2U DpnI (New England BioLabs) for 1h at 37°C, followed by self-ligation overnight, at 16°C, using 10U T4 polynucleotide kinase and 400U T4 ligase (both enzymes from New England BioLabs). The resulting product was transformed in *E. coli* DH5 α competent cells by classical transformation and constructs verified by Sanger sequencing.

3.3. Azole susceptibility testing of the clinical isolates collected in this study

A total of 479 *C. albicans* and *C. glabrata* isolates were profiled for their resistance to fluconazole and voriconazole. In an initial step, the isolates were cultivated for 17h in YPD in 96-microwell plates (at 30°C and with an orbital agitation of 200 rpm) after which cell suspensions were prepared (in water) and inoculated (at an initial OD_{530 nm} of approximately 0.0125) in 96-microwell plates containing RPMI either or not supplemented with: 4 mg/L of fluconazole or 0.25 mg/L of voriconazole for *C. albicans* strains, and

32 mg/L of fluconazole or 2 mg/L of voriconazole for *C. glabrata* strains. After 24h, the optical density of the cultures was determined and isolates whose growth in the presence of the azoles was, at least, 25% lower than the one observed in drug-free medium, were considered candidates as being resistant strains and were selected for downstream analysis. For these strains, it was determined the MIC (minimum inhibitory concentration) for fluconazole or voriconazole using the highly standardized microdilution method recommended by EUCAST [298]. To classify the strains as resistant or susceptible to these azoles we compared the MICs with the breakpoint values established for fluconazole (32 mg/L for *C. glabrata* and 4 mg/L for *C. albicans*) and with the ECOFF value established for voriconazole (1 mg/L for *C. glabrata* and 0.25 mg/L for *C. albicans*).

3.4. Sequencing of CgPDR1 allele encoded by the azole-resistant *Candida glabrata* isolates.

To sequence the CgPDR1 gene encoded by the azole-resistant *C. glabrata* isolates, genomic DNA was obtained and used as a template to amplify, by PCR, the CgPDR1 gene. To obtain DNA from the isolates two loops of biomass were added to approximately 100 μ L of glass beads (0.5 mm) and 200 μ L lysis buffer (Tris 50 mM, EDTA 50 mM, NaCl 250 mM, SDS 0.3 %). The tubes were vortexed for 2 min at maximum speed, incubated at 65°C for 1h and put on ice for 2 min. The disrupted cell suspension was afterwards vortexed, centrifuged at 13000 rpm for 15 min at 4°C and DNA precipitation was promoted by adding 20 μ L of NaAc 3M (pH 4.8) plus 400 μ L of cold ethanol to the recovered supernatant. The samples were left at -20°C for at least 30 min and then centrifuged at 13000 rpm, during 20 min at 4°C. The pellet obtained was washed with 500 μ L of ethanol 70%, and then centrifuged at 13000 rpm during 8 min at 4°C. The supernatant was discarded, and the pellet dried in speed vacuum. The obtained DNA was resuspended in 30 μ L deionized water. The extracted DNA was used as a template to amplify CgPDR1 by PCR and the corresponding PCR was sequenced (at least twice and using independent PCR products) at STAB Vida (Portugal) as a paid service.

3.5. Assessment of CgCDR1 and CgPUP1 expression in azole-resistant strains.

The transcript levels of CgCDR1 and CgPUP1 genes were compared in seven azole-resistant strains and in CBS138 during exponential growth by RT-PCR. For this, cells were grown in YPD at 30°C with orbital agitation (250 rpm) overnight and then inoculated in 150 mL of RPMI with an initial OD of 0.1 and grown at 30°C and 250 rpm orbital shake. When the OD₆₀₀ nm of the cultures were achieved approximately an OD of 2 cells were harvested by centrifugation (8000xg, 7 min, 4°C – Beckman J2.21 Centrifuge, rotor JA.10) and immediately frozen at -80°C until further use. RNA extraction was performed using the hot-phenol method. Conversion of the recovered RNA from the different cultures into cDNA was performed using 1 μ g of RNA in the C1000 Thermal Cycler (Bio-Rad, Hercules, USA). The subsequent quantitative PCR step was performed using 2.5 μ L of the cDNA and SYBR® Green super mix (BioRad)

in the 7500 Real-Time PCR System (Applied Biosystems). Primer sequences used are available in Table IV. 1.

3.6. Comparative transcriptomics of azole resistant isolates FFUL443, FFUL674 and ISTB218 with laboratory strain CBS138

Transcriptomic profile of isolates FFUL443, FFUL674 and ISTB2018 was compared during exponential growth in RPMI medium using a species-specific DNA microarray for *C. glabrata* [281]. For this, an individual colony of the FFUL443, FFUL674 and ISTB218 isolates was inoculated in YPD at 30°C with orbital agitation (250 rpm) overnight and then re-inoculated (at an initial OD_{600nm} of 0.1) in 150 mL of RPMI and left to grow at 30°C and 250 rpm orbital shake. When the OD_{600nm} of the cultures achieved 2 (corresponding to mid-exponential phase) cells were harvested by centrifugation and immediately frozen at -80°C until further use. RNA extraction was performed using RiboPure™ RNA Isolation Kit (Ambion, Life Technologies, CA). The quality and integrity of the purified RNA was confirmed in a Bioanalyzer. cDNA synthesis, hybridization, and scanning were performed using the Agilent protocol for two-color Microarray-Based Gene Expression Analysis Low Input Quick Amp Labeling v6.9 (Agilent Technologies), according to the manufacturer's instructions. One hundred nanograms of total RNA were used to synthesize labeled cDNA (with Cyanine 3-CTP), using Agilent T7 Promoter Primer and T7 RNA polymerase Blend (Agilent Technologies, Cat.5190–2305). Six hundred nanograms of labelled cDNA were hybridized in the microarray. Hybridizations were carried out using Agilent gasket slides in a rotating oven for 17 h at 65°C. Slides were then washed following manufacturer's instructions and scanned in an Agilent G2565AA microarrays scanner. Probes signal values were extracted using Agilent Feature Extraction Software. Data were normalized using median centering of signal distribution with Biometric Research Branch BRB-Array tools v3.4.0 software [299]. Final statistical analysis was carried out using LIMMA package in MeV software (MultiExperiment Viewer 4.8.0) [300] with a cut-off *p*-value of 0.1. Data was deposited at GEO with reference number GSE166841.

3.7. Genomic profiling of isolates ISTB218 (azole-resistant) and ISTA29 (azole-susceptible)

ISTB218 and ISTA29 cells were cultivated in YPD growth medium (up to an OD_{600nm} of ~3.0) and then centrifuged at 5000 rpm for 5 min at 4°C. The pellet was resuspended in 1 ml solution A (1 M Sorbitol (Sigma); 0.1 M EDTA (tetrasodium salt dehydrate) at pH 7.5). Afterwards, 10 mg/mL zymolyase (Zymo research) was added to the cellular suspension and the solution was incubated at 37°C until protoplast formation. The suspension was centrifuged at 5000 rpm for 5 min and the pellet resuspended in 1 mL solution B (50 mM Tris-HCL at pH 7.4 (Sigma-Aldrich), 20 Mm EDTA). After this step, 30µL of SDS (10%) was added to the mixture and this was left for 30 min at 65°C. Potassium acetate (250µL, 5 M; Merck) was subsequently added and the mixture was left for 1 h on ice. The suspension was clarified by centrifugation (10000 rpm for 10 min), and the supernatant was transferred to two fresh microfuge tubes. One volume of cold isopropanol was used to precipitate the pellet followed by centrifugation at 5000 rpm

for 15 min. Supernatant was discarded, and the resulting pellet was incubated in 1 mL ethanol 70% during 5 min and washed with ethanol 70% twice. The pellet was then dried in speed vacuum and resuspended in 200 μ L TE (pH7.4). Whole-genome sequencing was performed using Illumina HiSeq at CD Genomics, as a paid-service. Two rounds of paired-end sequencing were performed resulting in approximately 16 million reads for ISTB218 and 7 million reads for ISTA29, with an average size of 150 bp. The obtained reads for the two isolates were trimmed based on quality and then mapped against the genome of CBS138 for calling of SNPs and Indels using the tools available on CLC Genomics Workbench V21.0.1. Data concerning this whole-genome sequencing project was deposited at NCBI under the tag of Bioproject PRJNA699880.

3.7. Susceptibility assays to fluconazole of Δ Cg*pdr1* and Δ Cg*pdr1* Δ Cg*gal11a* *Candida glabrata* cells expressing different Cg*PDR1* alleles.

SKY107 (Δ Cg*pdr1*) cells or LYS2 (Δ Cg*pdr1* Δ Cg*gal11a*) cells were transformed with the pYR29-MycHis_Cg*PDR1* plasmid to drive the expression of the wild-type Cg*PDR1* allele; or with the engineered plasmids pYR29_Myc-HIS_Cg*PDR1*^{A820C}, pYR29-Myc-HIS_Cg*PDR1*^{T1176G} and pYR29-Myc-His_Cg*PDR1*^{T2408C} to drive the production of the GOF variants K274Q, I392M or I803T, respectively. The transformants were cultivated overnight, at 30°C and with an orbital agitation of 250 rpm, in minimal medium without uracil and on the next day the cells were re-inoculated in fresh MM medium at an OD_{600nm} of 0.1. The cells were left to grow (at 30°C and with an orbital agitation of 250 rpm) until mid-exponential phase (DO_{600nm}~0.8) and used to prepare a cell suspension (in PBS) with an OD_{600nm} of 0.05. 4 μ L of this cell suspension and of corresponding 1:4 and 1:16 of it were applied as spots onto the surface of solid MM or YPD either or not supplemented with the indicated concentrations of fluconazole. For the determination of MICs for fluconazole in these transformants the same procedure detailed above for the clinical isolates was used.

Table IV. 1. List plasmids and primers used in this study. In the case of the plasmids it is also provided their origin while in the case of the primers it is indicated for which their application was used for.

Plasmid	Plasmid Description	Reference
pSP76	Plasmid that drives expression of <i>CgPDR1</i> from its natural promoter and terminator	Khakhina, S, <i>et al.</i> 2018
pYR29_Myc-HIS_CgPDR1 ^{WT}	Plasmid that drives expression of <i>CgPDR1</i> from its natural promoter and terminator	This study
pYR29_Myc-HIS_CgPDR1 ^{A820C}	Plasmid that drives the gene expression and consequent production of the K274Q CgPdr1 mutant from its natural promoter and terminator	This study
pYR29-Myc-HIS_CgPDR1 ^{T1176G}	Plasmid that drives gene expression and consequent production of the I392M CgPdr1 mutant from its natural promoter and terminator	This study
pYR29-Myc-His_CgPDR1 ^{T2408C}	Plasmid that drives gene expression and consequent production of the I803T CgPdr1 mutant from its natural promoter and terminator	This study
Primer ID	Sequence (5' - 3')	Used for
CgPDR1_FW1	CTTCCATTACTTCGTACCC	CgPDR1 amplification and sequencing
CgPDR1_FW2	GCCTAGTACAAGAAGAACAAAAGTTG	CgPDR1 sequencing
CgPDR1_FW3	TCCATTGACGCCATTGAGTTACAAC	CgPDR1 sequencing
CgPDR1_FW4	TTACGACCGCAATTTGGACTCAGAGG	CgPDR1 sequencing
CgPDR1_REV4	CACACTAAGATCCATTGGCTTTTGAAT	CgPDR1 sequencing
CgPDR1_REV3	CAGAGTGCCAAAGTATGCAGCCTT	CgPDR1 sequencing
CgPDR1_REV2	CGGCGAGGGTAAATTCAACTGATAC	CgPDR1 sequencing
CgPDR1_REV1	GACAGTGTGCATAGCCTG	CgPDR1 amplification and sequencing
K274Q_FW	AAGATTAATGAAAGTGCCACCACTCAGTC ACTTGAAACAAACTTG	Site directed mutagenesis
K274Q_RV	CAAGTTTGTTCCTCAAGTACTGAGTGGTGG CACTTTCATTAATCTT	Site directed mutagenesis
I392M_FW	GATATCGATGGCCAACCCGTTAG	Site directed mutagenesis
I392M_RV	GACTCTTCATTGATATGGTGAACAC	Site directed mutagenesis
I803T_FW	ATGAATGAACTATCCTAAGTATGG	Site directed mutagenesis
I803T_RV	TACTTTCCAGTGCTCATATAGTC	Site directed mutagenesis
CgPDR1_FW_RT	GCTTGCCCCGCACATTGA	qPCR
CgPDR1_REV_RT	CCTCAGGCAGAGTGTGTTCTTTC	qPCR
CgPUP1_FW_RT	CACTGGTGCCTGAAAGGTG	qPCR
CgPUP1_REV_RT	TGTCCCAGGCTATCTTTGCC	qPCR
CgRDN25_FW_RT	AACAACCTACCGGCCGAAT	qPCR
CgRDN25_REV_RT	CAAGCGTGTTACCTATACTCCGCCGTCA	qPCR

4. Results

4.1. Distribution of *Candida* species among a cohort of isolates recovered across epidemiological surveys undertaken in Portugal

For the present study, we made use of 1270 *Candida* clinical isolates collected from patients attending hospitals in the Lisbon area, in Portugal, between 2015 and 2017. *C. albicans* was, by far, the species more frequently isolated comprising 922 isolates, followed by *C. glabrata* (154 isolates), *C. tropicalis* (62 isolates), *C. parapsilosis* (61 isolates), *C. krusei* (40 isolates), *C. lusitanae* (12 isolates), *C. kefyr* (10 isolates) and the rare *C. guilliermondii* (2 isolates), *C. dubliniensis*, *C. sake* and *C. inconspicua* (1 isolate each) (Figure IV. 1 and Annex Table IV. 1). Around 92% of the isolates examined were retrieved from non-sterile sites including vaginal exudates, urine, skin, or feces, the remaining being retrieved from sterile products like hemocultures (Annex Table IV. 1). *C. albicans* was the more frequent species isolated from all types of products, in line with the described versatility of this species as a human colonizer [301]. *C. glabrata* was, in almost all cases, the second more frequently isolated species (Figure IV. 1). It was of note the isolation of *C. tropicalis*, *C. parapsilosis*, *C. krusei* and *C. kefyr* in hemocultures, consistent with their reported ability to cause invasive candidiasis, including *C. kefyr* whose relevance in candidemia is poorly studied but increasing [302, 303]. Since MALDI-TOF cannot clearly distinguish *C. albicans* from its closely related variant *C. albicans var africana* [304, 305] and in Portugal this biovariant has not been described, we profiled our cohort of *C. albicans* strains for growth in minimal media having N-acetylglucosamine as the sole source of carbon as *C. albicans var africana* cells are unable to use this carbon source [304]. Eight *C. albicans var africana* strains could be identified, seven being recovered from vaginal exudates, consistent with the human genitourinary tract being its primary colonization niche [304, 305](Annex Table IV. 1).

4.2. Profile of resistance to fluconazole and voriconazole among the *Candida albicans* and *Candida glabrata* strains

We randomly selected 401 *C. albicans* and 78 *C. glabrata* strains (details in Annex Table IV. 1) for a profile of resistance to fluconazole and voriconazole. The strains were first phenotyped for their ability to grow in the presence of concentrations of fluconazole and voriconazole equal to the resistance breakpoints defined by EUCAST (32 mg/L of fluconazole and 1 mg/L of voriconazole for *C. glabrata* and 4 mg/L of fluconazole and 0.25 mg/L of voriconazole for *C. albicans*). Isolates exhibiting a growth reduction in the presence of the azoles of, at least, 25% of the growth registered in drug-free medium were selected for individual determination of the MIC of the two azoles (Annex Table IV. 1). This analysis led to the identification of 13 *C. albicans* and 4 *C. glabrata* isolates with MICs for fluconazole and voriconazole above the resistance breakpoint, while two *C. albicans* isolates (ISTB16 and ISTB284) could only be considered resistant to fluconazole (further details in Annex Table IV. 1).

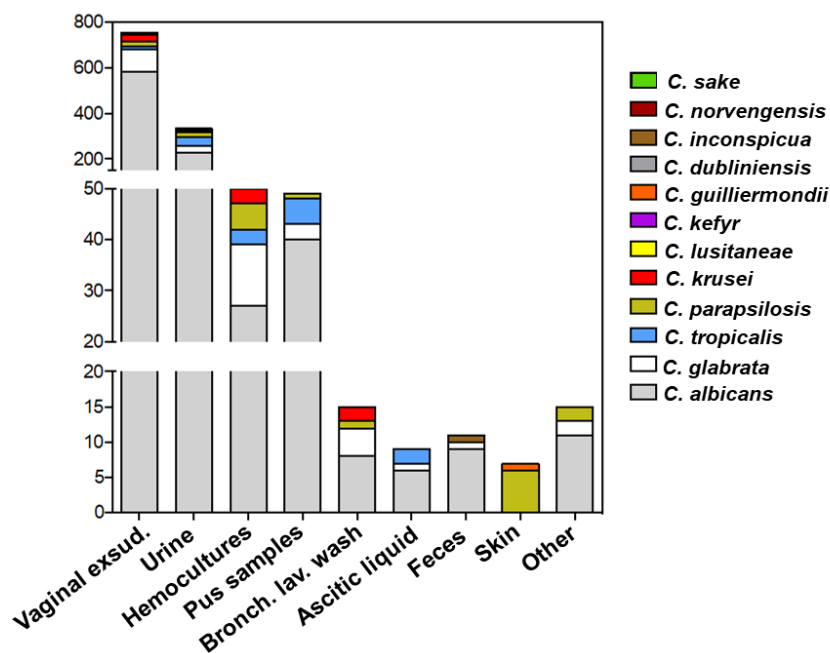


Figure IV. 1. Species distribution of the collection of *Candida* isolates examined in this work according to the product they were retrieved from. Species of the *Candida* genus were identified on MALDI-TOF profiling.

4.3. Sequencing of the *CgPDR1* allele encoded by the azole-resistant *Candida glabrata* isolates.

We focused then on the four identified *C. glabrata* azole-resistant strains identified in our cohort: ISTB218, ISTA56, ISTB607, ISTB556. We started by examining the sequence of the *CgPDR1* allele encoded by these strains with the results being shown in Table IV. 2. (Annex Table IV. 2 provides further details). We also included in this analysis six *C. glabrata* azole-resistant strains (FFUL412, FFUL443, FFUL674, FFUL830, FFUL866 and FFUL878) recovered from previous epidemiological surveys and that were also identified by our laboratory as azole resistance but whose underlying resistance mechanism was not further characterized [55](Chapter III). The *CgPDR1* gene encoded by all the examined strains exhibited the non-synonymous substitutions S76P, V91I, L98S, T143P and/or D243N, previously described to occur both in azole susceptible and resistant *C. glabrata* strains (Table IV. 2 and Annex Table II. 1). Two of the azole-resistant isolates encode the demonstrated R376W (ISTB556, ISTB607) GOF *CgPdr1* variant [51], while isolates FFUL866/FFUL830, FFUL412/FFUL443, ISTA56 and FFUL674 encode *CgPDR1* alleles with the E555K, I392M, G558C and I803T substitutions. All these substitutions were previously identified in azole-resistant strains but not in susceptible ones for which they were considered to represent *CgPdr1* GOF variants and to mediate the azole-resistance phenotype of the strains [6, 47, 51, 208, 296]. In line with this idea, isolates expressing these *CgPDR1* alleles (FFUL830, ISTA56 and ISTB607) over-express (comparing to the susceptible reference CBS138 strain) the *CgPdr1*-targets *CgCDR1* and *CgPUP1* during growth in unsupplemented RPMI medium, a phenotype observed in strains expressing *CgPDR1* GOF alleles [51] (Figure IV. 2 panel A). Isolate ISTB218 was found to encode a *CgPDR1* allele with no other modification besides those also observed in the susceptible strains (Table IV. 2).

Table IV. 2. Results obtained upon sequencing of the *CgPDR1* gene from the seven azole-resistant *Candida glabrata* strains examined in this study. The non-synonymous modifications found in the coding sequencing of the *CgPDR1* gene encoded by the strains are compared with the one of the azole-susceptible reference strain CBS138. Those modifications demonstrated before as CgPdr1 GOF variants are marked in black boxes, while those previously reported in azole-resistant strains but not in susceptible ones are indicated in grey boxes. SNPs described in azole susceptible and resistant strains are underlined. The herein described I392M and I803T substitution is indicated in the orange box.

Strain/Position	76	91	98	143	173	243	274	376	392	555	558	803
CBS138	S	V	L	T	D	D	K	R	I	E	G	I
FFUL412/FFUL443	<u>P</u>	<u>I</u>	<u>S</u>	<u>P</u>					M			
FFUL674		<u>I</u>	<u>S</u>			<u>N</u>						T
FFUL830/FFUL866		<u>I</u>	<u>S</u>			<u>N</u>				K		
FFUL878/FFUL887		<u>I</u>	<u>S</u>			<u>N</u>	Q					
ISTA56		<u>I</u>	<u>S</u>			<u>N</u>					C	
ISTB556/ISTB607		<u>I</u>	<u>S</u>			<u>N</u>		W				
ISTB218		<u>I</u>	<u>S</u>			<u>N</u>						

4.4. The I803T and I392M substitutions are new gain-of-function CgPdr1 variants.

The azole-resistant *C. glabrata* isolates FFUL443 and FFUL674 encode *CgPDR1* alleles, resulting in the aminoacid substitutions I392M and I803T respectively, that were observed in azole-resistant strains but not further studied [6, 51]. To test whether these two substitutions indeed represent new CgPdr1 GOF variants, the expression of the CgPdr1-target genes *CgCDR1* and *CgPUP1* was compared in isolates FFUL443 and FFUL674 and in the azole susceptible strain CBS138 during growth in drug-free RPMI medium (Figure IV. 2 panel A). These two genes were selected among those comprising the CgPdr1 regulon because they are the sole CgPdr1 targets consistently up-regulated by strains encoding *CgPDR1* GOF alleles [51]. The two isolates clearly over-expressed (comparing with the transcript levels produced in the azole-susceptible CBS138 strain) *CgCDR1*, while *CgPUP1* was only over-expressed in FFUL443 (Figure IV. 2 panel A). Global transcriptomic profiling of FFUL443, FFUL674 and CBS138 strains during growth in RPMI medium further revealed that, compared to the transcript levels of the CBS138 strain, the isolates over-express 87 (for the FFUL443 strain) and 44 (for the FFUL674 strain) genes described to be activated by CgPdr1, including 6 (*CAGL0K09702g*, *CgCDR1*, *CgPDH1*, *CgPUP1*, *CgQDR2*, *CAGL0A01650g*, *CgNCE103*) directly regulated by this transcription factor (Figure IV. 2 panel B and Annex Table IV. 3 and Annex Table IV. 4) - according with the information available in the PathoYeast database [141]. This observation supports the idea that the herein described I803T and I392M CgPdr1 variants are GOF mutants. To clearly demonstrate this, we ectopically expressed *CgPDR1* gene individually expressing these substitutions in a $\Delta Cgpdrl$ background (Figure IV. 2 panel C). The results obtained confirmed that both substitutions significantly enhance tolerance to fluconazole, compared with the tolerance provided by a wild-type *CgPDR1* allele (Figure IV. 2 panel C). The K274Q mutation described in the previous Chapter III [55] was confirmed to have the same protective effect as the other two GOFs.

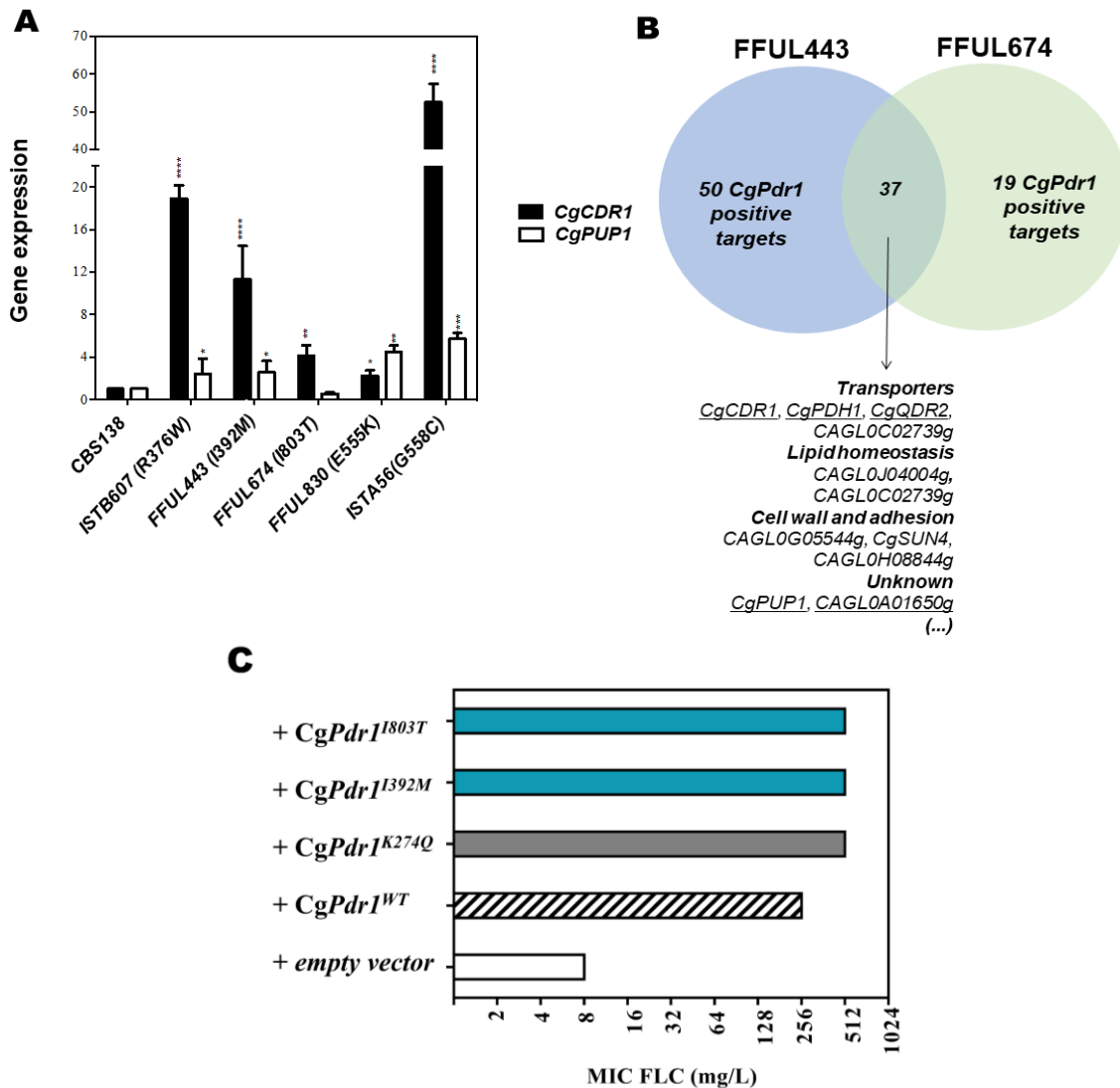


Figure IV. 2. Comparative gene and genomic expression between the azole-susceptible strain *Candida glabrata* CBS138 and the azole-resistant isolates FFUL443 and FFUL674, encoding a *CgPDR1* allele that harbors the not previously described non-synonymous substitution I392M and I803T. (A) The expression of *CgCDR1* and of *CgPUP1* was compared in CBS138, FFUL443 and FFUL674 cells during cultivation in drug-free RPMI medium until mid-exponential phase. The level of expression registered in the CBS138 was set at 1 and the other values compared with that. The transcript levels of *CgRDN25* were used as an internal control. The expression level of these two described *CgPdr1*-target genes was also monitored in isolates, FFUL830 and ISTA56 encoding, respectively, E555K and G558C, also found in azole-resistant isolates. As a positive control, the expression of *CgPUP1* and *CgCDR1* genes in ISTB607 strain was also monitored, encoding the demonstrated *CgPdr1* GOF variant R376W. (B) Venn diagram showing the number of *CgPdr1* documented activated genes (according to the information available in the PathoYeast database) found to be over-expressed in the transcriptome of isolates FFUL443 and FFUL674 cultivated in the same growth conditions (compared with transcript levels registered in the azole-susceptible strain CBS138). (C) MIC for fluconazole assessed by the recommended EUCAST microdilution method obtained for SKY107 cells transformed with plasmid pYR29-MycHis which drives expression of *CgPDR1* from its natural promoter and terminator and in the derived plasmids that encode the *CgPDR1* allele with the individual substitutions I392M and I803T. As a control, the described *CgPdr1* GOF variant K274Q was also used.

4.5. The I392M and K274Q CgPdr1 gain-of-function variants rely on the mediator subunit CgGal11A to enhance tolerance to fluconazole in *Candida glabrata*, while only a partial dependence for CgGal11A is observed for cells encoding the I803T variant.

The role of the CgGal11A mediator complex in activating CgPdr1 upon exposure of *C. glabrata* cells to azoles has been demonstrated [105, 181] but different CgPdr1 GOF variants have been found to depend on different degrees of this transcriptional regulatory complex component [181]. Therefore, we examined the effect of deleting this subunit in the ability of the CgPdr1^{I392M} and CgPdr1^{I803T} variants to increase resistance to azoles (Figure IV. 3). For the sake of comparison, we have also included in this experiment the previously characterized CgPdr1^{K274Q} GOF allele (Chapter III)[55]. As expected, the ability of a wild-type CgPDR1 allele to restore tolerance to fluconazole in a Δ Cgpdrl mutant was fully dependent on CgGAL11A (Figure IV. 3 and Annex Figure IV. 1). A similar dependence was also observed in cells producing the K274Q and I392M variants, although cells devoid of CgPDR1 and CgGAL11A were more tolerant to fluconazole in YPD when expressing the gene encoding the CgPdr1^{I392M} GOF variant than when expressing the wild-type (Figure IV. 3). In Δ Cgpdrl cells expressing the gene encoding the CgPdr1^{I803T} allele we could not detect a significant effect in tolerance to fluconazole upon the deletion of CgGAL11A, nor in YPD nor in minimal medium (Figure IV. 3). The results of these susceptibility assays undertaken in solid medium supplemented with fluconazole were consistent with the MICs for fluconazole obtained with the same Δ Cgpdrl and Δ Cgpdrl Δ Cggal11a strains expressing the different CgPDR1 alleles (shown in Annex Figure IV. 1).

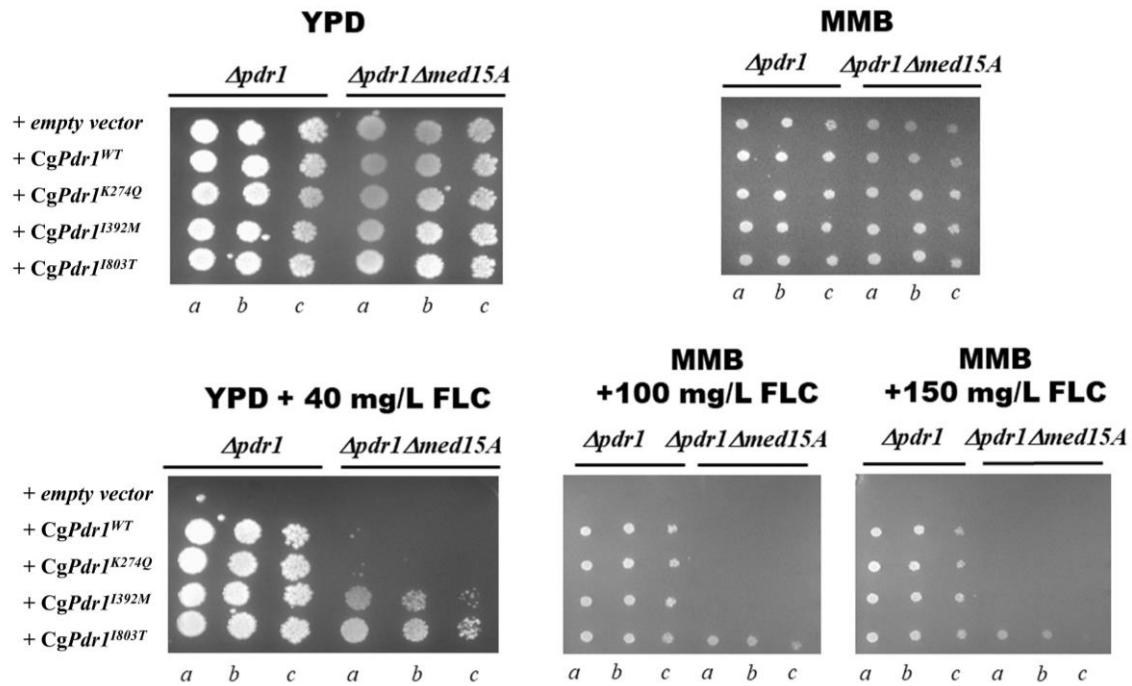


Figure IV. 3. Influence of the CgGal11A mediator subunit in tolerance to fluconazole of *Candida glabrata* cells producing the wild-type or the gain-of-function K274Q, I392M and I803T CgPdr1 variants. Δ Cgpd1 (SKY107) or Δ Cgpd1 Δ Cggal11a (LYS2) cells were transformed with the pYR29-MycHis_CgPDR1 plasmid (which drives expression of CgPDR1 from its natural terminator and promoter) or with the derived plasmids pYR29-MycHis_CgPDR1^{A820C}, pYR29-MycHis_CgPDR1^{T1176G} or pYR29-MycHis_CgPDR1^{T2408C}, encode the corresponding K274Q, I392M and I803T variants, and were used to compare susceptibility to fluconazole by spot assay in MM or in YPD rich medium. Final cell suspension of mid-exponential phase cells was prepared with an OD_{600nm} of 0.05 and dilutions of the cell suspension are spotted. Growth was compared after two to three days of incubation at 30°C, depending on the severity of growth inhibition.

4.6. OMICS profiling of the azole-resistant isolate *Candida glabrata* ISTB218, encoding a “wild-type” CgPDR1 allele

The azole-resistant isolate *C. glabrata* ISTB218 encodes a CgPDR1 allele not having non-synonymous substitutions that could be linked with azole-resistance and was therefore subjected to a genomic and transcriptomic profiling to elucidate the underlying resistance mechanism exhibited by this strain. During cultivation in RPMI growth medium 490 genes could be considered differently expressed (above a threshold level of 2-fold) in the ISTB218 isolate and in CBS138, 250 genes being more transcribed in the isolate and 240 genes more expressed in the lab strain (Annex Table IV. 5). Only 1 gene documented to be directly regulated by CgPdr1 was found among the genes up-regulated in ISTB218 (the ORF CAGLOA01650g, with unknown function) (Annex Table IV. 5). These observations are consistent with ISTB218 encoding a “wild-type” CgPdr1, inactive when cells are growing in the absence of a xenobiotic [62]. Three genes documented to confer protection against azoles in *C. glabrata* were found to be over-expressed in the ISTB218 isolate including the transcriptional regulator CgMIG1; CAGLO110923g, predicted to be involved in the biosynthesis of liponic acid; and CgRCN1, encoding a positive regulator of

the calcineurin pathway (Table IV. 3). *CgRCN2* and the two calmodulin-dependent protein kinases, described inhibitors of the *C. glabrata* calcineurin pathway [306], were down-regulated in the ISTB218 strain (Table IV. 3). Altogether these observations are consistent with the idea that calcineurin signaling can be more active in ISTB218 cells. The transcriptomic profiling also revealed the up-regulation in the ISTB218 strain of *CAGL0L03828g*, predicted to encode a cytochrome b5/NADH cytochrome b5 reductase electron transport system that in *S. cerevisiae* was shown to mediate sterol 14 α -demethylation (the reaction catalyzed by Erg11 [307]); and of *CAGL0F05137g*, encoding a predicted transporter of sterols between the ER and the plasma membrane (Table IV. 3). Sixteen genes whose deletion improves tolerance to azoles in *C. glabrata* were found to be down-regulated in ISTB218 out of which the more prominent was *CAGL0M08624g*, encoding a protein of unknown function (down-regulated around 15-fold), and the mitochondrial genes *CAGL0K01419g* and *CAGL0L12320g* (Table IV. 3 and Annex Table IV. 5).

Previous comparative genomic analyses involving *C. glabrata* clinical isolates and the CBS138 strain revealed a massive number of SNPs, making very difficult the establishment of relevant genotype to phenotype associations [55, 67, 283]. Thus, besides performing the whole-genome sequencing of ISTB218 we have also sequenced a randomly selected azole susceptible strain, ISTA29. The genomic structural alterations registered in these two strains, using CBS138 as a comparative platform, led to 700 non-synonymous SNPs that were only found in the azole-resistant strain ISTB218 (Annex Table IV. 6). It was evident that the genes involved in adhesion were those more divergent between ISTB218, ISTA29 and CBS138 strains (Figure IV. 4), this being in line with the results obtained in previous genomic comparisons involving CBS138 and clinical strains [55, 283]. Seventeen documented azole-resistance genes were found to harbor specific SNPs in the azole-resistant ISTB218 strain the adhesins *CAGL0L00157g* and *CAGL0C00231g*, the protein kinase *CgSLT2*, the ABC transporters *CgSNQ2* and *CgPDR12*, the *CgJJJ1* negative regulator of *CgPdr1* activity, the transcriptional regulator *CgRPN4* or the sterol transporters *CgTIR3* and *CAGL0F03267g* (Table IV. 4 and Annex Table IV. 6). We could not detect SNPs in the coding sequences of *CgMSH2* or *CgERG11*, in line with previous genomic analyses undertaken with other azole-resistant isolates that also failed to identify modifications in these genes [55, 283]. We could also identify 20 genes exhibiting frame-shifts leading to premature truncations in ISTB218 isolate (Annex Table IV. 6). Of these, only the inactivation of *CAGL0J00847g*, a subunit of the succinate dehydrogenase complex, results in improved tolerance to azoles [40] (Table IV. 4 and Annex Table IV. 6). The observed truncation in the ISTB218 strain of the aquaporine *CAGL0D00154g* (similar to ScAqy1) (reported previously in another clinical strain [283]) was also interesting considering that transcript levels of its homologue *CAGL0A01221g* were also strongly down-regulated in these cells (Annex Table IV. 5 and Annex Table IV. 6).

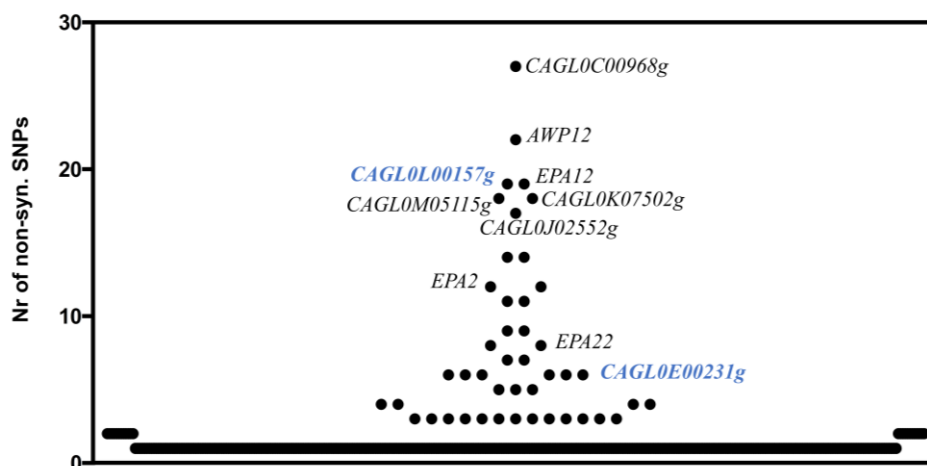


Figure IV. 4. Number of non-synonymous single-nucleotide polymorphisms found upon the comparison of gene sequences encoded by the azole-resistant strain ISTB218 and the azole-susceptible strains CBS138 and ISTA29. The names of adhesin-encoding genes are depicted in the figure to denote the high number of SNPs found in these sequences encoded by the azole-resistant strain ISTB218. Those adhesins that are described to provide protection against azoles in *C. glabrata* are highlighted in blue.

Table IV. 3. Results from the comparative transcriptomic analysis between the azole-resistant *Candida glabrata* strain ISTB218 and the azole-susceptible strain CBS138 during growth in RPMI medium until mid-exponential phase, as suggested by DNA microarray analyses. A selected set of genes found to be differently transcribed (above or below 2-fold) in the two strains (the full list is available in Annex Table IV. 5) is shown in this table, along with the description of their function and the reported outcome of gene deletion in tolerance to azoles in *C. glabrata* (green denotes a gene whose deletion results in improved tolerance to azoles; in red denotes a gene whose deletion results in decreased susceptibility to azoles).

<i>C. glabrata</i> ORF/ Standard Name	<i>S. cerevisiae</i> ortholog	mRNA ISTB218/ mRNA CBS138	Function
Metabolism and transport of sterols			
CAGL0L03828g	<i>CYB5</i>	2,92	Ortholog(s) have electron transfer activity and possible role in ergosterol biosynthetic process
CAGL0I10923g	<i>LIP5</i>	2,49	Ortholog(s) have role in protein lipoylation
CAGL0F05137g	<i>PRY2</i>	4,66	Ortholog(s) have a role in transport of sterols
Cell signalling			
CAGL0J04158g/Cg <i>RCN2</i>	<i>RCN2</i>	-2,50	Negative regulator of the calcineurin-Crz1p pathway
CAGL0F04741g	<i>CMK2</i>	-2,40	Predicted calmodulin-dependent protein kinase
CAGL0K10604g	<i>CMK1</i>	-2,36	Predicted calmodulin-dependent protein kinase
CAGL0E06248g/Cg <i>RCN1</i>	<i>RCN1</i>	2,10	Positive regulator of the calcineurin pathway
Other functions			
CAGL0A01221g	<i>AQY1</i>	-9,05	Predicted aquaporine
CAGL0F00957g/Cg <i>TPD3</i>	<i>TPD3</i>	-2,83	Putative serine/threonine protein phosphatase
CAGL0H00847g	<i>HUT1</i>	-2,28	Ortholog(s) are involved in UDP-glucose transmembrane transport
CAGL0K01243g	<i>MRPL25</i>	-2,02	Predicted mitochondrial large ribosomal subunit
CAGL0C01331g	<i>HPM1</i>	-2,18	Ortholog(s) have a role in positive regulation of translational fidelity and ribosomal large subunit assembly
CAGL0C02541g	<i>BDF1</i>	-2,22	Ortholog(s) have TFIID-class transcription factor complex binding
CAGL0K12056g	<i>RSM10</i>	-2,25	Predicted role in translation in the mitochondria
Unknown function			
CAGL0A02299g	no ortholog	-14,59	Unknown
CAGL0G01628g	<i>YNL035c</i>	-2,24	Unknown
Transcription			
CAGL0A01628g/Cg <i>MIG1</i>	<i>MIG1</i>	2,31	Transcriptional activator
CAGL0K01419g	<i>MTF2</i>	-3,02	Ortholog(s) are involved in mitochondrial translation
CAGL0L12320g	<i>GEP5</i>	-2,90	Ortholog(s) are involved in mitochondrial translation
CAGL0F05577g	<i>MSS116</i>	-2,60	Ortholog(s) have ATP-dependent RNA helicase activity
CAGL0I06380g/Cg <i>RPM2</i>	<i>RPM2</i>	-2,27	Mitochondrial RNase P precursor
CAGL0M08624g	<i>MSW1</i>	-2,24	Ortholog(s) have tryptophan-tRNA ligase activity
CAGL0C02541g	<i>BDF1</i>	-2,22	Ortholog(s) have TFIID-class transcription factor complex binding

Table IV. 4. SNPs identified in the gene sequences encoded by the azole-resistant ISTB218 strain but not by the azole susceptible strains ISTA29, as suggested upon whole-genome sequencing of the clinical strains and subsequent comparison with the available genomic sequence of CBS138. It is indicated the alteration found in the coding sequence of the gene encoded by the ISTB218 strain and the effect that deletion of genes have on azole tolerance. In green denotes a gene whose deletion results in improved tolerance to azoles; in red denotes a gene whose deletion results in decreased susceptibility to azoles. Fs, denote changes exhibiting frame-shifts resulting in premature truncation.

<i>C. glabrata</i> ORF/ Standard Name	<i>S. cerevisiae</i> ortholog	Function	ISTB218 amino acid modification (comparing with CBS138)
CAGL0F03267g	<i>LAM4</i>	Orthologs bind and perform inter-membrane transfer of sterols	Insertion of LysSerAspAlaHisSer between Ser231 and His232
CAGL0C03872g/Cg <i>TIR3</i>	<i>TIR3</i>	Putative GPI-linked cell wall protein involved in sterol uptake	Deletion between Val152 and Ser166
Cell signaling			
CAGL0J01892g/ Cg <i>PAN1</i>	<i>PAN1</i>	Ortholog(s) have a role in actin cortical patch assembly,	Gln104fs
CAGL0I06512g/ Cg <i>BEM2</i>	<i>BEM2</i>	Ortholog(s) have a role in actin cytoskeleton organization	Val1095Ile
CAGL0B02211g/Cg <i>CCH1</i>	<i>CCH1</i>	Putative calcium transporter; required for viability upon prolonged fluconazole stress	Tyr1585Ser
CAGL0J09702g/ Cg <i>ACK1</i>	<i>ACK1</i>	Ortholog(s) have a role in the regulation of the cell wall integrity pathway	Gly627fs
CAGL0J00539g/ Cg <i>SLT2</i>	<i>SLT2</i>	Protein kinase mediates the cell wall integrity pathway	Lys275Gln
Transcription			
CAGL0K01727g/Cg <i>RPN4</i>	<i>RPN4</i>	Transcription factor required for regulation of proteasome-encoding genes	Insertion of AlaGln between Gln99 and Met100
CAGL0L00583g	<i>USV1</i>	Ortholog(s) have a role in carbon catabolite activation of transcription from RNA polymerase II promoter	Lys175fs
CAGL0J07370g/ Cg <i>JJJ1</i>	<i>JJJ1</i>	Negative regulator of fluconazole resistance; mutation causes elevated expression of multidrug transporters <i>CDR1</i> and <i>CgPDR1</i>	Ala270Thr
Transport			
CAGL0I04862g/ Cg <i>SNQ2</i>	<i>SNQ2</i>	Plasma membrane ABC transporter	Pro1104His
CAGL0M07293g	<i>PDR12</i>	Plasma membrane ABC transporter	Tyr25His
CAGL0D00154g/Cg <i>AQY1</i>	<i>AQY1</i>	Has domain(s) with predicted channel activity	Phe49fs
CAGL0J00847g	<i>YJL045W</i>	Ortholog(s) have succinate dehydrogenase activity	Ala41fs

5. Discussion

In this study we shed light into the mechanisms of resistance to azoles in *C. glabrata* clinical strains, essential knowledge to understand how this pathogenic species acquires resistance *in vivo*, especially considering that many observations concerning azole resistance in laboratory strains often differ in clinical strains [reviewed e.g. in 4, 7]. Azole resistance of ten of the eleven *C. glabrata* resistant isolates that we characterized in this work was linked with the possible expression of CgPdr1 gain-of-function variants including the already confirmed GOF R376W, and the suggested G558C, E555K, I392M and I803T. Like many gain-of-function mutations described in CgPdr1, I392M, G558C, E555K and I803T substitutions map in the CRD of CgPdr1, with I803T being already close to the transactivation domain - located approximately in the fifty C-terminal amino acids [62]. While mutations embedded in the central regions of the CRD are believed to relieve its inhibitory effect over the transactivation domain, the effect of those located more closely to the transactivation domain is less clear, as recently shown [62, 181]. Comparative analysis of the transcriptomes of FFUL674, FFUL443 and FFUL887 isolates, encoding, respectively, the I803T, I392M and K274Q CgPdr1 variants, reveals an overlap of only 16 documented targets of CgPdr1 (Figure IV. 2 and Annex Table IV. 3 and Annex Table IV. 4). This reflects well the differential effect displayed by different GOF mutations over *C. glabrata* genomic expression, as observed before [46, 55, 117]. With the exception of CgCDR1 and CAGL0M08426g genes, all the 14 other presumed CgPdr1-targets over-expressed in the clinical isolates don't have a PDRE motif (the binding site for CgPdr1) in their promoter, as detailed in Annex Table IV. 3 and Annex Table IV. 4. This suggests that the effect of the GOF mutations in the CgPdr1-mediated alterations of the transcriptome is mostly indirect. Furthermore, it is particularly interesting the herein reported observation that cells expressing the CgPdr1^{I803T} variant have little dependence of the mediator complex subunit CgGal11A to induce azole tolerance, contrasting with the strong dependence exhibited by cells expressing the K274Q or I392M variants. These observations support the idea that GOFs modify the CgPdr1 interactome, this being an interesting issue to address in more dedicated studies.

The sole azole-resistant *C. glabrata* isolate identified in our study encoding a CgPDR1 allele not having substitutions linked with azole resistance was subjected to comparative transcriptomic and genomic analyses with two azole susceptible strains, this being the first exhaustive analysis of a clinical strain with these characteristics. The fact that in a cohort of eleven azole-resistant strains only one does not encode a gain-of-function CgPdr1 allele demonstrates the preponderance of this mechanism in driving resistance in *C. glabrata*, as also observed in *in vitro* evolution studies [63]. Two genes previously documented to confer protection against azoles were over-expressed in the ISTB218 strain including CgMIG1, poorly characterized in *C. glabrata* but known in *S. cerevisiae* for its role in glucose repression; and CgRCN1, a positive regulator of calcineurin. On the other hand, the two calmoduline kinases and CgRCN2, described inhibitors of calcineurin signaling [306], were down-regulated in ISTB218. Altogether these observations suggest that the calcineurine pathway can be more active in ISTB218 cells, a trait that favors azole tolerance in *C. glabrata* [306] and in other *Candida* species [308]. The over-expression in the ISTB218 strain of CAGL0L03828g, orthologous to the *S. cerevisiae* Cyb5 cytochrome, was another interesting response,

considering that ScCyb5 restores ergosterols biosynthesis in compensation of Erg11 inhibition [307, 309] and that Cyb5 protects *C. albicans* [310] against azoles. In this line, it was also noticeable the up-regulation of *CAGLOF05137g*, similar to the exporter of toxic sterols ScPry2 [311], and the prominent insertions detected in the coding sequences of *CAGLOF03267g*, involved in the inter-membrane transport of sterols from the ER to the plasma membrane [312](Table IV. 4). The inhibition of Erg11p by azoles induces the accumulation of toxic sterol intermediates in the plasma membrane and it is possible that modulation of the activity of sterols transporters can contribute for detoxification, either by promoting the export of toxic sterols (preventing their accumulation in the plasma membrane) or by enhancing the compensatory uptake of exogenous sterols. Interestingly, inactivation of the *CAGLOF03267g* that orthologue ScYps2 improves tolerance to azoles in *S. cerevisiae* [313] and the observed insertion detected in the coding sequence of *CgAQY1* of ISTB218 was also observed in another azole-resistant strain [55].

High-throughput phenotypic analyses undertaken in *C. glabrata* have been showing that the inactivation of multiple genes can result in improved azole tolerance, albeit the underlying mechanisms remain elusive [57, 314]. Sixteen genes described to enhance azole sensitivity were down-regulated in the ISTB218 strain, including proteins with a described role in mitochondrial function, in RNA metabolism, among others of unknown function. One of these genes, *CAGLOJ00847g*, encoding a subunit of the mitochondrial succinate dehydrogenase complex was also truncated in the ISTB218 strain (Table IV. 4). Although it is long known that loss of mitochondrial chromosome enhances azole resistance by activating CgPdr1 [4, 7, 55], inactivation of specific mitochondrial functions are also suggested to result in increased azole tolerance in a CgPdr1-independent manner [40]. Consistently, ISTB218 cells were found to be non-petite since they grow well on various non-fermentable carbon sources (results not shown). Altogether the transcriptomic profiling of the ISTB218 strain, in comparison with the lab strain CBS138, reveals a number of adjustments in the expression of genes that can modulate tolerance in *C. glabrata*, including the increase in expression of genes favoring protection and down-regulation of those that can augment azole toxicity.

Concerning the comparative genomic analysis, two of the genes found to differ more in ISTB218 and in the azole susceptible strains CBS138 and ISTA29, were *CAGLOL00157g* and *CAGLOE00231g*, encoding adhesins with a described positive role in tolerance to fluconazole [315]. Recently, it has also been described the beneficial effect of the adhesin Epa3 in azole tolerance contributed, among other aspects, to reduce the internal concentration of the azole [63]. Adhesion is under strong selective pressure in *C. glabrata* cells *in vivo* [55, 283, 287, 316] and although this has been attributed to the need of facilitating attachment and colonization of epithelial tissues, it is possible that such re-organization of proteins protruding from the cell envelope may positively influence resistance to azoles, for example, by restricting their entry inside the cells. Within this line of thinking it was also interesting the observed strong down-regulation and early truncation of two aquoglyceroporines, *CAGLOA01221g* and *CAGLOD00154g* as mounting evidence pointing to a mechanism of facilitated diffusion underlying entry of azoles to the inside of *Candida* cells [317].

On the overall, this study contributes to improve current understanding of acquired azole resistance in *C. glabrata* clinical isolates either by identifying two novel gain-of-function CgPdr1 variants that were not previously demonstrated, I803T and I392M, and by disclosing insights into possible CgPdr1-independent responses. These responses may include the up-regulation of genes maximizing protection to

azoles, the down-regulation of genes favoring susceptibility to azoles and/or the alteration of multiple genes connected with the metabolism of sterols that can compensate the azole-induced inhibition of Erg11. Necessarily a subsequent detailed genetic analysis should be performed to understand how these different mechanisms contribute, alone or in combination, for the azole-tolerance phenotype of the ISTB218 strain, however, such study is only possible upon the release of what can be the more promising candidates, information that is uncovered for the first time in this work and that is expected to pave the way for a deeper understanding of the acquisition to azoles *in vivo* in *C. glabrata*.

IV. Impact of gain-of-function mutations in different biochemical aspects of the activity of the transcription factor Pdr1 from *Candida glabrata*

1. Abstract

Increased activity of CgPdr1 gain-of-function variants is the main mechanism underlying resistance to azoles in clinical strains of *C. glabrata*. To date, the mechanisms by which these GOF mutations affect the biochemical activity of CgPdr1 remain elusive and in this chapter these were further investigated with emphasis on modifications described along the development of this thesis, K274Q, I392M and I803T. Starting from a reliable prediction of what can be the tri-dimensional structure of CgPdr1 an *in silico* analysis on the impact of GOF modifications was performed, with the results suggesting that these modifications happen in relevant structural features including the predicted fluconazole docking site, the transactivation domain and core structural regions involved in the control of the activity of the transactivation domain (specifically in restraining its activity). Two further exposed regions of the protein were identified to be enriched in CgPdr1 GOF variants, that may interfere with other regulatory mechanisms of CgPdr1 activity. Using ChIP-seq, it was examined whether the set of CgPdr1 promoter directly recognized *in vivo* was changed when the same *C. glabrata* cells express the wild-type or the CgPdr1^{K274Q} GOF variant. The results obtained showed that the set of genes recognized by the two CgPdr1 is essentially the same showing that the changes that prompt the expression of target genes are not determined by a different occupancy of the transcription factor in the promoters. Despite this, a different effect in expression of target gene of the two CgPdr1 variants was observed. To examine the impact of K274Q in CgPdr1 interactome, ChIP-SICAP accoupled with MS analysis was performed. The preliminary results did not allowed a clear set of proteins that could be considered as specifically interacting with one of the two CgPdr1 variants (for example, proteins that could only specifically interact with the K274Q variant), however, identifying several interactors of CgPdr1 were unveiled, including proteins involved in histone methylation, recently described to have a role in azole response in *C. glabrata*.

2. Introduction

The current shortage of antifungals in the market increases the need to understand, in a comprehensive manner, the molecular mechanisms that govern resistance of fungal cells to conventional molecules. Until thus far, in *C. glabrata* the emergence of gain-of-function mutations in the transcriptional regulator CgPdr1 remains the most predominant mechanism underlying resistance to azoles in clinical strains [7](Chapter IV). Further knowledge of the structural and regulatory effect of GOFs in the CgPdr1 protein could prove essential in the design of new potential antifungals that could complement azole antifungal therapy or even improve azole therapeutic molecules design. In this line, Nishikawa, J. L. *et al.* 2016 [212] have identified and subsequently characterized a new antifungal molecule, named iKIX1, that acts by destabilizing the interaction of CgPdr1 with the mediator complex (by binding to the KIX domain of CgGal11A which was found to bind CgPdr1) and consequently sensitizing *C. glabrata* azole-resistant strains. A second study, authored by Usher, J. and Haynes, K. 2019 [159], reported the ability of γ -butyrolactone (a molecule with medical uses for the treatment of sleeping disorders and alcohol withdrawal treatment [318]) to sensitize azole-resistant strains expressing CgPDR1 GOF alleles by inhibiting the histone acetyltransferase CgGcn5, identified as a strong genetic interactor of CgPdr1 hyperactive form (the deletion of CgGcn5 in a strain expressing different CgPDR1 GOF alleles was proven to be lethal or highly inhibiting of growth of the cells) albeit for unknown reasons [159]. These two studies represent clear examples of how the dissection of azole tolerance mechanisms can contribute to the design of new antifungals. Nonetheless, both molecules were found to have different degrees of inhibitory effects against the same strain of *C. glabrata* depending on the CgPdr1 GOF variant they encode [159, 212], which is in agreement with the idea that distinct GOF mutations act through independent mechanisms in mediating activation of CgPdr1 [62].

As discussed in Chapter III and IV of this thesis, the idea that different GOF mutations affect the biochemical activity of CgPdr1 distinctly has come from the differential effect these modifications exert in the genomic expression of *C. glabrata*, even if these modifications are found in the same predicted regulatory domain of the transcription factor [50, 54, 117, 194]. Despite this, the different genetic backgrounds of the strains examined are an important confounding factor that can difficult a more accurate interpretation of the results and detail what is the individual contribution of each CgPdr1 GOF modification. More recently, other evidence contributing to the idea that GOF mutations differently affect the biochemical activity of CgPdr1 were obtained, with the demonstration that different GOF variants exhibited different levels of dependence of the mediator subunit CgGal11A [54, 181, 212]. Specifically, a strain expressing a CgPDR1 allele that encodes the D1082G mutation (occurring in the trans-activation domain of the protein) was much less dependent on CgGal11A for inducing expression of target genes than when expressing alleles encoding CgPdr1 variants with GOF mutations occurring in the central regulatory domain (CRD) [181]. Furthermore, different levels of dependence of CgGal11A were also observed for strains expressing CgPDR1 GOF variants that occur inside the CRD domain, including P822L or the herein studied I803T [181](Chapter III). Different modifications occurring in the TAD of CgPdr1 were also found to affect the activity of CgPdr1 differently [181]. For example, while cells producing the D1082G CgPdr1 GOF variant dispensed Gal11A for activity, cells producing a CgPdr1 LWG1097AAA variant are highly dependent of

it [181]. Interestingly, the D1082G and LWG1097AAA modifications when individually combined with GOFs in the CDR domain reduce the hyperactivation of CgPdr1, the same being observed when combined with the deletion of the CRD [181]. All combined, these results appear to suggest that different CgPdr1 GOF variants can distinctively impact the interactome of this transcription factor.

In line with these observations obtained at a more molecular level, *C. glabrata* strains expressing different GOF mutations exhibit considerable differences in phenotypes attributable to CgPdr1 activity. For instance, while the CgPdr1^{L280F} variant was found to promote the up-regulation of CgEPA1 gene expression in various genetic backgrounds, the CgPdr1^{G346D} variant has a repressive effect in the transcription of this gene, with a corresponding lower ability of cells expressing this variant to adhere to epithelial cells [54, 229]. Interestingly, both of these variants were found to up-regulate CgEPA12, independently of the genetic background [54, 229]. Among adhesin encoding genes, the transcriptional regulation of CgEPA1 has been the more thoroughly studied showing a complex and intertwined network of different mechanisms. Two independent CgEPA1 silencing mechanisms have been described. The first depends on the sirtuin protein complex Sir involved in the silencing of genes located at the sub-telomeres [319-321], which is alleviated during NAD⁺ limitation [173]. The second mechanism is telomere-independent and involves the recognition of a *cis*-negative element by the Ku complex of DNA repair [322], that represses the transcription of CgEPA1 during cell division. This repression is alleviated after inoculation in a fresh medium and is rapidly silenced after one cell division [322]. The observation that some CgPdr1 GOFs constitutively up-regulate the expression of CgEPA1 suggests a cross-talk between this regulator and these mechanisms. Interestingly, both CgPdr1^{L280F} and CgPdr1^{G346D} mentioned contrary effects on CgEPA1 expression were dependent on the increased binding of CgPdr1 to PDRE [54, 229](although this interaction was found to have a low signal in ChIP-qPCR experiments possibly by being transient [54, 229]). These results might suggest that CgPdr1 can less efficiently bind to the promoters of some of its direct targets or that is only recruited to target promoters in certain conditions that depend on the chromatin state. Interestingly, repression of CgEPA1 transcription by Pdr1^{G346D} depends on enhanced recruitment of CgGal11A, while deletion of CgGAL11A has no effect in the ability of a wild-type CgPdr1 variant to induce CgEPA1 transcription [54].

This thesis chapter aims to shed some light on what can be the effect in the biochemical activity of CgPdr1 of the occurrence of different GOF modifications, with emphasis on the K274Q, I392M and I803T modifications herein characterized and in the GOFs G346D, P822L, D1082G, LWG1097AAA previously identified as resulting in different effects in CgPdr1 activity [54, 181, 229](Chapter III, IV). The limited knowledge of the structural organization of CgPdr1 reduces the characterization of domains based on the sequence homology to the conserved domains of the class of zinc transcription factors masking possible structural features that may have independent roles in the regulation of the activity of the protein. Therefore, in a first approach, it is presented an *in silico* look into what can be the effect of the different GOF modifications in the 3D structure of the protein, using the recently simulated CgPdr1 protein by the AlphaFold Protein Structure Database [323]. At the experimental level, it was assessed, by ChIP-seq coupled with transcriptomic analyses, how the occurrence of the GOF modification K274Q, identified in Chapter III, affected *C. glabrata* genomic expression including the set of promoters bound *in vivo* by CgPdr1, this being the first time that a study is performed to address in detail the effect of a GOF

modification has in CgPdr1 DNA binding in the same genetic background. Results of a preliminary analysis of how the interactome of CgPdr1 could be affected by the occurrence of the K274Q modification was explored using a ChIP-SICAP approach.

3. Material and methods.

3.1. Modelling of CgPdr1 tridimensional structure and visualization

To model how the different GOF modifications might affect the 3D structure of CgPdr1 predicted by the AlphaFold Protein Structure [323] the UCSF Chimera program [324] was used for better visualization and manipulation of the 3D CgPdr1 structure. Prediction of fluconazole docking in CgPdr1 was obtained using the Chimera integrated AutoDock Vina tool [325]. Protein structural changes that might result from gain-of-function mutations were further analysed using the Chimera integrated Rotamer tool to change the residues of the GOFs in study in the CgPdr1 structure backbone. To further explore if the non-synonymous mutation alters the interaction of the residue with the surrounding amino acids the Find Clashes/Contacts tool was used [324, 326]. In all cases the default settings of the bioinformatic tools were used. Chimera software was also used to calculate the CgPdr1 surface hydrophobicity potential according to the scale of Kyte and Doolittle and the electrostatic charged surface was calculated according to Coulomb's law. CgPdr1 protein sequence secondary structures were predicted in the PSIPRED workbench [327], and residue propensity for protein and DNA binding were predicted using the DisoRDPbind server [328].

3.2. Growth media, strains and plasmids used

SKY107 (Δ Cg*pdr1*) *C. glabrata* strain was used in this work, as further detailed in Table IV. 1. These cells were transformed, whenever needed, with plasmids pYR29_Myc-HIS_Cg*PDR1* and pSP76 (both allowing the expression of wildtype Cg*PDR1* from its natural promoter and terminator) and with the derived plasmids pYR29_Myc-HIS_Cg*PDR1*^{A820C} and pSP76_*PDR1*^{A820C} that allow production of the K274Q variant, obtained by site-directed mutagenesis (described in Chapter III and further detailed in Table IV. 1 and Table V. 1). Cells were cultivated in RPMI medium (2 g/L glucose, 2.08 g/L RPMI, 6.9 g/L MOPS, 0.03 g/L L-glutamine) at pH 7 with 250 rpm agitation at 30°C.

Table V. 1. *Primers and plasmids used in this study.* In the case of the plasmids, it is also provided their origin while in the case of the primers it is indicated for which their application was used for.

Primers	Sequence	Use
BamHI_End <i>PDR1</i> _FW1	CAGTCACTGCGGCCGCAACAAGTA AACATCAGAAAATAGGTC	Cloning of promoter and <i>CgPDR1</i> sequence of pSP76's in pYR29's
NotI_End <i>PDR1</i> _REV1	CAGTCACTGCGGCCGCAACAAGTA AACATCAGAAAATAGGTC	Cloning of promoter and <i>CgPDR1</i> sequence of pSP76's in pYR29's
PrCg <i>YHB1</i> -F	GGGGGTTTTCTCGAAGAG	Used for ChIP results control by qPCR in <i>CgYHB1</i> promoter
PrCg <i>YHB1</i> -R	GGTTGGTCTAGGAAAAAGCA	Used for ChIP results control by qPCR in <i>CgYHB1</i> promoter
Prom <i>PDR1</i> _REV	CTTTCCACGGAATAGGAGGCTC	Used for ChIP results control by qPCR in <i>CgPDR1</i> promoter
Prom <i>PDR1</i> _FW	GTAGACTCATTCCACGGAGC	Used for ChIP results control by qPCR in <i>CgPDR1</i> promoter
Prom <i>CDR1</i> _FW	GCAAGTCCACGGAATATTTCC	Used for ChIP results control by qPCR in <i>CgCDR1</i> promoter
Prom <i>CDR1</i> _REV	CATCGTTGCTCCTCGCTCC	Used for ChIP results control by qPCR in <i>CgCDR1</i> promoter
Plasmid	Plasmid Description	Reference
pSP76	Plasmid that drives the expression of <i>CgPDR1</i> from its natural promoter and terminator	Khakhina, S, <i>et al.</i> 2018
pSP76_ <i>CgPDR1</i> ^{A820C}	Plasmid that drives the expression of the <i>CgPDR1</i> ^{A820C} allele from its natural promoter and terminator and consequent production of the <i>CgPdr1</i> ^{K274Q} mutant	This study

3.3. Fluconazole susceptibility testing of Δ *Cgpdrl* *Candida glabrata* cells expressing different *CgPDR1* alleles.

SKY107 (Δ *Cgpdrl*) cells were transformed with plasmids pYR29_MycHIS_ *CgPDR1* and pSP76 and with the derived plasmids pYR29_MycHIS_ *CgPDR1*^{A820C} and pSP76_ *PDR1*^{A820C} that allow the production of the K274Q variant. The MIC obtained for fluconazole in the different transformants was determined using the highly standardized microdilution method recommended by EUCAST [298]. To classify the strains as resistant or susceptible to fluconazole the MICs obtained were compared with the 32 mg/L breakpoint resistance values defined for *C. glabrata*.

3.4 Transcriptomic analysis of *C. glabrata* cells expressing the *CgPdr1*^{WT} and the *CgPdr1*^{K274Q}

The comparative transcriptomic analysis of SKY107 cells transformed with pYR29_MycHIS_ *CgPDR1*^{WT} or with the variant pYR29_Myc-HIS_ *CgPDR1*^{A820C} was based on the use of species-specific DNA microarrays. For this, each strain was cultivated, at 30 °C, in 15 mL of RPMI (at pH7) until mid-exponential phase (OD 1), flash frozen in two volumes of cold ethanol, harvested by centrifugation and kept at -80°C until further use. RNA extraction, conversion to cDNA, and subsequent labelling were

performed as described previously [297]. Briefly, cells lysis was performed mechanically, resorting to glass beads and a Fastprep®24 bead beater (MP Biomedicals). Total RNA extraction was carried out using the RNeasy extraction kit (Qiagen) following the manufacturer's instructions. The concentration of RNA in each sample was quantified in a NanoPhotometer® spectrometer (IMPLEN), and RNA integrity was confirmed in an agarose gel. 1 µg of total RNA was used for fluorescent cDNA synthesis according to the amino-allyl protocol [297]. The cDNAs of each condition were labelled with Cy3 or Cy5 and hybridized in a custom *C. glabrata* Agilent array (in an 8 × 60 k format, array express accession number: A-MEXP-2402) as previously described at Merhej, J. *et al.* 2015 [297]. A second biological replicate was performed with switched cyanine dyed samples. After overnight hybridization and washing, the slides were scanned using a 2-micron Agilent microarray scanner. The images were analyzed using the feature extraction software (Agilent Technologies) and normalized using global LOWESS. The mean expression of every gene in the cells producing the wild-type CgPdr1 or the CgPdr1^{K274Q} variant was based on the average obtained for the two biological replicates performed. A gene was considered differentially expressed if its mean absolute Log2 fold change value was higher than 0.5 and if its expression variation was considered statistically significant using the LIMMA package with a cut-off p-value of 0.05 [329].

3.4. Chromatin immunoprecipitation sequencing assay

SKY107 cells transformed with pYR29_MycHIS_CgPDR1^{WT} or with pYR29_MycHIS_CgPDR1^{A820C} were cultivated in RPMI medium until mid-exponential phase (OD₆₀₀ between 0.8-1), the same conditions used for the comparative transcriptomic analysis. Cross-linking was performed by adding 1 % of formaldehyde to the medium. After 15 min, 340 mM glycine was added, and the incubation proceeded for another 10 min. Both steps were performed at room temperature with casual agitation. After this, cells were centrifuged, the pellet washed two times with Tris-buffered saline solution (TBS) and kept at -80°C until further use. Cell lysis was performed by resuspending the pellet in lysis buffer (containing 50 mM Hepes-KOH pH 7.5, 140 mM NaCl, 1 mM EDTA, 1 % Triton X100, 0.1 % Na-Deoxycholate, 1 mM phenylmethanesulfonyl fluoride (Fluka), and O-complete Protease Inhibitor (Roche Diagnostics)) containing 500 mL of glass beads and using the FastPreP®-24 instrument shaker (MP Biomedical). Cellular debris was centrifuged and the supernatant containing the DNA was recovered. The chromatin was then sonicated to yield ~300 bp DNA fragments using a Bioruptor® standard sonication device (Diagenode). The cell debris was centrifuged, and the soluble fraction was further used in the immunoprecipitation steps. Myc-tagged CgPdr1 was immunoprecipitated overnight with gentle shaking at 4°C using an anti-c-Myc antibody (Roche Applied Science) bound to Dynabeads® magnetic beads (Invitrogen) plus O-complete Protease Inhibitor (Roche Applied Science). Before immunoprecipitation, the anti-c-Myc-magnetic beads were prepared. For such, Dynabeads® magnetic beads were washed two times with phosphate-buffered saline with bovine serum albumin (PBS-BSA), followed by incubation with minimal agitation for at least 4 h at 4°C with 0.4 mg/mL anti-c-Myc antibody. On the next day, the immunoprecipitated DNA complexes (IP sample) were washed two times with lysis buffer, two times with lysis buffer supplemented with 360 mM NaCl, two times with wash buffer (10 mM Tris HCl at pH 8, 250 mM LiCl, 0.5 % NonidetP40, 0.5 % Na-Deoxycholate and 1 mM EDTA) and a final wash with TE at pH

8. Reversion of the cross-linked in the IP DNA was done by heating the samples for 4 h at 65°C with shaking at 600 rpm in a TE elution buffer containing 0.5 % SDS. After incubation, the samples were centrifuged, and the supernatant was conserved. DNA was extracted using the wash iDeal ChIP-seq kit (Diagenode). ChIP-seq of untagged *C. glabrata* cells grown in glycerol as a carbon source was used as control sample (mock) [330]. To confirm a correct CgPdr1 immunoprecipitation a qPCR was performed aiming to amplify the promoter region of CgPDR1 and CgCDR1 from the IP DNA. The CgYBH1 promoter sequence was used as a negative control since this is not a described CgPdr1 target (primer sequences are detailed Table V. 1). MicroPlex v2 kit from Diagenode (using the supplier recommendations) was used to construct single-read libraries from the IP samples. Sequencing was performed using NextSeq 500 device (Illumina technology available at the transcriptome platform at Ecole Normale Supérieure: [Http://www.transcriptoe.ens.fr/sgdl/](http://www.transcriptoe.ens.fr/sgdl/), Paris France). Each sample was sequenced in duplicate. After quality controls and filtering of low-quality bases, between 15 and 20 million sequences (IP sample) and 10 and 20 million sequences (control sample) were obtained. Three biological IP replicates were obtained for each analysis.

3.5. Peak calling and network construction

The reads obtained by sequencing were mapped in the *C. glabrata* genome, using the Bowtie algorithm [331]. SAMTOOLS suite [332] was used to convert the output SAM files to BAM files. BAM files of the sequence replicates were merged to increase the sequence coverage and then converted to BED files, using the 'genomeCoverageBed' tool, available from BEDTOOLS suite [333]. Peak calling was performed using the software bPeaks [334] using the mock IP as reference. The final threshold parameters used were the following: T1=2, T2=4, T3=0.7, T4=0.9. The final list of peaks detected was then manually curated using the IGV genome browser [335] removing artificial peaks such as peaks overlapping ORF regions, without a gene sequence in the vicinity, or found in the vicinity of a tRNA locus. Whenever a peak was found in between two coding sequences, if only one of the genes encoded was found overexpressed in the ChIP-seq results of the CgPdr1^{K274Q} variant it was considered that the transcription factor regulated only that gene. In case of equal expression of both genes was observed then both encoded genes were considered potential direct targets of CgPdr1.

3.6. Chromatin immunoprecipitation selective isolation of chromatin-associated proteins (ChIP-SICAP)

For ChIP-SICAP, SKY107 cells transformed with pYR29_MycHIS_CgPDR1^{WT} or with pYR29_MycHIS_CgPDR1^{K274Q} were cultivated under the same conditions as those used for the ChIP-seq and the comparative transcriptomic analysis. A mock sample, obtained using SKY107 cells transformed with an empty plasmid, was used as control. Two samples of each transformant strain were analyzed. The same protocol used for ChIP-seq was followed until the overnight immunoprecipitation and beads washing step. The remaining experimental steps used for the ChIP-SICAP are described in Rafiee, M.R. *et al.* 2016 [336] and further optimized by Wijick, V. *et al.* 2021 (in press)[337]. Briefly, after two steps of washing

with the wash buffer (10 mM Tris HCl at pH 8, 250 mM LiCl, 0.5 % NonidetP40, 0.5 % Na-Deoxycholate, and 1 mM EDTA), the beads were further washed four times with 100mM tris pH 8.0 to remove EDTA. The DNA was then biotinylated by incubation of the beads with biotin using 60U TdT enzyme (Thermo Fisher Scientific) and 0.2 mM biotin-11-ddUTP (Jena Bioscience) for 45 min at 37°C with 600 rpm agitation. Beads were then washed with ice-cold lysis buffer four times, resuspended in elution buffer containing 7.5 % SDS and 200 mM DTT (dithiothreitol), and incubated for 30 min at 37°C with 600 rpm agitation. After incubation, the samples were centrifuged, and the supernatant was conserved. The protein-DNA complex was then captured with streptavidin-coated beads previously equilibrated with lysis buffer by incubation with rotation for 1 h at room temperature. Beads were then washed three times with SDS wash buffer (10 mM Tris-HCL, 1 mM EDTA, 1% SDS, and 0.2 M NaCl₂), once with BW2x buffer (10 mM Tris-HCL, 1 mM EDTA, 0.1% Triton X100, 2 M NaCl₂), twice with isopropanol 10% and twice with acetonitrile 20%. Reverse crosslinking was carried out by resuspending the mixture in 14 µl digestion buffer (ammonium bicarbonate 50 mM, 10 % SDS) supplemented with 1 µl of 100 mM DTT, and incubated for 30 min at 95 °C. After cooling down, 1 µl of 0.2 M iodoacetamide was added and beads were incubated for 10 min at room temperature. Beads were pelleted, and the proteins in the supernatant were digested overnight at 37 °C with 300 ng trypsin (Promega, Madison, WI, USA) in a 25 mM NH₄HCO₃ buffer (0.2 µg trypsin in 20 µL). The resulting peptides were desalted using ZipTip µ-C18 Pipette Tips (Pierce Biotechnology, Rockford, IL, USA). Peptides were obtained by adding 5 µl of water pre-washed hydrophobic and hydrophilic Sera-mag beads to the samples (Carboxyl Magnetic Beads) plus 195 µl acetonitrile (100%) followed by vortex and 10 min incubation at room temperature. 10 µl of 2% DMSO was then added, and the sample was vortexed followed by pelleting of the beads. After pelleting the beads again, the tubes were sonicated in a water bath for 5 min with a high output. Finally, the samples were spinned, and the supernatant was transferred to a clean tube and washed with 1µl of 1% formic acid

3.7. High pH fractionation and mass spectrometry

Samples containing the peptides isolated in 3.6 were analyzed using an Orbitrap Q-Exactive Plus, coupled Nano-LC Proxeon 1000, equipped with an easy spray ion source (Thermo Scientific, Waltham, MA, USA). Peptides were loaded with an online preconcentration method and separated by chromatography using a Pepmap-RSLC C18 column (0.75 x 500 mm, 2 µm, 100 Å) from Thermo Scientific, equilibrated at 50°C and operated at a flow rate of 300 nL/min. Peptides were eluted by a gradient of solvent A (H₂O, 0.1% FA) and solvent B (100% ACN, 0.1% FA). The column was first equilibrated for 5 min with 95% of solvent A, then solvent B was raised to 35 % for 93 min, and finally, the column was washed with 80% solvent B during 10 min and re-equilibrated at 95% solvent A during 10 min. Peptides masses were analyzed in the Orbitrap cell in full ion scan mode at a resolution of 70,000 with a mass range of *m/z* 375-1500 and an AGC (automatic gain control) target of 3x10⁶. MS/MS was performed in a Top 20 DDA mode. Peptides were selected for fragmentation by Higher-energy C-trap Dissociation with a Normalized Collisional Energy of 27% and a dynamic exclusion of 30 seconds. Fragment masses were measured in the Orbitrap cell at a resolution of 17,500, with an AGC target of 2x10⁵. Monocharged peptides

and unassigned charge states were excluded from the MS/MS acquisition. The maximum ion accumulation times were set to 50 ms for MS and 45 ms for MS/MS acquisitions, respectively.

3.8. MS data analysis

Raw data was processed on Proteome Discoverer 2.2 with the mascot node (Mascot version 2.5.1) with a *Candida glabrata* Genome Database v2020 from <http://www.candidagenome.org>. Tryptic digestion was used with a maximum of 2 missed cleavage authorized. Precursor and fragment mass tolerances were set to 6 ppm and 0.02 Da. Spectra were filtered using a 1 % false discovery rate (FDR) with the percolator node. Proteins were identified and quantified by at least one unique peptide. Only proteins with at least two quantified intensity values in a condition and with a proportion of observed values superior to 0 % in each condition are kept. In each condition, the intensity values were normalized by centering on the mean of the medians of intensities in each sample. Proteins absent in one condition and present in another were directly assumed differentially abundant. Two biological replicates were used for each condition in the study. Only proteins identified in the ChIP-SICAP of CgPdr1^{WT} or CgPdr1^{K274Q} samples but not in the mock-IP sample were considered. Usual contaminant peptides of IP-MS, such as ribosomal proteins and core histones, were discarded from the analysis [338].

4. Results and Discussion

4.1 General overview of the predicted structure of the zinc finger transcription factor and nuclear receptor CgPdr1

Until recently, the reduced knowledge of the structural organization of CgPdr1 limited the characterization of regulatory domains based on sequence homology to the class of zinc transcription factors and partial gene disruption studies. This limitation can mask possible structural features that may have independent roles in the regulation of the activity of the protein and their better study could help in understanding different effects underlying regulation of CgPdr1 activity, for example in GOF variants. In order to shed some light into how the different gain-of-function mutations could impact the structure of CgPdr1, the recent structure predicted by this regulator by the AlphaFold project (an artificial intelligence system that makes state-of-the-art accurate protein structure predictions [323]), represented in Figure V. 1 panel A, was studied. It is clear that the prediction has a higher local quality in the core region and lower confidence of prediction in the predicted disorder sequences of the protein (Figure V. 1 panel A and Figure V. 2 panel A)[327]. These disordered structures in CgPdr1 correlate with the predicted C-terminal and N-terminal, that unstructured features are described to be essential for the ability to bind to DNA or other proteins (Figure V. 2 panel B), that in the case of transcription factors can act as co-factors in transcriptional regulation [147, 328]. Conserved structural features found in fungal nuclear ligand-binding transcription factors are clearly identified in the predicted CgPdr1 structure [147](Figure V. 1 panel B and C in yellow), including the Zn₂-Cys₆ DNA binding domain (between D32 and I52 residues) and the disordered structure linker region, located between the DBD and the structured core of the protein (between residues T152 and S197) (Figure V. 1 panel B and C in light grey). Both regions precede the conserved extruding coiled-coil structure, in which is visible the exposed hydrophobic stretch characteristic of the dimerization domain (between residues Y212 and N255) (Figure V. 1 panel B and C in grey and in panel D) [147, 224]. The Central Regulatory Domain (CRD) (between positions W256 and M957) is visible as a globular structural domain, while the TAD domain structure is defined at the C-terminal, as expected (Figure V. 1 panel B and C in green). The main structural features conserved in TAD domains of zinc fingers transcription factors are a two-short alpha-helix structure enriched in hydrophobic and negatively charged residues, between residues Y1076 and D1104 (Figure V. 1 panel E). This structure is adjacent to a disordered region composed of residues with a high propensity to interact with proteins (from T1017 to F1064) and also DNA (from residue N998 to V1011)(Figure V. 2 panel B). Notably, both the two structural features of TAD are required for the maximum activity of ScPdr1 [225].

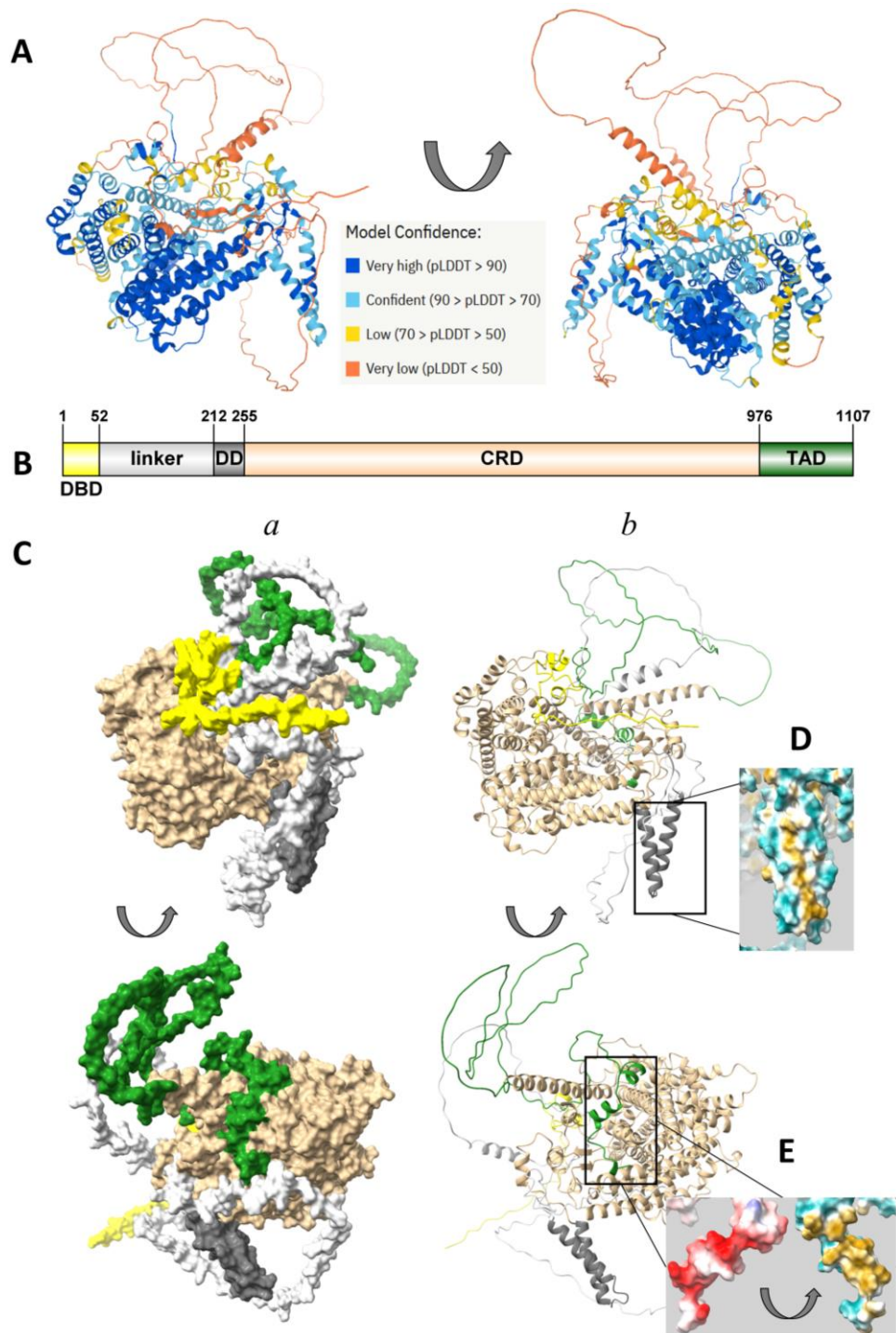


Figure V. 1. The modelling of the *CgPDR1* protein structure allows the characterization of the conserved structural domains of zinc-finger nuclear receptor transcription factors. (A) Structural modelling of *C. glabrata* Pdr1 according to AlphaFold Protein Structure Database with confidence modelling representation. (B) The *CgPdr1* protein structure is composed of four different structural features: the DNA-binding domain (DBD, yellow), the linker sequence (light grey) the dimerization domain (DD, dark grey), the core structure central regulatory domain (CRD, beige), and the transactivation domain (TAD, green). (C) Representation of two sides of the *CgPdr1* protein in surface view (a) and backbone view (b), respectively. (D) Representation of the *CgPdr1* hydrophobic properties of the dimerization domain and (E) of the hydrophobic and electrostatic properties of the individualized *CgPdr1* TAD domain. The hydrophobicity potential is represented from blue for the most hydrophilic residues, to white if neutral, and to yellow if hydrophobic, while the electrostatic charged surface is represented from red for the most negative potential, to white if neutral, and to blue if positive.

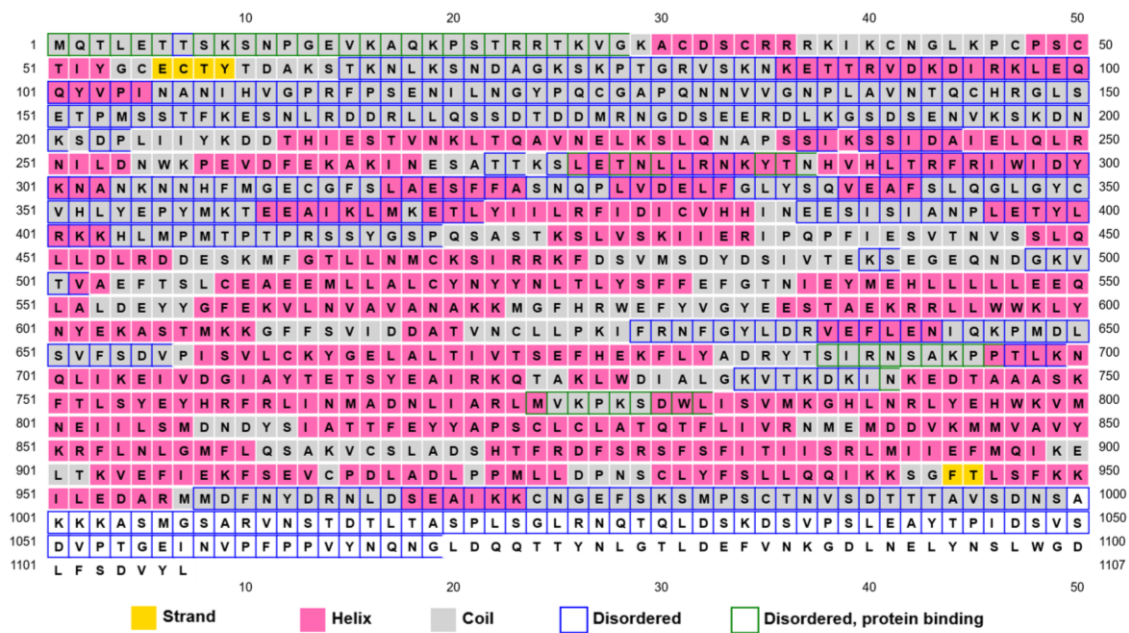
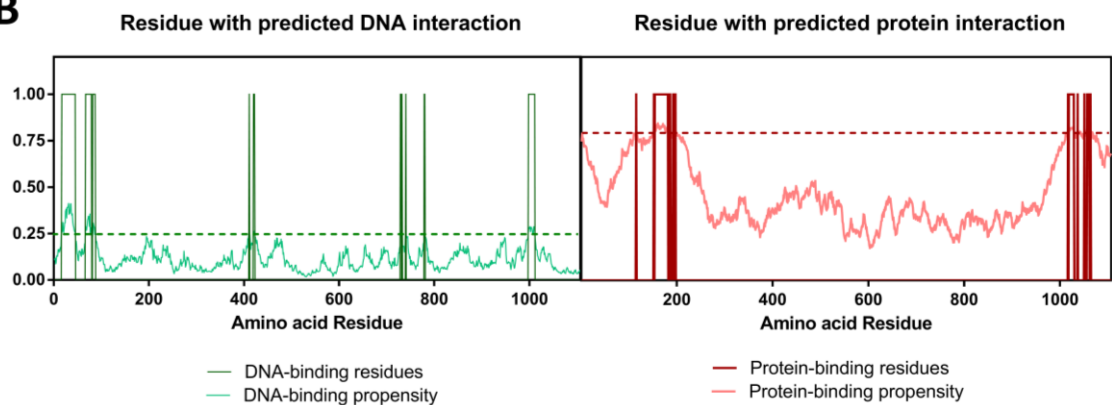
A**B**

Figure V. 2. Prediction of the secondary structure of CgPdr1 and of the residue's propensity for DNA and protein binding. (A) Secondary structure prediction along the CgPdr1 amino acid sequence was obtained in PSIPRED workbench. (B) DisoRDPbind was used to predict the propensity for the different residues of CgPdr1 to bind to DNA and Proteins.

An interesting result that comes from this structural prediction is the close proximity of the transactivation domain and the CRD which is likely to facilitate their interaction, something that is essential to maintain CgPdr1 at a low activity in non-stressful conditions (Figure V. 1 panel C)[62]. In this context, it was noteworthy the observed positive electrostatic charges in the docking region for TAD domain predicted in CRD (Figure V. 3 panel Bc in blue) while TAD domain is predicted to be negatively charged (Figure V. 3 panel Cc in red), a trait that can contribute for the interaction of these two domains [62]. The interaction of the TAD with the CRD may also depend on its hydrophobic residues (Figure V. 3 panel Db) to be buried in the core domain, which also has hydrophobic patches (Figure V. 3 panel Bb). This hydrophobic stretch of TAD in ScPdr1 of *S. cerevisiae* was previously characterized to be essential for the interaction of the domain with ScGal11A [105], suggesting that Gal11 could directly compete for the interaction of this region with the core of the protein, which is in the agreement with the model that TAD needs to be released to interact with the mediator complex [62].

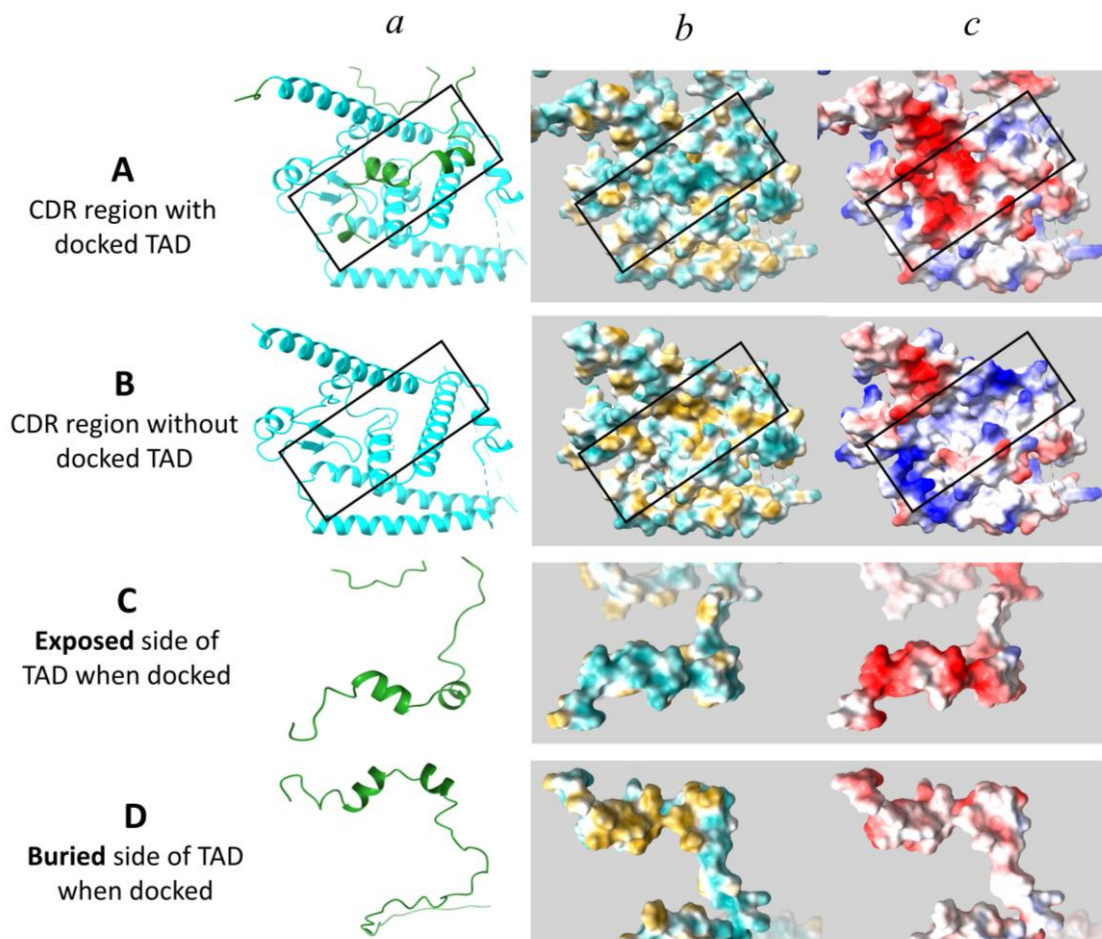


Figure V. 3. Analysis of the properties of the CgPdr1 structures involved in the interaction between the transactivation domain and the central regulatory domain. (A) The 3D structures of the TAD and CRD interacting were individualized from the rest of the CgPdr1 structure for further analysis. Further individualization of the TAD region (C and D) from the CRD domain (B) was obtained to characterize the hydrophobic (b) and electrostatic (b) properties of the interacting surfaces. The hydrophobicity potential is represented in blue for most hydrophilic surfaces, in white, for neutral residues, and in yellow for hydrophobic ones. The electrostatic charged surface interaction is represented in red for the most negative potential, in white if neutral, and in blue if positive. The backbone view is also represented in (a), marking in cyan the CDR structures predicted to interact with TAD, which is itself highlighted in green. The region of the TAD docking in the CRD structure is further marked in a black box.

Inspection of the contacts made by the amino acids located in CgPdr1 TAD domain (Figure V. 4 panel A and B, TAD represented in green and contacts represented in yellow lines) with the amino acids of the CRD (Figure V. 4 panel A and B, with residues interacting with TAD represented in dark blue and in green along the amino acid sequence in panel C), revealed that the interaction is more likely to involve three distinct helix structures located in the core of the protein (L344 to Y357, E361 to A393 and G943 to N975) that are represented in Figure V. 4 panel A and B in cyan. This *in silico* prediction is concordant with previous studies, that demonstrated that activation of ScPdr1 could be achieved by the deletion of a small sequence in the CDR that encodes the corresponding amino acid region in CgPdr1 that includes the L344 to Y357 helix and part of the region of the E361 to A393 helix (amino acid region defined as the inhibitory domain (Figure II. 6 and Annex Figure II. 1) [225]). The adjacent C-terminal amino acid sequence of the L344 to Y357 helix and N975 to G943 helix also includes several small structural features that are predicted to interact with amino acids of the TAD, including a small two-beta sheet structure (H288 to I298), small α -helixes (Y300 to K305 and C930 to I936) and surrounding loops (Figure V. 4 panel A and B in cyan). Exposed short helix structures are often associated with bioactive regions that can interact with proteins, DNA, or even RNA [339]; therefore, the sequestration of the TAD domain by the CgPdr1 core could affect, or be affected, by modification in these structures resulting from different interactions. Altogether these structural features allowed to identify what can be three main inhibitory domains in the CDR (ID) (Figure V. 4 panel D): i) domain IDI, comprised of 288 to 393 amino acid sequences that includes two of the main large α -helix interacting with the TAD domain, a small helix and a small two-beta sheet structure (Figure V. 4 A, B and D in red); ii) domain IDII, comprised by a small loop of amino acids (M774 to S779) found to interact with the most C-terminal residues of the TAD domain and that could be important for its tight sequestration (Figure V. 4 panel A, B and D in green); iii) domain IDIII, comprised by the 926 to 975 amino acid sequence located at the N-terminal of the disordered region of TAD domain, that includes the third main large α -helix structure of the CRD interacting with the TAD domain and a short α -helix (Figure V. 4 panel A, B and D in black).

To predict the fluconazole docking site in the CgPdr1 protein structure the Chimera integrated AutoDock Vina tool was used. For this, the previously defined minimum xenobiotic binding domain (XBD)[105] was defined as the receptor (Figure V. 5, panel A), predicting only one probable region of docking (the same analysis using the entire CgPdr1 protein structure was used as the receptor returned the same best score results). Fluconazole is predicted to be docked in a channel that crosses the globular part of the protein of the CgPdr1 structure (Figure V. 5 panel B marked with a yellow arrow). This analysis allowed the prediction of the amino acids that interact with A552 and D554, with the residues from the aminoacid stretch Y811 to E818 and from the stretch D876 to S880, as those interacting directly with fluconazole during binding (Figure V. 5 panel C). In specific, it was found that fluconazole was predicted to contact the residues in the loop between the α -helixes composed by the aminoacid stretches I537 to A552 and T573 to Y572, extending outwards of the protein core (Figure V. 6 panel A in dark blue). Both these two α -helixes' sequences are part of the XBD (Figure II. 6 and Annex Figure II. 1), and the exposed T573-Y572 α -helix is also part of the Middle homology domain (Figure II. 6 and Annex Figure II. 1). Notably, the identified structures to contact to fluconazole contain only part of the structure previously identified as being the minimum XBD (Figure V. 5 panel B)[105]. Fluconazole was also predicted to interact with the D810-E830 and H872-I898 α -helixes buried in the core of the protein (Figure V. 6 panel A). Interestingly, from the residues defined to be relevant for the interaction with fluconazole (Figure V. 5 panel C) only the properties of the residues found in the H872-E897, not belonging to the XBD, appear to be conserved in CgPdr1, ScPdr1, and ScPdr3 (Annex Figure II. 1). From these identified structures, H872 to E897 amino acid stretch appears to be the main α -helix interacting with the previously predicted TAD docking structures (Figure V. 6, panels Ba in cyan). The Y572-T556 and D810-E830 α -helixes also form a few contacts with the predicted TAD docking structure, suggesting a smaller impact in this structure (Figure V. 6, panels Bb and c). Altogether, the H872-E897 α -helix structure may relay the xenobiotic docking to the structures that interact with the TAD domain. The remaining structures, including those encoded by the previously minimum defined XBD should be mostly involved in the structuring of the docking domain.

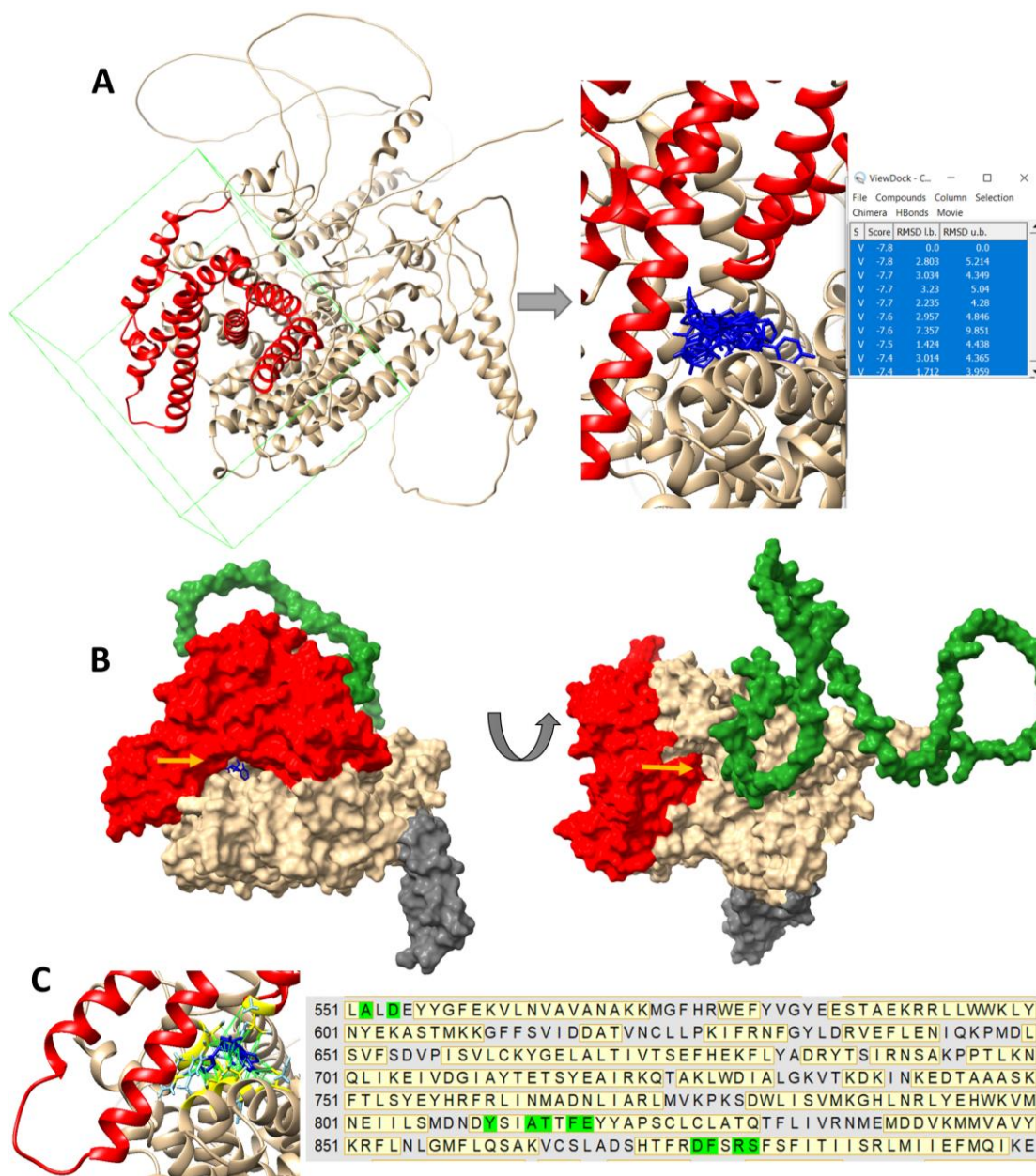


Figure V. 5. Modelling of fluconazole docking in the CgPdr1 nuclear receptor transcription factor structure. The Chimera software integrated AutoDock Vina tool was used to simulate the most probable docking regions for fluconazole molecule in CgPdr1. (A) For the simulation, the minimum XBD was defined as the receptor (defined in Thakur, J. K. *et al.* 2008, represented in red), predicting only one probable region of docking. The different scores of qualities in prediction are summarized in the table. (B) The predicted fluconazole (represented in blue and signal by an orange arrow) docking site occurs in a channel that crosses the core structure of the CgPdr1. The DBD and linker domain were removed for better visualization. (C) The Chimera Find Contact tool was used to predict the residues capable of interacting with the best scored simulated fluconazole (-7.8) binding modes and are marked in green in the amino acid sequence.

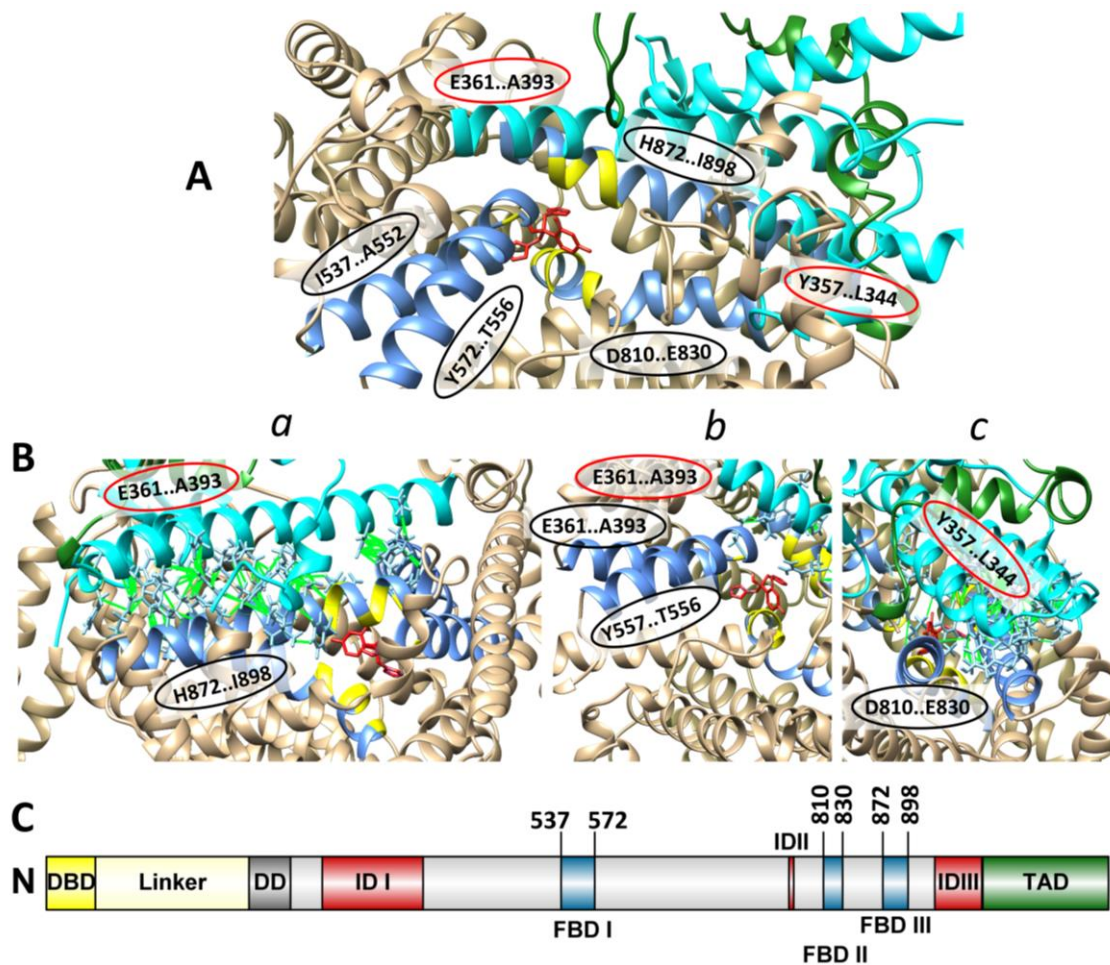


Figure V. 6. Definition of the CgPdr1 protein structural features that interact with fluconazole antifungal molecule. (A) The predicted structural features of CgPdr1 that are predicted to be involved in the interaction and possibly modified by the binding of the fluconazole molecule (red) are marked in dark blue, with amino acid residue stretch circled in black, with the specific residues predicted to interact with fluconazole marked in yellow. The structures previously predicted to contact with the docked TAD domain are also represented in cyan and residues circled in red (B) The contacts formed by the different functional structures were further analyzed and are marked in green. (C) The undertaken prediction allowed the identification of three predicted fluconazole binding domains (FBD, blue) marked as three stretches along the central regulatory domain of CgPdr1 (grey).

4.2. Distribution of gain-of-function mutations across the different structural features predicted for CgPdr1

After the thorough *in silico* analysis performed over CgPdr1 3D structure, including the identification of some functionally relevant structural domains, it was possible to examine, *in silico*, the effect that might be caused by different mutations, including those that are GOF (Annex Table II. 1) (Figure V. 7 panel A). In particular, it was possible to examine the impact of GOF mutations K274Q, I392M and I803T, all confirmed to drive hyperactivation of CgPdr1 during the course of this thesis, as well as of GOFs previously describe to differently influence CgPdr1 activity. Careful examination of the places where the different confirmed GOF modifications in the literature appear revealed an enrichment in mutations

occurring in the central CRD globular structural domain (Figure V. 7, marked in red) affecting specially predominantly buried residues in the α -helix surrounding the structures that are predicted to interact with fluconazole (Figure V. 7 panel A, dark blue). These amino acid changes could alter the stability of the core structure and promote a distancing between the multiple α -helices, thus mimicking what appears to be the CgPdr1 restructuring happening after ligand (fluconazole) binding. Interestingly, modification to a tyrosine of the Asp876 residue, predicted to interact with fluconazole, was found to result in a gain-of-function CgPdr1 mutation (Figure V. 5 panel C). Two particularly interesting GOFs located in the CDR globular structural domain are P822L and I803T (identified in Chapter IV), two non-synonymous mutations shown to result in CgPdr1 hyperactivation partially dependent of CgGal11A [181](Chapter IV). Both residues are found on the same side of the core structure of the protein (Figure V. 7, panel B) and are part of two close α -helix structures with multiple residue connections (Figure V. 7, panel Ba). Both residues are encoded in the homologous NLS sequence defined in ScPdr1 suggesting that this region could regulate CgPdr1 activity independently of CgGal11A (Annex Figure II. 1, Figure V. 7, panel B marked in dark grey). Since CgPdr1 is constitutively found in the nucleus interacting with the PDRE of target promoter genes, it is unlikely that changes in the homologous NLS sequence could affect CgPdr1 localization resulting in changes in CgPdr1 activity [71]. Although this sequence was found to be fundamental for the nuclear import, the ScPdr1 does not interact with the ScPse1 importer and is indirectly imported through the possible interaction of another uncharacterized factor [227]. Concordantly, the electrostatic surface of this region of the CgPdr1 structure reveals enrichment of exposed negative charges (Figure V. 7, panel Bb) that might interact with positively charged regions of other proteins, that may affect the CgPdr1 activity. Furthermore, the α -helix Q830-D810 interacts with both fluconazole and the α -helix L344-Y357 involved in the TAD sequestering domain, meaning that changes in this structural region could still simulate the CgPdr1 xenobiotic activation through a possible release of TAD, even if these GOF mutations in this region regulates the activation of CgPdr1 partially independently of CgGal11A.

Several residues of the α -helices predicted to be involved in TAD sequestration (Figure V. 7 panel C in cyan) were also found to serve as points for the emergence of GOF mutations in CgPdr1, in agreement with the described critical role of this domain for regulation of CgPdr1 activity. One of such mutations is the GOF I392M (Chapter IV), a residue buried in the core structure of the protein. To explore what may be the impact that this modification may have on CgPdr1 structure, the Chimera software was used to modify the Ile392 residue to a methionine. This change originates clashes to surrounding amino acids and could therefore originate a shift of this structure that can result in destabilization of the TAD docking structure and, consequently, in its release and activation of the protein.

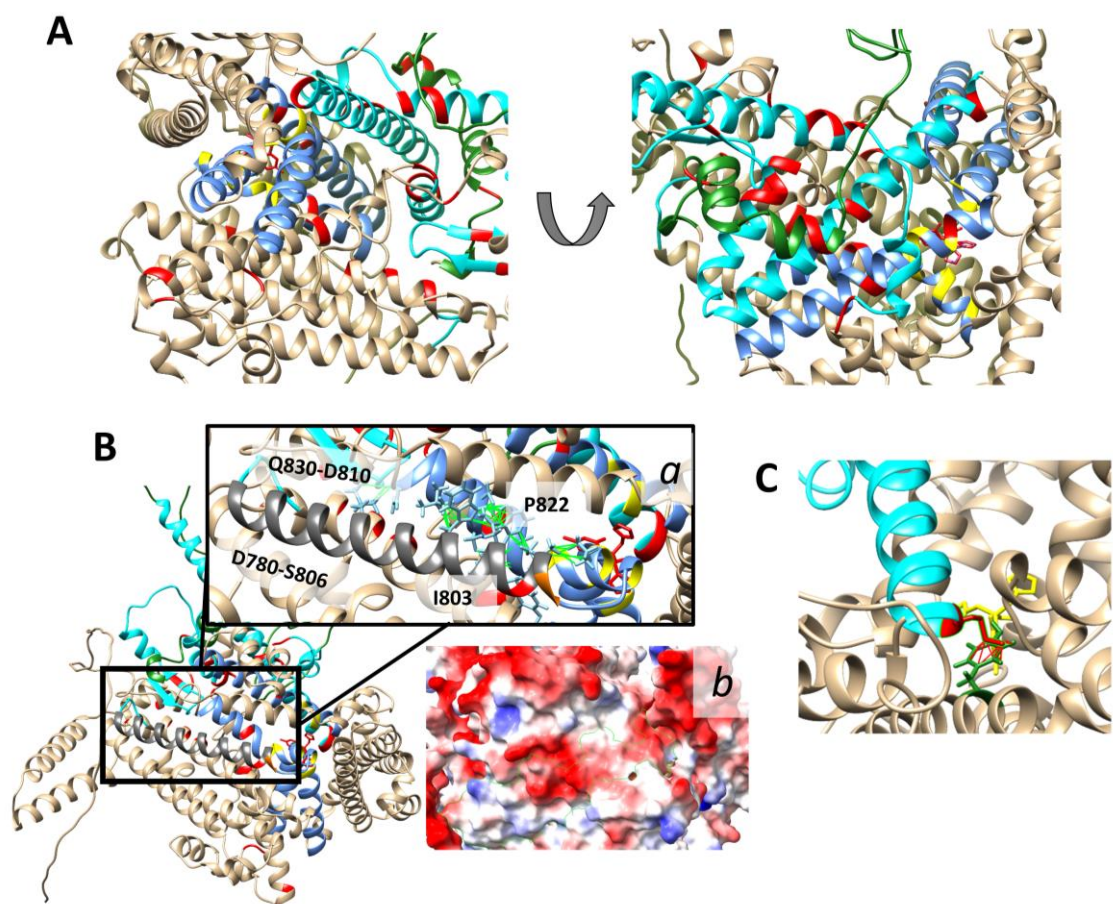


Figure V. 7. Gain-of-function mutations are distributed in the central regulatory domain of the *CgPdr1* transcription factor protein. The Chimera visualization software was used to inspect closely the distribution of residues affected by GOF mutations (red) along with the structure of *CgPdr1*. (A) The influence that the change of these residues of the core structure of *CgPdr1* can have on the fluconazole docking structure (dark blue), with residues that interact with fluconazole (highlighted in yellow), the TAD domain (green) and the structural features that interact with the TAD (cyan) were carefully analyzed. (B) Analyses of the effect that the residues (red) changes P822L and I803T in the core of *CgPdr1*, reported resulting in *CgGal11A* partially independent *CgPdr1* hyperactivation, might have on *CgPdr1* protein structure. (a) Influence of the mentioned GOFs and the connected (represented with green lines) α -helix structures where they are located might have on the *CgPdr1* structure and specifically the nuclear localization signal region (dark grey) (b) The surface region of this *CgPdr1* structure region is specially enriched in negative charges (red). (C) The 392 residue (red) is buried in the *CgPdr1* structure and located in an α -helix structure involved in TAD domain sequestration (cyan) that is also located near the fluconazole (yellow) predicted docking site. The modification to a Met amino acid generates clashes (red lines) to the near T520 residue (green).

Residues located within the TAD domain itself (Figure V. 8 panel A) are also found to serve as points for the emergence of GOF mutations. As described before, different modifications in the TAD domain can have different dependencies on *CgGal11A* in the hyperactivity of *CgPdr1* [181]. Interestingly, analysis of these specific changes revealed that modifications in this region may affect relevant properties of this structural domain. Specifically, while D1082E GOF mutation (which relies partially on *CgGal11A* for *CgPdr1* activation) appears to change the overall negative charge of the TAD, and LWG1097AAA modification (highly dependent of *CgGal11A* for activation of *CgPdr1*) significantly affects the hydrophobic nature of the domain (Figure V. 8 panel B) [181]. These results suggest that reduction of the hydrophobicity enrichment of the domain may increase the dependency of *CgGal11A* for *CgPdr1* activity,

while the reduction of the overall negative electrostatic charge may reduce this dependency. Interestingly, it was previously described that the CgPdr1^{P822L} affecting in the CRD, also as mentioned showing a decreased dependence in CgGal11A, and CgPdr1^{D1082E} of the TAD variants have a similar transcriptional profile (~0.87) when expressed in the same isogenic strain while presenting transcription profiles with lower similarities when compared to other GOFs, even if in the same domain. Furthermore, both CgPdr1^{P822L} and the CgPdr1^{D1082G} variants originate higher transcript levels of various CgPdr1 target genes (e.g. CgCDR1, CgCDR2, CgSNQ2, or CgYBH1), compared to the transcript levels that are produced in strains expressing other CgPdr1 GOF variants [181]. This result suggests that the partially independent CgGal11A activity regulation exerted by both GOF mutations could involve the same players and correspondent structural regions affected.

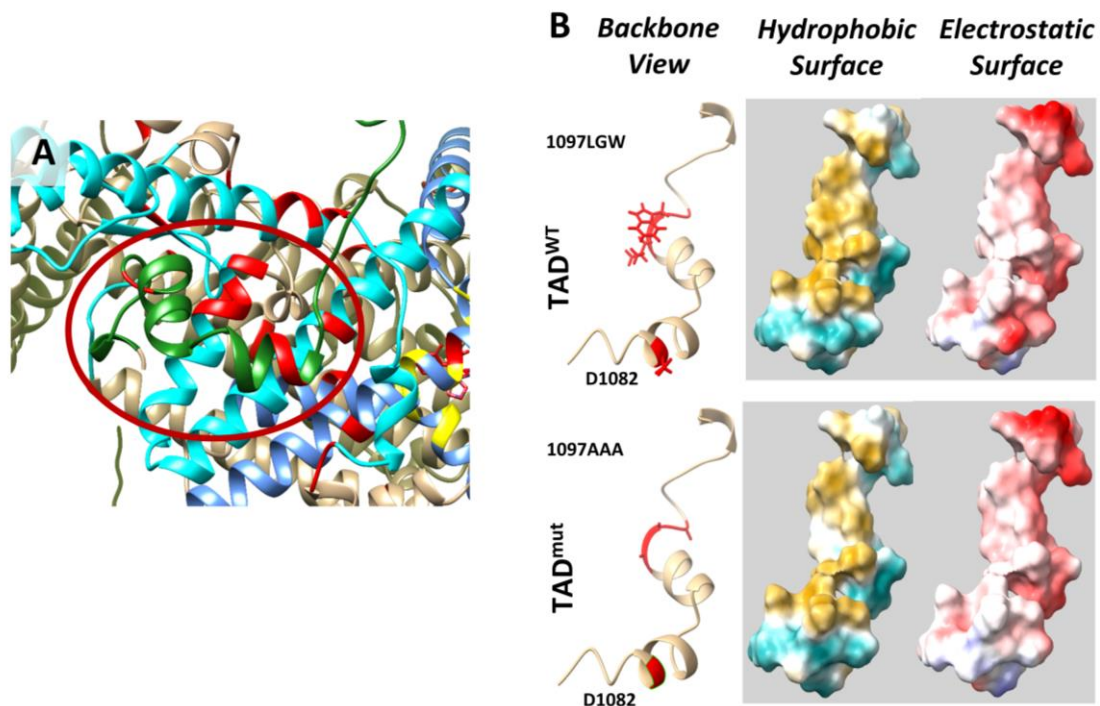


Figure V. 8. Gain-of-function mutations distributed in the transactivation domain of the CgPdr1 transcription factor protein. The Chimera visualization software was used to inspect closely the distribution of residues affected by GOF mutations (red) along with the structure of CgPdr1. (A) The influence that the change of these residues in the TAD (green) was carefully analyzed. (B) Analysis of the distinct effect of the modifications LWG1097AAA and D1082G, different dependencies on CgGal11A for hyperactivation of CgPdr1, have on the TAD domain overall negative electrostatic charge (red) and hydrophobic surface (yellow).

The GOF modifications occurring in two exposed regions, between F575 to T588 residues (Figure V. 9) and the W256 to Y336 residues (Figure V. 10) are more elusive to understand. The first of these regions is composed of two α -helix structures protruding from the fluconazole docking site to the exterior of the protein (Figure V. 9 panel A). Most of the GOFs described to affect this structural region (e.g. F575L, H576Y, Y584C, T588A) occur in residues located in the surface of CgPdr1 and thus it is possible that a change of the protein surface in this region can underlie the hyper-activation of the protein. The GOFs in this region affect two α -helices structures forming a channel leading to the predicted fluconazole docking site (Figure V. 9 panel B). The amino acid sequence of these helices is part of the middle homology region

(Figure II. 6 and Annex Figure II. 1) present in most yeast zinc transcription factors and whose function is not clear, although in *S. cerevisiae* it was found dispensable for the activity of ScPdr1 [225]. Thus, changes in this MHR region may affect the activity of CgPdr1 in a mechanism that is independent of the TAD release. MHR was suggested to assist target discrimination of zinc transcription factors by aiding the DBD and linker sequence interaction to DNA [224] and, interestingly, GOFs occurring in CgPdr1 occur predominantly in aromatic amino acids that may play a role in mediating protein contacts with DNA (Figure V. 9 panel A) [340]. Therefore, it would be interesting to study if GOF mutations in this domain could change CgPdr1 DNA binding specificity or even tighten the transcription factor interaction with the DNA, the mechanism suggested to explain the CgPdr1 hyperactivation in N-terminal tagging of CgPdr1 [207].

Middle homology domain

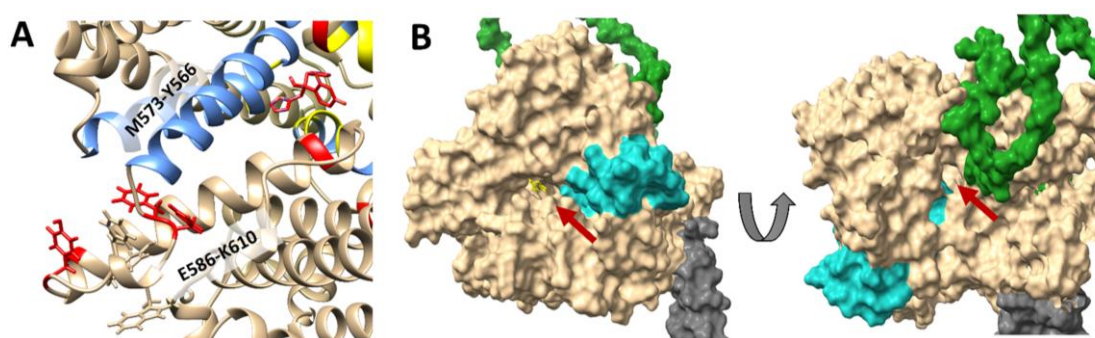


Figure V. 9. Gain-of-function mutations distributed in the exposed region of the middle homology domain of the CgPdr1 transcription factor protein. The Chimera visualization software was used to inspect closely the distribution of residues affected by GOF mutations (red) along with the structure of CgPdr1. (A) Several residues of the middle homology region (MHR) were also identified to be affected by GOF mutations; specifically, aromatic amino acids enriched in this region. (B) This zinc transcription factor conserved region is a structural part of the channel where fluconazole docks (highlighted in blue). The predicted fluconazole molecule (yellow) docking channel structure is signaled in surface representation with a red arrow.

The second mentioned exposed region comprising the W256 to Y336 residues, in which GOF CgPdr1 mutations appear to occur at high frequency, is located within the CRD and links the dimerization domain with the TAD docking region (inhibitory domain I) (Figure V. 10 panel A). Since small structural features in this region are also predicted to interact with the TAD domain (Figure V. 4), it is possible that these GOF mutations may affect TAD sequestration by the core structure. Interestingly, however, one of the GOF identified in this region is the L280P that when expressed in different genetic backgrounds was demonstrated to have a positive influence on the expression of *CgEPA1* [229], which is normally repressed by chromatin silencing, raising the question of whether this structural region of CgPdr1 has an effect in gene expression resulting from changes in the activity of chromatin remodelling proteins. Contrarily, the G346D mutation, located in the first ID motif, has a negative effect or a null effect in the expression of the *CgEPA1* gene depending on the genomic background [54]. Altogether, these results suggest that the region linking the dimerization domain to the globular structure of the protein might have a specific regulatory function in CgPdr1 protein. Concordantly this region has several small exposed secondary structures that are known to have a role in protein-protein interaction [339]. Interestingly, the

4.2. Overview of the insights brought by the *in silico* structural analysis over CgPdr1 activity

With the structural information obtained, it was possible to better detail the regulatory domains that might be involved in the regulation of CgPdr1 activity and also anticipate what can be the effect of the occurrence of distinct GOF mutations in CgPdr1 activity. A schematic representation of these identified regulatory domains, along with the description of CgPdr1 GOF mutants described, is presented in Figure V. 11. The regulatory domains identified across the central regulatory domain include three inhibitory domains that might be involved in maintaining TAD in its inactive form; and domains predicted to be involved in the direct interaction of CgPdr1 with fluconazole (indicated as FDB). Due to the promiscuous nature of CgPdr1 in binding xenobiotics [105] other regions of the protein may be involved in binding rather than only the herein identified FDB domain. Hyper-activating mutations found to occur in the MHR and the regulatory domain (indicated as RD) are localized in the surface of the protein and, according with the structural model herein presented, appear to be far from the FBD and ID domains, thus leading to the idea that they influence CgPdr1 activity by a mechanism that might not be related with the sequestration of TAD. Regarding NLS, two proven GOF mutations were found in this region to result in partially CgGal11A independent CgPdr1 hyperactivation [181](Chapter III). As observed in Figure V. 11 panel A, the distribution of the GOFs reported in the literature affects directly the described regions, strongly backing the *in silico* predictions of the relevance of these individual domains in the CgPdr1 protein activity.

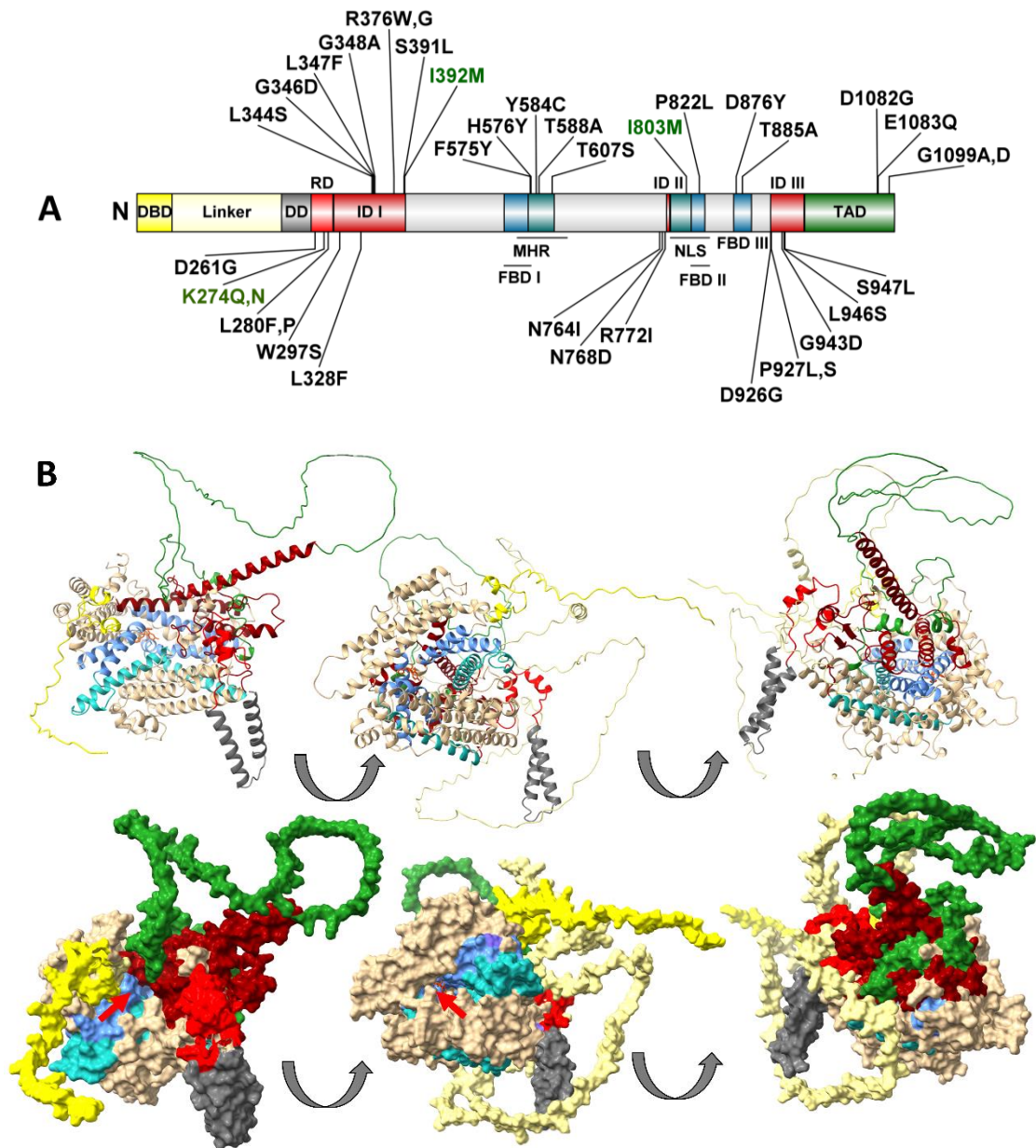


Figure V. 11. *Redefinition of the regulatory domains of CgPdr1 based on the predicted structure features, the effect of gain-of-function mutations in CgPdr1 activity, and literature information.* (A) The different regulatory domains of CgPdr1 identified include the DNA-binding domain (DBD), the linker region, the dimerization domain (DD), the regulatory domain (RD), three inhibitory domains (ID), three domains involved in fluconazole binding signalling (FBD), the middle homology region (MHR) the nuclear localization signalling (NLS) and the transactivation domain (TAD). The distribution of the gain-of-function mutations found in the literature in the amino acid sequence of CgPdr1 is also represented, including in green the GOFs characterized in this thesis. The structural representation of the different domains is represented with the same color in (B) backbone and (C) surface structural representation.

Notably, no significant mutations have been described to occur in the DNA-binding or dimerization domains of CgPdr1 suggesting that the changes in these domains could have a negative effect in mechanisms governing the activity of this protein. Another interesting observation is that several modifications, not associated with azole resistance, have been described to occur in the alleles encoded by clinical strains and not by the laboratory strain CBS138 including S76P, located in the DBD; V91I, L98S, L139I, T143P, located in the linker DNA; or D243N, located in the dimerization domain. Further studies will be required to investigate the relevance of these modifications.

4.5 Effect of the CgPdr1^{K274Q} variant in *Candida glabrata* genomic expression

To examine in detail how the K274Q modification in CgPdr1 affects the genomic expression of *C. glabrata*, cells of the SKY107 strain (devoid of CgPDR1 gene) were transformed with plasmid pYR29-MycHis_CgPDR1, or with its derived version pYR29-MycHis_CgPDR1^{A830C} (both engineered in chapter III of this thesis), to allow the expression of the wild-type CgPdr1 or its CgPdr1^{K274Q} variant in the same genetic background. As expected, cells expressing CgPdr1^{WT} variant exhibited a considerably lower MIC for fluconazole than those expressing the CgPdr1^{K274Q} variant, 128 and 258 mg/L, respectively (Table V. 2). Notably, the MIC obtained for cells expressing the wild-type CgPdr1 was already the defined resistance breakpoint for fluconazole in *C. glabrata* (which is set at 32 mg/L). Previous results described in the literature indicate that modifications in the C-terminal portion of CgPdr1 results in enhanced activity of this regulator, probably by affecting the functionality of the transactivation domain [51, 54, 56, 117, 196, 207], and therefore it is possible that the obtained higher MIC resulted from the Myc-tagging. Indeed, when SKY107 cells were transformed with plasmids pSP76 or pSP76_CgPDR1^{A830C}, that drive expression of non-tagged CgPdr1 proteins, the MICs obtained were significantly lower. Despite this, the beneficial impact of K274Q in improving azole tolerance is still observed, either in cells expressing the pYR29-MycHis or the PS76 plasmid (Table V. 2). The following work was performed with the pYR29-MycHis plasmid.

Table V. 2. Minimum inhibitory concentration values of fluconazole obtained for SKY107 cells ($\Delta pdr1$) transformed with plasmid pSP76 and pYR29-MycHis which drives expression of CgPDR1 from its natural promoter and terminator and in the derived plasmids that encode the CgPDR1 allele with the individual substitutions K274Q.

	CgPDR1-MYC (pYR29-MycHis Plasmid)	CgPDR1 (pS76 plasmid)
+empty vector	4	4
+CgPdr1 ^{WT}	128	8
+CgPdr1 ^{K274Q}	258	64

Comparison of the transcriptome of SKY107 cells expressing the CgPdr1^{WT} or the CgPdr1^{K274Q} variants (from the Myc-plasmid) resulted in the identification of 20 genes that could be considered differently expressed (above or below a threshold of 0.5 log₂F, corresponding to 1.4-fold) when cells were cultivated in RPMI medium. It is important to stress that under these experimental conditions, only the K274Q variant is expected hyperactivated thus allowing a more thorough study of the individual effect exerted by the GOF mutation. The dataset of genes differently expressed between CgPdr1^{WT} activated only under basal conditions and CgPdr1^{K274Q} hyperactivated variant (described in detail in Table V. 3) includes seven genes previously reported to be direct targets of CgPdr1, including Cg*CDR1*, Cg*PDH1*, and Cg*YOR1*, all encoding ABC drug-efflux pumps; Cg*PUP1*, a mitochondrial protein with unknown function; Cg*RTA1*, with a predicted role in lipid homeostasis; and the stress response genes Cg*YIMI* and Cg*AFT2*. The genes Cg*EPA2* and Cg*EPA3*, encoding poorly characterized adhesins, were also found to be up-regulated (1,43 and 1,42 fold, respectively, in the cells producing the K274Q variant, while gene Cg*AWP12* was down-regulated. Notably, expression of *CAGL0A01584g*, an ortholog of Sc*AGA2* involved in cellular agglutination in this species, was also found to be up-regulated in the K274Q variant. These results associating CgPdr1 and the expression of adhesin-encoding genes are of interest considering the close proximity of the K274 modification to the L280 residue whose modification to a proline was also described to result in up-regulation of Cg*EPA1* [229]. Also similar to what was herein observed with the K274Q variant, cells expressing a L280P hyper-active variant were also found to repress Cg*AWP12* expression [51]. On the overall, these results turn interesting a further study of the involvement of CgPdr1^{K274Q} and CgPdr1^{L280F} variants in *C. glabrata* adhesion and subsequent ability to form biofilms on biotic and abiotic surfaces. Neither Cg*EPA2* nor Cg*EPA3* ORFs promoters were found to harbour a putative PDRE motif suggesting an indirect effect of CgPdr1. Both these two ORFs are located at the telomeric region of chromosome E, after the Cg*EPA1* ORF. For this reason, it would also be interesting to investigate whether the effect of CgPdr1 K274Q modification in expression of these genes may be indirect and linked with modifications of the chromatin that might enhance transcription.

Table V. 3. Comparative transcriptomic analysis of *C. glabrata* SKY107 cells ($\Delta pdr1$) transformed with *pYR29_Myc-HIS_CgPDR1^{WT}* or *pYR29_Myc-HIS_CgPDR1^{AS20C}* plasmids, which drive the production of the wild-type or K274Q hyperactive variant, during growth in RPMI medium. Mid-exponential phase cells cultured in an RPMI medium were collected at a DO~1. A gene was considered differentially expressed if its mean absolute Log2 fold change value of two independent biological experiments was higher than 0.5 or lower than -0.5, with a cut-off p-value of 0.05. The PathoYeast database [141] was used to identify which of the differentially expressed genes are direct (in bold) or indirect targets of CgPdr1 (in underline). The information regarding the protein encoded function was summarized from the CGD database.

<i>C. glabrata</i> ORF/Standard Name	<i>S. cerevisiae</i> ortholog	Log2Fold (CgPdr1 ^{K274Q} vs CgPdr1 ^{WT})	Description
<i>CAGL0M12947g/</i> CgPUP1	no ortholog	1,44	Mitochondria-localized protein with unknown function
<i>CAGL0M01760g/</i> CgCDRI	PDR5	1,26	Multidrug transporter of ABC superfamily
<i>CAGL0E06666g/</i> CgEPA2	no ortholog	1,195	Epithelial adhesion protein
<i>CAGL0M09713g</i>	YIM1	1,085	Putative aldehyde reductase involved in DNA damage response
<i>CAGL0D00374g</i>	no ortholog	1,08	Protein of unknown function
<i>CAGL0L00561g</i>	<i>SSO1</i>	0,88	Putative plasma membrane t-SNARE involved in vesicle fusion
<i>CAGL0F02717g/</i> CgPDHI	PDR15	0,87	Multidrug transporter of ABC superfamily
<i>CAGL0E06688g/</i> CgEPA3	no ortholog	0,8	Epithelial adhesion protein involved in biofilm formation
<i>CAGL0M00704g</i>	no ortholog	0,73	Protein of unknown function
<u><i>CAGL0K03509g/</i></u> <u>CgHFD1</u>	<u>HFD1</u>	0,69	Putative dehydrogenase involved in ubiquinone biosynthesis and sphingolipid metabolism
<i>CAGL0L12496g</i>	no ortholog	0,68	Protein of unknown function
<i>CAGL0K00715g/</i> CgRTAI	RTA1	0,605	Putative membrane protein with unknown function of the lipid-translocating exporter family
<i>CAGL0D02244g</i>	<i>MEK1</i>	0,6	Putative meiosis-specific serine/threonine protein kinase
<i>CAGL0M06435g</i>	<i>PCH2</i>	0,57	Putative nuclear component of the pachytene checkpoint, which prevents chromosome segregation when recombination and chromosome synapsis are defective
<u><i>CAGL0F02651g</i></u>	<u>DIT1</u>	0,56	<i>S. cerevisiae</i> ortholog has a role in ascospore wall assembly
<i>CAGL0C04213g</i>	<i>RCR1</i>	0,56	Putative plasma membrane ubiquitin ligase-substrate adaptor involved in vesicle-mediated transport and chitin localization
<i>CAGL0G00242g/</i> CgYORI	YORI	0,545	Putative ABC transporter involved in multidrug efflux
<i>CAGL0D05918g/</i> CgATF2	ATF2	0,515	Putative alcohol acetyltransferase involved in steroid detoxification
<i>CAGL0A01584g</i>	<i>AGA2</i>	0,51	Putative adhesion subunit of a-agglutinin involved in cellular agglutination
<u><i>CAGL0G10219g/</i></u> <u>CgAWP12</u>	no ortholog	-0,49	Adhesin-like protein

It was previously suggested that distinct transcription profiles of different CgPdr1 GOF variants could occur by a bias in interaction to promoters with a different number of PDRE motifs (that could enhance recruitment of the transcription factor) or to the ability of CgPdr1 to recognize slightly different PDRE sequences (and with that recognize other target genes not recognized by the wild-type variant)[27]. Similar effects are proposed to explain the differences in ScPdr1 and ScPdr3 regulons [77, 97]. Therefore, in complement with the comparative transcriptomic analysis, it was also examined the direct binding of CgPdr1^{WT} or the CgPdr1^{K274Q} variant to the promoter region of target genes using for that a ChIP-seq approach. Necessarily, the cells were cultivated under the same conditions as those used for the transcriptomic analysis, that is, RPMI medium. The results of this analysis led to the identification of the promoters where CgPdr1^{WT}/CgPdr1^{K274Q} were found bound, these being summarized in Annex Table V. 2. A few examples of the peaks obtained are detailed in Figure V. 12. Representation and the final list of predicted direct targets (upon the application of filters to remove non-reliable results) considered to be directly bound in the promoters by CgPdr1 *in vivo* under these conditions are summarized in Table V. 4.

Table V. 4. Genes identified to be directly regulated by the CgPdr1^{K274Q} and CgPdr1^{WT} variants in this study using ChIP-seq analysis. Information regarding the protein encoded function was summarized from the CGD database [140].

<i>C. glabrata</i> ORF/ Standard Name	<i>S. cerevisiae</i> Ortholog	Log2F (CgPdr1 ^{K274Q} vs CgPdr1 ^{WT})	Description
CAGL0A00451g/ CgPDR1	PDR1	-0.11	Zinc finger transcription factor, the activator of drug resistance genes via pleiotropic drug response elements
CAGL0C03289g/ CgYBT1	YBT1	0.33	Putative ABC transporter involved in bile acid transport
CAGL0D05918g/ CgATF2	ATF2	0.52	Putative alcohol acetyltransferase involved in steroid detoxification
CAGL0F02717g/ CgPDH1	PDH1	0.87	Multidrug transporter of ABC superfamily
CAGL0G00242g/ CgYOR1	YOR1	0.55	Putative ABC transporter involved in multidrug efflux
CAGL0I04862g/ CgSNQ2	SNQ2	0.20	Predicted plasma membrane ABC transporter, putative transporter involved in multidrug resistance
CAGL0I07249g	BAG7	0.03	Putative RhoGAP involved in the homeostasis of the cell wall and cytoskeleton
CAGL0K01727g/ CgRPN4	RPN4	0.30	Transcription factor regulator of proteasome genes and ergosterol metabolism genes
CAGL0L10142g/ CgRSB1	RSB1	0.14	Putative sphingolipid flipase with the role in the incorporation of sphingolipid in the plasma membrane
CAGL0L10120g/ CgRTA1	RTA1	0,61	Putative membrane protein with the unknown function of the lipid-translocating exporter family
CAGL0M01760g/ CgCDR1	CDR1	1.26	Multidrug transporter of ABC superfamily
CAGL0M09713g	YIMI	1.09	Putative aldehyde reductase is involved in DNA damage response
CAGL0M12947g/ CgPUP1	PUP1	1.44	Mitochondria-localized protein

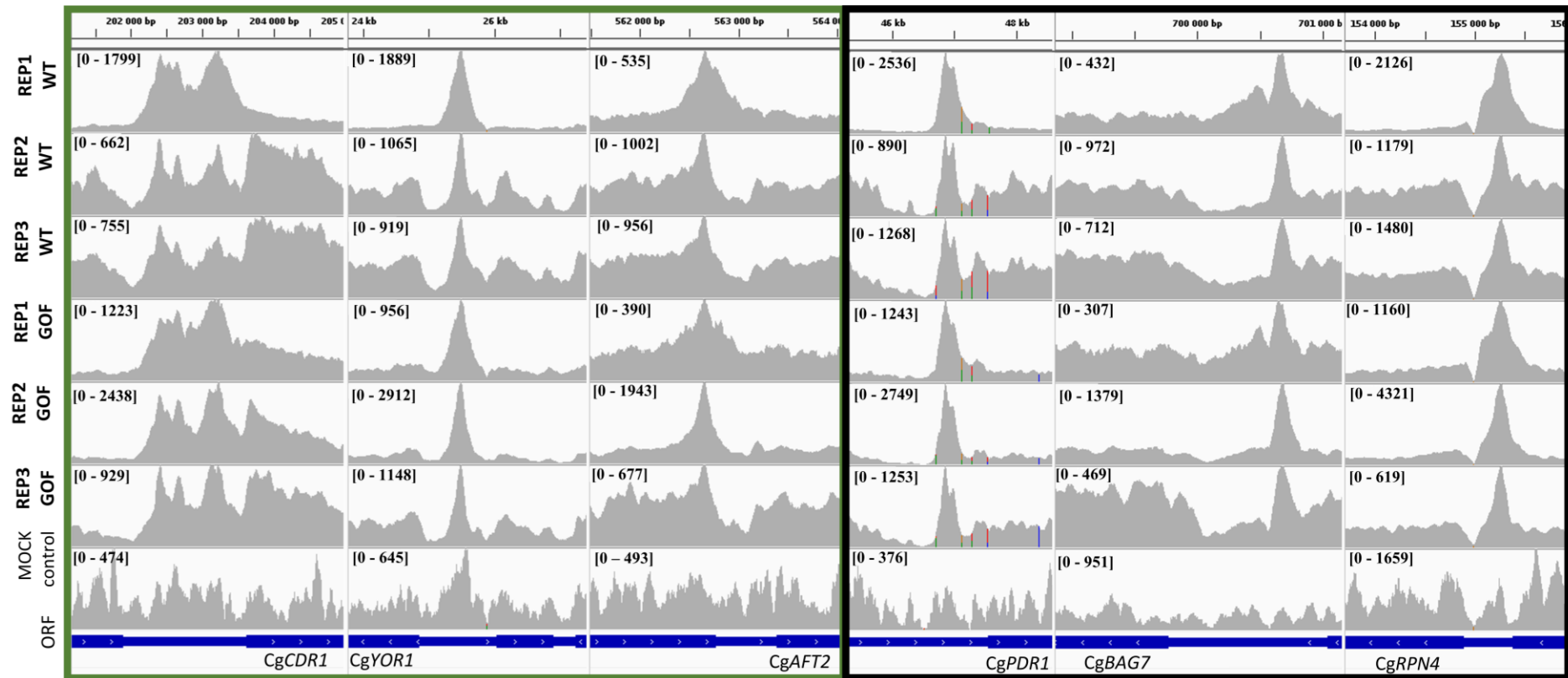


Figure V. 12. Representation of the *CgPdr1*^{K274Q} and *CgPdr1*^{WT} interaction with the promoter of some *CgPdr1* identified direct targets. Three examples of peaks of reads obtained in ChIP-seq analysis in the promoters of found upregulated genes by *CgPdr1*^{K274Q} vs *CgPdr1*^{WT} (green) and without change (black). Images were obtained in IGV viewer using ChIP-seq sequence files of three different replicates of each *CgPdr1* variant. The MOCK IP reads used as the control for peak calling using bPeaks software are also represented.

The results render clear that the set of promoters recognized *in vivo* by the wild-type CgPdr1 or by the CgPdr1^{K274Q} variant is the same, demonstrating that the hyper-activating mutation did not result in an expansion in the set of targets recognized by the transcription factor (Table V. 4, Figure V. 13). Out of the 13 direct targets of CgPdr1 herein identified, only 7 showed significantly increased (log2 fold change >0.5) expression in cells expressing the CgPdr1^{K274Q} variant, suggesting that other mechanisms are also involved in prompting the regulation of CgPdr1 target genes, besides the direct binding of the transcription factor to the promoter region (Table V. 4). The ChIP-seq analysis of promoters bound by CgPdr1^{K274Q} did not demonstrate an evident enrichment in reads (associated with occupancy of the transcription factor), compared to those obtained from the expression of wild-type CgPdr1, not even in promoters of genes whose expression was enhanced in cells expressing the K274Q variant (Figure V. 12). It is possible that we couldn't see an increase in occupancy in the K274Q variant because in our work we resorted to the use of a C-terminal tagged version of CgPdr1, a condition that has been described to increase protein activity (in other words, our wild-type could already be at a higher activity, compared to the one exhibited by a non-tagged inactive CgPdr1) [51, 54, 56, 117, 196, 207]. This observation was intriguing considering that in the work of Paul *et al.* 2014 [71], exploring a wild-type CgPdr1 activated due to mitochondrial dysfunction it was observed enrichment in occupancy of up-regulated target genes, in comparison with the occupancy observed in rho⁺, using an anti-CgPdr1 antibody in the ChIP-seq experiments. However, the same work demonstrated that when immunoprecipitating a tag-CgPdr1 significantly reduced the number of genes with enriched CgPdr1 promoter occupation in a rho⁰ strain when compared to a rho⁺ strain, but enrichment was still reported [71]. A relevant factor to have in consideration is the lack of stress activation signaling in a CgPdr1 gain-of-function since retroactive signalling effectors could alter the ability of CgPdr1 to bind to the DNA. An example of such is the dependence of ScPdr3 on ScLge1 recruitment of ScPdr3 protein to its promoter in rho⁰ cells [98].

The 13 potential direct targets of CgPdr1 herein identified (in the non-active CgPdr1^{WT} and in the hyperactive K274Q variant) coincide with those described in a previous study that aimed at characterizing the set of genes recognized by a wild-type CgPdr1 encoded in a petit strain and therefore activated [71](Figure V. 13). This similarity of the “different” CgPdr1 regulons, regardless of its activation status (and also despite differences in medium and growth conditions used, and even in ChIP protocol used) shows that the impact of CgPdr1 in genomic expression of *C. glabrata* is strongly associated with a well-defined set of genes. It was noticeable a higher number of promoters bound *in vivo* by CgPdr1 in the study that examined the wild-type CgPdr1 activated in the petite strain due to mitochondrial dysfunction, as detailed in the Venn diagram shown in Figure V. 13. This difference can result from a lower sensitivity of our ChIP-seq approach or can result from a different capacity of CgPdr1 to recognize different promoters dependent on the activation mechanism. In this context, a closer analysis of the promoters recognized by CgPdr1^{WT}, by the CgPdr1^{K274Q} variant or by the active CgPdr1 encoded in a petite mutant [71] revealed that promoters of genes only bound by the activated CgPdr1 coming from the petite mutant contain PDRE motifs having at their 5' terminus, AT, TC, CT, or CC, while promoters recognized by the non-active wild-type or K274Q CgPdr1 variants harbour PDRE motifs that have at their 5' terminus a TT (

Table V. 5). When comparing the promoters of genes found to be up-regulated in the cells expressing the K274Q variant, it is noticeable that these genes harbour multiple PDRE motifs that have at their 5' terminus a TT, while those genes whose promoter harbored only one PDRE motif having the two thymines in the 5' position were found to be equally transcribed in the wild-type and in the K274Q variant. Notably, *CgCDR1* and *CgPUP1*, the two genes found to be up-regulated in most strains expressing *CgPdr1* GOF mutants, were among those having multiple TTCCGTGG PDRE motif in their promoter. Further studies focused on quantifying the strength and occupancy in the binding of *CgPdr1* to the different PDRE sequence motifs could confirm whether or not the affinity towards the TTCCGTGG motif is preferable.

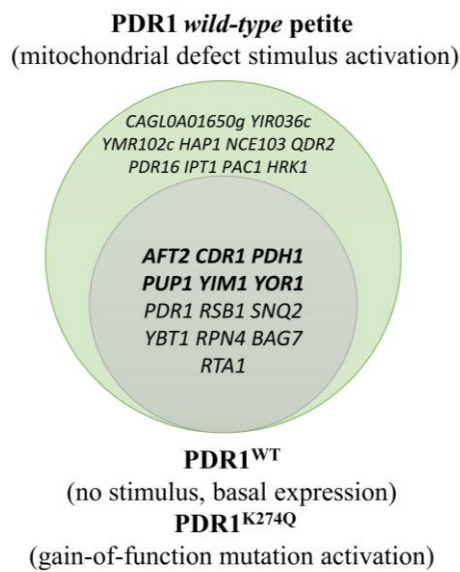


Figure V. 13. The K274Q gain-of-function mutation does not affect the *CgPdr1* promoter binding preference. ChIP-seq analyses of the *CgPdr1* Myc-tagged versions expressed in the SKY107 strain and immunoprecipitated in mid-exponential growth in RPMI pH7. ChIP-seq analyses identified the same direct regulated genes for *CgPdr1*^{K274Q} and *CgPdr1*^{WT}. Genes represented in bold have increased expression in a strain expressing *CgPdr1*^{K274Q} variant compared *CgPdr1*^{WT}. This set of genes was previously confirmed in Paul S. *et al.* 2014 directly regulated targets of *CgPdr1* activated in a petite strain. From those, only identified direct targets with a PDRE found in the promoter were considered in the present comparative analysis.

Table V. 5. Adapted table from Paul, S. et al. 2014 summarizing the direct CgPdr1 direct targets in rho⁰ cells predicted by the interaction of CgPdr1 with the promoter with PDRE motifs. Gray lines indicated the genes defined as possible targets only in ChIP-seq results in rho⁰ cells but not in this work. The PDRE motifs identified in the promoters of the gene targets are summarized. A central sequence highlighted in blue is conserved in most PDRE detected. Change of at least one of the two initial thymine is highlighted in red.

<i>C. glabrata</i> ORF/ Standard Name	<i>S. cerevisiae</i> Ortholog	PDRE(s)	Fold change in rho ⁰ cells vs rho ⁺	Fold change in CgPdr1 ^{K274Q} vs CgPdr1 ^{WT}
CAGL0A01650g	no ortholog	CCCCGTGGGA ATCCATGGGA	12	1
CAGL0C02937g	PAC1; HRK1	TCCCCGTGGAC	<2.2	1
CAGL0G01540g/CgNCE103	NCE103	CCCCGTGGGA	7	1.2
CAGL0G05313g	IPT1	ATCCGTGGAA	<2.2	1.1
CAGL0G08624g/CgQDR2	QDR2	ATCCGTGGAG	2.3	1
CAGL0J05852g	YIR036c	TCCCCGTGGAA	8	1.1
CAGL0J07436g/CgPDR16	PDR16	TTCCGTGGGA	3	1.1
CAGL0K03377g	YMR102C	ATCCGTGGAG TCCCATGGAA	3	1
CAGL0K05819g	HAP1	ATCCGTGGAA	3	1.1
CAGL0C03289g/CgYBT1	YBT1	TTCCGGGGAA TTCCGTGGGT	5	1.3
CAGL0D05918g/CgATF2	ATF2	CTCCGTGGAA	10	1.4
CAGL0F02717g/CgPDH1	PDH1	TTCCGTGGAA TTCCGTGGAA	18	1.8
CAGL0G00242g/CgYOR1	YOR1	TTCCCCGGGT TTCCGTGGAA	22	1.5
CAGL0I04862g/CgSNQ2	SNQ2	TCCCGTGGAG TTCCGTGGAA		1.1
CAGL0K00715g/CgRTA1	RTA1	TTCCGTGGAG	12	1.5
CAGL0K01749g/CgRPN4	RPN4	CTCCGTGGAC TTCCGTGGAA	3	1
CAGL0L10142g/CgRSB1	RSB1	TTCCGTGGAA	7	1.1
CAGL0M01760g/CgCDR1	CDR1	TTCCGTGGAC TTCCGTGGAA TCCCGTGGAA TCCCGTGGAG	4	2.4
CAGL0M09735g/ CgMEC3; CAGL0M09713g	MEC3; YIM1	TTCCGTGGAA TTCCGTGGAA	9	2.1
CAGL0M12947g/CgPUP1	PUP1	TTCCGTGGAT TTCCGTGGAC	57	2.7

4.7. Comparison of the interactomes of wild-type CgPdr1 and of K274Q GOF mutant

In order to better understand how the occurrence of GOF modifications may shape the ability of CgPdr1 to interact with other proteins at the chromatin site, a ChIP-SICAP followed by MS approach was used [336]. This technique allows discrimination of the proteins interacting near a given protein-DNA complex. For this, an immunoprecipitation step is undertaken that will pulldown the Myc-CgPdr1-DNA

complex and also interacting proteins that could be nearby. After the immunoprecipitation, the DNA immunoprecipitated together with myc-tagged CgPdr1 is biotinylated and afterwards captured with streptavidin, while other proteins not interacting with DNA are washed [336]. For this experiment, the cells were cultivated under the same conditions as those used for the comparative transcriptomic and ChIP-seq analyses, that is, in RPMI. Under the experimental conditions used a total of 26 proteins with predicted nuclear localization were identified as interacting with CgPdr1^{WT} and/or with CgPdr1^{K274Q} (Annex Figure V. 1 and Table V. 6). Overall, few nuclear proteins were identified to be immunoprecipitated with CgPdr1 and these experiments should be optimized in the future. These results, as they are, limit the confidence in the following analysis, especially when it comes to comparing the quantitative intensities of the same proteins between both CgPdr1^{WT} and CgPdr1^{K274Q}, but also in the analysis of proteins exclusively found in one of the datasets. Therefore, the following analysis will focus only the proteins identified as general possible interactors of CgPdr1 (regardless of whether they had been retrieved from the wild-type or the K274Q variant) these being listed in Table V. 6.

As expected, CgPdr1 and CgGal11A were pulled down from the immunoprecipitated protein extracts recovered from CgPdr1^{WT} and CgPdr1^{K274Q} samples, demonstrating that the IP step was correctly performed. Among the retrieved proteins, only these two had been before implicated in azole resistance in *C. glabrata*. Notably, most of these CgPdr1 interactors have a biological function that relates to DNA binding (Figure V. 14) including components of different complexes involved in transcriptional elongation or in chromatin remodelling (Table V. 6, Figure V. 14). The herein identification of subunits of the FACT complex as putative CgPdr1 interactors was interesting considering the previous demonstration on the involvement of this complex in up-regulation of *ScPDR5* transcription in *S. cerevisiae* [149, 150]. Three proteins predicted to have a role in histone methylation were identified in the set of CgPdr1 interactors, CAGL0J04510g, CAGL0B01375g and CAGL0L04774g (Figure V. 14, Table V. 6). As mentioned before, azole stressed *C. glabrata* cells show a decreased level of histone methylation and a consequent decrease in H3 and H4 histones protein levels [164]. Specifically, the two herein identified Paf1 complex proteins (the orthologs of ScCtr6 and ScCdc73) and the ortholog of ScSpt6 have a positive role in H3K36 trimethylation, which was described to exert a negative effect in the expression of genes of the CgPdr1-regulon in *C. glabrata* [164, 341]. This observation and the herein identification of these proteins involved in histone methylation as interactors of CgPdr1 suggests histones present in the promoter region of target genes can be undergoing methylation/de-methylation processes, with consequences in their expression. One interesting aspect that would be interesting to test, if whether this interaction between histone methylating-proteins would be less pronounced in cells encoding GOF CgPdr1 variants which could explain the higher expression of CgPdr1 target genes in these cells. Other CgPdr1 interactors identified include CAGL0J01177g, an orthologue of ScAbf1, a zinc transcription multifunctional global regulator involved in chromatin silencing and remodelling [342]; and CAGL0E02315g, similar to the ScHtz1 histone variant implicated in the silencing of telomeric located genes like adhesins [343]. The immunoprecipitation of both these proteins is especially relevant in light of the well-reported role of CgPdr1 in prompting the expression of telomerically located adhesin genes expression *CgEPA2* and *CgEPA3* in cells expressing the K274Q GOF variant. The co-immunoprecipitation of CgPdr1 with CAGL0L02013g, an ortholog of ScIxr1, a transcriptional repressor of genes involved in response to hypoxia [344], was also very intriguing

considering that in a screening, taking advantage of *S. cerevisiae* mutant library, to identify genes that when deleted the growth could be affected by the expression of Cg*PDR1* GOF variants, the expression of Cg*PDR1* (including GOF variants) in a Sc*IXR1* deletion mutant led to defect in growth [159]. However, this genetic interaction was not further confirmed in *C. glabrata*.

Table V. 6. (Part 1) *Interactome of the CgPdr1^{WT} and CgPdr1^{K274Q} analyzed by mass-spectrometry of the immunoprecipitated CgPdr1 variants with interacting proteins through ChIP-SICAP technique.* Only proteins identified in the MS of CgPdr1^{WT} or CgPdr1^{K274Q} immunoprecipitated samples but not in the MOCK sample were considered. Two biological replicates were used for each condition in the study. Furthermore, the usual contaminants peptides of IP-MS such as ribosomal proteins and core histones were discarded from the analysis. Information herein detailed regarding the protein function summarized from the CGD and SGD databases. In bold are marked encoding genes that deletion was demonstrated to influence azole resistance and protein was demonstrated to interact with CgPdr1.

Sample	Uniprot accession	<i>C. glabrata</i> protein/ Standard Name	<i>S. cerevisiae</i> Ortholog	Function
WT and K274Q	Q6FPG2	CAGL0J04070g	<i>RPB8</i>	Predicted central subunit RNA polymerases
	Q6FXB0	CAGL0B01375g	<i>CTR9</i>	Predicted component of the Paf1p complex involved in transcription elongation that binds to the basal transcription machinery
	Q6FPE2	CAGL0J04510g	<i>CDC73</i>	Predicted component of the Paf1p complex involved in transcription-coupled nucleotide excision repair, mRNA 3'-end processing, and histone H3 methylation. It binds to the basal transcription machinery
	Q6FPT2	CAGL0J01177g	<i>ABF1</i>	Predicted zinc finger transcription factor in transcriptional activation, gene silencing, and DNA replication and repair
	Q6FXU7	CAGL0A00451g/ CgPDR1	PDR1	Zinc finger transcription factor that positively regulates drug resistance genes via pleiotropic drug response elements
	Q6FX01	CAGL0C01573g	<i>ARO4</i>	Predicted 3-deoxy-D-arabino-heptulosonate-7-phosphate synthase; catalyzes the first step in aromatic amino acid biosynthesis. In <i>S. cerevisiae</i> the protein distribution to the nucleus increases upon DNA replication stress
	Q6FPL0	CAGL0J02992g	<i>THO1</i>	Predicted nuclear protein that binds to dsDNA, RNA, and chromatin and is involved in transcription, nuclear poly(A) ⁺ mRNA export, and ribonucleoprotein complex assembly
	Q6FSB6	CAGL0H01815g/ CgCBF1	<i>CBF1</i>	Predicted basic helix-loop-helix protein homodimer that binds to the E-box consensus sequence CACGTG present at MET gene promoters and centromere DNA element I and associates with other transcription factors to mediate transcriptional activation or repression
	Q6FRS9	CAGL0H06215g/ CgGAL11A	MED15A	Component of the transcriptional Mediator complex
	Q6FWT4	CAGL0C03047g	<i>SPT16</i>	Predicted subunit of the heterodimeric FACT complex (Spt16p-Pob3p) that is involved in the reorganization of the nucleosomes to facilitate access to DNA by RNA and DNA polymerases
	Q6FLN7	CAGL0L02013g	<i>IXR1</i>	Predicted transcriptional repressor that regulates hypoxic genes during normoxia
	Q6FKI2	CAGL0L11352g	<i>POB3</i>	Predicted subunit of the heterodimeric FACT complex (Spt16p-Pob3p)
	B4UN11	CAGL0H08541g	<i>NHP6B</i>	Predicted high-mobility group protein that binds to and remodels nucleosomes and is involved in the recruiting of FACT complex and other chromatin remodelling complexes to the chromosomes

Table V. 6. (Part 2)

Sample	Uniprot accession	<i>C. glabrata</i> ORF/ Standard Name	<i>S. cerevisiae</i> Ortholog	Function
WT	Q6FMY5	CAGL0K04235g	<i>NQM1</i>	Predicted nuclear transaldolase involved in oxidative stress response
K274Q	Q6FND0	CAGL0K00913g	<i>ADE3</i>	Predicted cytoplasmic enzyme C1-tetrahydrofolate synthase is involved in the biosynthesis of purines, histidine, methionine, or pantothenic acid
	Q6FVH0	CAGL0E01947g	<i>HRP1</i>	Predicted subunit of cleavage factor I required for the cleavage and polyadenylation of pre-mRNA 3' ends
	B4UMZ4	CAGL0E02315g	<i>HTZ1</i>	Predicted histone variant H2AZ involved in transcription activation, prevention of the ectopic spread of heterochromatin, and genome integrity
	Q6FVB4	CAGL0E03245g	<i>NSR1</i>	Predicted nucleolin required for pre-rRNA processing and ribosome biogenesis
	Q6FIV9	CAGL0M11374g	<i>SWI3</i>	Predicted subunit of the SWI/SNF chromatin remodelling complex
	Q6FMA4	CAGL0K09702g	<i>YNL134C</i>	Predicted NADH-dependent aldehyde reductase, involved in detoxification of furfural
	Q6FXZ3	CAGL0A01430g/ CgTRP5	<i>TRP5</i>	Tryptophan synthase
	Q6FWK4	CAGL0C04983g/ CgADO1	<i>ADO1</i>	Predicted adenosine kinase that may be involved in recycling adenosine
	Q6FUV3	CAGL0F00407g	<i>LIA1</i>	Predicted deoxyhypusine hydroxylase metalloenzyme that catalyzes hypusine formation unique amino acid to eIF-5A
	Q6FRZ5	CAGL0H04697g	<i>SPT5</i>	Predicted Spt4p/5p (DSIF) subunit of the transcription elongation factor complex that binds to the basal transcription machinery
	Q6FRA6	CAGL0H10142g/ CgARO3	<i>ARO3</i> (best homology hit)	Predicted 3-deoxy-D-arabino-heptulosonate-7-phosphate synthase that catalyzes the first step in aromatic amino acid biosynthesis
	Q6FLB1	CAGL0L04774g	<i>SPT6</i>	Predicted nucleosome remodelling protein is required for the fidelity of promoter selection through maintenance of chromatin structure during transcription and is required for H3K36 trimethylation by Set2p.

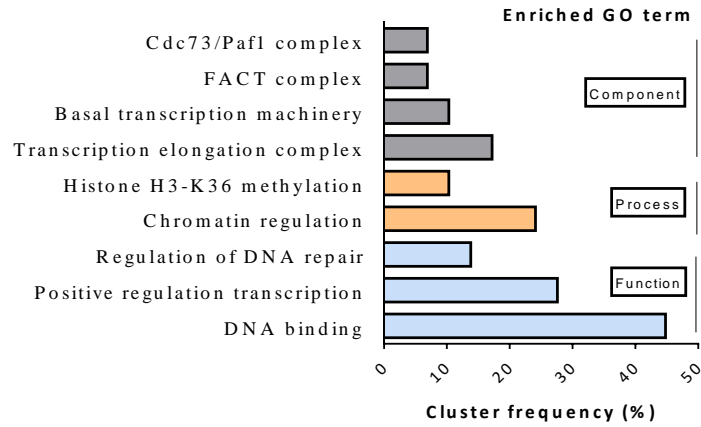


Figure V. 14. Mass spectrometry identification of the nuclear proteins immunoprecipitated with the Myc-tag *CgPDR1* wild-type variant and *K274Q* gain-of-function variant using ChIP-SICAP methodology. Gene ontology (GO) categories in the proteins identified were defined using the CGD database “GO term finder” tool [345].

VI. Effect of CgHaa1 and of CgHaa1-regulon in *Candida glabrata* ability to form biofilms and in virulence against the infection model *Galleria mellonella*

1. Abstract

Candida glabrata is today the second major causative agent of candidiasis, with the increased incidence of this species being associated with its high resilience to currently used antifungals, in particular, to azoles. In result of this, the development of new therapies focused on targets other than those targeted by currently used antifungals is needed and, in this context, proteins that contribute for the persistence of *C. glabrata* as a human colonizer, even if as a commensal, are interesting since inhibition of their activity can reduce competitiveness and lead to eradication. The CgHaa1 transcription factor has been recently described as the major response element of *C. glabrata* to stress induced by acetic acid, an organic acid which the yeast has to cope with considering its presence in the vaginal environment as the result of the metabolic activity of commensal bacteria. The described CgHaa1-regulon was extensive and included proteins with different biological functions contributing to maximize response to acetic acid stress standing out the plasma-membrane pump encoding gene CgPMA1, several regulators of CgPma1, the MDR transporter CgTPO3 and various predicted adhesin-encoding genes. In this work, the role of CgHaa1 and of its target genes CgAWP12, CgAWP13, CAGL0H07469g, and CAGL0K10164g, all encoding adhesins, in the ability of *C. glabrata* in adherence to biotic and abiotic surfaces was scrutinized, along with the impact of these genes in biofilm formation. Furthermore, it is also herein demonstrated that the expression of CgHAA1 gene and of its target genes CgAWP12, AWP13, CAGL0K10164g, CAGL0I07249g, CAGL0E03740g and CAGL0G05632g, maximizes virulence of *C. glabrata* against the wax *Galleria mellonella* infection model, expanding the biological function of this regulatory system beyond response and tolerance to acetic acid stress.

2. Introduction

C. glabrata is very well adapted to the human host, having acquired in its evolution several traits that are believed to improve its capacity as a human colonizer [346, 347]. Among these, *C. glabrata* has evolved strategies to avoid the activity of the host immune system such as a capability to survive inside macrophages, being even capable of inducing lysis of these cells after extensive replication and increased cell load [348]. This strategy of immune evasion differs greatly from that of *C. albicans*, which appears to depend more on escaping phagocytosis rather than adapting to the harsh environment of the phagosome. To do so, *C. albicans* cells shift to hyphal growth shortly after macrophage internalization disrupting the macrophage membrane [349, 350]. One of the responses that *C. glabrata* cells have been described to undergo while “colonizing macrophages” includes an extensive remodeling of chromatin to allow an extensive modification of its genomic expression and with that improved capability to respond to different stressors posed by the environment [351]. These modifications in the transcriptome profile of *C. glabrata* phagocytized cells includes the up-regulation in expression of genes involved in DNA damage repair and cell wall integrity, but also an extensive shift in metabolic genes expression presumed to result from a response to the glucose starving conditions registered in the phagosome [201, 351, 352]. Among the alterations registered in transcriptome of *C. glabrata* phagocytosed cells is the up-regulation of genes involved in gluconeogenesis, in β -oxidation of fatty acids, and in glyoxylate cycle [201, 351, 352]. These changes suggest a change to consume carbon sources that could be more available than glucose, such as fatty acids [351, 352]. At the cellular level, it is observed the mobilization of intracellular resources via autophagy (especially pexophagy) this being essential for the survival of *C. glabrata* engulfed cells [201, 353]. The increase in the expression of genes involved in high-affinity reductive iron uptake systems and the transport of siderophore-iron complexes was also observed as a response of phagocytized *C. glabrata* cells, attributed to the iron starvation conditions deprived macrophage cytosol [354, 355]. Responses that involve the modification of the phagosome environment were also observed to take place including the inhibition of phagosome acidification [348, 356]. The lack of pH reduction results in the blockage of macrophage maturation and the reduction of the function of acidic hydrolases [348].

In this study, it is described the involvement of the CgHaa1 regulator and of some of its regulated genes in the formation of biofilms under acidic conditions (pH 4) prompted by the presence of acetic acid, an aspect that has not been much addressed in prior studies focusing on biofilm development that use neutral pHs [347, 357] or other acidifying agents (like HCl or lactic acid, for example) [358, 359]. This involvement of CgHaa1 in biofilm formation was anticipated taking into account the demonstrated positive effect of this regulator in mediating adherence of *C. glabrata* to vaginal epithelial cells at low pH and in up-regulating the expression of several adhesin-encoding genes (as described in the introduction of this thesis, see Chapter II), a trait that was not observed for the orthologous network active in *Saccharomyces cerevisiae* and controlled by the orthologue transcription factor ScHaa1 [252, 262]. These aspects are detailed in the introduction section of the thesis and therefore they won't be described herein. The set of genes regulated by CgHaa1 in response to acetic acid include *CAGL0H07469g*, *CAGL0J11176g*, *CAGL0K10164g* and *CAGL0L06424g* with known orthologues in *S. cerevisiae* and *CgEPA2*, *CgAWP12*, *CgAWP13*, *CAGL0F09273g* and *CAGL0H00110g* *C. glabrata*-specific predicted adhesion genes [262]. Few studies have investigated the binding specificity of these adhesins and the

conditions leading to its gene expression, knowledge primarily limited to the observation of the expression of some of these adhesions genes or the protein production in conditions of oxidative stress, low pH or azole antifungal exposure [63, 358, 360-362], as consequence these adhesins remain largely uncharacterized. Adhesion is a fundamental aspect of the virulence of *Candida* species and of their ability to colonize the human host and this was also found to be the case of *C. glabrata* whose genome appears to encode an exceptionally high number of these proteins (~60 to 100) [363-365], compared to the number encoded by *S. cerevisiae* (~10) [366, 367]. This expansion of adhesion-involved genes is a possible consequence of the necessity of this yeast to successfully adhere (and subsequently form a biofilm) on different host surfaces and make quick adaptations of the adhesion capacity to changing conditions in the niche [346, 347, 363]. Recently, a *de novo* assembly of the CBS138 laboratorial strain performed with more accurate sequencing methods (and that therefore bypassed the problems with the sequencing of large telomeric genes, as is the case of those encoding adhesins) predicted that the *C. glabrata* adhesin-encoding genes exhibit long tandem repeats not observed in other Fungi, this being believed to favor may interaction with ligands at some distance from the cell [368]. Interestingly, proteomic studies also revealed a high number of adhesion-related proteins in the biofilm matrix of *C. glabrata*, compared to the one registered in a biofilm formed by *C. albicans* cells [369, 370]. It is suggested that the higher contribution of adhesion in *C. glabrata* may compensate for the lack of filamentation, a trait that is crucial for adhesion and biofilm formation in *C. albicans* [363, 369, 371]. Concordantly with the importance of adhesion in *C. glabrata*, several genome-wide studies report enrichment of non-synonymous mutations, increased copy number, small insertions and deletions of adhesin genes in clinical isolates, even when comparing clonal isolates recovered from different sites of infection of the same patient [55, 67, 283, 287, 316, 372, 373]. These genetic differences are believed to result largely from the sub-telomeric localization of these adhesin-encoding genes which renders them hotspots for large copy variations and SNP variations [372, 374, 375]. Adhesin gene expansions and rapid evolution results in the higher capability of *C. glabrata* to establishment biofilm in different substrates, both *in vivo* and *in vitro*, with consequences in the reduction of the efficacy of antifungal treatment due to reduced drug access (reviewed in [371]). Few transcriptional regulators have been characterized so far as mediating *C. glabrata* ability to form biofilms, specially under acidic conditions, a trait that, as said above, is relevant in the scope of vaginal colonization [34]. Among those transcription factor described to influence biofilm formation are CgCst6, a negative regulator of *in vitro* formed biofilms, presumably by downregulating *CgEPA6* gene expression [376]; CgEfg1 and CgTec1, required for the maximum production of polysaccharides and protein content in the extracellular matrix, respectively, and maximizing adherence of *C. glabrata* to human vaginal epithelial cells [377]. While CgEfg1 was shown to be involved in the regulation of several adhesion genes in biofilm cells, CgTec1 played more relevant role in regulating the expression of genes involved in cell wall organization or filamentous growth during biofilm formation [377]. Notably, CgEfg1 was found to down-regulate the expression of a reduced number of adhesion-encoding genes during *C. glabrata* planktonic growth demonstrating that the activity of these regulators is also largely influenced by the morphological state of the cells and even their density [377].

The involvement of CgHaa1 and of its poorly characterized target adhesins genes *CgAWP12*, *CgAWP13*, *CAGL0H07469g*, and *CAGL0K10164g* in the ability of *C. glabrata* cells to form biofilms is scrutinized in this work, shedding light into the panoply of players that influence this complex phenotype in this pathogenic yeast species. Furthermore, the role of the CgHaa1-regulon in virulence of *C. glabrata* against the infection model

Galleria mellonella was also scrutinized expanding the portfolio of biological functions described for this system beyond tolerance to acetic acid at low pH.

3. Materials and Methods

3.1. Strains and growth medium

The *C. glabrata* strains used in this study are listed in Table VI. 1. The different strains were batch-cultured at 30°C at 250 rpm orbital agitation in liquid YPD rich medium, MM, or RPMI growth medium. YPD contains, per liter, 20 g of glucose (Merck), 20 g bactopectone (Difco) and 10 g yeast extract (Difco). The MM medium contains, per liter, 20 g glucose (Merck), 1.7 g yeast nitrogen base without ammonium and amino acids (Difco), and 2.65 g (NH₄)₂SO₄ (Merck). RPMI contains, per liter, 20 g of RPMI-1640 synthetic powder medium without glutamine (Sigma), 20 g of glucose (Merck), 0.3 g of glutamine (Sigma), and 0.165 mol/L of MOPS (Sigma). When needed, the pH of the medium used was adjusted to pH 4 using HCl as the acidulant. Solid media was obtained by supplementing the corresponding liquid medium with 20 g (per liter) of agar (Iberagar).

3.2. Gene disruption

The KUE100 strain [277] was used as the host for the individual disruption of the following CgHaa1 target genes: CgAWP12, CgAWP13, CAGL0H07469g, CAGL0K10164g, CAGL0L00649g, CAGL0L08008g, CgICL1, and CgMLS1. The remaining deletion mutants used in this work were previously described in Bernardo *et al.* 2017 [262]. These mutants were created by replacing their sequence with a DNA cassette containing the CgHIS3 gene using homologous recombination. The replacement cassette was prepared by PCR using an appropriate set of primers and using the pHIS906 plasmid containing the CgHIS3 sequence as a template. The transformation procedures of KUE100 cells were performed as described before in Ueno, K. *et al.* 2011 [277]. The recombination locus and gene deletion were verified by PCR using appropriate primers.

3.3. Assessment of the deletion of CgHAA1 gene and of the target adhesins CgAWP12, CgAWP13, CAGL0H07469g, and CAGL0K10164g genes in *Candida glabrata* ability form biofilms in the presence of acetic acid

Cell viability in the biofilm formed by *C. glabrata* KUE100_chr606 cells or by the mutants Δ CgHaa1, Δ Cgawp12, Δ Cgawp13, Δ CAGL0H07469g, and Δ CAGL0K10164g was tested, using the Presto blue method. Briefly, an initial suspension of the different strains (containing approximately 2×10^6 cells/ml) was inoculated in the wells of polystyrene microtiter plates (Greiner) containing 200 μ L of RPMI (at pH 4) or of this medium supplemented with 30 mM acetic acid. The cells were cultivated, at 30 °C, with orbital shaking of 100 rpm for 6 h and 24 h. After 6 and 24h, the medium was carefully removed from each well, and cells were washed twice with 100 μ L PBS to remove non-adherent cells. PrestoBlue reagent (ThermoFisher Scientific) was then diluted with RPMI (at pH 4) in a proportion of 1:10 (prestoBlue reagent:medium). To determine viability, 100 μ L of this solution was added to the cells and the mixture left for 30 min at 37°C. Afterwards, absorbance at 570 nm and 600 nm was measured in a microplate reader (SPECTROstar Nano, BMG Labtech).

Table VI. 1. List of strains used in this study

Strain	Genotype	Predicted function of the encoded protein	Reference
KUE100	Parent strain derived from the <i>C. glabrata</i> strain 2001H; histidine auxotroph; the recipient enables highly efficient gene targeting in which <i>yku80</i> is repressed with a <i>SAT1</i> flipper	-	Ueno, K. <i>et al.</i> 2011 [277]
KUE100_chr606	Control strain derived from KUE100 parental strain in which the <i>CgHIS3</i> marker was ectopically integrated at a non-coding locus	-	Ueno, K. <i>et al.</i> 2011 [277]
KUE100Δ <i>Cghaa1</i>	Δ <i>Cghaa1</i> strain, ORF CAGL0L09339g was replaced with <i>CgHIS3</i> marker	Transcription factor, involved in the regulation of response to acetic acid stress	Bernardo, R. <i>et al.</i> 2017 [262]
KUE100Δ <i>Cgawp12</i>	Δ <i>Cgawp12</i> strain, ORF CAGL0G10219g was replaced with <i>CgHIS3</i> marker	Predicted cell wall adhesin	This study
KUE100Δ <i>Cgawp13</i>	Δ <i>Cgawp13</i> strain, ORF CAGL0H10626g was replaced with <i>CgHIS3</i> marker	Predicted cell wall adhesin	This study
KUE100Δ <i>CAGL0H07469g</i>	Δ <i>CAGL0H07469g</i> strain, ORF CAGL0H07469g (<i>ScICS2</i> orthologue) was replaced with <i>CgHIS3</i> marker	Predicted cell wall adhesin	This study
KUE100Δ <i>CAGL0K10164g</i>	Δ <i>CAGL0K10164g</i> strain, ORF CAGL0K10164g (<i>ScSED1</i> orthologue) was replaced with <i>CgHIS3</i> marker	Predicted cell wall adhesin	This study
KUE100Δ <i>CAGL0C03740g</i>	Δ <i>CAGL0C03740g</i> strain, ORF CAGL0C03740g (<i>ScMIT1</i> best hit) was replaced with <i>CgHIS3</i> marker	Protein of unknown function	Bernardo, R. <i>et al.</i> 2017 [262]
KUE100Δ <i>CAGL0G05632g</i>	Δ <i>CAGL0G05632g</i> strain, ORF CAGL0G05632g (<i>ScYDL218W</i> orthologue) was replaced with <i>CgHIS3</i> marker	Protein of unknown function	Bernardo, R. <i>et al.</i> 2017 [262]
KUE100Δ <i>CAGL0I07249g</i>	Δ <i>CgCAGL0I07249g</i> strain, ORF CAGL0I07249g (<i>ScBAG7</i> orthologue) was replaced with <i>CgHIS3</i> marker	Putative GTPase-activating protein involved in the cell wall and cytoskeleton homeostasis	Bernardo, R. <i>et al.</i> 2017 [262]
KUE100Δ <i>CAGL0K07337g</i>	Δ <i>CAGL0K07337g</i> strain, ORF CAGL0K07337g (<i>ScHSP30</i> best hit) was replaced with <i>CgHIS3</i> marker	Predicted ion channel with a role in the regulation of the plasma membrane ATPase activity	Bernardo, R. <i>et al.</i> 2017 [262]
KUE100Δ <i>Cgrsb1</i>	Δ <i>Cgrsb1</i> strain, ORF CAGL0L10142g was replaced with <i>CgHIS3</i> marker	Putative sphingolipid flippase	Bernardo, R. <i>et al.</i> 2017 [262]
KUE100Δ <i>Cgicl1</i>	Δ <i>Cgicl1</i> strain, ORF CAGL0J03058g was replaced with <i>CgHIS3</i> marker	Predicted isocitrate lyase of the glyoxylate cycle	This study
KUE100Δ <i>CAGL0L00649g</i>	Δ <i>CAGL0L00649g</i> strain, ORF CAGL0L00649g (<i>ScACS1</i> orthologue) was replaced with <i>CgHIS3</i> marker	Predicted acetyl-coenzyme A synthetase	This study

3.4. Assessment of the expression of *CgHAA1*, *CgAWP12*, *CgAWP13*, *CAGL0H07469g*, and *CAGL0K10164g* genes during biofilm formation in the presence or absence of acetic acid

To assess the expression of *CgHAA1* and of the *CgHaa1*-regulated genes *CgAWP12*, *CgAWP13*, *CAGL0H07469g*, and *CAGL0K10164g* genes in biofilms formed by *C. glabrata* in the presence or absence of acetic acid, the same experimental setup described above was used with the difference that the assay was conducted in 6-well polystyrene microtiter plates (Orange Scientific). Around 6h after the inoculation of the cells in the 6-well plates, the medium was carefully removed and the biofilm formed was washed twice with PBS to remove non-adherent cells, scraped with a pipette tip and finally resuspended in 1 mL PBS. The cells were centrifuged for 2 min at 15 000 rpm at 4°C and stored at -80°C until RNA extraction. For the RNA extraction, the MasterPure™ Yeast RNA Purification Kit (Lucigen) was used. The cDNA synthesis step was performed in a real-time PCR machine and resorting to 1 µg of total RNA collected from each sample. This reverse transcription step was performed using the multiscribe reverse transcriptase kit (Applied Biosystems) in a C1000 Thermal Cycler (Bio-Rad, Hercules). Approximately 250 ng of the synthesized cDNA was used for the subsequent quantitative PCR step. In all experiments, the transcript level of *CgACT1* mRNA was used as an internal control. The primers used for the amplification of the probes selected to monitor gene expression were designed using Primer Express Software and are detailed in Table VI. 2.

Table VI. 2. List of primers used in this study

Primer	Sequence
<i>CgACT1</i> _ Forward	5'-AGAGCCGTCCTCCCTTCCAT- 3'
<i>CgACT1</i> _ Reverse	5'-TTGACCCATACCGACCATGA- 3'
<i>CgAWP12</i> _ Forward	5'-CGATTGCTTTTGATACCCCAAT- 3'
<i>CgAWP12</i> _ Reverse	5'-CGGACCTTCCAGGAAAAAGAC- 3'
<i>CgAWP13</i> _ Forward	5'-AATATCTTGCTGGGCTTTTGGA- 3'
<i>CgAWP13</i> _ Reverse	5'-AGCGTAGCACTGTCTATGATTATTTCTT- 3'
<i>CAGL0H07469g</i> _ Forward	5'-GGGATCTCCAAGGCGGTATAA- 3'
<i>CAGL0H07469g</i> _ Reverse	5'-GGCAAATATAGCTCCTCTGGTGTAC- 3'
<i>CAGL0K10164g</i> _ Forward	5'-ACGTTCTTCTCTTGCTGCACAA- 3'
<i>CAGL0K10164g</i> _ Reverse	5'-GCCGTTAACGTGTTGGGTAAC- 3'
<i>CAGL0E03740g</i> _ Forward	CATGGAGTCAAGGAGAAGATCACA
<i>CAGL0E03740g</i> _ Reverse	GGCACAATCACCCTCATGGT

3.5. Effect of *CgHaa1* and *CgHaa1*-regulated adhesin genes *CgAWP12*, *CgAWP13*, *CAGL0H07469g*, and *CAGL0K10164g* in adherence of *Candida glabrata* to the reconstituted human vaginal epithelium

The capability of the control strain KUE100_chr606 or of the mutants $\Delta Cg\text{haa1}$, $\Delta Cg\text{awp12}$, $\Delta Cg\text{awp13}$, $\Delta CAGL0H07469g$, and $\Delta CAGL0K10164g$ to colonize a commercially available reconstituted human vaginal epithelium (RHVE) was compared (Skin Ethic 335 Laboratories; Nice, France). The method used is detailed in Alves, S. *et al.* 2014 [378]. Briefly, RHVE tissues were inoculated for 24 h with 1 mL of standardized suspensions of the different *C. glabrata* strains (using 2×10^6 cells/mL) in RPMI medium adjusted to pH 4, either or not supplemented with 30 mM acetic acid. As a control, two RHVE tissue preparations incubated only with 1 mL

RPMI, supplemented or not with acetic acid, were also prepared. The infected and non-infected tissues were incubated at 37°C in a 5 % CO₂ environment in saturated humidity for 12h and after this quantification of *C. glabrata* cells in the different tissue preparations was performed based on the quantification of genomic DNA. For this, the infected tissues were placed in sterile 1.5 mL microcentrifuge tubes (Eppendorf AG, Hamburg, Germany) with approximately 300 µL of 367 glass beads (0.5 mm diameter – Sigma, St. Louis, Mo.) and 600 µL of sorbitol buffer GriSP, Porto, Portugal). This final mix was homogenized three times for 60 s, using a Mini-Beadbeater-8 (Stratech Scientific, Soham, UK). After tissue disruption, the supernatant was carefully removed and placed in another sterile microcentrifuge tube. Then, DNA extraction was performed using the GRS Genomic DNA kit – Tissue (GriSP), following the manufacturer’s protocol. After extraction, the DNA from each experimental condition was quantified using the NanoDrop 1000 Spectrophotometer (Thermo Fisher Scientific, Wilmington, DE, USA). *C. glabrata* genomic DNA was quantified using real-time PCR in a CF X96 Real-Time PCR System (Bio-Rad, Berkeley, USA). Each reaction mixture consisted of 10 µl of working concentration of SsoFast EvaGreen Supermix (Bio-Rad, Berkeley, USA), 0.2 µl of each primer (50 µM) (forward- TTTGCATGCGCTTGCCACGAATCC and reverse- GGTGGACGTTACCGCCGCAAGCAATGTT), and 4 µl of DNA, in a final reaction volume of 20 µl. Negative controls were performed using a reaction mixture with ddH₂O (Cleaver Scientific Ltd, UK) substituting for the template DNA. Template DNA for each positive control was obtained from RHVE tissues after the step of DNA extraction described above. PCR cycling conditions consisted of an initial denaturation step at 98 °C for 2 min, followed by 40 cycles of denaturation at 98°C for 5 s and primer annealing at 60°C for 5 s. In each cycle, a dissociation stage at 60°C was run to generate a melting curve for confirming the specificity of the amplification product. Previously, calibration curves (Ct vs. Log cells) for each *C. glabrata* strain were constructed using the same PCR protocol as described above. For these, serial dilutions of the *Candida* cells were prepared and the DNA for PCR analysis was extracted from the planktonic cell pellet using the DNA extraction kit (QIAamp® DNA FFPE Tissue, Qiagen, Crawley, UK) with some modifications [262].

3.6. Effect of CgHAA1 and of CgHaa1-regulated genes in virulence of *Candida glabrata* against *Galleria mellonella*

To study the effect of CgHAA1 and of the CgHaa1-regulated genes CgAWP12, CgAWP13, CAGL0H07469g, CAGL0K10164g, CgBAG7, CAGL0E03740g, CAGL0G05632g, CAGL0H07469g, CgHSP30, CgRSB1 and CAGL0C03740g in virulence of *C. glabrata* against the infection model *Galleria mellonella*, killing and proliferation assays used before with success [116] were explored. Briefly, cells of the wild-type or of mutants devoid of the above mentioned genes were cultivated overnight in YPD medium, harvested by centrifugation and resuspended in an appropriate volume of PBS to yield a cellular concentration of ~1.4 x 10¹⁰ cells/mL. Afterwards 3.5 µL of this cell suspension was used to inject the larvae in the hindmost left proleg. As control larvae were also injected with the same volume of sterile PBS. To confirm the cellular concentration present in each cell suspension prepared, serial dilutions were prepared and the number of CFUs estimated. At least 3 replicas were performed and for each a total of 10 larvae were injected. The viability of the larvae was recorded at 24 h, 48 h, and 72 h. Larvae were considered dead if in response to shaking of the petri dish or touch with a pipette tip the larvae displayed no movement.

3.7. Effect of CgHAA1 and of CgHaa1-regulated genes in the ability of *Candida glabrata* to proliferate inside *Galleria mellonella* hemocytes

The effect of CgHAA1 and of CgHaa1-regulated genes CgAWP12, CgAWP13, CAGL0K10164g, CAGL0I07249g, CAGL0E03740g, CAGL0G05632g, CAGL0H07469g, CgHSP30, CgRSB1 and CAGL0C03740g in the ability of *C. glabrata* to proliferate in the presence of hemocytes collected from the hemolymph of the larvae *Galleria mellonella* was determined following an adapted protocol of an experimental setup previously described [116]. To isolate the hemocytes from *G. mellonella* hemolymph the larvae (in the last-instar stage) were anesthetized on ice and after sterilization of the abdomen surface with ethanol, the larvae were punctured with a sterile needle to collect the hemolymph to an anticoagulant buffer (98 mM NaOH, 145 mM NaCl, 17 mM EDTA, and 41 mM citric acid pH 4.5) in a 1:1 proportion. The hemolymph was then centrifuged at 250 g for 10 min at 4°C, washed twice with PBS, and centrifuged again at 250 g for 5 min at 4°C. The hemocytes obtained were gently suspended in 1 mL of Grace's insect medium (GIM) (Thermo Fisher Scientific) supplemented with 10 % (v/v) fetal bovine serum, 1 % (w/v) glutamine, and 1% (w/v) antibiotic/antimycotic solution composed of 10,000 units of penicillin G, 10 mg of streptomycin and 25 mg/L amphotericin B. Suspended hemocytes were counted in a hemocytometer and incubated overnight at 25 °C, in 24-well plates, at a concentration of 2×10^5 cell/mL. On the next day, the hemocyte monolayers were washed with PBS, and the medium was replaced with GIM without antibiotics. After this, *C. glabrata* cells of the control strain KUE100_chr606 or the derived mutants Δ Cg*haa1*, Δ Cg*awp12*, Δ Cg*awp13*, Δ CAGL0K10164g, Δ CAGL0I07249g, Δ CAGL0E03740g, Δ CAGL0G05632g were put in contact with the hemocyte monolayers (at a density of 7×10^2 yeast/mL). After inoculation, cells were centrifuged at 500 g for 1 min and incubated for 1h at 37°C with 5% CO₂, the time at which the *Candida* strains that did not interact with the hemocyte monolayers were removed (by washing the monolayer two times with PBS 500 μ l) and then the medium was replaced with GIM without antibiotics. The viability of the different strains interacting with the hemocytes was quantified after 1 and 8 hours after infection. For that, the monolayer of monocytes and yeasts was exposed for 20 minutes to 0.5 % (v v⁻¹) Triton X-100, allowing the release of internalized *Candida* cells, and quantifying the number of CFUs present in the lysate obtained.

3.9. Effect of the deletion of CgHAA1 and of CgHaa1-regulated genes CAGL0L00649g, CgICL1, and CgMLS1 in *Candida glabrata* tolerance to acetic acid at a low pH and in co-consumption of acetate and glucose.

The susceptibility of *C. glabrata* control strain KUE100_chr606 and of the derived deletion mutants Δ Cg*haa1*, Δ CAGL0L00649g and Δ Cg*icl1*, was compared in liquid and in solid MM medium. For the assessment of the susceptibility in solid medium spot assays were used. For that, cells of the different strains were cultivated at 30°C with 250 rpm agitation in liquid MM medium at pH 4.0, until the mid-exponential phase (OD_{600nm} of 0.5.). After this, cells were diluted, in PBS, to obtain a suspension with a standardized OD_{600nm} of 0.05. 4 μ l of this cell suspension and of two subsequent dilutions (1:5 and 1:25) were then applied as spots onto the surface of agarized MM plates at pH 4.5 either or not supplemented with 50 mM acetic acid. The plates were incubated at 30°C for 3 days and the growth of the different strains was compared. For the assessment of the susceptibility in liquid medium, the strains were cultivated for about 72 h at 30 °C with 250 rpm agitation, in liquid MM medium at pH

4.0, either or not supplemented with 30, 45 and 60 mM acetic acid. Samples of culture supernatants were taken at appropriate time intervals and then separated in an Aminex HPX-87H column, eluted at room temperature with 0.005 M H₂SO₄ at a flow rate of 0.6 ml/min, for 30 min. A refractive index detector was used to quantify glucose while acetic acid was detected using a UV-Vis detector set at 210 nm. Under the conditions used glucose and acetic acid had retention times of 9.2 and 14.3 min, respectively. Reproducibility and linearity of the method were tested, and concentrations of the compounds were estimated based on appropriate calibration curves.

4. Results

4.1. In the presence of acetic acid, the expression of *CgHAA1* and of the *CgHaa1*-regulated genes *CgAWP12*, *CgAWP13*, *CAGL0H07469g*, and *CAGL0K10164g* is necessary for the proper formation of *Candida glabrata* biofilms in biotic and abiotic surfaces

Considering the demonstrated positive effect of *CgHaa1* in adherence of *C. glabrata* to vaginal epithelial cells during exposure to acetic acid stress [262] and its positive effect in the regulation of the adhesin encoding genes *CgAWP12*, *CgAWP13*, *CAGL0H07469g*, and *CAGL0K10164g* [262], it was decided to examine, in closer detail, the effect of these players of the *CgHaa1*-regulon in biofilm formation prompted by this yeast species. For that, it was compared the ability of the control strain KUE100_chr606 and of mutants devoid of the above mentioned adhesin-encoding regulated by *CgHaa1* to form biofilms in the abiotic surface of polystyrene. In the absence of acetic acid the results obtained showed that only the expression of *CAGL0H07469g* and *CAGL0K10164g* genes resulted in a slight, but detectable, reduction of the biofilm formed, but this was only observed for the early time period of 6h not being detected differences after 24h (shown in Figure VI. 1 panel A). Exposure of wild-type cells to 30 mM acetic acid (at pH 4), a physiological relevant concentration in the vaginal environment, had only a small effect in reducing biofilm formation, compared to the control (Figure VI. 1 panel A). Differently, after 6h all the 5 mutants tested exhibited a reduced formation of the biofilm in the presence of the acid, with the more evident reductions being observed for the strains deleted for the *CgHAA1* and *CAGL0H07469g* genes. Interestingly, the deletion of *CgHAA1* slightly increased (~17%) early biofilm formation (Figure VI. 1 panel A). Exposure to a higher concentration of acetic acid, 45 mM (at pH 4), led to a similar pattern of results (Annex Figure VI. 1). Since at 24h the differences in the viability of the different strains in the biofilms formed were not observed, it seems conceivable to hypothesize that the expression of *CgHAA1* and of its *CgHaa1*-regulated adhesins *CgAWP12*, *CgAWP13*, *CAGL0H07469g*, and *CAGL0K10164g* contributes to increase the rate at which the biofilm is formed when acetic acid is present, affecting the early stages of adhesion. Consistent with the positive effect of the expression of *CgHAA1*, *CgAWP13* and *CAGL0H07469g* for cell adhesion during the early formation of the biofilm, the expression of the corresponding encoding genes was found to be higher (in a range of 4 to 6 times) in these conditions, compared to the transcript levels attained in control biofilm cells (Figure VI. 1 panel B). Unlike what was observed in planktonic conditions [262], the deletion of *CgHAA1* gene had no significant impact on the expression of these adhesin-encoding genes in the presence of acetic acid (only the expression of *CAGL0K10164g* was very slightly reduced in the $\Delta Cg\text{haa1}$ mutant in the presence of acetic acid, compared to the levels registered in cells of the parental strain) (Figure VI. 1 panel B). Surprisingly, in non-acetic acid-stressed cells, the expression of *CgAWP13* and *CAGL0H07469g* was higher in the $\Delta Cg\text{haa1}$ mutant, compared to the wild-type (Figure VI. 1 panel B).

In the second step, we focused on the adhesion to the biotic surface of vaginal epithelial cells. We hypothesized that the expression of the adhesins *CgAWP12*, *CgAWP13*, *CAGL0H07469g*, and *CAGL0K10164g* could contribute to the formation of a biofilm on this surface, as it was observed to occur with *CgHaa1* [262]. The results obtained confirmed the important role of the adhesins *CgAwp12*, *CgAwp13* and *CAGL0K10164g*, in augmenting the ability of *C. glabrata* to adhere to the surface of vaginal epithelial cells; however, except for the

strain deleted for the *CAGL0H07469g* gene, the beneficial effect exerted by these adhesins is independent of the presence of acetic acid as the reduction in colonization in the mutants was identical in the presence or absence of the acid (Figure VI. 1 panel C).

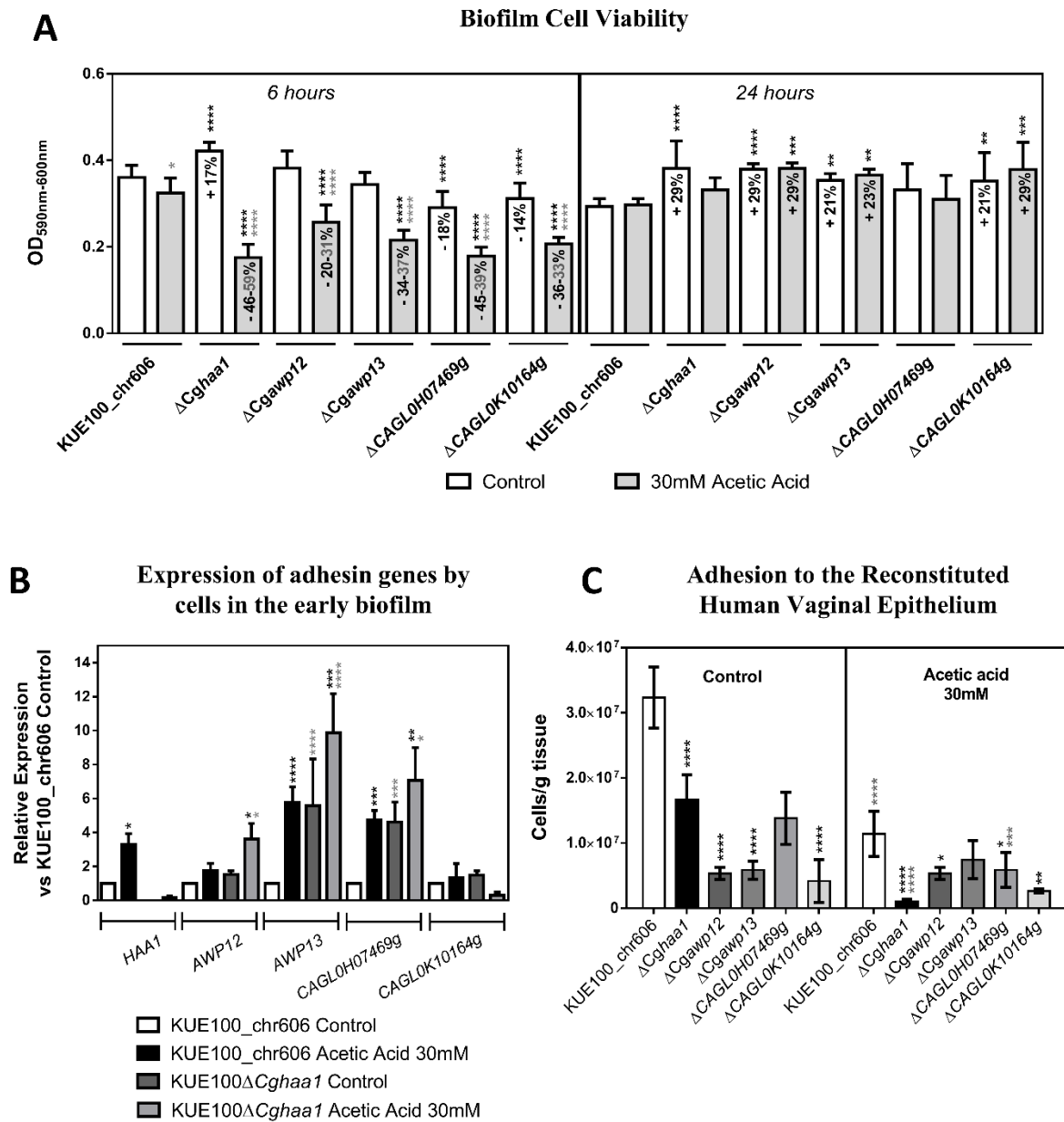


Figure VI. 1. Assessment of the effect and expression of CgHAA1 and CgHaa1-regulated adhesion genes CgAWP12, CgAWP13, CAGL0H07469g, and CAGL0K10164g in biofilm formation in biotic and abiotic surfaces. (A) Cell viability in biofilm was measured using PrestoBlue after 6 h and 24 h growth in RPMI at pH4, with or without acetic acid. Results represent the means of ten independent experiments. (B) Comparison, measured by real-time PCR, of transcription levels of the CgHaa1-regulated adhesion genes in the control KUE100_chr606 and Δ Cg $haa1$ strain in control or acetic growth conditions, after 6 h in RPMI growth at pH 4. (C) Effect in RHVE cells in adhesion of *C. glabrata* of the deletion of the CgHAA1, CgAWP12, CgAWP13, CAGL0H07469g, and CAGL0K10164g when compared to the KUE100_chr606 control strain, after 12 hours growth in RPMI at pH 4, with or without 30 mM acetic acid. Significant differences in adhesion of the deletion mutants with the wild-type strain are signaled in black, while significant differences in adherence of the same strain when grown in control or acetic acid stressed conditions are marked in grey. Results represent the means of a minimum of three independent experiments. Statistical significance of the data shown was assessed using ANOVA considering different replicas performed (* $p > 0.05$, ** $p \leq 0.01$, *** $p \leq 0.01$, **** $p \leq 0.0001$).

4.2. Effect of CgHaa1 and of CgHaa1-regulated genes in virulence of *Candida glabrata* against the infection model *Galleria mellonella*

Considering the positive described effect of CgHaa1 expression in of the CgHaa1-regulated genes in adherence of *C. glabrata* to vaginal epithelial cells, which is a trait linked to the virulence of this pathogenic yeasts, we have decided to examine whether the expression of these genes could also affect the virulence of *C. glabrata* in the *Galleria mellonella* model. This infection model is successfully used to test the virulence of *C. glabrata* and for the evaluation of *in vivo* activity of antifungal molecules [379]. In this context, the *G. mellonella* larvae were inoculated with cells of the control parental strain KUE100_chr606, of CgHAA1 mutant and the mutants of the CgAWP12, CgAWP13, CAGL0H07469g, and CAGL0K10164g adhesion genes mutant strains previously characterized. Besides these, six other mutant strains devoid of genes described to be under the regulation of CgHaa1 were also examined. The selection of these genes took into account their level of responsiveness to acetic acid stress and the role played by CgHaa1 in inducing that response, as well as their biological functions and its eventual contribution to virulence related phenotypes. The mutants tested were Δ CAGL0I07249g, devoid of a gene encoding a predicted GTPase-activating protein involved in the cell wall and cytoskeleton homeostasis [380]; Δ Cgrsb1, devoid of a predicted sphingolipid flippase involved in the incorporation of sphingolipids into the plasma membrane in *C. glabrata* [381]; Δ CAGL0K07337g, devoid of a predicted regulator of the plasma membrane proton pump [262]; Δ CAGL0C03740g [382], devoid of a predicted transcription factor whose *S. cerevisiae* orthologue regulates pseudohyphal growth; and Δ CAGL0E03740g and Δ CAGL0G5632g, devoid of genes of unknown function but that were selected considering a response fully dependence of CgHaa1p in CAGL0E03740g expression during the response to acetic acid and the potent up-regulation of CAGL0G05632g gene (1,51 and 6,95 fold, respectively). The results obtained showed that only the deletion of CgHAA1, of the adhesin-encoding genes CgAWP12, CgAWP13, and CAGL0K10164g; of the predicted GTPase activator CAGL0I07249g, CAGL0E03740g and CAGL0G5632g reduced virulence of *C. glabrata* against *G. mellonella* (Figure VI. 2, panel A). The reduced killing of *G. mellonella* when infected with these different mutants, compared to the levels registered when the infection was prompted by the wild-type strain, does not appear to be correlated with differences in capabilities of the strains to establish colonization of the larvae since the number of viable cells of the different strains present in the larvae hemolymph was identical (results not shown).

In order to determine whether the reduced virulence of the above-mentioned mutant strains against *G. mellonella* could be explained by a lower capability to surpass the activity of the larvae's primary immune system, a co-culture between the different yeast strains and larvae hemocytes was performed. In specific, the assay used was designed to detect differences in the ability of the strains to proliferate inside the hemocytes, considering that proliferation of *C. glabrata* inside macrophages had been highlighted as a major virulence factor of this pathogenic yeast [348]. The results obtained showed that after 1 hour of co-cultivation no significant differences in the interaction of the different strains inside hemocytes were obtained, however, after 8h, the number of viable yeast cells that could be retrieved from the inside of hemocyte cells was smaller for the Δ Cghaa1 and Δ Cgawp13 mutants than for the wild-type strain (Figure VI. 2, panel B). Surprisingly, the deletion of CAGL0G05632g gene significantly increased proliferation inside the hemocytes (Figure VI. 2, panel B), a phenotype that was surprising considering that this same deletion reduced virulence of *C. glabrata* towards *G. mellonella* (Figure VI. 2, panel A).

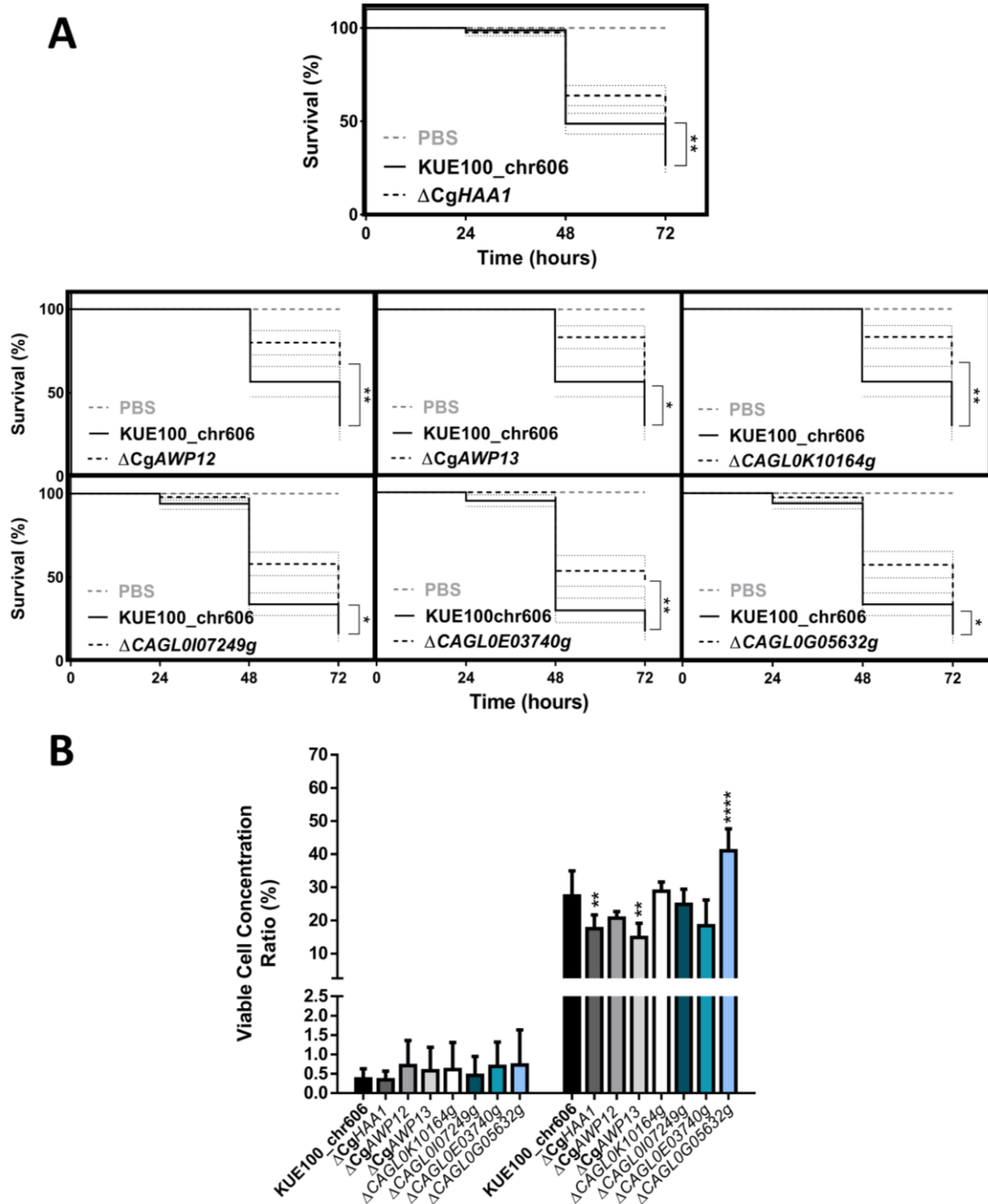


Figure VI. 2. Importance of *CgHaa1* and *CgHaa1* regulated adhesins genes for virulence in *Candida glabrata* of the *Galleria mellonella* infection model (A) *G. mellonella* survival after injection with *C. glabrata* control KUE100_chr606 strain, and the deletion mutants $\Delta CgHaa1$, $\Delta Cgawp12$, $\Delta Cgawp13$, $\Delta CAGL0K10164g$, $\Delta CgCAGL0I07249g$, $\Delta CAGL0E03740g$ and $\Delta CAGL0G05632g$. Differences in survival rates were calculated by using a log-rank (Mantel-Cox) statistical test ($P < 0.01$, for comparison of the wild-type and the mutant). (B) *In vitro* infection of hemocytes with *C. glabrata* control KUE100_chr606 strain, and the mutants of $\Delta CgHaa1$, $\Delta Cgawp12$, $\Delta Cgawp13$, $\Delta CAGL0K10164g$, $\Delta CgCAGL0I07249g$, $\Delta CAGL0E03740g$ and $\Delta CAGL0G05632g$. *Candida* load in the hemocytes was assessed upon 1 and 8 h of internalization by the *G. mellonella* hemocytes, using a MOI of 1:5. The displayed results are relative to the concentration of viable cells inoculated at time zero. Statistical significance differences shown comparing the KUE100_chr606 with the mutant strains were assessed using one-way ANOVA considering the different replicas performed (** $p \leq 0.01$, **** $p \leq 0.0001$). All the results represent the means of a minimum of three independent experiments.

4.3. Role of CgHaa1 in co-consumption of glucose and acetate by *C. glabrata*

The consumption of acetate was described to be an important factor for the survival of *C. glabrata* inside macrophages [351, 352] and it was previously shown that this species is capable of consuming acetic acid/acetate even when glucose is present in the environment [249]. The CgHaa1-regulon includes two genes of the glyoxylate cycle [262] that are predicted to be involved in acetate metabolism: *CAGL0L00649g*, encoding an orthologue of the acetyl CoA-synthetase *ScACSI* and *CgICLI*, encoding an orthologue of the isocitrate lyase of *S. cerevisiae*. CgHaa1 maximizes virulence of *C. glabrata* against *G. mellonella* and increases proliferation of the yeast inside hemocytes and therefore we decided to test whether CgIcl1 and *CAGL0L00649g* could be involved in these phenotypes as well. Indeed, the deletion of *CgICLI* and of *CAGL0L00649g* significantly reduced the virulence of *C. glabrata* against *G. mellonella* (Figure VI. 3 panel A). Unfortunately, during the time that took to complete this thesis, it was not possible to ascertain whether these genes also contributed to the increased proliferation of *C. glabrata* cells inside the hemocytes, however, this is certainly an aspect that must be looked over afterwards. Consistent with the previously established idea that protection against acetic acid stress involves an ability of *C. glabrata* to consume acetate via the glyoxylate cycle [249], as observed in other acetic acid-tolerant yeast species [257], mutants devoid of *CgICLI* and *CAGL0L00649g* genes showed enhanced susceptibility to acetic acid stress (Figure VI. 3 panel B and Figure VI. 3 panel C) and reduced capability to co-consume acetate/acetic acid in the presence of glucose (Figure VI. 3 panel C). A slight reduction in fitness of Δ *CAGL0L00649g* strain was also registered in the absence of acetic acid, albeit can be related to a loss of fitness of the strain (Figure VI. 3, panels B and C). A noticeable feature that emerged from the analysis of the patterns of co-consumption of acetate and glucose by all strains was that upon glucose exhaustion no more acetate appears to be consumed (more evident in the data obtained with 45mM; Annex Figure VI. 2).

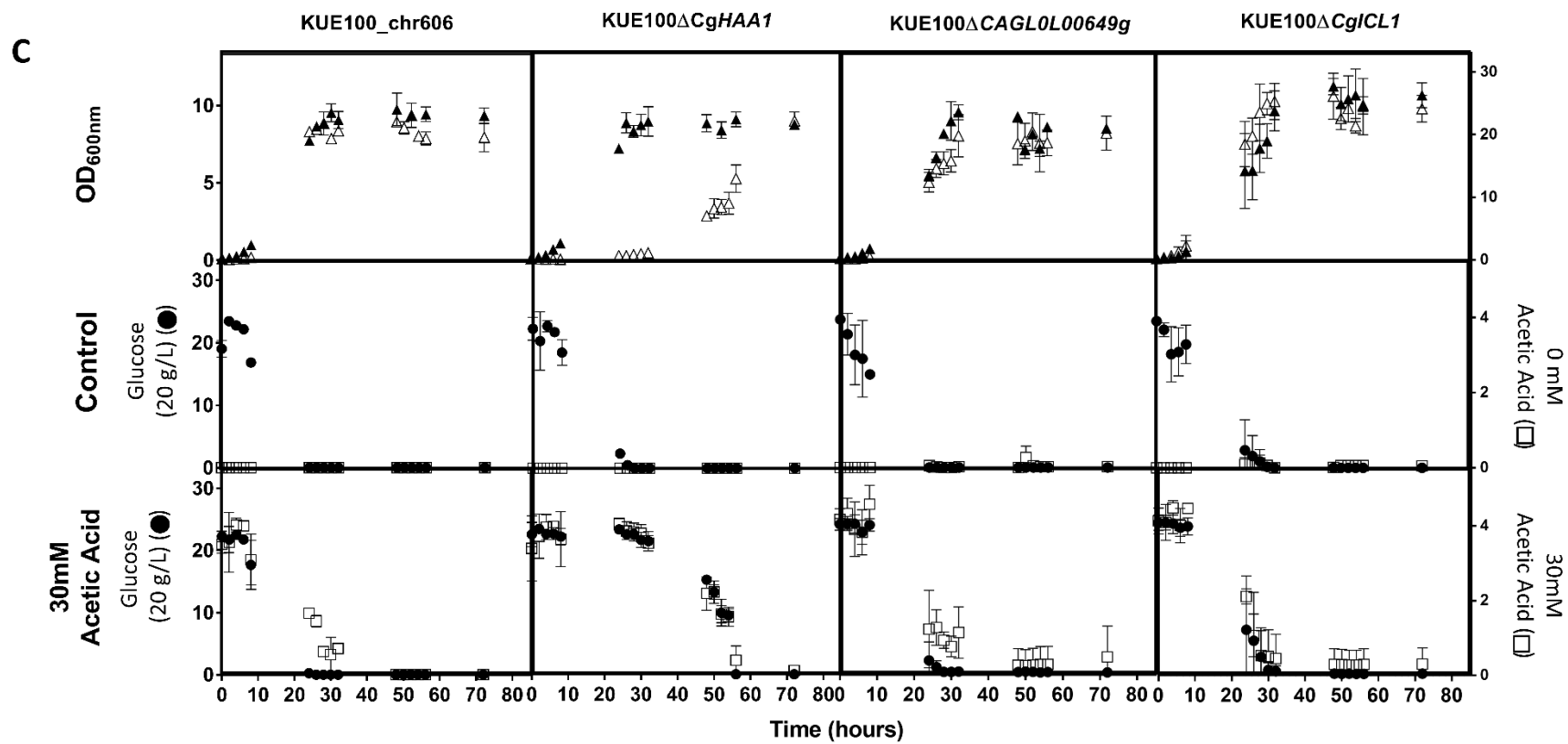
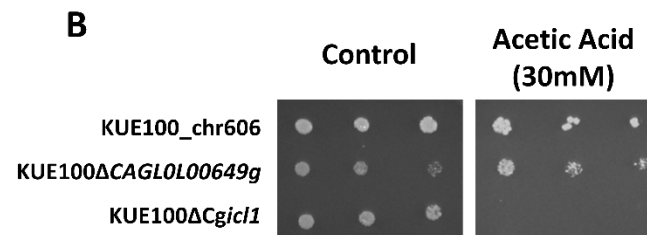
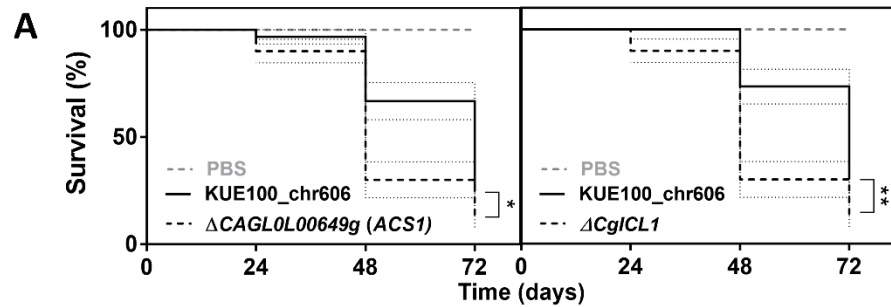


Figure VI. 3. Importance of *CgHaa1* and *CgHaa1* regulated acetate metabolism genes for the co-consumption of acetic acid with glucose and the role in virulence. (A) *G. mellonella* survival after injection with *C. glabrata* control KUE100_chr606 strain, and the deletion mutants Δ CAGL0L00649g and Δ Cgic11. Differences in survival rates were calculated by using a log-rank (Mantel-Cox) statistical test ($P < 0.01$, for comparison of the wild-type and the mutant). (B) Comparison of the susceptibility of control *C. glabrata* KUE100_chr606 and deletion mutants Δ CAGL0L00649g and Δ Cgic11 to inhibitory concentrations of acetic acid. Cells used to prepare the spots in MM at pH 4.5 were cultivated until the mid-exponential phase, harvested by centrifugation. The final cell suspension was prepared with an OD_{600nm} of 0.05 and dilutions of the cell suspension were spotted. (C) For evaluating the consumption of acetic acid and glucose, the control KUE100_chr606 strain, and the deletion mutant strains Δ CAGL0L00649g and Δ Cgic11 were cultivated in liquid MM medium at pH 4.0 either or not supplemented with acetic acid. Growth was followed for approximately 72 h during which samples of culture supernatants were harvested and used for the quantification of acetic acid and glucose concentrations by HPLC. The results shown are means of the results obtained in three independent experiments.

5. Discussion

In its adaptation to the human host, *C. glabrata* has evolved strategies to successfully colonize the different niches and these include the avoidance of the immune system but also the capability to adhere and subsequently form a biofilm at the surface of epithelial cells or to other cells of the co-colonizing microbiota. Recently, the CgHaa1-regulon was identified as mediating tolerance and response of *C. glabrata* cells to acetic acid [262], a response that is relevant to avoid exclusion of this species from the vaginal tract considering that concentration of this organic acid can increase prominently, specially when dysbiosis occurs [137, 232, 234]. One of the observations that stood out from the characterization of the CgHaa1-regulon, in comparison with its orthologous network in *Saccharomyces cerevisiae*, was the inclusion of several adhesins (CgAWP12, CgAWP13, CgEPA2, CAGL0K10164g, CAGL0H07469g, CAGL0H00110g, CAGL0F09273g, CAGL0M11726g, and CAGL0E06666g)[252, 262]. Part of this can result from the background of the *S. cerevisiae* strain used to define the ScHaa1 regulon, BY4741, a strain that has reduced adhesive properties. Indeed, studies undertaken with adherent *S. cerevisiae* strains demonstrated a positive effect of ScHaa1 in the regulation of FLO genes and also in improving adhesion [383]. Taking into account all these observations gathered in *C. glabrata* and in *S. cerevisiae* in this work we have decided to examine, in closer detail, the role of CgHaa1 in *C. glabrata* adherence and in the formation of biofilms in the presence of acetic acid. Only recently, the effects that low pH has on biofilm formation in *C. glabrata* have been described, contrasting with the considerable knowledge that has been gathered in biofilms formed at pH 7. The change from a neutral pH 7 to a low pH4 adjusted with lactic acid was found to increase biomass and viability in *C. glabrata* biofilms [358, 369]. Interestingly, the opposite effect was observed for *C. albicans* [188]. The matrix composition of *C. glabrata* biofilms cultured at pH 4 was also found to have a decreased content of (1,3)- β -D-glucan and proteins, compared to those obtained when biofilms were established at pH 7 [188, 369]. Interestingly, a substantial portion of the proteins specifically found in the matrix of *C. glabrata* biofilms formed under acidic conditions was of unknown function, while others have functions previously related with adhesion or virulence, such as yapsins [369]. Notably, CgPdr1 and CgHaa1 were predicted *in silico*, to be the major potential regulators of the genes encoding the biofilm matrix proteins found in the acidic formed biofilms of *C. glabrata* [369]. Interestingly, in a different study 16% of genes found to be upregulated in biofilm cells formed at the acidic pH of 5.6 (pH of the SDB medium used in the study) [377] were previously described as CgHaa1 targets [262]. Altogether these observations prompt a more thorough examination of the role played by the CgHaa1 regulon in biofilm formation in *C. glabrata*, both in the presence or absence of acetic acid, an aspect that has not yet been addressed in other studies and that is relevant considering the toxicity exerted by this acid against *C. glabrata*, something that was not observed for lactic acid [237].

In the presence of acetic acid, the expression of *CgHAA1* was required for the formation of the biofilm over the surface of polystyrene, however, this defect was only detectable at the early time point of 6h, while at 24h no differences between the two strains were detected (Figure VI. 1). Interestingly, despite the viability of the biofilm cells being the same at the later time point, microscopic imaging of biofilms showed some morphological differences specially in what concerns the compactness of the biofilm (as shown by the images in Annex Figure VI. 3, even in control conditions). During the time that this thesis

took it was not possible to further study these observations but it would be interesting not only to obtain a more thorough microscopic characterization of the biofilms formed by wild-type and $\Delta CgHaa1$ cells, but also of the mutants devoid of CgHaa1 target genes that were also found to positively influence biofilm formation. One hypothesis is that the biofilm formed by *C. glabrata* cells devoid of CgHAA1 is “weaker” than the one formed by cells of the parental strain, which could be of high relevance considering that the strength of the biofilm is expected to play a very relevant role to sustain survival of *C. glabrata* against environmental stressors [371]. The results obtained herein demonstrate that the CgHaa1-target adhesins CgAWP12, CgAWP13, CAGL0H07469g and CAGL0K10164g, also affect the rate at which biofilms are formed on the surface of polystyrene plates in the presence of acetic acid. Not much is known concerning the biological role of these adhesins, although CgAwp12 had been found in the extracellular matrix of biofilms formed during growth in YPD rich medium [384] and its expression is enhanced in biofilm cells formed during growth in SDB medium at pH 5.6 [377] or in RPMI medium (both at pHs 7 and pH 4 adjusted with lactic acid [369]); CgAwp13 was identified in the biofilms formed by hyper-adhesive clinical isolates but not by the reference strain CBS138 in YPD rich medium [384] and was further reported to be upregulated in cells grown in hydrogen peroxide osmotic stress [362]. Regarding CAGL0H07469g, the ortholog of the *ScICS2* gene with unknown function is expressed in mature 24h biofilm growth in SDB medium at pH 5.6 when compared to planktonic growth [362]. As for CAGL0K10164g, no information has been gathered until thus far beyond its resemblance to the *S. cerevisiae* GPI protein ScSEDI [140].

Consistent with playing a role in the formation of biofilms under *in vitro* conditions, CgAwp12, CgAwp13, and CAGL0K10164g and CAGL0H07469g were also found to contribute for adhesion of *C. glabrata* to vaginal epithelial cells in the presence of acetic acid. The beneficial effect of CgAwp12, CgAwp13, and CAGL0K10164g, and even of CgHaa1, in facilitating adhesion to vaginal epithelial cells is, apparently, independent of the presence of acetic acid since it was also observed even when the cells were cultivated in RPMI at pH4, using HCl as the acidulant. Although under planktonic conditions the expression of the adhesins CgAWP12, CgAWP13 and CAGL0K10164g was shown to be under the control of CgHaa1 [262], in the biofilm-forming cells this was not the case. Chromatin immunoprecipitation experiments (described in the next chapter of this thesis) revealed that the effect of CgHaa1 over the regulation of these adhesin-encoding genes is indirect (no direct binding to promoter regions was detected) and therefore it is possible that the interactor(s) of CgHaa1 directly involved in regulation of adhesin-encoding genes under planktonic conditions may not be active under biofilm-forming conditions. This lack of correlation between CgHaa1 and the expression of adhesin-encoding genes leaves elusive the molecular reasons underneath the positive effect exerted by this regulator in adherence. It is possible that this might result from a role of this regulator over several other adhesins, however, very few *C. glabrata* adhesins were demonstrated to mediate adhesion of the yeast to vaginal human cells and therefore the identification of which candidate(s) to test is challenging considering the wide number of adhesins encoded by the *C. glabrata* genome. Also of note was the observation that the presence of acetic acid drastically reduced adhesion of *C. glabrata* wild-type cells to vaginal epithelial cells (and reduced even more the deletion strains), something that was not observed when the biofilms were formed on the surface of polystyrene plates. This observation shows that the adherence phenotype of *C. glabrata in vivo*, in the vaginal tract, is

likely to be modulated by the many small molecules present therein as a result of the metabolic activity of a large microbiota, with acetic acid included.

Besides the effect of CgHaa1 in adhesion and biofilm formation, the role of the CgHaa1-regulon in general virulence of *C. glabrata* towards the wax *Galleria mellonella* was studied. Furthermore, the transcriptional profile of *C. glabrata* engulfed by murine macrophage-like cell line and human THP-1 macrophages belong to the CgHaa1-regulon accounting for approximately 14 and 26 % of the upregulated genes, respectively [262, 351, 352], further increasing the interest in the study of this more systemic virulence phenotypes. Compared to less expensive and ethically unconstrained models (like the murine infection model), the use of *G. mellonella* offers advantages for the study of systemic infections prompted by *Candida* species, including *C. glabrata*, such as it is less ethically challenging, offers the possibility of using a temperature of 37°C and allows tight control of the inoculum used for the infection assay [385]. Also, the *G. mellonella* immune response has similarities to that of the innate immune system response in mammals, including a humoral and a cellular response (reviewed in [386]). The cellular response is mediated by hemocytes present in the circulatory system that are capable of inducing phagocytic capacity, produce antimicrobial compounds, and are further involved in coagulation, nodulation and melanization of the wax [386, 387]. The results clearly show CgHaa1 contributes for maximal virulence of *C. glabrata* towards *G. mellonella* and this was correlated with a beneficial effect of this transcription factor in mediating proliferation of the yeast inside hemocytes. The effect of *CgHAA1* expression in inducing virulence against the wax can result from it contributing for the over-expression of genes also involved in this phenotype and, in line with this, at least 5 described targets were also found to positively improve killing of the larvae: the adhesins *CgAWP12*, *CgAPW13*, and *CAGL0K10164g*; the predicted GTPase *CAGL0I07249g* orthologue of *ScBAG7* that was described to play a role in structuring the *S. cerevisiae* cell wall; and *CAGL0C03740g* and *CAGL0G05632g*, that have an unknown biological function. Among these, only *CgAwp13* was found to improve proliferation of the yeast in hemocytes, as it was also found with *CgHaa1*. Notably, two other genes of the CgHaa1 regulon, *CgIcl1* and *CAGL0L00649g* (*ScAcs1* orthologue), were also herein demonstrated to contribute for virulence of *C. glabrata* towards *G. mellonella*, also being required for tolerance of the yeast to acetic acid stress. This data is interesting considering that the use of carbon sources other than glucose has been shown to be essential for survival of pathogens, including of *Candida*, when engulfed by immune cells [351, 388]. In particular, the use of acetate as a carbon source by phagocytosed *C. glabrata* cells is suggested by the increased expression of the *CgADY2* acetate transporter gene [352] and of genes involved in acetate catabolism [351]. Recently, the deletion of *CgICL1* in *C. glabrata* was reported to affect the growth in alternative carbon sources, the survival of *C. glabrata* inside macrophages, and to attenuate the virulence in a mouse model of invasive candidiasis [389], which is in line with the results reported herein. Concordantly, players of the glyoxylate pathway *CaICL1* and *CaMLS1*, were also found to be detrimental for phagocytosis survival of *C. albicans* [388]. The fact that CgHaa1-regulon also includes the acetate metabolism genes *CAGL0L00649g*, *CgICL1*, and *CgMLS1* (all genes overexpressed during internalization of *C. glabrata* by macrophages [351, 352]), suggests that regulation of these genes expression could also contribute for the beneficial role exerted by CgHaa1 in proliferation of *C. glabrata* inside *G. mellonella* hemocytes. Notably, *S. cerevisiae* Haa1 was recently shown to become activated upon direct binding of acetate to the N-terminal 150-residue region [390]. The

similarity between ScHaa1 and CgHaa1 suggests that the same might also occur in *C. glabrata*. The composition of the *G. mellonella* is not well characterized but acetate was never detected in the hemolymph [391], however, its presence inside the hemocytes is conceivable considering that there is strong evidence *C. glabrata* cells use available acetate as a carbon source in the phagosome macrophages [351, 352, 392-394]. Therefore, exposure to an endogenous source of acetate inside *G. mellonella* can explain the activation of CgHaa1 and, consequently, the up-regulation of its target genes including those enhancing virulence. The reduction of protein acetylation in engulfed *C. glabrata* cells (resulting in part from an epigenetic signature diminished in euchromatic acetylation marks) [351] can also provide an internal acetate pool for the cells that could trigger CgHaa1 activation.

In conclusion, in this work, other biological functions other merely the acetic acid stress response were attributed CgHaa1, including an important role in biofilm formation, adhesion to vaginal epithelial cells and a contribution for virulence against *Galleria mellonella*. The poorly characterized adhesins CgAwp12, CgAwp13, CAGL0K10164g and CAGL0H07469g, were herein implicated to affect the rate at which biofilms are formed in acidic conditions in the presence of acetic acid on the surface of polystyrene plates. CgAwp12, CgAwp13, and CAGL0K10164g further influence the adherence to epithelial cells and the virulence of *C. glabrata* against the *G. mellonella* infection model. These results enhance the knowledge about what is known concerning these important mediators of *C. glabrata* pathogenesis, specially relevant for the study of how these yeasts interact with the vaginal epithelia, an issue that remains elusive, specially in what concerns the identification of the players underneath the yeast-epithelium interaction. The results obtained in this work, specially the identification of CgHaa1 and of the adhesins CgAwp12, CgAwp13 and CAGL0K10164g as mediators of adhesion of *C. glabrata* to vaginal epithelial cells, advance new targets for the design of novel anti-*Candida* drugs that can inhibit relevant traits underlying the colonization and pathogenic potential of this yeast and, eventually, resulting in its eradication.

VII. Elucidation of the CgHaa1-regulatory network by ChIP-seq analysis

1. Abstract

CgHaa1 is the main transcription regulator of the response of *Candida glabrata* cells to acetic acid stress, a function that was conserved during the evolution from its ortholog in *Saccharomyces cerevisiae* ScHaa1. However, comparative transcriptomic analyses (under comparable experimental setups) revealed that the genes under CgHaa1 and ScHaa1 regulation differ in a considerable extent, suggesting that the structure of the regulatory network may have changed between these two yeasts. In order to shed light into this aspect, and contribute for a more general perspective on how transcription regulatory networks change across evolution in Yeasts, the present work aimed at dissecting the genes directly bound *in vivo* by CgHaa1 using ChIP-seq analysis. The results obtained led to the identification of 22 promoter regions bound *in vivo* by CgHaa1 under acetic acid, which is considerably smaller compared to the number of genes found to be regulated by this transcription factor under the same conditions (90 identified target genes). The genes that are under direct regulation of CgHaa1 include the MDR transporter CgTPO3; the transcription factor CgFKH1, the adhesin CgEPA21, the regulator of the H⁺-proton pump CgPMP1 or the poorly characterized proteins CgYRO2 or CgYGPI. Interestingly out of these 20% of the predicted direct targets identified were not found under the regulation of ScHaa1. Further *in silico* analysis of the promoters where CgHaa1 was bound, suggested that the ScHaa1 binding site can be recognized by CgHaa1, and also resulted in the identification of a new putative binding site for this transcription factor, kAAATGGsy, whose interaction with a recombinant peptide containing the CgHaa1 DBD was attempted.

2. Introduction

To succeed as a human colonizer *Candida glabrata* cells have to face multiple challenges including the activity of the host immune system, variations in nutrient availability, ability to adhere to the epithelial cells and also the presence of a co-colonizing microbiota that, among other aspects, produces small molecules that can constrain growth of *Candida* (reviewed in [395, 396]). Acetic acid is one of such molecules that is known to be produced by commensal vaginal *Lactobacilli* species. At low pH, acetic acid is known to have a potent antimicrobial effect [237] against *C. glabrata* and, even more prominently, for *C. albicans* [237]. To cope with environmental stresses *C. glabrata* cells make use of dedicated regulatory systems and recently the transcription factor CgHaa1 was identified to control the reprogramming of genomic expression in response to acetic acid [262], similar to what was described for its *S. cerevisiae* orthologue ScHaa1 [252, 256]. All the functional aspects concerning the description of this network, as well as its cross-comparison with the one controlled by ScHaa1 is provided in the introductory chapter of this thesis (Chapter II). In this chapter, we focused on addressing a more systematic comparison of these two orthologous networks addressing their evolution. Prior studies addressing the evolution of regulatory networks across Yeasts have shown the need of using for similar experimental setups in order to avoid introducing confounding factors in the analysis [264]. In this context, it is important to mention that the previous transcriptomic analysis undertaken to elucidate the genes whose transcription is promoted during acetic acid stress in *S. cerevisiae* and in *C. glabrata* and the specific importance of the transcriptional regulation by Haa1 were conducted under similar conditions including the use of the same growth medium, the same inhibitory concentrations of acetic acid and the same pH, 4.0. A comparison of the dataset of genes regulated by ScHaa1 and CgHaa1 revealed some similarities (Figure II. 9)(such as the regulation of the *TPO3* drug efflux pump with a role in determining the amount of acetic acid accumulated intracellularly), however, there are clear divergences as well (Figure II. 9)[252, 262]. The specific genes only found in the CgHaa1 regulon include several genes involved in adhesion genes (e.g. CgEPA2, CgAWP12 or CgAWP13), cell-wall genes involved in the synthesis of β -1,3/ β -1,6-glucans and genes involved in the regulation of internal pH homeostasis, like CgPMA1, encoding the membrane plasma proton pump or CgPMP1, a predicted regulator of CgPma1 [262].

Analysis of other regulatory networks unveiled several mechanisms as responsible for the evolution of transcriptional networks between different Yeast species including the loss and/or gain of cis-regulatory elements in target promoters (reviewed in [397, 398]). Due to a low density of functional nucleotides in the promoter sequences and to the reduced constraints in the positioning and ordering of binding sites without affecting their functionality, it is observed that the frequency of occurrence of modifications in promoter regions is considerably higher than the one registered in coding sequences [397, 398]. While inversions and insertions allow the conservation of the *cis*-regulatory element in the promoter, DNA-binding motifs can also be deleted with high frequency or lose functionality through single nucleotide polymorphisms. In this case, the pressure to preserve the regulation of the controlled genes may result in the appearance of a new *cis*-element in the promoter through a high occurrence of single nucleotide polymorphisms that compensate for the loss of a functional element [397, 398]. This rapid evolution allows the conservation of directly regulated genes in a transcriptional network and the gain of *cis*-regulatory

elements in the promotor of new genes leading to a direct regulon expansion [398]. If there is no selective pressure to maintain the influence of a specific DNA-binding motif in the gene expression, this rapid evolution within promotor regions allows loss of *cis*-regulatory elements in given sets of genes, thus facilitating specialization of the transcriptional network between species. An important example in the context of the opportunistic pathogenic yeast *C. glabrata*, is the expansion of the CgPdr1 transcriptional network from that of ScPdr1 by the appearance of a new *cis*-element PDRE motif in the promotor of adhesion gene CgEPA1 with impact in epithelial cell adhesion [54, 229]. The evolution of the transcriptional networks can also result from modifications in the transcription factor itself, generally known as a *trans* evolution process. For instance, compared to its *S. cerevisiae* orthologue ScRpn4, CaRpn4 from *C. albicans* was found to recognize an additional *cis*-element due to the loss of homology in a small region of the C₂H₂ finger in the DNA binding [398]. Consequently, both species share part of the Rpn4 regulon through a commonly recognized motif, while the distinct uncommon regulated targets are determined by the specific recognition of variant sequences [398]. The differentiation of networks can also combine both *cis*- and *trans*- coordinate evolution. A striking example demonstrates that one single non-synonymous mutation in CgAp1 DBD in *C. glabrata*, R60K, is responsible for the changes in binding specificity, compared to its ortholog ScYap1. The change alters the preference of the transcription factors of the Yap family to bind to the response element YRE-A motif rather than the YRE-O [264, 399]. Despite this, in response to benomyl stress, it was found that both orthologs, even recognizing different motifs, share the regulation of a set of overlapping target genes as the result of the appearance of the new *cis*-element recognized by CgAp1 in the promoters of *C. glabrata* overlapping target genes [264, 399]. In this context, *trans*- and *cis*-evolution co-evolve in a compensatory fashion to maintain transcriptional regulation of the network [399].

The differences detected in the set of genes regulated by ScHaa1 or CgHaa1 under similar experimental settings prompted us to examine, in close detail, how these two networks may have changed. However, the studies that had been conducted both in *S. cerevisiae* and in *C. glabrata* concerning the action of ScHaa1/CgHaa1 were only based on results from transcriptomic analysis leaving unclear what are the set of genes directly or indirectly regulated by these transcription factors. To better answer this issue and clarify the direct effect of CgHaa1 in *C. glabrata* transcriptome in response to acetic acid, the present work aimed to dissect the set of genes directly regulated by CgHaa1 using the ChIP-seq approach. Using the results obtained from the ChIP-seq analysis, putative DNA motifs that could serve as binding sites for CgHaa1 were also unveiled and an attempt to test their interaction with a recombinant peptide harboring the CgHaa1 DNA binding domain was made.

3. Material and methods

3.1. Strains and growth medium

The strains used in this work (Table VII. 2) are derived from the background strain KUE100 [277]. Myc-tagging of the strain KUE100 at the *CgHAA1* locus was performed as described previously [75]. Briefly, a myc-His cassette was amplified by PCR from the pFA6a-13Myc-His3MX6 plasmid of the Longtine's collection [400]. The oligonucleotides used in the amplification contain 5' homology sequences flanking the desired genomic insertion points are detailed in Table VII. 1. At least 10 µg of the purified PCR product were used to transform KUE100 cells using the standard AcLi yeast transformation protocol. Genotyping of the clones growing on the selective media CSM-HIS media (2 % glucose, 0,67 % yeast nitrogen base, recommended amounts of CSM-HIS from MP Bio) was performed by PCR. Correct insertion of the cassettes at the targeted genomic loci (and the corresponding absence of wild-type versions of the targeted gene) were confirmed by PCR and subsequent Western blot using an anti-Myc antibody (Roche). All the oligonucleotides used for cassette preparation and integration verification are listed in Table VII. 2. The different strains were batch cultured at 30°C at 250 rpm orbital agitation in minimal medium (MM) at pH 4 adjusted with HCL as the acidulant. MM contains per liter, 20 g glucose (Merck), 1.7 g yeast nitrogen base without amino acids (Difco), and 2.65 g (NH₄)₂SO₄ (Merk), supplemented with 0.2 % of histidine (Sigma).

3.2. Chromatin immunoprecipitation of CgHaa1 and sequencing of the interacting DNA

The *CgHAA1*-Myc tagged strain was cultivated in 50 mL of MM at pH 4 at 30°C and using an orbital agitation of 250 rpm. When the OD_{600nm} of culture was between 0.8 and 1, 30 mM acetic acid was added (using a stock solution of 2 M, prepared in water and adjusted to pH 4 using NaOH pellets). After 30 minutes of growth, cross-linking was performed following the same experimental setup described in Chapter IV. The subsequent immunoprecipitation and sample purification steps were also performed according to the protocol described therein. ChIP-seq of untagged *C. glabrata* cells grown in glycerol as a carbon source was used as the control sample (MOCK) [330]. qPCR from the IP DNA of a promoter sequence of *CgPMA1* was used to confirm correct immunoprecipitation, using as control the promoter of *CgYBH1* gene that is not under the regulation of CgHaa1, according to Bernardo *et al.* [262]. MicroPlex v2 kit from Diagenode (using the supplier recommendations) was used to construct single-read libraries from the IP samples. Sequencing was performed using NextSeq 500 device (Illumina technology available at the transcriptome platform at Ecole Normale Supérieure: <http://www.transcriptoe.ens.fr/sgdl/>, Paris France). Three biological IP replicates were obtained for acetic acid-exposed cells and each sample was sequenced in duplicate. After quality controls and filtering of low-quality bases, between 15 and 20 million sequences (IP sample) and 10 and 20 million sequences (control sample) were obtained.

3.3. Peak calling, motif retrieving, and network construction

The reads obtained by sequencing were mapped in the *C. glabrata* genome, using the bowtie algorithm [331]. SAMTOOLS suite [332] was used to convert the output SAM files to BAM files. BAM files of the sequence replicates were merged to increase the sequence coverage and then converted to BED files, using the ‘genomeCoverageBed’ tool, available from the BEDTOOLS suite [333]. Peak calling was performed using the software bPeaks [334] using the mock IP as reference. The final threshold parameters used were the following: T1=5, T2=6, T3=1.9, T4=0.9. The final list of peaks detected was then manually curated using the IGV genome browser removing artificial peaks such as peaks overlapping ORF regions, without a gene sequence in the vicinity, or the vicinity of tRNA locus. Whenever a peak was found in between two coding sequences, if only one of the genes encoded was found overexpressed in the KUE100_chr606 vs KUE100Δ*Cghaa1* during acetic acid stress it was considered that the transcription factor regulated only that one gene. If none of the encoded ORF genes expression was found modified, both encoded genes were considered potential direct targets. To find enriched DNA motifs in the promoters considered to be directly regulated by CgHaa1, the FASTA files describing the DNA sequences obtained by bPeaks were used as the input for the ‘peak-motif’ tool available in the RSATools databases (<http://rsat.ulb.ac.be/>) [401]. For this motif analysis, peak motifs with low complexity (e.g., CCCCCCCC) motifs were discarded.

3.4. Transcriptomic analyses of the CgHaa1 influence during 30 mM acetic acid stress

Transcriptomic analysis of KUE100_chr606 and KUE100_Δ*Cghaa1* cells was performed (in duplicated) using the same experimental setting established for the ChIP-seq analysis. RNA extraction, purification and microarray analysis was performed using the same protocol detailed in Chapter IV. The images were analyzed using the feature extraction software (Agilent Technologies) and normalized using global LOWESS, and the mean of the biological replicates was calculated. A gene was considered differentially expressed by CgHaa1 whenever the mean expression absolute log₂ fold change in the KUE100_chr606 strain was above 0.5, compared with the expression obtained by the KUE100_Δ*Cghaa1* during growth in the same stress conditions used for the ChIP-seq analyses (MM at pH 4 at 30°C supplemented with 30 mM acetic acid) and if the variation was considered statistically significant (p-value of 0.05 or lower, calculated using the LIMMA package).

3.5. Heterologous expression in *E. coli* of CgHaa1-DBD peptide and subsequent purification by affinity chromatography

The peptide that could comprise the predicted DNA binding domain (DBD) of *CgHAAI*, mapped between residues 1 and 153 (CgHaa1-DBD) (Figure VII. 4) was heterologously expressed in *E. coli* with a protocol similar to the one described in Mira, N. *et al* 2011 [253]. Briefly, the construct based on the expression pET23a+ was engineered to allow over-expression of the candidate *CgHAAI* DBD sequence upon isopropyl β -D-1-thiogalactopyranoside (IPTG) induction. For this, the *CgHAAI* DBD coding sequence was amplified from *C. glabrata* genome by PCR using the primers described in Table VII. 2. The product of amplification was subsequently digested with BamHI and HindIII (Takara) and ligated to pET23a+ (using a 1:5 plasmid to fragment proportion) using 400U of T4 DNA ligase (NEB). The product of ligation was transformed into *E. coli* DH5 α cells and the transformants recovered in LB solid medium supplemented with ampicillin. Plasmid DNA was extracted from the recovered *E. coli* transformants and the correct insertion of the *CgHAAI* DBD sequence in the vector was afterward confirmed by Sanger sequencing. To drive the expression of the peptide, the corresponding plasmid was transformed into *E. coli* BL21-CodonPlus(DE3)-RIL cells (Stratagene) and the transformants were cultivated at 37°C, with 250 rpm orbital agitation, in LB medium supplemented with 30 μ g/mL of chloramphenicol and 150 μ g/mL of ampicillin, until mid-exponential phase (corresponding to an OD_{640nm} of approximately 0.6). At this point, 0.3 mM IPTG was added to the culture and after 3 h cells were harvested by centrifugation (at 8000 rpm, 8 min, 4°C), washed twice with ice-cold distilled water, and stored at -80°C until further use. The cell pellet was afterwards sonicated, centrifuged at 15 000 rpm for 45 min at 4°C and the crude soluble protein extract obtained was loaded into a His-trap column (GE Healthcare). Prior to sample addition, the column was equilibrated with 10 mL of ice-cold washing buffer (10 mM phosphate buffer pH 7.4, 150 mM NaCl, 10mM imidazole). Elution of the trapped CgHaa1-DBD-His₆ peptide was performed using a stepwise increasing gradient of imidazole, with concentrations ranging from 20 mM to 500 mM. The fractions containing the purified peptide (identified upon SDS-PAGE analysis of the eluted fractions) were then applied in a 75 Sephadex HR10-300 GL3-kDa-70kDa column (GE Healthcare) for subsequent fast protein liquid chromatography (FPLC) purification. Confirmation of the expression and purification of the peptide was performed by western blot using an anti-His₆ antibody (Santa Cruz Biotech).

Table VII. 2. List of strains, plasmids and primers used in this work

Strains	Description and genotype	Reference
KUE100	Parental strain, $\Delta his3 yku80::SAT1$ flipper	Ueno <i>et al.</i> 2007 [277]
KUE100_chr606	Control strain, <i>CgHIS3</i> marker was ectopically integrated at a non-coding locus of chromosome F, position 605,901 - 606,015	Ueno <i>et al.</i> 2011 [277]
KUE100_Δ <i>Cghaa1</i>	Δ <i>Cghaa1</i> mutant strain, ORF <i>CAGL0L09339g</i> was replaced by <i>CgHIS3</i> gene marker	Bernardo <i>et al.</i> 2017 [262]
KUE100_Haa1-Myc	<i>CgHAA1</i> tagged strain, a 13Myc- <i>HIS3</i> tag was inserted in the C-terminal region of the coding sequence	This study
Plasmids	Description	Reference
pET23a(+)	Bacterial vector for expression of N-terminally T7 His-Tag tagged proteins	Novagen ®
<i>CgHaa1</i> -153DBD	IPTG-inducible plasmid that drives the expression of <i>CgHaa1</i> N-terminal DNA-binding domain from 1 to 153 fused tagged with 6HIS at C-terminal	This study
pFA6a-13Myc-His3MX6	Plasmids that allow the C-terminal protein tagging with 13Myc, with <i>CgHIS3</i> gene marker	Longtine <i>et al.</i> 1998 [400]
Primers	Sequence	Use
<i>CgHAA1</i> end-F1	ACAGGTAGTGTCTCCTCCAAGCCAATTATTATCTGACGAAGGTTTCGCTGAATTCC ATAATTTTATCACATC	<i>CgHAA1</i> -Myc- <i>HIS</i> insertion cassette construction
<i>CgHAA1</i> ter-R1	CATTGACTGATCCTCACCAGG	<i>CgHAA1</i> -Myc- <i>HIS</i> insertion cassette construction
<i>CgHAA1</i> terverif-R1	CCACTGCGAATAAAAAAGGAAAAAAGACATGGTAATTTCAAAGTTCCTCCCCGA ACCATTTCACTACATAT	<i>CgHAA1</i> -Myc- <i>HIS</i> insertion screening
pFA6a_verif1_FW	GCTAGGATACAGTTCTCACATC	Myc- <i>HIS</i> insertion screening
Prom <i>CgYHB1</i> -FW	GGGGGTTTCTCGAAGAG	ChIP followed by qPCR in <i>CgYHB1</i> promoter
Prom <i>CgYHB1</i> -REV	GGTTGGTCTAGGAAAAAGCA	ChIP followed by qPCR in <i>CgYHB1</i> promoter
Prom <i>PMA1</i> -FW	CACAGAGTCCACAGGCTCC	ChIP followed by qPCR in <i>CgPMA1</i> promoter
Prom <i>PMA1</i> -REV	GTGTGTTGGGGTTCTGTCGTC	ChIP followed by qPCR in <i>CgPMA1</i> promoter
pET23a(+)_ <i>CgHAA1</i> DBD_FW	CGGGATCCATGGTTTTGATAAATGGCGTTAAATACGCTTG	<i>CgHaa1</i> DBD sequence amplification for ligation to pET23a(+) plasmid
pET23a(+)_ <i>CgHAA1</i> DBD_REV	CCCAAGCTTCGTCAGATTCGTAGATTCATCATTTTCATTCAAAG	<i>CgHaa1</i> DBD 1-153 amino acid sequence amplification for ligation to pET23a(+) plasmid
Oligo_ <i>TPO3</i> _SPRHaa1_FW	GACCTATTGGCCATTTACGAAAGG	SPR oligo
Oligo_ <i>TPO3</i> _SPRHaa1_REV	CCTTTCGTGAAATGGCCAATAGGTC	SPR oligo
Oligo_ <i>EPA21</i> _SPRHaa1_FW	AAAAGTGGGCCCATTTTCCCAATC	SPR oligo
Oligo_ <i>EPA21</i> _SPRHaa1_REV	GATTGGGAAAATGGGCCCACTTTT	SPR oligo
Oligo_ <i>FKH1</i> _SPRHaa1_FW	GGGTATTAATAATGGCGCGGGATCCG	SPR oligo
Oligo_ <i>FKH1</i> _SPRHaa1_REV	CGGATCCC GCGCCATTTTAATACCC	SPR oligo
Oligo_SPRnegcontrol_FW	CACAGAGAGAGAGCACTACACGTA	SPR oligo
Oligo_SPRnegcontrol_REV	TACGTGTAGTGTCTCTCTCTGTG	SPR oligo

4. Results and Discussion

4.1. Identification of promoter regions recognized *in vivo* by CgHaa1 in acetic acid-stressed *Candida glabrata* cells and prediction of the set of directly regulated genes

To identify direct genes targets regulated by CgHaa1, the interaction of the transcription factor to promoter regions in *C. glabrata* cells exposed to acetic acid stress was examined by ChIP-seq. Transcriptomic analysis was undertaken in *C. glabrata* and also in *S. cerevisiae* have clearly shown that CgHaa1/ScHaa1 proteins are largely dispensable for genomic expression of the two yeasts in the absence of acetic acid [252, 262], which is consistent with the recent demonstrations that ScHaa1 is only activated upon direct binding of acetate [390]. In this context, we decided to undertake the ChIP-seq experiments only in the presence of acetic acid. For this, KUE100_Haa1-Myc exponential cells were suddenly challenged with 30 mM acetic acid (at pH 4) and after 30 minutes of exposure cross-linking was performed. Gene expression of the wild-type and $\Delta Cg\text{haa1}$ mutant cells in the presence of acetic acid was also performed in the same conditions as the ChIP-seq to understand if the interaction of the transcription factor to the promoter of the gene results in its transcription. Comparison of the transcriptome of KUE_chr606 wildtype strain and the KUE100 $\Delta Cg\text{haa1}$ mutant strain resulted in the identification of 88 upregulated genes and 17 downregulated genes (above or below a threshold of 0.5 log₂F, corresponding to 1.4-fold) when cells were cultivated in MM medium at pH 4 under 30 mM acetic acid stress. Of those, ~70% (72 genes) were concordant to the transcriptomic analyses undertaken in Bernardo *et al.* 2017 [262].

A noticeable aspect concerning the profile of the ChIP-seq read peaks upon immunoprecipitation of the DNA associated with CgHaa1 was the generalized low intensities of reads in the IP samples, compared to those obtained in the MOCK condition. Consequently, it is not possible to identify always a very clear peak indicative of binding of the transcription factor to the DNA, although enrichment in reads is indeed observed (Figure VII. 1 and Figure VII. 2). This fact is rendered clear if we compare the profile of peaks obtained in this study and the ChIP-seq results of the CgPdr1 DNA, obtained using the same protocol (Chapter V, Figure V. 12). This difference in the ChIP profile obtained could result from a more transient binding of CgHaa1 to its target promoters, compared to a stronger and constitutive binding exerted by CgPdr1. Similar to what is described for ScHaa1, it is possible that CgHaa1, upon activation by dephosphorylation upon acetic acid stress, can be translocated from the cytosol to the nucleus [390, 402, 403]. Differently, CgPdr1 is found to be constitutively bound to its promoters [71](Chapter V). A closer analysis of the CgHaa1 ChIP-seq results obtained resulted in a division in two of the target DNA sequences to which CgHaa1 was found bound under acetic acid: i) a first set, including 15 genes whose promoters contain peaks of reads identified the bPeaks software as being consistently enriched in the IPed samples obtained from the different biological replicates (represented in Figure VII. 1 and summarized in Table VII. 3) stress (peaks identified are summarized in Annex Table VII. 2). Interaction of CgHaa1 to these promoters in the conditions of growth and stress used in the current work appears to influence directly the expression of 10 genes of those genes (log₂ fold > 0.5) (Table VII. 3, white lines); ii) a second set of genes, including 6 genes whose promoter's interaction with CgHaa1 requires further confirmation by coupling ChIP of CgHaa1 with qPCR, since the intensity of peaks identified was low compared to mock and may have not

been identified as consistently present in all biological replicates. In a second step, a guided analysis was performed in which the promoter region of those 88 genes found to be up-regulated by CgHaa1 in the herein carried out transcriptomic analysis were individually searched, this resulting in the identification 4 genes with possible low-intensity peaks in the promoters (represented in Figure VII. 2 and summarized in Table VII. 3). Finally, the promoter of several “chipable” ORFs identified in all three replicates when compared to the MOCK (genes that are usually highly expressed and that are frequently identified in chromatin immunoprecipitation with high reads in the ORF region, sometimes in an unspecific manner, due to indirect cross-linking effects or non-specific interactions of the antibodies with RNA polymerases [404-406]) was searched for enriched peaks in the promoters, compared to the intensity found in the mock sample. The identification of peaks in the promotor of these genes could have been masked due to the closeness to high intensity of reads in the ORF and not been detected by bPeaks. In a final step, this list of the second set of genes was compared with the list of genes whose transcription was found to decrease in the $\Delta Cg\text{haal}$ mutant, to compile a list of probable CgHaa1 direct targets, resulting in the identification of 7 presumed targets summarized in Table VII. 3 (highlighted in grey), although it has to be said that further confirmations by qPCR should be performed in order to clearly define this analysis (represented in Figure VII. 2 and peaks are summarized in Table VII. 3). The identified set of peaks with lower confidence located in promoters of genes with unchanged expression could still be potential targets under different conditions of growth and stress and are therefore represented in Annex Figure VII. 2 and summarized in Annex Table VII. 3 After all the analysis was carried out, a comprehensive list of 22 candidate promoters to which CgHaa1 can be found bound *in vivo* under acetic acid stress was compiled and is shown in Table VII. 3.

Table VII. 3. (Part I) *Genes to which CgHaa1 was found to be bound to the promoter in acetic acid-stressed C. glabrata cells, as indicated by ChIP-seq analysis.* The table describes the list of genes presumed to be directly regulated by CgHaa1 *in vivo* under acetic acid stress (30 mM, pH 4), using the experimental setting detailed in materials and methods. The effect of CgHaa1 in the expression of these genes is also indicated, based on the results of the transcriptomic analysis herein carried out, as well as the predicted *S. cerevisiae* orthologue and the existence of an eventual regulatory association with ScHaa1. Encoded protein function was retrieved from CGD or SGD databases [140, 407]. The second set of genes, in grey lines, represents a set of possible direct targets that interaction of CgHaa1 to the promoter needs to be confirmed since the peaks observed in the ChIP-seq experiments have often low intensities and were not detected by bPeaks, at least not in all replicates.

<i>C. glabrata</i> ORF/ Standard Name	Log2 Fold (KUE100/ mRNA KUE100ΔCg $haa1$)	Function	<i>S. cerevisiae</i> Ortholog	<i>S. cerevisiae</i> ortholog regulation by ScHaa1
<i>CAGL0A01782g</i> / CgHXT4	0.64	Predicted glucose transmembrane transporter	HXT4	
<i>CAGL0D06732g</i> / CgEPA21	-	Putative adhesin	-	
<i>CAGL0G02893g</i>	0.47	Presumable NADH kinase with a predicted role in NADP biosynthesis	POS5	
<i>CAGL0G03289g</i> / CgSSA3	0.57	Heat shock protein of the HSP70 family	SSA4	Indirect evidence under acetic acid stress growth conditions [408]; HRE is found in the promoter [253]
<i>CAGL0G03267g</i>	0.93	Putative lipid raft-associated protein, with a role in protein targeting to membrane	AST2	
<i>CAGL0G08866g</i>	1.33	Putative forkhead transcription factor with a predicted role in the regulation of cell cycle and morphogenesis	FKH1	
<i>CAGL0H10076g</i>	2.49	Putative plasma membrane chaperone protein of unknown function	YRO2	Indirect evidence under acetic acid stress growth conditions [408]
<i>CAGL0I10384g</i> / CgTPO3	1.86	Multi-drug resistance transporter of the Major Facilitator Superfamily	TPO2	Direct during acetic acid stress [390]
<i>CAGL0J06050g</i>	1.2	Putative highly glycosylated cell-wall secreted protein	YGPI	Indirect evidence under acetic acid stress growth conditions [408]; HRE in the promoter [253]
<i>CAGL0J08316g</i>	0.36	Putative homoserine O-acetyltransferase	MET2	
<i>CAGL0K05357g</i> / CgGLN1	0.01	Putative glutamate-ammonia ligase involved in ammonia assimilation	GLN1	Indirect evidence under non-stress conditions [409]; HRE is found in the promoter [141]
<i>CAGL0L08008g</i>	1.19	Putative regulatory subunit of the plasma membrane H ⁺ -ATPase Pma1	PMP1	
<i>CAGL0L08030g</i>	1.14	Putative mitochondrial asparagine-tRNA ligase	SLM5	
<i>CAGL0L06864g</i>	0.79	Protein of unknown function	SIP5	Indirect evidence under non-stress conditions [409]
<i>CAGL0M11902g</i>	-0.11	Protein of unknown function	FUN19	

Table VII. 3. (Part II)

<i>C. glabrata</i> ORF/ Standard Name	mRNA gene KUE100/ mRNA KUE100ΔCg <i>haa1</i>	Function	<i>S. cerevisiae</i> Ortholog	<i>S. cerevisiae</i> ortholog regulation by ScHaa1
<i>CAGL0A00495g/</i> <i>CgPMA1</i>	0.62	Putative plasma membrane proton pump with a role in the internal pH homeostasis	<i>PMA1</i>	
<i>CAGL0C02893g</i>	0.99	Putative kinase is implicated in the activation of the Pma1 ATPase	<i>HRK1</i>	Indirect evidence under acetic acid stress growth conditions [408]; HRE in the promotor [253]
<i>CAGL0C03740g</i>	1.21	Best hit of <i>S. cerevisiae</i> ScMIT1 gene that regulates pseudohyphal growth	-	
<i>CAGL0E05566g</i>	1.17	Putative transcriptional activator of glycolytic genes	<i>TYE7</i>	Indirect evidence under non-stress conditions [409]
<i>CAGL0G05632g</i>	2.16	The ortholog in <i>S. cerevisiae</i> is a putative protein with unknown function that is induced during starvation	<i>YDL218W</i>	
<i>CAGL0I04246g/</i> <i>CgSUT1</i>	1.55	Putative transcription factor involved in sterol uptake	<i>SUT1</i>	
<i>CAGL0L09339g/</i> <i>CgHAA1</i>	3.155	Transcription factor involved in acetic acid stress response	<i>HAA1</i>	Indirect evidence under non-stress conditions [409]; HRE is found in the promotor [141]

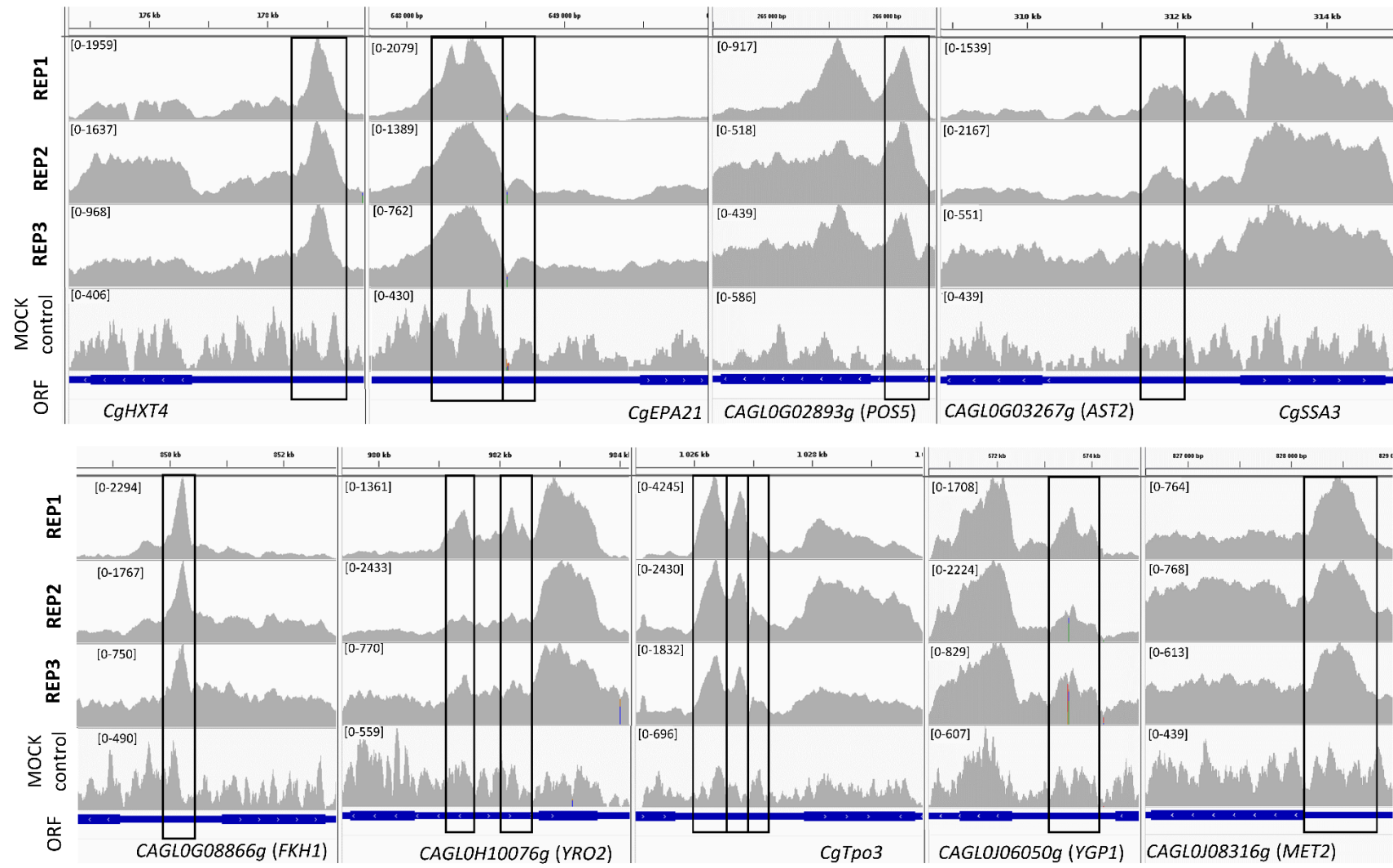


Figure VII. 1. (Part I)

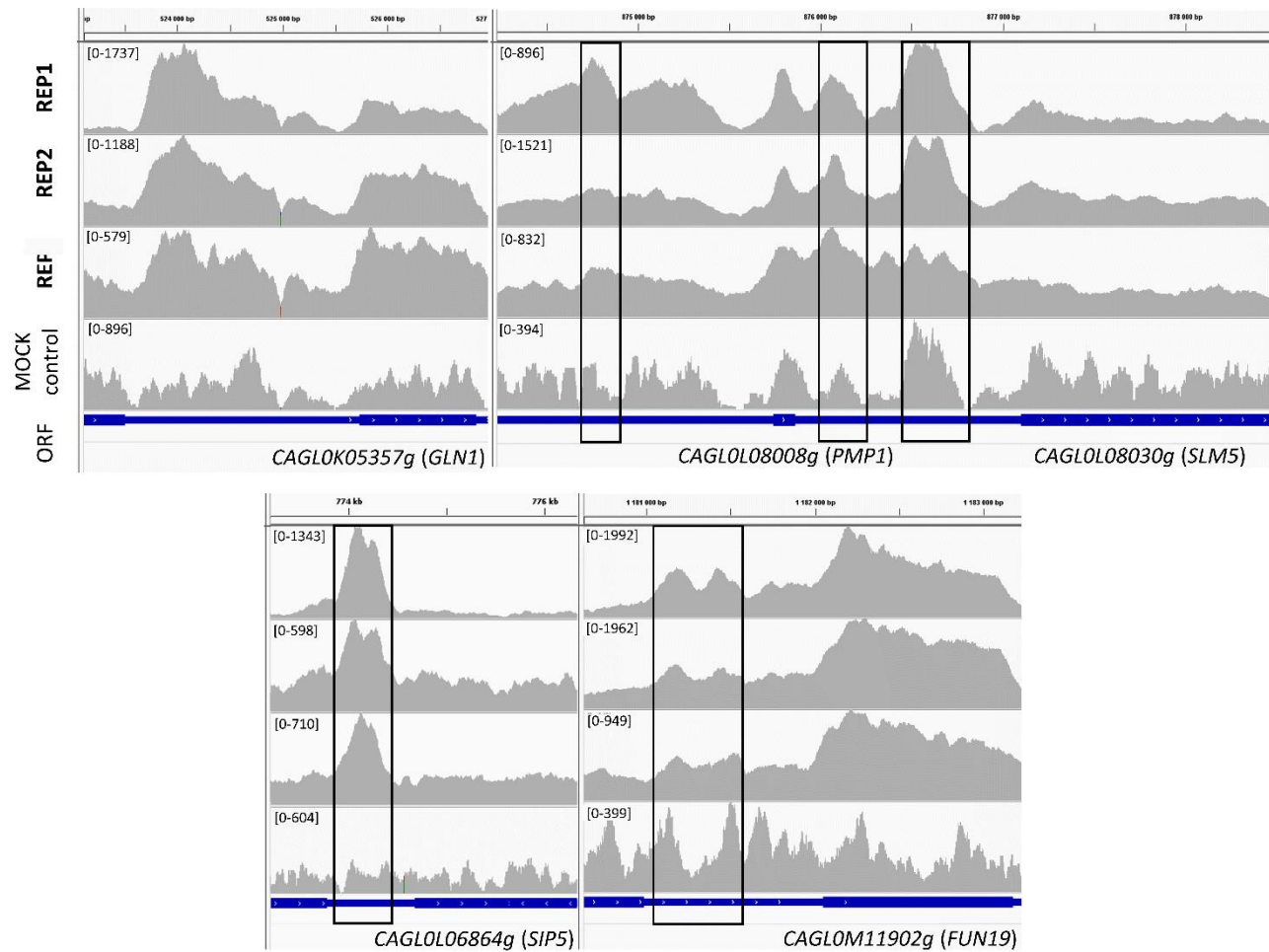


Figure VII. 1. (Part II) *Representation of the CgHaa1 interaction with the promoter of potential direct targets genes.* Images were obtained in IGV and represent visually the alignment to the *C. glabrata* genome of the sequenced reads obtained by the three biological replicates of CgHaa1 ChIP-seq, specifically in the promoter regions where high intensity of reads (peaks) were identified by bPeaks software (black boxes) when compared to the MOCK control.

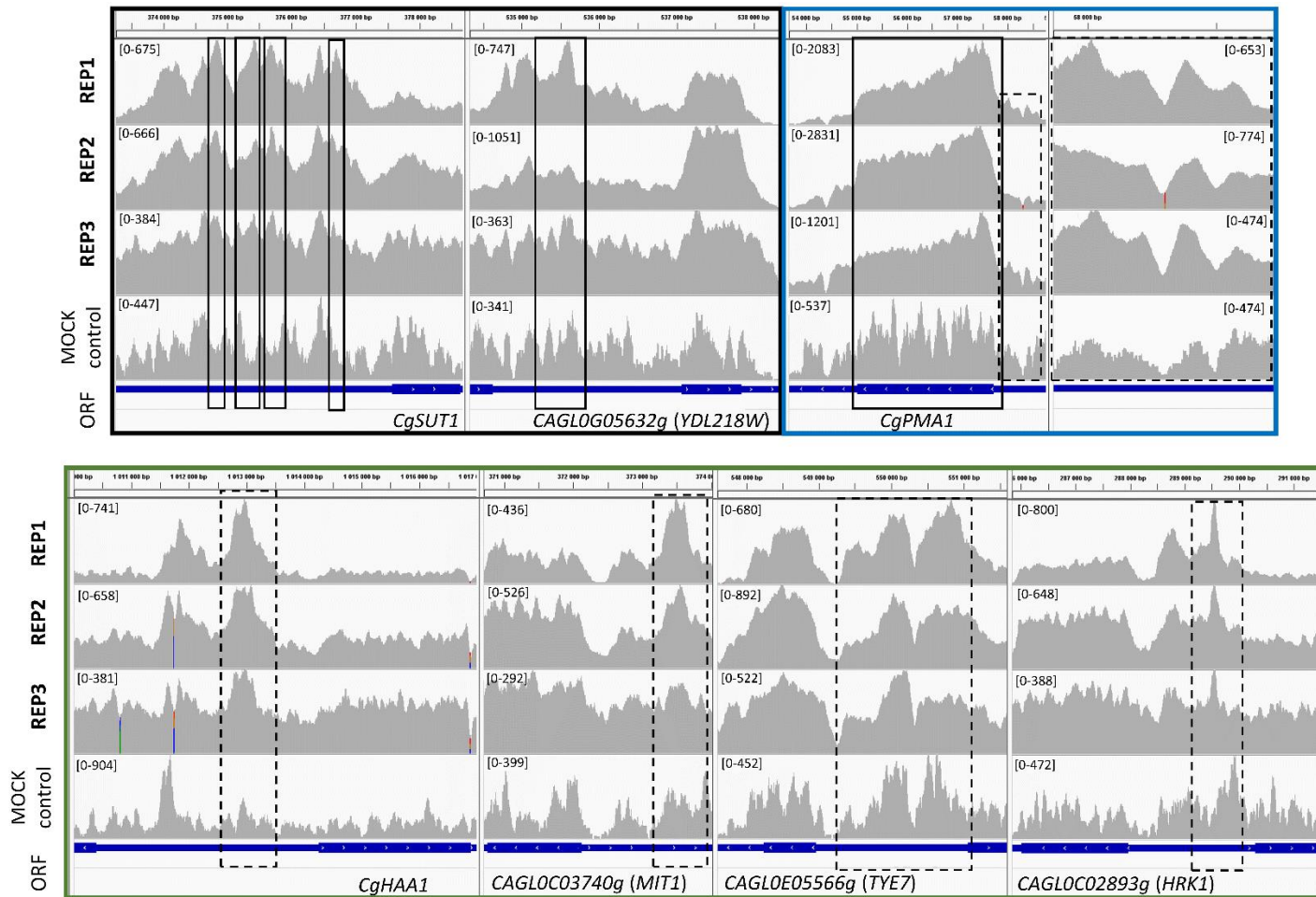


Figure VII. 2. Representation in IGV of possible *CgHaa1* interaction with the promoters of upregulated genes. These interactions require further confirmation, since they are low in intensity and not always identified by bPeaks, at least consistently in all replicates (black), were found in the promoters of chipable genes (blue, possible peaks in promoters highlighted in dashed boxes) or found in the promoter up-regulated genes (green, possible peaks in promoters highlighted in dashed boxes)

Examining the results herein obtained, it is clear that CgHaa1 regulates several different cellular processes in response to acetic acid stress. When comparing the preliminary CgHaa1-transcription network to that of the predicted ScHaa1 [253], some genes appear to be conserved as direct targets. Specifically, *ScTPO2* is confirmed to be a direct target of ScHaa1 during acetic acid stress [390], while *ScYGPI*, *ScSSA4* and *ScHRK1* were described as probable direct targets of CgHaa1 since, besides being dependent on ScHaa1 for expression during acetic acid stress, an HRE motif is also found in both genes' promotor [141, 252, 410]. Four other genes, *ScGLN1*, *ScSIP5*, *ScTYE7* and *ScHAA1* orthologues in *S. cerevisiae* were also described to be (at least) indirectly regulated positively by ScHaa1 under non-stressful growth in YPD [409], however, only *ScGLN1* and *ScHAA1* genes had an HRE motif in their promotor [141]. Another putative direct target of ScHaa1 in response to acetic acid stress is the *ScFKH2* transcription factor gene [253] that is a paralogue of *ScFKH1*, orthologue of the herein identified CAGL0G08866g as a potential direct target of CgHaa1. In *S. cerevisiae* both paralogues have distinct functions, even displaying different promotor occupancy [411, 412]. However, they appear to have redundant roles in the activation of mitotic cell cycle regulation [412]. The conservation of one of the paralogues in the CgHaa1 network suggests some significance of this transcriptional system in the overall Haa1-regulatory network. The deletion of this transcription factor in *C. glabrata* however, does not appear to affect acetic acid resistance (Annex Figure VII. 2).

The above-mentioned set of orthologues that appear to be under Haa1 regulation both in *C. glabrata* and in *S. cerevisiae* only accounts for approximately ~30% of the genes, which indicates a noteworthy divergence between the two transcriptional networks in both species. From the set of genes found to be regulated directly only by CgHaa1, of special significance is the possible direct regulation of *CgPMA1* which is fundamental for the internal pH homeostasis and survival of yeast cells in response to insults that perturb internal pH homeostasis, as it occurs under acid stress [242]. Interestingly, the function of CgPma1 was already reported to be regulated by the CgHaa1 possible indirect target *CgHSP30*, which is a homolog of *CgYRO2* [262]. It would be of great interest to further investigate if *CgYRO2* conserves the function of its homologue, since it is a commonly a direct target of both CgHaa1 and ScHaa1. Furthermore, CgHaa1 directly regulates the expression of *CgPMP1* which encodes the putative regulatory subunit of the proton H⁺-ATPase pump [413]. It further regulates the expression of *CgAST2*, encoding a putative lift raft-associated protein whose *S. cerevisiae* orthologue was involved in the correct targeting of ScPma1 to the plasma membrane [414]. Concordantly, during the screening of a large-scale deletion mutant library [57] (preliminary results, not published), the *CgAST2* deletion mutant was found to be highly defective during growth when cells are exposed to high concentrations of acetic acid (Annex Figure VII. 2). In *S. cerevisiae* the ScHaa1 transcription factor is reported to be a possible direct regulator of *ScHSP30*, but not of *ScPMP1* or *ScAST2*, neither are these genes upregulated during acetic acid exposure in *S. cerevisiae* stressed cells [252, 253]. These results suggest that the genetic elements of the Haa1 network responsible for the regulation of Pma1 activity have diverged between species. This result is quite interesting considering that both species have distinct mechanisms underlying the regulation of internal pH. Specifically, even though *S. cerevisiae* shows higher growth rates at low external pH, *C. glabrata* maintains a higher pH_{int} independently of the pH of the medium [415]. Differences in activity and regulation of CgPma1 could help explain these differences in pH_{int} regulation. If so, these differences may be reflected in the evolution of

transcriptional networks that respond to stresses with consequences in the pH homeostasis. Nevertheless, it was previously reported that both species recover from the decrease in pH_{int} caused by weak-organic acids at the same rate [415]. Other exclusive CgHaa1 target genes include CgHXT4, predicted glucose importer; CAGLOG02893g required for mitochondrial detoxification of reactive oxygen; CAGL0J08316g and CAGL0L08030g involve in aminoacid metabolism. These genes may all give an important contribution to the response to acetic acid by acting on to energy depletion and amino acid starvation in acetic stressed cells promoting and in the response to oxidative stress [242]. The observed direct interaction of CgHaa1 with the promoter of CgEPA21, a putative adhesin gene, was also an interesting observation considering the demonstrated involvement of CgHaa1 system in the adhesion phenotype (Chapter VI). Interestingly, this gene was recently described to play an important role in biofilm formation [184, 416] and could be an important effector of the observed role of CgHaa1 in the biofilm structure as reported in Chapter V. The adhesin genes studied in the past chapter (CgAWP12, CgAWP13, CAGL0H07469g, and CAGL0K10164g) do not appear to be part of the CgHaa1 network suggesting that the previously reported influence of CgHaa1 in transcription must be indirect, being concordant to the lack of impact of the CgHaa1 in their expression during biofilm formation (Figure VI. 1).

Altogether the preliminary defined CgHaa1 direct network accounts for around 20% of the overall change in gene upregulation that was herein observed to depend on CgHaa1 expression (Annex Table VII. 1). This divergence may result from some lack of identification of direct CgHaa1 targets (for example weaker interactions may have escaped the undertaken IP step) but it is more likely that it results from the activity of other transcription factors that, afterwards, impact the transcriptional regulatory network, as it was also suggested to be the case for *S. cerevisiae* [253]. Besides CgFkh1, four other putative transcription factors were identified as possible direct targets of CgHaa1, albeit in some of the cases the reported interaction was weak and should involve additional confirmation by qPCR. These transcription factors include the CgHAA1 itself, suggesting a positive autoregulatory transcription loop; CAGL0E05566g, an orthologue of ScTYE7 encoding a transcriptional activator of glycolytic genes and that was described to be upregulated during acetic acid exposure [408], being also an important genetic factor for maximum acetic acid resistance [252]; CgSUT1, a regulator of sterol uptake; and CAGL0C03740g whose best homologue in *S. cerevisiae* is ScMIT1, a regulator of pseudohyphal growth [382]. Interestingly, in Chapter VI, the deletion of CAGL0C03740g reduced the virulence of *C. glabrata* against *G. mellonella*. Mit1 transcription factor is poorly characterized in both species and the conditions and molecular mechanisms that stimulate *C. glabrata* pseudohyphal growth are poorly understood. It would be interesting, to further study the involvement of this gene in tolerance to acetic acid in both species and also whether it influences pseudohyphal growth both in response to acetic acid but also during internalization in *G. mellonella* hemocytes

4.2. *In silico* identification of a putative CgHaa1 DNA-binding site

To identify the regulatory element of CgHaa1, the promoter regions that were found to be directly recognized by CgHaa1 *in vivo* in acetic acid-stressed cells by bPeaks (detailed in Annex Table VII. 2) were used to search for over-represented DNA motifs, candidates to serve as binding site for CgHaa1. For this analysis, only the sequences of the peaks with higher confidence profiles obtained after ChIP-seq analysis were used, resulting in a total of 15 DNA sequences (Table VII. 3, Annex Table VII. 2). The DNA sequences of these promoters recovered in the ChIP-seq analysis by the bPeaks software were loaded in the RSAT – DNA pattern tool [417]. First, the presence in these promoters of the minimal defined DNA motif recognized by ScHaa1 (SMGGSG [253]) in these sequences was accessed to understand if there was a conservation of the motif recognized. This similarity search was performed considering the high similarity existing between ScHaa1 and CgHaa1 DBDs (Figure VII. 4) (63.87% identity at the amino acid level) which suggests that the two transcription factors may interact with DNA in a relatively similar manner, even though only part of the direct network appears conserved. A found HRE motif was only considered relevant for the establishment of a potential regulatory association if it was found on the high coverage regions of the peak sequence (Annex Figure VII. 3). This careful analysis was guided by the report that an unguided search for the ScHaa1 binding motifs in the promoters of *S. cerevisiae* returns a much greater number of potential targets than the documented predicted targets of ScHaa1 based on transcription dependence [418]. With these conditions, an HRE motif was considered to be present in the promoters of CgSSA4, CgTPO3, CgYGP1, CgSLM5 and CgYRO2, the first three being predicted direct targets of ScHaa1 as well. The CgYRO2 and CgSLM5 recruitment to the CgHaa1 regulon may be explained by the appearance of an HRE motif in its promoter that is not present in the corresponding Sc orthologue. Notably, all these five genes were herein observed to be prominently up-regulated prominently in response to acetic acid (all above log2 fold of 0.5). Since the HRE motif used by ScHaa1 was present in a small number of target gene promoters a *de novo* search for over-represented DNA motifs was performed using RSAT – DNA pattern tool [401]. The list of motifs provided by the tool is available in Annex Table VII. 4. Two main DNA motifs, shown in Figure VII. 3, emerged as being over-represented in the promoter regions recognized by CgHaa1: i) rrTAGCGGd, a motif showing some similarities to HRE with the final CG stretch resembling the previously identified minimal functional motif of ScHaa1, SMGGSG [253]. This motif is well localized in the peak of three upregulated genes CgSLM5, CgTPO3, CgFKH1 and CgGLN1 (the same is not true for the same motif found in the CgEPA21 promotor)(Annex Figure VII. 3); ii), kkAAATGGsy, found in 80% of the CgHaa1 target promoters and is usually located well within the peak of reads (Table VII. 4, Annex Figure VII. 3). Notably, this second motif was found in the promoter of all upregulated target genes by CgHaa1. Interestingly, through close inspection, it is possible to observe that this motif usually precedes an HRE or an HRE-like motif (highlighted Annex Figure VII. 3 with blue arrows). The motif itself may be followed by a CG stretch similar to the HRE as well (highlighted in the Table VII. 4 in bold). Therefore, CgHaa1 interaction with the promoter of its target genes could be mediated by the proximity of a kkAAATGGsy to an HRE-like motif. It is possible that this second adjacent motif could regulate the interaction of a CgHaa1 transcription co-factor. Concordantly, spacing between different regulatory

elements in the promoter is usually conserved due to mechanistic constraints in the transcriptional machinery interaction [397, 398]. Nevertheless, this motif is found in higher frequency than the *S. cerevisiae* HRE and the HRE-like motif, which suggests that it might be recognized by CgHaa1 directly.

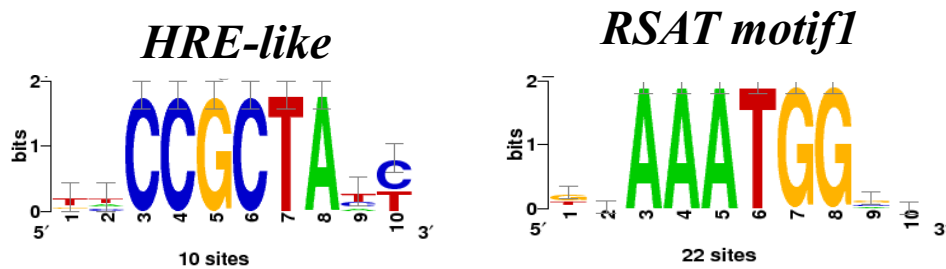


Figure VII. 3. Representation of the two most significant consensus binding motifs for CgHaa1 during acetic acid stress predicted from the ChIP-seq peaks sequences using the RSAT tools. The sequences of high reads peaks identified by the bPeaks software, located at gene promoters regions, that result from the sequencing of DNA immunoprecipitated with the Myc tagged CgHaa1 *in vivo* in response to acetic acid stress (30 mM, pH 4), were used to find the most represented motifs using the RSAT tools.

Table VII. 4. Listing of the sequences of the different motifs identified by RSAT tools within the peaks sequence identified by bPeaks software. The sequences of high reads peaks identified by the bPeaks software, located at gene promoters regions, that result from the sequencing of DNA immunoprecipitated with the Myc tagged CgHaa1 *in vivo* in response to acetic acid stress (30 mM, pH 4), were used to find the HRE motif recognized by ScHaa1 using RSAT tools. *De novo* search for the most represented motifs identified two main motifs denominated HRE-like motif - due to the similarity to HRE, and RSAT motif 1 – the motif with higher incidence identified by the RSAT tools. The HRE-like motifs that were identified by RSAT tools *in novo* motif search that corresponds to the previously identified ScHaa1 HRE motif are underlined. Bold RSAT motif 1's have a stretch of CG nucleotides that resemble the HRE motif. The motifs found in the reverse strand of the DNA are highlighted in italic.

<i>C. glabrata</i> ORF/ Standard Name	<i>S. cerevisiae</i> Ortholog	Motifs found in peaks		
		HRE (SMGGSG)	HRE-like (yhCCGCTAhy)	RSAT motif 1 (kkAAATGGsy)
<i>CgHXT4</i>	<i>HXT4</i>	-	-	GGAAATGGGG TGAGGAAATCT ATAGGAAATAG
<i>CgEPA21</i>	-	-	<i>ACCTCCCCCCCC</i>	TAAAATGGGT TTAAATGGGA CGAAATGGCG TTAGGCAATAC GAAAATGGGC GAAAATGGGC ATAGGAAATCT
<i>CAGL0G02893g</i>	<i>POS5</i>	-	-	-
<i>CgSSA3/ CgAST2</i>	<i>SSA4/AST2</i>	ggccGAGGGGaagg	-	CTAAATGGCC CCAAATGGGT
<i>CAGL0G08866g</i>	<i>FKH1</i>	-	<i>TCCCGCTACT</i> TAATAGCGGAA <i>AACCGCTACT</i> <i>TATTCCCCCAT</i> <i>TCCCGCTAAC</i> <i>CACTCCCCGAG</i>	TAAAATGGCG
<i>CAGL0H10076g</i>	<i>YRO2</i>	<i>tactCAGGGGcagt</i>	-	CTAGGAAATTG <i>GTAAATGGGT</i>
<i>CgTPO3</i>	<i>TPO2</i>	<i>gtggGAGGGGcagt</i> <i>atctGCGGGGggga</i> <i>ttccGAGGGGttt</i>	<u>CCCTCCCACCGA</u> <u>AGTTCCCCCCCG</u>	TGAAATGGCC AGAAATGGCC AAAGGCAATCG GGAAATGGGA
<i>CAGL0J06050g</i>	<i>YGP1</i>	ggggGAGGGGgggg	-	-
<i>CAGL0J08316g</i>	<i>MET2</i>	-	-	TTAAATGGAC
<i>CgGLN1</i>	<i>GLN1</i>	-	<i>CAAAAGCGGTA</i>	GTAAATGGCT <i>TTAGGAAATGA</i>
<i>CAGL0L08008g</i>	<i>PMP1</i>	-	-	<i>GCAAATGGAT</i>
<i>CAGL0L08030g</i>	<i>SLM5</i>	<i>ttatCCGGGGtatac</i>	<u>TTCCGCTATC</u> <u>TTCCGCTACC</u>	<u>TTCCGCTATC</u> <u>TTCCGCTACC</u>
<i>CAGL0L06864g</i>	<i>SIP5</i>	-	-	<i>GAAAATGGGA</i>
<i>CAGL0M11902g</i>	<i>FUN19</i>	-	-	-

4.3. Heterologous expression of the CgHaa1 DNA binding domain and study of its interaction with the candidate DNA motifs

To confirm a possible interaction of the CgHaa1 with the identified candidate motifs a strategy similar to the one used before to elucidate the ScHaa1 recognition site [253] was explored. In specific, it

The heterologous expression of the peptide was successfully performed in *E. coli* and the peptide was purified by affinity chromatography resorting to His-Trap columns. In Figure VII. 5 are shown the results of demonstrating the success of the experimental setting used for the heterologous expression. However, during the time of this thesis it was not possible to optimize the SPR experiments to be conducted and therefore it was not possible to determine if the purified CgHaa1 peptides was indeed able to interact with the DNA motifs.

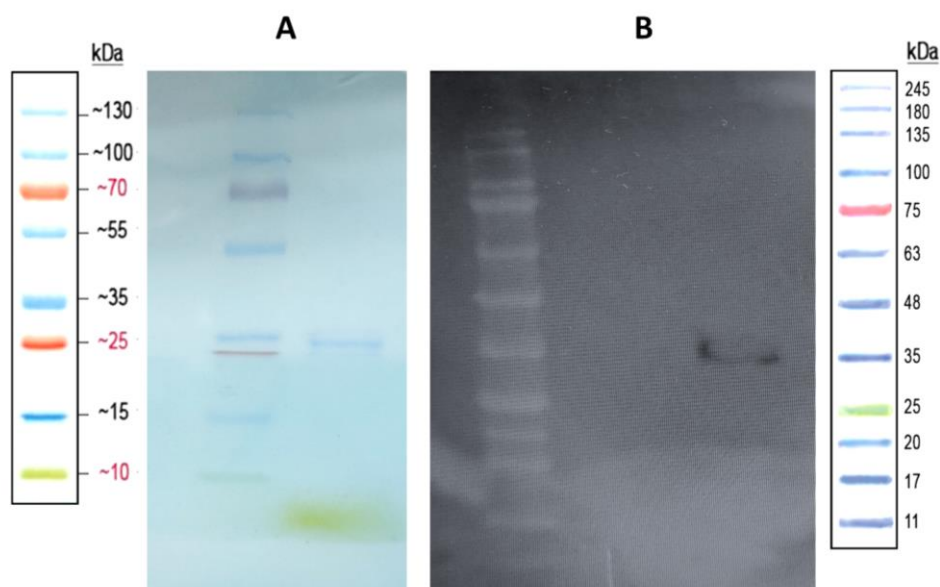


Figure VII. 5. *Heterologous expression of the CgHaa1-153DBD.* The CgHaa1-153DBD His tagged peptide was heterologously expressed in *E. coli* BL21-CodonPlus(DE3)-RIL cells from the pET23a+ plasmid. The peptide was afterwards purified by the sonicated cell pellet using a His-trap column and further concentrated and through fast protein liquid chromatography. Confirmation of the expression and purification of the peptide was performed by SDS (A) and detection of the His-tag by western blot (B).

5. Final Remarks

Overall, the Haa1-transcription networks of *S. cerevisiae* and *C. glabrata* appear to have diverged significantly, taking into account the significant differences in the direct regulated genes predicted. In this context, differences detected in the set of genes regulated by ScHaa1 or CgHaa1 may result from differences in the binding site recognized by these two regulators. It is also noteworthy an observed differentiated regulation of transcription regulator genes that can account for the indirect CgHaa1-transcription network. The final direct CgHaa1 regulon identified in this work is illustrated in Figure VII. 6.

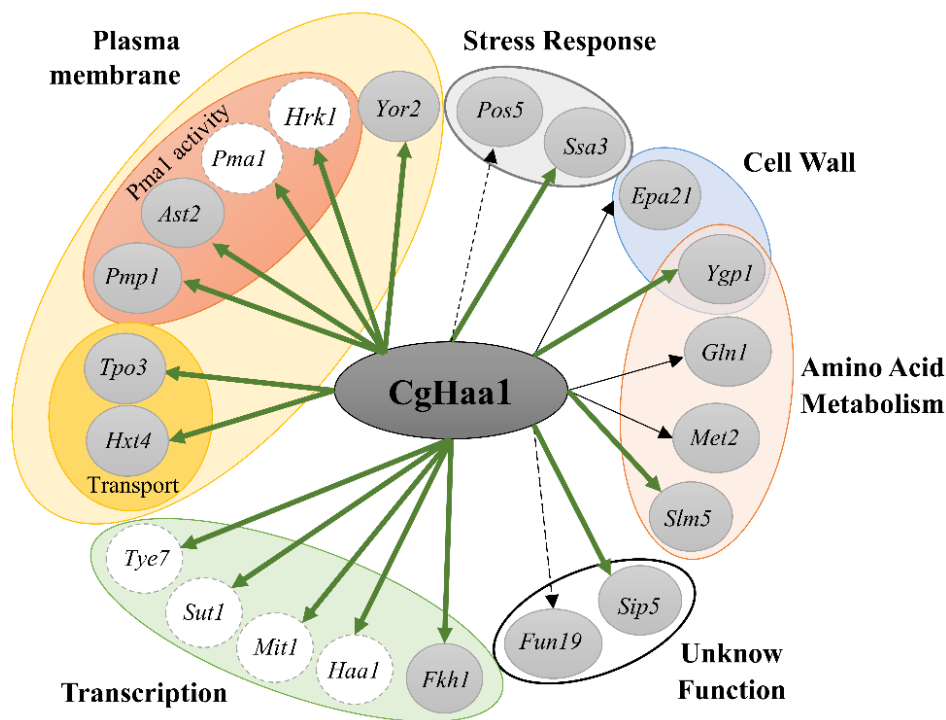


Figure VII. 6. Representation of the preliminary regulatory network of CgHaa1 during acetic acid stress. The network constructed has two levels of confidence: 1) interaction of CgHaa1 transcription factor with the promoter of the gene confirmed by ChIP-seq analysis during acetic acid growth conditions; 2) Using the same growth conditions, confirmation of CgHaa1 dependence for gene expression using microarray assay (market in green arrows). A dashed arrow represents the lack of a predicted DNA binding site in the promoter ChIP-seq peaks. Genes circled in dashed lines require further confirmation of CgHaa1 interaction to the promoter. Gene name was defined by the orthologue in *S. cerevisiae*.

VIII. Final Discussion

The increased resilience of *C. glabrata* to antifungal therapy and the persistent emergence of resistant strains is highly problematic, specially considering the high rates of morbidity and mortality associated with infections caused by this pathogenic yeast. The current shortage of antifungals in the market increases the need to understand, in a comprehensive manner, the molecular mechanisms that govern the resistance of fungal cells to conventional molecules. It is expected that this effort can foster the identification of novel therapeutic targets and also identify new molecules that can be used alone, or in combination with classical antifungals, to control the emergence of resistant strains. In this context, it is particularly relevant the study of underlying mechanisms of resistance in clinical strains undertaken in this thesis since these have the potential to reflect, in a more accurate manner, the *in vivo* path towards resistance. Indeed, as demonstrated in the introductory section of the thesis, it has been observed that a substantial part of the mechanisms described to mediate azole resistance in laboratory strains of the *Candida* genus (with *C. glabrata* included) has not been confirmed to play a role in mediating the resistance phenotype exhibited by clinical strains. Although it is possible that this divergence in findings obtained in the laboratory and clinical strains may reflect difficulties to mimic *in vitro* the conditions that *in vivo* can shape the molecular mechanisms of azole resistance, it is also possible that these mechanisms can be “hidden” by others that play a stronger role in the phenotype. In Chapters III and IV of the thesis, extensive libraries of *Candida* clinical isolates were screened for antifungal susceptibility/resistance. In number of strains examined, this study represents one of the largest reported in Portugal until today. Furthermore, by broadening the study to include not only isolates associated with candidemia (that is, isolates retrieved from the blood of infected patients), the results offer a more general epidemiological view of *Candida spp.* in the community. In line with similar epidemiological studies undertaken in different parts of the world, we found that *C. glabrata* was the second more frequent species isolated from all instances, following *C. albicans*. The incidence of azole resistance (in the range of 16% in study described in Chapter III and 5.4% in the study reported in Chapter IV) is in line with those described in Portugal but also in worldwide epidemiological studies (4.3-15.7%) [2, 3, 419, 420]. Several rare *Candida spp.* clinical isolates could be identified in these studies, including *C. guilliermondii*, *C. dubliniensis*, *C. sake*, *C. keyr* and *C. inconspicua*, with a noticeable presence of *C. keyr* in blood samples, which demonstrates the great variability of human-infecting *Candida* species and may raise some awareness for the study of those that are today out of the spotlight. Eight *C. albicans* of the *africana* variant were further identified, which as far as our knowledge represents the first description of this sub-species in Portugal. This gathered collection of clinical isolates and their further characterization was a fundamental asset for the results herein described and will comprise a useful tool for future studies focused on the characterization of lesser studied *Candida spp.*, or for the fostering knowledge of resistance mechanisms in other *Candida spp.* clinical isolates besides *C. glabrata*, the species focused in this work.

From both antifungal resistance screening studies presented in this thesis, a total of eleven isolates of *C. glabrata* were found to be cross-resistance to fluconazole and voriconazole antifungals, with 2 of them being subjected to comparative genomic and transcriptomic analyses with the laboratory strain CBS138. Besides contributing to the understanding of the azole-resistance phenotype, these global analyses also have the potential to provide clues into the adaptive responses that are evolved by *C. glabrata* during colonization of the human host advancing the current knowledge on the biology and physiology of this

yeast species. As observed in other studies, extreme genetic diversity was observed between the clinical strains and the lab strain CBS138 and even between the clinical strains, which greatly difficult the establishment of relevant genotype-phenotype associations. Among the profiled azole-resistance strains, 10 were found to encode gain-of-function variants of the CgPdr1 transcription factor, demonstrating the preponderance of this mechanism in the acquisition of azole resistance in *Candida glabrata* clinical isolates. Three of these CgPDR1 GOF alleles, encoding the variants K274Q, I392M and I803T were herein characterized in further detail, demonstrating that their expression alone in the background of a susceptible strain is sufficient to induce resistance to fluconazole and voriconazole. However, the comparative transcriptome of the isolates carrying the different GOF CgPDR1 variants against the laboratorial strain CBS138 demonstrated that these alleles may influence differently the direct regulon of CgPdr1 since only two direct targets were commonly regulated, CgCDR1 and CgPDH1 (Figure VIII. 1). Further ectopic expression of these CgPDR1 variants in a $\Delta Cgpdrl\Delta Cgmed15A$ demonstrated that I803T is less dependent on CgMed15A for azole resistance than the other GOFs. Following these results, in Chapter V we aimed to further understand how distinct GOFs may result in different transcription profiles and interactomes.

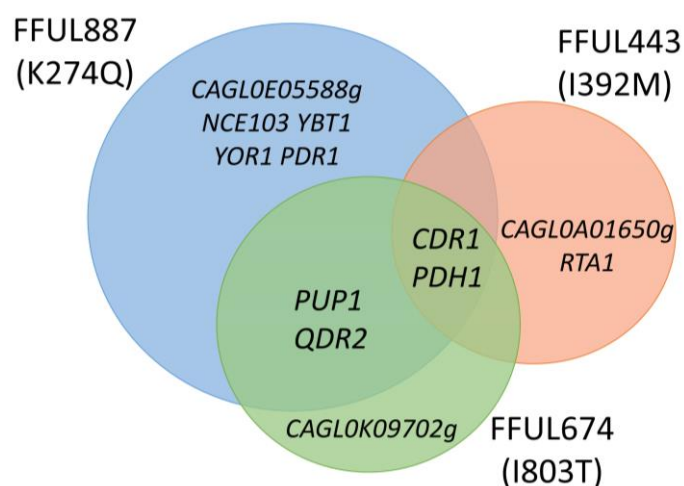


Figure VIII. 1. Different effects of gain-of-function mutations identified in the course of this thesis in the CgPdr1-direct regulon. The upregulated known direct CgPdr1 target genes of the clinical isolates with distinct CgPdr1 gain-of-function variants when compared to de CBS138 azole sensitive laboratorial strain show little overlap.

The sole azole-resistant *C. glabrata* clinical isolate ISTB218 exhibiting a phenotype of cross-resistance to fluconazole and voriconazole that was found to encode a “wild-type” allele of CgPdr1 was also studied in detail in this thesis. The identification of this isolate demonstrates that there are CgPdr1-independent mechanisms governing azole resistance *in vivo*, although these mechanisms may be often masked by the appearance of CgPDR1 gain-of-function mutations that arise as to the most stable resistance factor. Using genomic and transcriptomic comparative approaches indicates that this strain up-regulates a few genes that were previously described to confer resistance to azoles in *C. glabrata*, while it down-regulates the expression of genes described to augment the toxicity of azoles. Examples include the upregulation of CAGL0L03828g, predicted to be capable of mediating the reaction catalyzed by Erg11, and

of *CAGLOF05137g*, encoding a predicted transporter of sterols. These changes in the transcription profile in ISTB218 could help compensate for the diminished CgErg11 function by azole exposure. Also noteworthy is the prediction that the calcineurin pathway can be more active in ISTB218 thus influencing azole resistance. Specifically, the *CgRCN1* positive regulator of the calcineurin pathway was found to be upregulated, while *CgRCN2* and two calmodulin-dependent proteins that inhibit calcineurin kinases were down-regulated. The transcriptomic profiling also revealed the downregulation of genes whose deletion improves tolerance to azoles in *C. glabrata* including the mitochondrial genes *CAGLOK01419g* and *CAGLOL12320g*. Further genomic analysis revealed truncations in genes that disruption results in improved tolerance to azoles, including the aquaporine *CAGLOD00154g* and the *CAGLOJ00847g* predicted to encode a subunit of the succinate dehydrogenase complex. In Figure VIII. 2. are schematically represented the mechanisms involved in the acquisition of resistance to azoles in the isolates that were addressed in this thesis. Further studies will help to understand the individual contribution of the different mechanisms highlighted, alone or in combination, to the azole-tolerance phenotype of the strains. The herein carried out methodology was performed in drug-free medium to uncover constitutive mechanisms that could influence the resistance phenotype of the ISTB218, similar to what is observed when studying CgPdr1 GOF variants. It will also be relevant, specially in the case of this strain, to assess the modifications of the transcriptome in the presence of fluconazole, since the presence of the xenobiotic may induce the triggering of other responses that may have not yet emerged from the analysis.

The extensive genomic and transcriptomic information obtained has the potential to picture possible “intermediate stages” of azole resistance that were overcome by the CgPdr1 GOFs. Concordantly, using an approach to filter non-synonymous SNPs found in a susceptible clinical isolate (ISTA29) also found in *C. glabrata* resistant clinical isolates comparative to CBS138 strain as well (that could reflect prevalent modifications found in clinical isolates but not laboratorial strains) still preserved a great number of non-synonymous SNPs that could influence azole resistance (Annex Table IV. 6). In that line of thought, it would be further interesting to study prevalent mutations in “azole-resistance” genes even in azole resistant strains encoding CgPdr1 GOFs. The transcriptomic/genomic analyses can also highlight important colonization mechanisms such as the role of adhesion observed by the evolutionary pressure in adhesion genes. Further studies could also focus on identifying similarities or dissimilarities in clinical isolates collected from different niches and how these genes/processes reflect the evolutionary capacity of *C. glabrata* to adapt to those niches. The information gathered through these analyses can in the future be explored to identify new therapeutic targets against newly discovered azole responsive mechanisms but also aim to limit important factors of colonization in *C. glabrata*. Furthermore, the gathered knowledge may also pave the way for the development of tools that can facilitate the early diagnosis of resistant strains, a pressing issue since appropriate antifungal treatment according to the clinical isolate resistance profile has been found to play an important role in determining mortality rates of patients suffering from invasive candidiasis. Specifically, it would be of relevance to develop a method for the rapid assessment of CgPdr1 GOFs, since it remains the most prevalent mechanism of resistance observed in *C. glabrata* clinical strains.

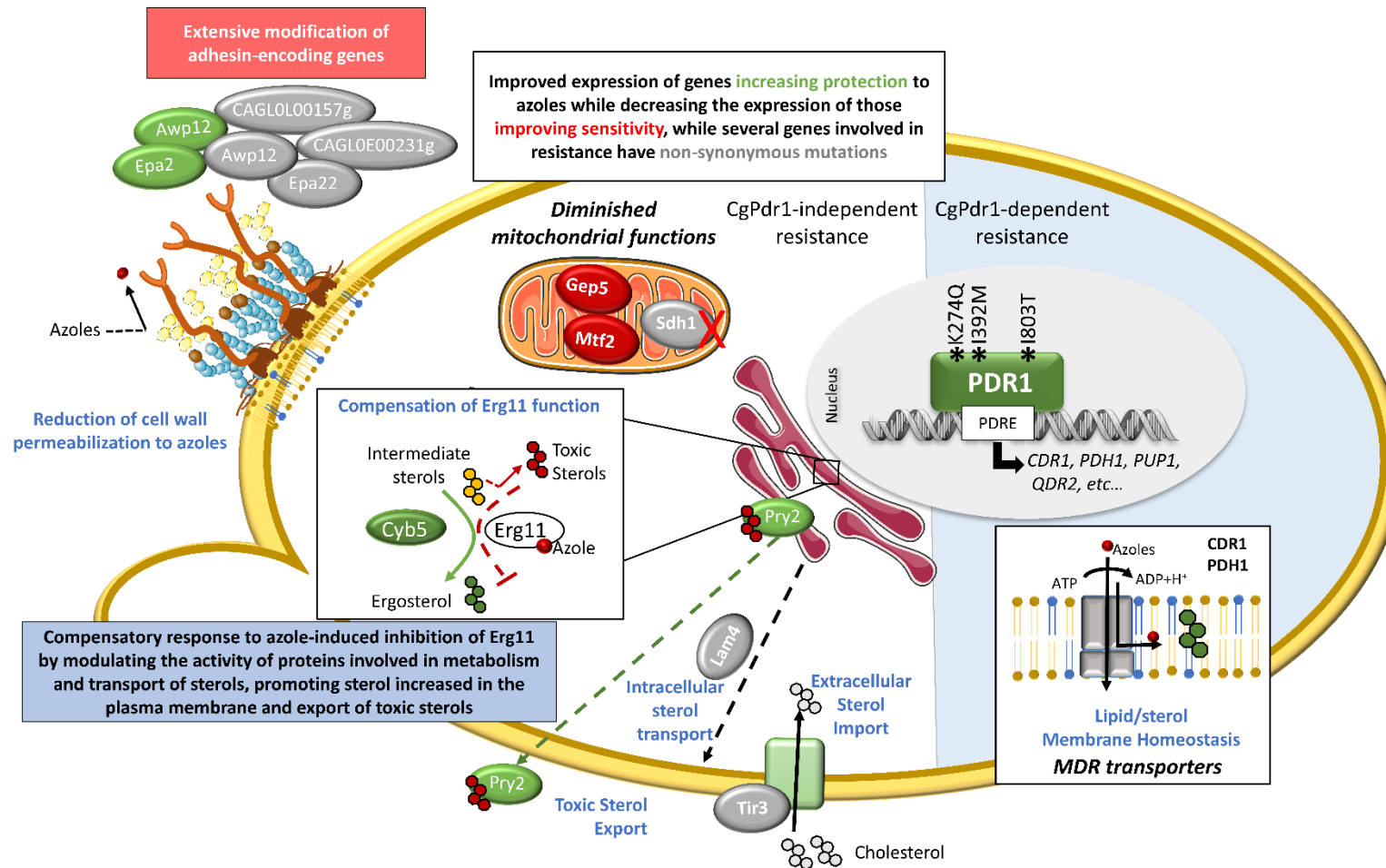


Figure VIII. 2. Genome and transcriptome-wide studies results were used to identify changes in resistance factors in azole-resistant clinical isolates. During the current thesis, a total of ten clinical isolates were found to have an azole resistance phenotype. Azole resistance of ten clinical isolates was associated with non-synonymous mutations in CgPdr1, including K274Q, I392M and I803T demonstrated herein for the first time to be gain-of-function mutations. One azole resistance clinical isolate was found to encode a CgPdr1 “wild-type” allele. OMICs studies helped identified several non-synonymous mutations (grey) or changes in transcription (green if upregulated and red if downregulated) of known azole resistance genes that can be in the future scrutinized as important mechanisms of resistance.

To further study the impact of gain-of-function mutations on the hyperactivity of the CgPdr1, specially of *CgPDR1*^{I392M}, *CgPDR1*^{K274Q} and *CgPDR1*^{I803T}, a more thorough analysis was carried out. Like many gain-of-function mutations described in CgPdr1, the GOFs substitutions identified in this study are mapped in the central regulatory domain of CgPdr1 that serves to restrain of the potent activity of the transactivation domain [62]. Taking advantage of the recently predicted structure of CgPdr1 by the AlphaFold project [323], an *in silico* study of how these GOF mutations impact the 3D structure of the protein was carried out, along with a structural characterization of some functional domains of CgPdr1. In this context, it is important to note that the limited knowledge of the structural organization of CgPdr1 reduces the characterization of functional domains to those that could be identified based on the sequence homology with what has been studied for zinc finger transcription factors in general. Consequently, possible structural features with independent roles in the regulation of the activity of the protein could remain unidentified. The herein carried out analysis narrowed the regulatory domains to a small subset of regions with functional impact, including the place where transactivation domain docks (that is, the region responsible for the restrain of TAD activity by the CRD) or the docking region of fluconazole. With the information obtained by structural *in silico* analysis and gathered in the literature on the different effects that distinct GOF mutations have on CgPdr1 activity helped elucidate how different small structural features could have different functions in the biochemical activity in CgPdr1. For instance, the majority of the GOFs found, inclusively in the current thesis, are usually distributed in the central regulatory domain and are dependent on CgGal11A activity [54, 181, 212]. One striking example is the I803T GOF, found in the NLS region, where other GOFs were also described to result in the hyperactivity of CgPdr1 partially independent of CgGal11A (Figure VIII. 3). Another example is the observation that although the GOFs K274Q and I392M are found both at the N-terminal of the central regulatory domain, they are found in distinct structural features with potential different functions in the activity of CgPdr1 (Figure VIII. 3). Specifically, while the I393 residue is part of the predicted inhibitory domain involved in the sequestration of the TAD domain in its inactive state, the K274 residue is located in a more disordered region where other GOFs are evidenced to regulate the expression of normally chromatin repressed genes, which might indicate a possible impact on the function of chromatin regulators [229]. This narrowing of CgPdr1 structural and regulatory domains can guide the ongoing research to understand the different mechanisms of regulation existing in this essential MDR factor in *C. glabrata* and in the understanding of why different GOFs result in different transcriptional profiles in the same background. Furthermore, it would help improve the finding of new molecules that could potentiate azole treatment independently of GOF distinct effects. The opportunity to understand how xenobiotics interact with CgPdr1 could also prove to be an important tool for the design of new generation azole molecules that would present a limited interaction with CgPdr1 or even design antagonists that upon interacting with the protein could lock its function.

To further pursue how gain-of-function mutations can differently affect CgPdr1 activity it was examined in the same genetic background the impact of Pdr1 wildtype or K274Q variant expression in the ability of Pdr1 to bind promoters *in vivo*. ChIP-seq results rendered clear that the promoters recognized *in vivo* by the CgPdr1^{WT} or by the CgPdr1^{K274Q} variant were identical, indicating that the non-synonymous mutations do not result in a capability of the transcription factor to recognize novel promoters (Figure VIII. 3). It was also noticeable that the impact of CgPdr1 binding in the expression of these directly regulated

genes was not always identical with some being up-regulated in the K274Q variant such as *CgCDR1* and *CgPUP1*, while others were not (despite the protein being found in the promoter region) like *CgRPN4* and *CgSNQ2* (Figure VIII. 3). A closer analysis of the PDRE motif present in the promoter of those genes whose expression was increased by the *CgPdr1*^{K274Q} variant, compared to the *CgPdr1*^{WT}, suggests that the presence of two timines before the PDRE sequence, TTCCGTGG, can be involved since this sequence was enriched in the promoters of those genes that were bound and also up-regulated by the GOF variant. An assessment of the interactome of *CgPdr1*^{WT} and *CgPdr1*^{K274Q} was also undertaken through the use of a ChIP-SICAP experiment accoupled with MS. Several interesting possible co-factors of *CgPdr1* activity were identified that could in the future be further studied with the prospect of identifying new antifungal targets that could limit azole resistance. Important examples include proteins involved in H3K36 trimethylation which was recently described to have a negative effect on PDR gene transcription [164, 341] and proteins with roles in chromatin and telomeric silencing that could play a role in *CgPdr1* involvement in adhesin genes expression. The relevance of these proteins in *CgPdr1* activity should be studied in more detail and the different contribution to the distinct *CgPdr1* GOF variants activity should also be explored to get a clearer and more accurate picture of this drug-responsive critical regulatory system, a knowledge that is relevant to understand the complex and intertwined mechanisms governing gene expression in eukaryotes.

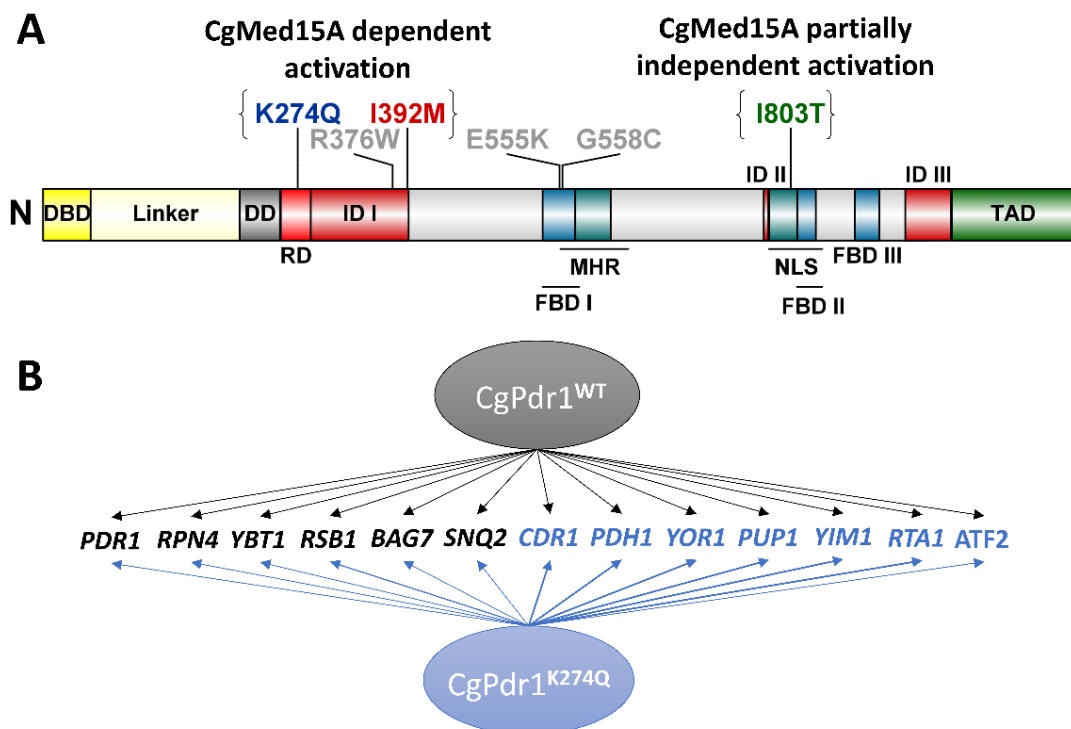


Figure VIII. 3. *Different effects of gain-of-function mutations identified in the course of this thesis in the CgPdr1 protein structure and activity.* (A) The GOFs K274Q and I392M that are dependent on CgGal11A for *CgPdr1* hyperactivity are located in the regulatory domain (RD) and inhibitory domain (IDI), while the I803T GOF, that *CgPdr1* hyperactivity is less dependent on CgGal11A, is located in the nuclear localization signalling domain (NLS). (B) ChIP-seq analysis revealed that *CgPdr1*^{K274Q} variant (blue) as the same distribution has the wild-type variant (orange) in the promoter region of its target genes despite having a different influence on their expression. The genes upregulated using transcriptomic analysis by the *CgPdr1*^{K274Q} variant compared to the *CgPdr1*^{WT} variant are marked in blue.

In Chapter VI and Chapter VII, the characterization of the CgHaa1 transcriptional network and its importance as a virulence factor against *Galleria mellonella* is described. CgHaa1 is required for maximal tolerance and response to these cells to high concentrations of acetic acid found prominently during bacterial vaginosis [262]. The understanding of how *Candida* persists in the vaginal niche and is not excluded from the vaginal tract in adverse conditions could prove essential to foster novel therapeutic targets that could underlie the ability of this pathogenic yeast to persist during vaginal colonization. In Chapter V, it was demonstrated that CgHaa1 biological functions go beyond governing response and tolerance to acetic acid stress. Specifically, CgHaa1 was confirmed to be a relevant factor for the maximum biofilm formation in the presence of acetic acid determining adherence to both biotic and abiotic surfaces. The expression of CgHAA1 was also found to enhance virulence of *C. glabrata* against the infection model *G. mellonella* and this phenotype was correlated with a contribution of the regulator for increased survival of the yeast inside the larvae's monocytes, a response that can help counteract the activity of the primary immune response of the wax. Further examination of the role played by previously identified CgHaa1-target genes in these two phenotypes, capability to form biofilms and virulence towards *G. mellonella*, led us to imply, for the first time, the poorly characterized adhesins CgAWP12, CgAWP13, CAGL0K10164g and CAGL0H07469g in adherence of *C. glabrata* to vaginal epithelial cells. However, under these conditions, there was no effect of CgHaa1 expression in the control of these genes' transcription thus leaving an open perspective of a more thorough transcriptomic analysis of this *C. glabrata*-vaginal cells co-culture system that can help elucidate what are other genes regulated by CgHaa1 that could mediate the observed impact in adherence to vaginal epithelial cells. These results are quite relevant since, as far as our knowledge, only two other transcription factors, besides CgHaa1 [262](Chapter VI), have been recently described to be important for maximum adherence of *C. glabrata* to human vaginal epithelial cells, specifically CgEfg1 and CgTec1 [377]. Also as far as our knowledge, no other adhesin was so far characterized for its relevance in *C. glabrata* in this phenotype.

Like CgHAA1, the expression of CgAWP12, CgAWP13, CAGL0H07469g, CAGL0I07249g, CAGL0I07249g, CAGL0C03740g and CAGL0G05632g target genes was also found to increase virulence of *C. glabrata* against *G. mellonella*, however, out of these only the expression of CgHAA1 and CgAWP13 could be linked with a contribution for survival inside the larvae's hemocytes. This observation suggests that the role of CgHaa1 regulatory system for the increased virulence phenotype can correlate with the larvae's hemocytes survival but further studies will be required to understand the players involved. Considering that CgHaa1 was described to regulate the expression of genes involved in acetate catabolism and that the presence of this metabolite inside the larvae's hemocytes can be a triggering factor for the activation of this regulator, it was examined whether the expression of CgICL1 and CAGL0L00649g (ScACSI orthologue), two enzymes involved in the mobilization of acetate via glyoxylate cycle, contribute for tolerance to acetic acid and enhance virulence of *C. glabrata* towards *G. mellonella*. The results demonstrate that indeed this is the case, however, during the time that this thesis took it was not possible to determine the impact that these genes have in the survival inside the larvae's hemocytes, something that is definitely required to complete this model of how CgHaa1 regulates this phenotype.

The final chapter of this thesis, Chapter VI, is focused on the dissection of the CgHaa1-dependent transcriptional regulatory network and the understanding of how this system differed and evolved from the one described in the budding yeast *Saccharomyces cerevisiae*. Previous transcriptomic analyses carried out under very similar experimental setups in *S. cerevisiae* and in *C. glabrata* demonstrated that the CgHaa1 and ScHaa1 networks are quite different, with the first being larger and comprising a set of genes involved in biological functions that were not under the regulation of ScHaa1 [252, 262]. At the development stage of this current project, a provisory CgHaa1 transcriptional network was built using two levels of information, similar to what was previously described in Merhej J. *et al.* 2016 [421]. First, a regulatory interaction is proposed if the transcription factor binding to a gene promoter is confirmed in the ChIP-seq results. In a second analysis, the confidence that this interaction can result in the transcription of the gene is obtained through transcriptomic analysis. Using ChIP-seq analysis, a total of 22 direct targets of CgHaa1 were defined, including CgTPO3 predicted to encode an acetate transporter, or CgPMP1 and CgAST2 predicted to encode proteins involved in the regulation of the CgPma1 proton pump activity. Under acetic acid stress the binding to the promoter by CgHaa1 has a positive influence on the transcription of 70% of the target genes. It is important however to stand out that for some of the genes herein suggested to be direct targets of CgHaa1, further confirmation by qPCR will be required since there was a low-intensity profile of the reads in the regions where CgHaa1 is presumably bound. This can result from technical difficulties associated with the ChIP-seq methodology used, but it can also reflect a transient and weak interaction of the regulator with the promoter. In Figure VII. 6 it is then schematically represented the set of genes that are herein suggested to be direct targets of CgHaa1 (with those obtained at lower confidence degrees being identified with an asterisk) in comparison with those characterized in *S. cerevisiae*. Several common predicted direct targets of the Haa1 of *C. glabrata* and *S. cerevisiae* regulatory network were identified to be conserved possibly through the same *cis*-regulatory element, the HRE element (SMGGSG). However, only around 20% of the direct regulated network was predicted to be conserved with that of *S. cerevisiae* during acetic acid stress and the elucidation of the molecular mechanisms underneath these differences will require a better and unequivocal identification of what is the DNA element recognized *in vivo* by CgHaa1. In this thesis, the first step towards that identification has been taken with the identification of two DNA sequences enriched in the regions where CgHaa1 was mapped to bind in the promoter of target genes, yhCCGCTAhy and kkAAATGGsy. Further studies will now be required to complete the work herein initiated and demonstrate whether or not CgHaa1 binds to these motifs and to what affinity. Among the possibilities that could explain the differences in the two networks, are the addition of *cis*-regulatory HRE-like elements to the promoter of *C. glabrata* unique Haa1 target genes (including CgSLM5 or the ScFKH1 orthologue) and the possible recognition of a new *cis*-responsive element, kkAAATGGsy. The low conservation of indirect Haa1 transcriptional network between species is also reported [252, 262], which could be explained by the loss and gain of transcription regulators genes as direct targets of CgHaa1.

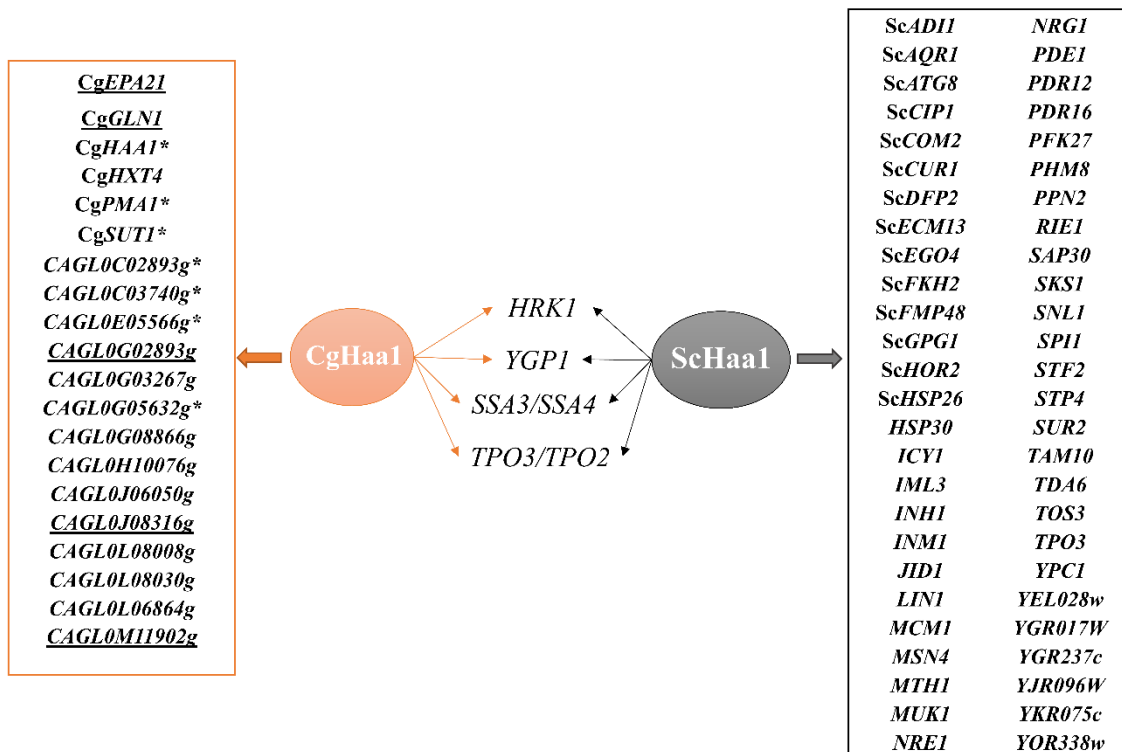


Figure VIII. 4. Comparison of the CgHaa1 and ScHaa1 predicted direct regulatory network during acetic acid stress. The CgHaa1 regulatory network was defined in this thesis for the first time based on the ChIP-seq analysis explored in Chapter VII. CgHaa1 dependence for gene expression was confirmed by microarray assay to predict if CgHaa1 interaction with a gene promotor could result in gene upregulation (when that is found not to be the case, the gene is underlined). Genes marked with * required further validation by ChIP-qPCR since a low-intensity profile of the reads in the regions where CgHaa1 is presumably bound was observed. The ScHaa1 regulatory network was predicted by Mira, NP. *et al.* 2011 [253], based on the presence of the identified binding motif HRE in the promotor of genes that expression is dependent of ScHaa1 during acetic acid stress. The effect in transcription on the target genes by CgHaa1 and ScHaa1 were accessed under similar growth conditions, mid-exponential phase cells grown in minimal medium at pH4 after 30 min acetic acid exposure.

IX. List of Publications and Communications

Peer-reviewed scientific publications:

Salazar SB, Simões RS, Pedro NA, Pinheiro MJ, Carvalho NFNN, Mira NP. An overview on conventional and non-conventional therapeutic approaches for the treatment of candidiasis and underlying resistance mechanisms in clinical strains. *J Fungi (Basel)*. 2020; 10;6(1), doi: 10.3390/jof6010023

Lourenço A, Nuno Pedro N, Salazar SB and Mira NP. Effect of acetic acid and lactic acid at low pH in growth and azole resistance of *Candida albicans* and *Candida glabrata*. *Front Microbiol*. 2019; 9: 3265, doi: 10.3389/fmicb.2018.03265

Marques L, Alves MM, Eugénio S, Salazar SB, Pedro N, Grenho L, Mira NP, Fernandes MH and Montemor MF. Potential anti-cancer and anti-*Candida* activity of Zn-derived foams. *Journal of Materials Chemistry B*. 2018; 6, 2821-2830, doi: 10.1039/C7TB02726E

Alves MM, Marques LM, Nogueira I, Santos CF, Salazar SB, Eugénio S, Mira NP and Montemor F. In silico, *in vitro* and antifungal activity of the surface layers formed on zinc upon this biomaterial degradation. *Applied Surface Science*. 2018; 447:401-407, doi: 10.1016/j.apsusc.2018.03.164

Salazar SB, Wang C, Musterkötter M, Okamoto M., Takahashi-Nakaguchi A, Chibana H, Lopes M, Güldener U, Butler G and Mira NP. Comparative genomic and transcriptomic analyses unveil novel features of azole resistance and adaptation to the human host in *Candida glabrata*. *FEMS Yeast Res*. 2018; 1;18(1), doi: 10.1093/femsyr/fox079

Submitted (in Press):

Salazar SB, Pinheiro MJF, Sotti-Novais D, Soares AR, Lopes MM, Ferreira T, Rodrigues V, Fernandes F. and Mira NP. Disclosing azole resistance mechanisms in resistant *Candida glabrata* strains encoding wild-type or gain-of-function CgPDR1 alleles through comparative genomics and transcriptomics (*in press* at G3)

Oral communication in national or international meetings:

Salazar SB, Valez N, Sotti-Novais D, Simões R, Souza JA, Faustino MJ, Faustino C, Mendonça C, Lopes MM, Rodrigues V, Mira NP. Unveiling azole resistance mechanisms in *Candida glabrata* clinical isolates encoding wild-type or gain-of-function CgPdr1 alleles. Oral presentation at the *Candida* and Candidiasis, May 2021 online edition.

Salazar SB, Pedreira T; Chibana H; Lopes MM; Güldener U and Mira NP. Genomic Adaptive Mechanisms mediating Azole Resistance and Adaptation to the Human Host in *Candida glabrata*, with emphasis on the role of CgPDR1 regulon. Oral presentation at the XXI Jornadas de Biologia de Leveduras, Professor Nicolau van Uden, June 2018, Braga, Portugal.

Salazar SB, Bernardo R, Cunha DV, Wang C, Chibana H, Silva S, Pereira L, Sá-Correia I, Azeredo J, Butler G, Mira NP. Genetic adaptive mechanisms mediating response and tolerance to acetic acid stress in the human pathogen *Candida glabrata*: role of the CgHaa1-dependent signalling pathway, oral presentation at the Microbial Stress Meeting: Systems to Molecules and Back, April 2018, Kinsale, Ireland.

Poster communication in national or international meetings:

Salazar SB, Valez N, Pinheiro MJ, Pedro NA, Lourenço A, Mira NP. Modulation of *Candida glabrata* response and resistance to azoles in the presence of acetic and lactic acids at low pH. *Candida and Candidiasis*, May 2021 online edition.

Salazar SB, Silva S, Mil-Homens D, Pimenta AI, Chibana H, Azeredo J, Fialho AM, Mira NP. The *Candida glabrata* CgHaa1-dependent system is required for biofilm formation, adhesion to epithelial cells and maximal virulence against *Galleria mellonella*. Advanced Lecture Course on Human Fungal Pathogens. May 2019, Nice, France.

Salazar SB, Pedreira T, Henriques R, Wang C, Musterkotter M, Okamoto M, Takahashi-Nakaguchi A, Chibana H, Lopes MM, Güldener U, Butler G, Mira NP. Comparative genomic and transcriptomic analysis unveil novel features of azole resistance and adaptation to the human host in *Candida glabrata*. Microbiotec'17, December 2017, Porto, Portugal

Seixas I, Barbosa C, Salazar SB, Mendes-Faia A, Güldener U, Mendes-Ferreira A and Mira NP. Genome sequence and annotation of the non-conventional yeast *Hanseniaspora guilliermondii* UTAD222. Microbiotec'17, December 2017, Porto, Portugal

Seixas I, Barbosa C, Salazar SB, Mendes-Faia A, Güldener U, Mendes-Ferreira A and Mira NP. Genome sequence and annotation of the non-conventional yeast *Hanseniaspora guilliermondii* UTAD222. 33rd International Specialized Symposium on Yeasts, June 2017, University College Cork, Ireland

Awards:

Best talk by an Early Career Researcher sponsored by the journal Genes, at Microbial Stress Meeting: From systems to Molecules and Back, 2018, Kinsale, Ireland.

First Prize for best communication by poster awarded by The American Society for Microbiology, at "Microbiotec'15", 2015, Évora, Portugal.

X. References

1. Brown, G.D., et al., *Hidden killers: human fungal infections*. *Sci Transl Med*, 2012. **4**(165): p. 165rv13.
2. Pfaller, M.A., et al., *Results from the ARTEMIS DISK Global Antifungal Surveillance Study, 1997 to 2007: a 10.5-year analysis of susceptibilities of Candida Species to fluconazole and voriconazole as determined by CLSI standardized disk diffusion*. *J Clin Microbiol*, 2010. **48**(4): p. 1366-77.
3. Pfaller, M.A., et al., *Twenty Years of the SENTRY Antifungal Surveillance Program: Results for Candida Species From 1997-2016*. *Open Forum Infect Dis*, 2019. **6**(Suppl 1): p. S79-S94.
4. Sanguinetti, M., B. Posteraro, and C. Lass-Flörl, *Antifungal drug resistance among Candida species: mechanisms and clinical impact*. *Mycoses*, 2015. **58 Suppl 2**: p. 2-13.
5. Castanheira, M., et al., *Activity of echinocandins and triazoles against a contemporary (2012) worldwide collection of yeast and moulds collected from invasive infections*. *Int J Antimicrob Agents*, 2014. **44**(4): p. 320-6.
6. Won, E.J., et al., *Fluconazole-Resistant Candida glabrata Bloodstream Isolates, South Korea, 2008-2018*. *Emerg Infect Dis*, 2021. **27**(3): p. 779-788.
7. Salazar, S.B., et al., *An Overview on Conventional and Non-Conventional Therapeutic Approaches for the Treatment of Candidiasis and Underlying Resistance Mechanisms in Clinical Strains*. *J Fungi (Basel)*, 2020. **6**(1).
8. Carolus, H., et al., *Amphotericin B and Other Polyenes-Discovery, Clinical Use, Mode of Action and Drug Resistance*. *J Fungi (Basel)*, 2020. **6**(4).
9. Allen, D., et al., *Azole antifungals: 35 years of invasive fungal infection management*. *Expert Rev Anti Infect Ther*, 2015. **13**(6): p. 787-98.
10. Mroczynska, M. and A. Brillowska-Dabrowska, *Review on Current Status of Echinocandins Use*. *Antibiotics (Basel)*, 2020. **9**(5).
11. Vermes, A., H.J. Guchelaar, and J. Dankert, *Flucytosine: a review of its pharmacology, clinical indications, pharmacokinetics, toxicity and drug interactions*. *J Antimicrob Chemother*, 2000. **46**(2): p. 171-9.
12. Lees, N.D., et al., *Cloning of the late genes in the ergosterol biosynthetic pathway of Saccharomyces cerevisiae--a review*. *Lipids*, 1995. **30**(3): p. 221-6.
13. Lewis, J.S., 2nd and J.R. Graybill, *Fungicidal versus Fungistatic: what's in a word?* *Expert Opin Pharmacother*, 2008. **9**(6): p. 927-35.
14. Kumar, A., et al., *Fungicidal versus fungistatic therapy of invasive Candida infection in non-neutropenic adults: a meta-analysis*. *Mycology*, 2018. **9**(2): p. 116-128.
15. Pappas, P.G., et al., *Guidelines for treatment of candidiasis*. *Clin Infect Dis*, 2004. **38**(2): p. 161-89.
16. Hull, C.M., et al., *Two clinical isolates of Candida glabrata exhibiting reduced sensitivity to amphotericin B both harbor mutations in ERG2*. *Antimicrob Agents Chemother*, 2012. **56**(12): p. 6417-21.
17. Hull, C.M., et al., *Facultative sterol uptake in an ergosterol-deficient clinical isolate of Candida glabrata harboring a missense mutation in ERG11 and exhibiting cross-resistance to azoles and amphotericin B*. *Antimicrob Agents Chemother*, 2012. **56**(8): p. 4223-32.
18. Bard, M., et al., *Sterol synthesis and viability of erg11 (cytochrome P450 lanosterol demethylase) mutations in Saccharomyces cerevisiae and Candida albicans*. *Lipids*, 1993. **28**(11): p. 963-7.
19. Kelly, S.L., et al., *Mode of action and resistance to azole antifungals associated with the formation of 14 alpha-methylergosta-8,24(28)-dien-3 beta,6 alpha-diol*. *Biochem Biophys Res Commun*, 1995. **207**(3): p. 910-5.
20. Morio, F., et al., *Screening for amino acid substitutions in the Candida albicans Erg11 protein of azole-susceptible and azole-resistant clinical isolates: new substitutions and a review of the literature*. *Diagn Microbiol Infect Dis*, 2010. **66**(4): p. 373-84.
21. Berkow, E.L., et al., *Multidrug Transporters and Alterations in Sterol Biosynthesis Contribute to Azole Antifungal Resistance in Candida parapsilosis*. *Antimicrob Agents Chemother*, 2015. **59**(10): p. 5942-50.
22. Choi, M.J., et al., *Resistance Mechanisms and Clinical Features of Fluconazole-Nonsusceptible Candida tropicalis Isolates Compared with Fluconazole-Less-Susceptible Isolates*. *Antimicrob Agents Chemother*, 2016. **60**(6): p. 3653-61.
23. Vandeputte, P., et al., *Mechanisms of azole resistance in a clinical isolate of Candida tropicalis*. *Antimicrob Agents Chemother*, 2005. **49**(11): p. 4608-15.
24. Kelly, S.L., et al., *The G464S amino acid substitution in Candida albicans sterol 14alpha-demethylase causes fluconazole resistance in the clinic through reduced affinity*. *Biochem Biophys Res Commun*, 1999. **262**(1): p. 174-9.

25. Feng, W., et al., *Mutations and/or Overexpressions of ERG4 and ERG11 Genes in Clinical Azoles-Resistant Isolates of Candida albicans*. *Microb Drug Resist*, 2017. **23**(5): p. 563-570.
26. Neji, S., et al., *Virulence factors, antifungal susceptibility and molecular mechanisms of azole resistance among Candida parapsilosis complex isolates recovered from clinical specimens*. *J Biomed Sci*, 2017. **24**(1): p. 67.
27. Tsai, H.F., et al., *Microarray and molecular analyses of the azole resistance mechanism in Candida glabrata oropharyngeal isolates*. *Antimicrob Agents Chemother*, 2010. **54**(8): p. 3308-17.
28. Sanguinetti, M., et al., *Mechanisms of azole resistance in clinical isolates of Candida glabrata collected during a hospital survey of antifungal resistance*. *Antimicrob Agents Chemother*, 2005. **49**(2): p. 668-79.
29. Berila, N., et al., *Mutations in the CgPDR1 and CgERG11 genes in azole-resistant Candida glabrata clinical isolates from Slovakia*. *Int J Antimicrob Agents*, 2009. **33**(6): p. 574-8.
30. Brun, S., et al., *Mechanisms of azole resistance in petite mutants of Candida glabrata*. *Antimicrob Agents Chemother*, 2004. **48**(5): p. 1788-96.
31. Geber, A., et al., *Deletion of the Candida glabrata ERG3 and ERG11 genes: effect on cell viability, cell growth, sterol composition, and antifungal susceptibility*. *Antimicrob Agents Chemother*, 1995. **39**(12): p. 2708-17.
32. Ksiezopolska, E., et al., *Narrow mutational signatures drive acquisition of multidrug resistance in the fungal pathogen Candida glabrata*. *Curr Biol*, 2021. **31**(23): p. 5314-5326 e10.
33. Vale-Silva, L.A., et al., *Azole resistance by loss of function of the sterol Delta(5),(6)-desaturase gene (ERG3) in Candida albicans does not necessarily decrease virulence*. *Antimicrob Agents Chemother*, 2012. **56**(4): p. 1960-8.
34. Richter, S.S., et al., *Antifungal susceptibilities of Candida species causing vulvovaginitis and epidemiology of recurrent cases*. *J Clin Microbiol*, 2005. **43**(5): p. 2155-62.
35. Sanglard, D., et al., *The ATP binding cassette transporter gene CgCDR1 from Candida glabrata is involved in the resistance of clinical isolates to azole antifungal agents*. *Antimicrob Agents Chemother*, 1999. **43**(11): p. 2753-65.
36. Sanglard, D., F. Ischer, and J. Bille, *Role of ATP-binding-cassette transporter genes in high-frequency acquisition of resistance to azole antifungals in Candida glabrata*. *Antimicrob Agents Chemother*, 2001. **45**(4): p. 1174-83.
37. Kumari, S., et al., *Unmasking of CgYor1-Dependent Azole Resistance Mediated by Target of Rapamycin (TOR) and Calcineurin Signaling in Candida glabrata*. *mBio*, 2022: p. e0354521.
38. Nakayama, H., et al., *The Candida glabrata putative sterol transporter gene CgAUS1 protects cells against azoles in the presence of serum*. *J Antimicrob Chemother*, 2007. **60**(6): p. 1264-72.
39. Costa, C., et al., *Clotrimazole Drug Resistance in Candida glabrata Clinical Isolates Correlates with Increased Expression of the Drug:H(+) Antiporters CgAqr1, CgTpo1_1, CgTpo3, and CgQdr2*. *Front Microbiol*, 2016. **7**: p. 526.
40. Gale, A.N., et al., *Identification of Essential Genes and Fluconazole Susceptibility Genes in Candida glabrata by Profiling Hermes Transposon Insertions*. *G3 (Bethesda)*, 2020. **10**(10): p. 3859-3870.
41. Santos, R., et al., *The multidrug resistance transporters CgTpo1_1 and CgTpo1_2 play a role in virulence and biofilm formation in the human pathogen Candida glabrata*. *Cell Microbiol*, 2017. **19**(5).
42. Pais, P., et al., *Membrane Proteomics Analysis of the Candida glabrata Response to 5-Flucytosine: Unveiling the Role and Regulation of the Drug Efflux Transporters CgFlr1 and CgFlr2*. *Front Microbiol*, 2016. **7**: p. 2045.
43. Sa-Correia, I., et al., *Drug:H+ antiporters in chemical stress response in yeast*. *Trends Microbiol*, 2009. **17**(1): p. 22-31.
44. Rizzo, J., et al., *Role of lipid transporters in fungal physiology and pathogenicity*. *Comput Struct Biotechnol J*, 2019. **17**: p. 1278-1289.
45. Khandelwal, N.K., et al., *Azole resistance in a Candida albicans mutant lacking the ABC transporter CDR6/ROA1 depends on TOR signaling*. *J Biol Chem*, 2018. **293**(2): p. 412-432.
46. Vermitsky, J.P. and T.D. Edlind, *Azole resistance in Candida glabrata: coordinate upregulation of multidrug transporters and evidence for a Pdr1-like transcription factor*. *Antimicrob Agents Chemother*, 2004. **48**(10): p. 3773-81.
47. Healey, K.R., et al., *Prevalent mutator genotype identified in fungal pathogen Candida glabrata promotes multi-drug resistance*. *Nat Commun*, 2016. **7**: p. 11128.
48. Abbes, S., et al., *Interactions between copy number and expression level of genes involved in fluconazole resistance in Candida glabrata*. *Front Cell Infect Microbiol*, 2013. **3**: p. 74.

49. Polakova, S., et al., *Formation of new chromosomes as a virulence mechanism in yeast Candida glabrata*. Proc Natl Acad Sci U S A, 2009. **106**(8): p. 2688-93.
50. Caudle, K.E., et al., *Genomewide expression profile analysis of the Candida glabrata Pdr1 regulon*. Eukaryot Cell, 2011. **10**(3): p. 373-83.
51. Ferrari, S., et al., *Gain of function mutations in CgPDR1 of Candida glabrata not only mediate antifungal resistance but also enhance virulence*. PLoS Pathog, 2009. **5**(1): p. e1000268.
52. Garnaud, C., et al., *Next-generation sequencing offers new insights into the resistance of Candida spp. to echinocandins and azoles*. J Antimicrob Chemother, 2015. **70**(9): p. 2556-65.
53. Ni, Q., et al., *CgPDR1 gain-of-function mutations lead to azole-resistance and increased adhesion in clinical Candida glabrata strains*. Mycoses, 2018. **61**(7): p. 430-440.
54. Tian, Y., et al., *A gain-of-function mutation in PDR1 of Candida glabrata decreases EPA1 expression and attenuates adherence to epithelial cells through enhancing recruitment of the Mediator subunit Gal11A*. Microbiol Res, 2020. **239**: p. 126519.
55. Salazar, S.B., et al., *Comparative genomic and transcriptomic analyses unveil novel features of azole resistance and adaptation to the human host in Candida glabrata*. FEMS Yeast Res, 2018. **18**(1).
56. Vermitsky, J.P., et al., *Pdr1 regulates multidrug resistance in Candida glabrata: gene disruption and genome-wide expression studies*. Mol Microbiol, 2006. **61**(3): p. 704-22.
57. Schwarzmueller, T., et al., *Systematic phenotyping of a large-scale Candida glabrata deletion collection reveals novel antifungal tolerance genes*. PLoS Pathog, 2014. **10**(6): p. e1004211.
58. Kaur, R., I. Castano, and B.P. Cormack, *Functional genomic analysis of fluconazole susceptibility in the pathogenic yeast Candida glabrata: roles of calcium signaling and mitochondria*. Antimicrob Agents Chemother, 2004. **48**(5): p. 1600-13.
59. Borah, S., R. Shivarathri, and R. Kaur, *The Rho1 GTPase-activating protein CgBem2 is required for survival of azole stress in Candida glabrata*. J Biol Chem, 2011. **286**(39): p. 34311-24.
60. Noble, J.A., et al., *STB5 is a negative regulator of azole resistance in Candida glabrata*. Antimicrob Agents Chemother, 2013. **57**(2): p. 959-67.
61. Vu, B.G., et al., *The Candida glabrata Upc2A transcription factor is a global regulator of antifungal drug resistance pathways*. PLoS Genet, 2021. **17**(9): p. e1009582.
62. Moye-Rowley, W.S., *Multiple interfaces control activity of the Candida glabrata Pdr1 transcription factor mediating azole drug resistance*. Curr Genet, 2019. **65**(1): p. 103-108.
63. Cavalheiro, M., et al., *A Transcriptomics Approach To Unveiling the Mechanisms of In Vitro Evolution towards Fluconazole Resistance of a Candida glabrata Clinical Isolate*. Antimicrob Agents Chemother, 2019. **63**(1).
64. Singh-Babak, S.D., et al., *Global analysis of the evolution and mechanism of echinocandin resistance in Candida glabrata*. PLoS Pathog, 2012. **8**(5): p. e1002718.
65. Kannan, A., et al., *Comparative Genomics for the Elucidation of Multidrug Resistance in Candida lusitanae*. mBio, 2019. **10**(6).
66. Demers, E.G., et al., *Evolution of drug resistance in an antifungal-naive chronic Candida lusitanae infection*. Proc Natl Acad Sci U S A, 2018. **115**(47): p. 12040-12045.
67. Carrete, L., et al., *Genome Comparisons of Candida glabrata Serial Clinical Isolates Reveal Patterns of Genetic Variation in Infecting Clonal Populations*. Front Microbiol, 2019. **10**: p. 112.
68. Goffeau, A., *Drug resistance: the fight against fungi*. Nature, 2008. **452**(7187): p. 541-2.
69. Alenquer, M., S. Tenreiro, and I. Sa-Correia, *Adaptive response to the antimalarial drug artesunate in yeast involves Pdr1p/Pdr3p-mediated transcriptional activation of the resistance determinants TPO1 and PDR5*. FEMS Yeast Res, 2006. **6**(8): p. 1130-9.
70. Fardeau, V., et al., *The central role of PDR1 in the foundation of yeast drug resistance*. J Biol Chem, 2007. **282**(7): p. 5063-5074.
71. Paul, S., T.B. Bair, and W.S. Moye-Rowley, *Identification of genomic binding sites for Candida glabrata Pdr1 transcription factor in wild-type and rho0 cells*. Antimicrob Agents Chemother, 2014. **58**(11): p. 6904-12.
72. DeRisi, J., et al., *Genome microarray analysis of transcriptional activation in multidrug resistance yeast mutants*. FEBS Lett, 2000. **470**(2): p. 156-60.
73. Khakhina, S., L. Simonicova, and W.S. Moye-Rowley, *Positive autoregulation and repression of transactivation are key regulatory features of the Candida glabrata Pdr1 transcription factor*. Mol Microbiol, 2018. **107**(6): p. 747-764.
74. Hallstrom, T.C. and W.S. Moye-Rowley, *Hyperactive forms of the Pdr1p transcription factor fail to respond to positive regulation by the hsp70 protein Pdr13p*. Mol Microbiol, 2000. **36**(2): p. 402-13.

75. Merhej, J., et al., *bPeaks: a bioinformatics tool to detect transcription factor binding sites from ChIPseq data in yeasts and other organisms with small genomes*. *Yeast*, 2014. **31**(10): p. 375-91.
76. Lucau-Danila, A., et al., *Early expression of yeast genes affected by chemical stress*. *Mol Cell Biol*, 2005. **25**(5): p. 1860-8.
77. Banerjee, D., et al., *Responses of pathogenic and nonpathogenic yeast species to steroids reveal the functioning and evolution of multidrug resistance transcriptional networks*. *Eukaryot Cell*, 2008. **7**(1): p. 68-77.
78. Salin, H., et al., *Structure and properties of transcriptional networks driving selenite stress response in yeasts*. *BMC Genomics*, 2008. **9**: p. 333.
79. van den Hazel, H.B., et al., *PDR16 and PDR17, two homologous genes of Saccharomyces cerevisiae, affect lipid biosynthesis and resistance to multiple drugs*. *J Biol Chem*, 1999. **274**(4): p. 1934-41.
80. Ghosh, A.K., G. Ramakrishnan, and R. Rajasekharan, *YLR099C (ICT1) encodes a soluble Acyl-CoA-dependent lysophosphatidic acid acyltransferase responsible for enhanced phospholipid synthesis on organic solvent stress in Saccharomyces cerevisiae*. *J Biol Chem*, 2008. **283**(15): p. 9768-75.
81. Thevissen, K., et al., *SKN1, a novel plant defensin-sensitivity gene in Saccharomyces cerevisiae, is implicated in sphingolipid biosynthesis*. *FEBS Lett*, 2005. **579**(9): p. 1973-7.
82. Kihara, A. and Y. Igarashi, *Cross talk between sphingolipids and glycerophospholipids in the establishment of plasma membrane asymmetry*. *Mol Biol Cell*, 2004. **15**(11): p. 4949-59.
83. Topolska, M., et al., *TORC2-Dependent Ypk1-Mediated Phosphorylation of Lam2/Ltc4 Disrupts Its Association with the beta-Propeller Protein Laf1 at Endoplasmic Reticulum-Plasma Membrane Contact Sites in the Yeast Saccharomyces cerevisiae*. *Biomolecules*, 2020. **10**(12).
84. Hallstrom, T.C., et al., *Coordinate control of sphingolipid biosynthesis and multidrug resistance in Saccharomyces cerevisiae*. *J Biol Chem*, 2001. **276**(26): p. 23674-80.
85. Warringer, J. and A. Blomberg, *Involvement of yeast YOL151W/GRE2 in ergosterol metabolism*. *Yeast*, 2006. **23**(5): p. 389-98.
86. Weider, M., et al., *Vhr1p, a new transcription factor from budding yeast, regulates biotin-dependent expression of VHT1 and BIO5*. *J Biol Chem*, 2006. **281**(19): p. 13513-13524.
87. Le Crom, S., et al., *New insights into the pleiotropic drug resistance network from genome-wide characterization of the YRR1 transcription factor regulation system*. *Mol Cell Biol*, 2002. **22**(8): p. 2642-9.
88. Onda, M., et al., *Analysis of gene network regulating yeast multidrug resistance by artificial activation of transcription factors: involvement of Pdr3 in salt tolerance*. *Gene*, 2004. **332**: p. 51-9.
89. Shahi, P., K. Gulshan, and W.S. Moye-Rowley, *Negative transcriptional regulation of multidrug resistance gene expression by an Hsp70 protein*. *J Biol Chem*, 2007. **282**(37): p. 26822-26831.
90. Kolaczowska, A., et al., *Compensatory activation of the multidrug transporters Pdr5p, Snq2p, and Yor1p by Pdr1p in Saccharomyces cerevisiae*. *FEBS Lett*, 2008. **582**(6): p. 977-83.
91. Vanacloig-Pedros, E., et al., *Live-cell assays reveal selectivity and sensitivity of the multidrug response in budding yeast*. *J Biol Chem*, 2019. **294**(35): p. 12933-12946.
92. Hallstrom, T.C. and W.S. Moye-Rowley, *Multiple signals from dysfunctional mitochondria activate the pleiotropic drug resistance pathway in Saccharomyces cerevisiae*. *J Biol Chem*, 2000. **275**(48): p. 37347-56.
93. Gulshan, K., et al., *Evidence for the bifunctional nature of mitochondrial phosphatidylserine decarboxylase: role in Pdr3-dependent retrograde regulation of PDR5 expression*. *Mol Cell Biol*, 2008. **28**(19): p. 5851-64.
94. Zhang, X. and W.S. Moye-Rowley, *Saccharomyces cerevisiae multidrug resistance gene expression inversely correlates with the status of the F(0) component of the mitochondrial ATPase*. *J Biol Chem*, 2001. **276**(51): p. 47844-52.
95. Devaux, F., et al., *Genome-wide studies on the nuclear PDR3-controlled response to mitochondrial dysfunction in yeast*. *FEBS Lett*, 2002. **515**(1-3): p. 25-8.
96. Zhu, Y. and W. Xiao, *Pdr3 is required for DNA damage induction of MAG1 and DDII via a bi-directional promoter element*. *Nucleic Acids Res*, 2004. **32**(17): p. 5066-75.
97. Mamnun, Y.M., et al., *The yeast zinc finger regulators Pdr1p and Pdr3p control pleiotropic drug resistance (PDR) as homo- and heterodimers in vivo*. *Mol Microbiol*, 2002. **46**(5): p. 1429-40.
98. Zhang, X., et al., *Transcriptional regulation by Lge1p requires a function independent of its role in histone H2B ubiquitination*. *J Biol Chem*, 2005. **280**(4): p. 2759-70.

99. Shahi, P., et al., *Differential roles of transcriptional mediator subunits in regulation of multidrug resistance gene expression in Saccharomyces cerevisiae*. Mol Biol Cell, 2010. **21**(14): p. 2469-82.
100. Delahodde, A., T. Delaveau, and C. Jacq, *Positive autoregulation of the yeast transcription factor Pdr3p, which is involved in control of drug resistance*. Mol Cell Biol, 1995. **15**(8): p. 4043-51.
101. Zhang, X., et al., *Cross-talk between transcriptional regulators of multidrug resistance in Saccharomyces cerevisiae*. J Biol Chem, 2001. **276**(12): p. 8812-9.
102. Nishida-Aoki, N., et al., *Activation of the mitochondrial signaling pathway in response to organic solvent stress in yeast*. Curr Genet, 2015. **61**(2): p. 153-64.
103. Ghaemmaghami, S., et al., *Global analysis of protein expression in yeast*. Nature, 2003. **425**(6959): p. 737-41.
104. Paul, S., J.A. Schmidt, and W.S. Moye-Rowley, *Regulation of the CgPdr1 transcription factor from the pathogen Candida glabrata*. Eukaryot Cell, 2011. **10**(2): p. 187-97.
105. Thakur, J.K., et al., *A nuclear receptor-like pathway regulating multidrug resistance in fungi*. Nature, 2008. **452**(7187): p. 604-9.
106. Mannhaupt, G., et al., *Rpn4p acts as a transcription factor by binding to PACE, a nonamer box found upstream of 26S proteasomal and other genes in yeast*. FEBS Lett, 1999. **450**(1-2): p. 27-34.
107. Owsianik, G., L. Balzi l, and M. Ghislain, *Control of 26S proteasome expression by transcription factors regulating multidrug resistance in Saccharomyces cerevisiae*. Mol Microbiol, 2002. **43**(5): p. 1295-308.
108. Pais, P., et al., *Candida glabrata Transcription Factor Rpn4 Mediates Fluconazole Resistance through Regulation of Ergosterol Biosynthesis and Plasma Membrane Permeability*. Antimicrob Agents Chemother, 2020. **64**(9).
109. Kapetanakis, G.C., et al., *Overlapping Roles of Yeast Transporters Aqr1, Qdr2, and Qdr3 in Amino Acid Excretion and Cross-Feeding of Lactic Acid Bacteria*. Front Microbiol, 2021. **12**: p. 752742.
110. Rios, G., et al., *Role of the yeast multidrug transporter Qdr2 in cation homeostasis and the oxidative stress response*. FEMS Yeast Res, 2013. **13**(1): p. 97-106.
111. Khandelwal, N.K., et al., *Vacuolar Sequestration of Azoles, a Novel Strategy of Azole Antifungal Resistance Conserved across Pathogenic and Nonpathogenic Yeast*. Antimicrob Agents Chemother, 2019. **63**(3).
112. Manente, M. and M. Ghislain, *The lipid-translocating exporter family and membrane phospholipid homeostasis in yeast*. FEMS Yeast Res, 2009. **9**(5): p. 673-87.
113. Siddiqah, I.M., et al., *Yeast ENV9 encodes a conserved lipid droplet (LD) short-chain dehydrogenase involved in LD morphology*. Curr Genet, 2017. **63**(6): p. 1053-1072.
114. Tiwari, R., R. Köffel, and R. Schreiber, *An acetylation/deacetylation cycle controls the export of sterols and steroids from S. cerevisiae*. Embo j, 2007. **26**(24): p. 5109-19.
115. Roetzer, A., et al., *Regulation of Candida glabrata oxidative stress resistance is adapted to host environment*. FEBS Lett, 2011. **585**(2): p. 319-27.
116. Pais, P., et al., *A new regulator in the crossroads of oxidative stress resistance and virulence in Candida glabrata: The transcription factor CgTog1*. Virulence, 2020. **11**(1): p. 1522-1538.
117. Ferrari, S., et al., *Contribution of CgPDR1-regulated genes in enhanced virulence of azole-resistant Candida glabrata*. PLoS One, 2011. **6**(3): p. e17589.
118. Klimova, N., et al., *Phenotypic analysis of a family of transcriptional regulators, the zinc cluster proteins, in the human fungal pathogen Candida glabrata*. G3 (Bethesda), 2014. **4**(5): p. 931-40.
119. Vu, B.G., G.H. Thomas, and W.S. Moye-Rowley, *Evidence that Ergosterol Biosynthesis Modulates Activity of the Pdr1 Transcription Factor in Candida glabrata*. MBio, 2019. **10**(3).
120. Harbison, C.T., et al., *Transcriptional regulatory code of a eukaryotic genome*. Nature, 2004. **431**(7004): p. 99-104.
121. Hahn, J.S., D.W. Neef, and D.J. Thiele, *A stress regulatory network for co-ordinated activation of proteasome expression mediated by yeast heat shock transcription factor*. Mol Microbiol, 2006. **60**(1): p. 240-51.
122. da Silva, S.M., et al., *Transcriptional regulation of FeS biogenesis genes: A possible shield against arsenate toxicity activated by Yap1*. Biochim Biophys Acta Gen Subj, 2018. **1862**(10): p. 2152-2161.
123. Teixeira, M.C., et al., *Refining current knowledge on the yeast FLR1 regulatory network by combined experimental and computational approaches*. Mol Biosyst, 2010. **6**(12): p. 2471-81.

124. Teixeira, M.C., et al., *Yeast adaptation to mancozeb involves the up-regulation of FLR1 under the coordinate control of Yap1, Rpn4, Pdr3, and Yrr1*. *Biochem Biophys Res Commun*, 2008. **367**(2): p. 249-55.
125. Akache, B., et al., *Complex interplay among regulators of drug resistance genes in Saccharomyces cerevisiae*. *J Biol Chem*, 2004. **279**(27): p. 27855-60.
126. Hellauer, K., et al., *Zinc cluster protein Rdr1p is a transcriptional repressor of the PDR5 gene encoding a multidrug transporter*. *J Biol Chem*, 2002. **277**(20): p. 17671-6.
127. Srikanth, C.V., A.K. Chakraborti, and A.K. Bachhawat, *Acetaminophen toxicity and resistance in the yeast Saccharomyces cerevisiae*. *Microbiology (Reading)*, 2005. **151**(Pt 1): p. 99-111.
128. Wendler, F., et al., *Diazaborine resistance in the yeast Saccharomyces cerevisiae reveals a link between YAP1 and the pleiotropic drug resistance genes PDR1 and PDR3*. *J Biol Chem*, 1997. **272**(43): p. 27091-8.
129. Tenreiro, S., A.R. Fernandes, and I. Sa-Correia, *Transcriptional activation of FLR1 gene during Saccharomyces cerevisiae adaptation to growth with benomyl: role of Yap1p and Pdr3p*. *Biochem Biophys Res Commun*, 2001. **280**(1): p. 216-22.
130. Rong-Mullins, X., et al., *Transcriptional Profiling of Saccharomyces cerevisiae Reveals the Impact of Variation of a Single Transcription Factor on Differential Gene Expression in 4NQO, Fermentable, and Nonfermentable Carbon Sources*. *G3 (Bethesda)*, 2018. **8**(2): p. 607-619.
131. Cui, Z., et al., *Yeast gene YRR1, which is required for resistance to 4-nitroquinoline N-oxide, mediates transcriptional activation of the multidrug resistance transporter gene SNQ2*. *Mol Microbiol*, 1998. **29**(5): p. 1307-15.
132. Akache, B. and B. Turcotte, *New regulators of drug sensitivity in the family of yeast zinc cluster proteins*. *J Biol Chem*, 2002. **277**(24): p. 21254-60.
133. Wang, X., et al., *The Absence of the Transcription Factor Yrr1p, Identified from Comparative Genome Profiling, Increased Vanillin Tolerance Due to Enhancements of ABC Transporters Expressing, rRNA Processing and Ribosome Biogenesis in Saccharomyces cerevisiae*. *Front Microbiol*, 2017. **8**: p. 367.
134. Gallagher, J.E., et al., *Divergence in a master variator generates distinct phenotypes and transcriptional responses*. *Genes Dev*, 2014. **28**(4): p. 409-21.
135. Larochelle, M., et al., *Oxidative stress-activated zinc cluster protein Stb5 has dual activator/repressor functions required for pentose phosphate pathway regulation and NADPH production*. *Mol Cell Biol*, 2006. **26**(17): p. 6690-701.
136. Ouyang, L., et al., *Integrated analysis of the yeast NADPH-regulator Stb5 reveals distinct differences in NADPH requirements and regulation in different states of yeast metabolism*. *FEMS Yeast Res*, 2018. **18**(8).
137. O'Hanlon, D.E., T.R. Moench, and R.A. Cone, *Vaginal pH and microbicidal lactic acid when lactobacilli dominate the microbiota*. *PLoS One*, 2013. **8**(11): p. e80074.
138. Ouyang, X., et al., *Yap1 activation by H2O2 or thiol-reactive chemicals elicits distinct adaptive gene responses*. *Free Radic Biol Med*, 2011. **50**(1): p. 1-13.
139. Lee, T.I., et al., *Transcriptional regulatory networks in Saccharomyces cerevisiae*. *Science*, 2002. **298**(5594): p. 799-804.
140. Skrzypek, M.S., et al., *The Candida Genome Database (CGD): incorporation of Assembly 22, systematic identifiers and visualization of high throughput sequencing data*. *Nucleic Acids Res*, 2017. **45**(D1): p. D592-D596.
141. Monteiro, P.T., et al., *YEASTRACT+: a portal for cross-species comparative genomics of transcription regulation in yeasts*. *Nucleic Acids Res*, 2020. **48**(D1): p. D642-D649.
142. Yang, H., et al., *Structural mechanism of ergosterol regulation by fungal sterol transcription factor Upc2*. *Nat Commun*, 2015. **6**: p. 6129.
143. Nagi, M., et al., *Transcription factors CgUPC2A and CgUPC2B regulate ergosterol biosynthetic genes in Candida glabrata*. *Genes Cells*, 2011. **16**(1): p. 80-9.
144. Whaley, S.G., et al., *UPC2A is required for high-level azole antifungal resistance in Candida glabrata*. *Antimicrob Agents Chemother*, 2014. **58**(8): p. 4543-54.
145. Pérez-de los Santos, F.J., et al., *Transcriptome Analysis Unveils Gln3 Role in Amino Acids Assimilation and Fluconazole Resistance in Candida glabrata*. *J. Microbiol. Biotechnol*, 2021. **31**(5): p. 659-666.
146. Gaspar-Cordeiro, A., et al., *Zap1 is required for Candida glabrata response to fluconazole*. *FEMS Yeast Res*, 2022.
147. Naar, A.M. and J.K. Thakur, *Nuclear receptor-like transcription factors in fungi*. *Genes Dev*, 2009. **23**(4): p. 419-32.

148. Glass, C.K. and M.G. Rosenfeld, *The coregulator exchange in transcriptional functions of nuclear receptors*. Genes Dev, 2000. **14**(2): p. 121-41.
149. Gao, C., et al., *On the mechanism of constitutive Pdr1 activator-mediated PDR5 transcription in Saccharomyces cerevisiae: evidence for enhanced recruitment of coactivators and altered nucleosome structures*. J Biol Chem, 2004. **279**(41): p. 42677-86.
150. Voth, W.P., et al., *A role for FACT in repopulation of nucleosomes at inducible genes*. PLoS One, 2014. **9**(1): p. e84092.
151. Miller, C., et al., *Mediator phosphorylation prevents stress response transcription during non-stress conditions*. J Biol Chem, 2012. **287**(53): p. 44017-26.
152. Verger, A., D. Monte, and V. Villeret, *Twenty years of Mediator complex structural studies*. Biochem Soc Trans, 2019. **47**(1): p. 399-410.
153. Borah, S., et al., *Pivotal role for a tail subunit of the RNA polymerase II mediator complex CgMed2 in azole tolerance and adherence in Candida glabrata*. Antimicrob Agents Chemother, 2014. **58**(10): p. 5976-86.
154. Espinola-Lopez, J.M. and S. Tan, *The Ada2/Ada3/Gcn5/Sgf29 histone acetyltransferase module*. Biochim Biophys Acta Gene Regul Mech, 2021. **1864**(2): p. 194629.
155. Martens, J.A., et al., *Transcriptional activation by yeast PDR1p is inhibited by its association with NGG1p/ADA3p*. J Biol Chem, 1996. **271**(27): p. 15884-90.
156. Yibmantasiri, P., et al., *Networks of genes modulating the pleiotropic drug response in Saccharomyces cerevisiae*. Mol Biosyst, 2014. **10**(1): p. 128-37.
157. Yu, S.J., Y.L. Chang, and Y.L. Chen, *Deletion of ADA2 Increases Antifungal Drug Susceptibility and Virulence in Candida glabrata*. Antimicrob Agents Chemother, 2018. **62**(3).
158. Kounatidis, I., et al., *A Host-Pathogen Interaction Screen Identifies ada2 as a Mediator of Candida glabrata Defenses Against Reactive Oxygen Species*. G3 (Bethesda), 2018. **8**(5): p. 1637-1647.
159. Usher, J. and K. Haynes, *Attenuating the emergence of anti-fungal drug resistance by harnessing synthetic lethal interactions in a model organism*. PLoS Genet, 2019. **15**(8): p. e1008259.
160. Yamada, Y., *RPD3 and UME6 are involved in the activation of PDR5 transcription and pleiotropic drug resistance in rho(0) cells of Saccharomyces cerevisiae*. BMC Microbiol, 2021. **21**(1): p. 311.
161. Borecka-Melkusova, S., et al., *RPD3 and ROM2 are required for multidrug resistance in Saccharomyces cerevisiae*. FEMS Yeast Res, 2008. **8**(3): p. 414-24.
162. Venters, B.J., et al., *A comprehensive genomic binding map of gene and chromatin regulatory proteins in Saccharomyces*. Mol Cell, 2011. **41**(4): p. 480-92.
163. Yamada, Y., *UME6 Is Involved in the Suppression of Basal Transcription of ABC Transporters and Drug Resistance in the rho(+) Cells of Saccharomyces cerevisiae*. Microorganisms, 2022. **10**(3).
164. Moirangthem, R., K. Kumar, and R. Kaur, *Two Functionally Redundant FK506-Binding Proteins Regulate Multidrug Resistance Gene Expression and Govern Azole Antifungal Resistance*. Antimicrob Agents Chemother, 2021. **65**(6).
165. Li, L. and Y. Wang, *Cross-talk between the H3K36me3 and H4K16ac histone epigenetic marks in DNA double-strand break repair*. J Biol Chem, 2017. **292**(28): p. 11951-11959.
166. McDaniel, S.L. and B.D. Strahl, *Stress-free with Rpd3: a unique chromatin complex mediates the response to oxidative stress*. Mol Cell Biol, 2013. **33**(19): p. 3726-7.
167. Carrozza, M.J., et al., *Histone H3 methylation by Set2 directs deacetylation of coding regions by Rpd3S to suppress spurious intragenic transcription*. Cell, 2005. **123**(4): p. 581-92.
168. Chakrabortee, S., et al., *Intrinsically Disordered Proteins Drive Emergence and Inheritance of Biological Traits*. Cell, 2016. **167**(2): p. 369-381 e12.
169. Luo, F., et al., *Constructing gene co-expression networks and predicting functions of unknown genes by random matrix theory*. BMC Bioinformatics, 2007. **8**: p. 299.
170. Kapitzky, L., et al., *Cross-species chemogenomic profiling reveals evolutionarily conserved drug mode of action*. Mol Syst Biol, 2010. **6**: p. 451.
171. Orta-Zavalza, E., et al., *Local silencing controls the oxidative stress response and the multidrug resistance in Candida glabrata*. Mol Microbiol, 2013. **88**(6): p. 1135-48.
172. Ma, B., et al., *High-affinity transporters for NAD+ precursors in Candida glabrata are regulated by Hst1 and induced in response to niacin limitation*. Mol Cell Biol, 2009. **29**(15): p. 4067-79.
173. Domergue, R., et al., *Nicotinic acid limitation regulates silencing of Candida adhesins during UTI*. Science, 2005. **308**(5723): p. 866-70.
174. Xie, J., et al., *Sum1 and Hst1 repress middle sporulation-specific gene expression during mitosis in Saccharomyces cerevisiae*. EMBO J, 1999. **18**(22): p. 6448-54.

175. Vazquez-Franco, N., et al., *Candida glabrata Hst1-Rfm1-Sum1 complex evolved to control virulence-related genes*. Fungal Genet Biol, 2021. **159**: p. 103656.
176. Reinberg, D. and R.J. Sims, 3rd, *de FACTo nucleosome dynamics*. J Biol Chem, 2006. **281**(33): p. 23297-301.
177. Lum, P.Y., et al., *Discovering modes of action for therapeutic compounds using a genome-wide screen of yeast heterozygotes*. Cell, 2004. **116**(1): p. 121-37.
178. Dudley, A.M., et al., *A global view of pleiotropy and phenotypically derived gene function in yeast*. Mol Syst Biol, 2005. **1**: p. 2005 0001.
179. Parsons, A.B., et al., *Integration of chemical-genetic and genetic interaction data links bioactive compounds to cellular target pathways*. Nat Biotechnol, 2004. **22**(1): p. 62-9.
180. Koschubs, T., et al., *Identification, structure, and functional requirement of the Mediator submodule Med7N/31*. EMBO J, 2009. **28**(1): p. 69-80.
181. Simonicova, L. and W.S. Moye-Rowley, *Functional information from clinically-derived drug resistant forms of the Candida glabrata Pdr1 transcription factor*. PLoS Genet, 2020. **16**(8): p. e1009005.
182. Hoepfner, D., et al., *High-resolution chemical dissection of a model eukaryote reveals targets, pathways and gene functions*. Microbiol Res, 2014. **169**(2-3): p. 107-20.
183. Huang, Z., et al., *A functional variomics tool for discovering drug-resistance genes and drug targets*. Cell Rep, 2013. **3**(2): p. 577-85.
184. Vandebosch, D., et al., *Genomewide screening for genes involved in biofilm formation and miconazole susceptibility in Saccharomyces cerevisiae*. FEMS Yeast Res, 2013. **13**(8): p. 720-30.
185. Thevissen, K., et al., *Miconazole induces changes in actin cytoskeleton prior to reactive oxygen species induction in yeast*. J Biol Chem, 2007. **282**(30): p. 21592-7.
186. Lee, K.K., et al., *Combinatorial depletion analysis to assemble the network architecture of the SAGA and ADA chromatin remodeling complexes*. Mol Syst Biol, 2011. **7**: p. 503.
187. Loewith, R., et al., *Pho23 is associated with the Rpd3 histone deacetylase and is required for its normal function in regulation of gene expression and silencing in Saccharomyces cerevisiae*. J Biol Chem, 2001. **276**(26): p. 24068-74.
188. Goncalves, B., et al., *Hormones modulate Candida vaginal isolates biofilm formation and decrease their susceptibility to azoles and hydrogen peroxide*. Med Mycol, 2020. **58**(3): p. 341-350.
189. Biermann, A.R., E.G. Demers, and D.A. Hogan, *Mrr1 regulation of methylglyoxal catabolism and methylglyoxal-induced fluconazole resistance in Candida lusitanae*. Mol Microbiol, 2021. **115**(1): p. 116-130.
190. Biermann, A.R. and D.A. Hogan, *Transcriptional response of Candida auris to the Mrr1 inducers methylglyoxal and benomyl*. bioRxiv, 2022.
191. Rodrigues, C.F., M.E. Rodrigues, and M. Henriques, *Candida sp. Infections in Patients with Diabetes Mellitus*. J Clin Med, 2019. **8**(1).
192. Jawale, C.V., et al., *Restoring glucose uptake rescues neutrophil dysfunction and protects against systemic fungal infection in mouse models of kidney disease*. Sci Transl Med, 2020. **12**(548).
193. Guo, P.C., et al., *Structural insights into the cofactor-assisted substrate recognition of yeast methylglyoxal/isovaleraldehyde reductase Gre2*. Biochim Biophys Acta, 2014. **1844**(9): p. 1486-92.
194. Tsai, H.F., et al., *Candida glabrata PDR1, a transcriptional regulator of a pleiotropic drug resistance network, mediates azole resistance in clinical isolates and petite mutants*. Antimicrob Agents Chemother, 2006. **50**(4): p. 1384-92.
195. Vandeputte, P., et al., *Hypersusceptibility to azole antifungals in a clinical isolate of Candida glabrata with reduced aerobic growth*. Antimicrob Agents Chemother, 2009. **53**(7): p. 3034-41.
196. Ferrari, S., et al., *Loss of mitochondrial functions associated with azole resistance in Candida glabrata results in enhanced virulence in mice*. Antimicrob Agents Chemother, 2011. **55**(5): p. 1852-60.
197. Weidberg, H. and A. Amon, *MitoCPR-A surveillance pathway that protects mitochondria in response to protein import stress*. Science, 2018. **360**(6385).
198. Bouchara, J.P., et al., *In-vivo selection of an azole-resistant petite mutant of Candida glabrata*. J Med Microbiol, 2000. **49**(11): p. 977-984.
199. Brun, S., et al., *Biological consequences of petite mutations in Candida glabrata*. J Antimicrob Chemother, 2005. **56**(2): p. 307-14.
200. Siscar-Lewin, S., et al., *Transient Mitochondria Dysfunction Confers Fungal Cross-Resistance against Phagocytic Killing and Fluconazole*. mBio, 2021. **12**(3): p. e0112821.

201. Fukuda, Y., et al., *Transcriptional profiling of Candida glabrata during phagocytosis by neutrophils and in the infected mouse spleen*. Infect Immun, 2013. **81**(4): p. 1325-33.
202. Schuller, C., et al., *Membrane-active compounds activate the transcription factors Pdr1 and Pdr3 connecting pleiotropic drug resistance and membrane lipid homeostasis in saccharomyces cerevisiae*. Mol Biol Cell, 2007. **18**(12): p. 4932-44.
203. Torelli, R., et al., *The ATP-binding cassette transporter-encoding gene CgSNQ2 is contributing to the CgPDR1-dependent azole resistance of Candida glabrata*. Mol Microbiol, 2008. **68**(1): p. 186-201.
204. Tantivitayakul, P., et al., *Missense mutation in CgPDR1 regulator associated with azole-resistant Candida glabrata recovered from Thai oral candidiasis patients*. J Glob Antimicrob Resist, 2019. **17**: p. 221-226.
205. Biswas, C., et al., *Whole Genome Sequencing of Australian Candida glabrata Isolates Reveals Genetic Diversity and Novel Sequence Types*. Front Microbiol, 2018. **9**: p. 2946.
206. Hou, X., et al., *Profiling of PDR1 and MSH2 in Candida glabrata Bloodstream Isolates from a Multicenter Study in China*. Antimicrob Agents Chemother, 2018. **62**(6).
207. Tian, Y., et al., *Sequence modification of the master regulator Pdr1 interferes with its transcriptional autoregulation and confers altered azole resistance in Candida glabrata*. FEMS Yeast Res, 2018. **18**(4).
208. Katiyar, S., et al., *Evaluation of Polymorphic Locus Sequence Typing for Candida glabrata Epidemiology*. J Clin Microbiol, 2016. **54**(4): p. 1042-50.
209. Sasse, C., et al., *The stepwise acquisition of fluconazole resistance mutations causes a gradual loss of fitness in Candida albicans*. Mol Microbiol, 2012. **86**(3): p. 539-56.
210. Hill, J.A., T.R. O'Meara, and L.E. Cowen, *Fitness Trade-Offs Associated with the Evolution of Resistance to Antifungal Drug Combinations*. Cell Rep, 2015. **10**(5): p. 809-819.
211. Demers, E.G., et al., *Balancing Positive and Negative Selection: In Vivo Evolution of Candida lusitanae MRR1*. mBio, 2021. **12**(2).
212. Nishikawa, J.L., et al., *Inhibiting fungal multidrug resistance by disrupting an activator-Mediator interaction*. Nature, 2016. **530**(7591): p. 485-9.
213. Paul, S., W.H. McDonald, and W.S. Moye-Rowley, *Negative regulation of Candida glabrata Pdr1 by the deubiquitinase subunit Bre5 occurs in a ubiquitin independent manner*. Mol Microbiol, 2018. **110**(2): p. 309-323.
214. Cohen, M., et al., *Ubp3 requires a cofactor, Bre5, to specifically de-ubiquitinate the COPII protein, Sec23*. Nat Cell Biol, 2003. **5**(7): p. 661-7.
215. Hallstrom, T.C., et al., *Regulation of transcription factor Pdr1p function by an Hsp70 protein in Saccharomyces cerevisiae*. Mol Cell Biol, 1998. **18**(3): p. 1147-55.
216. Prunuske, A.J., et al., *Role for the molecular chaperones Zuo1 and Ssz1 in quorum sensing via activation of the transcription factor Pdr1*. Proc Natl Acad Sci U S A, 2012. **109**(2): p. 472-7.
217. Ducett, J.K., et al., *Unfolding of the C-terminal domain of the J-protein Zuo1 releases autoinhibition and activates Pdr1-dependent transcription*. J Mol Biol, 2013. **425**(1): p. 19-31.
218. Eisenman, H.C. and E.A. Craig, *Activation of pleiotropic drug resistance by the J-protein and Hsp70-related proteins, Zuo1 and Ssz1*. Mol Microbiol, 2004. **53**(1): p. 335-44.
219. Meyer, A.E., et al., *The specialized cytosolic J-protein, Jjj1, functions in 60S ribosomal subunit biogenesis*. Proc Natl Acad Sci U S A, 2007. **104**(5): p. 1558-63.
220. Whaley, S.G., et al., *Jjj1 Is a Negative Regulator of Pdr1-Mediated Fluconazole Resistance in Candida glabrata*. mSphere, 2018. **3**(1).
221. Gillies, A.T., R. Taylor, and J.E. Gestwicki, *Synthetic lethal interactions in yeast reveal functional roles of J protein co-chaperones*. Mol Biosyst, 2012. **8**(11): p. 2901-8.
222. Souid, A.K., et al., *ELM1 is required for multidrug resistance in Saccharomyces cerevisiae*. Genetics, 2006. **173**(4): p. 1919-37.
223. Nebauer, R., et al., *The phosphatidylethanolamine level of yeast mitochondria is affected by the mitochondrial components Oxa1p and Yme1p*. FEBS J, 2007. **274**(23): p. 6180-90.
224. Schjerling, P. and S. Holmberg, *Comparative amino acid sequence analysis of the C6 zinc cluster family of transcriptional regulators*. Nucleic Acids Res, 1996. **24**(23): p. 4599-607.
225. Kolaczkowska, A., et al., *Functional dissection of Pdr1p, a regulator of multidrug resistance in Saccharomyces cerevisiae*. Mol Genet Genomics, 2002. **267**(1): p. 96-106.
226. Mistry, J., et al., *Pfam: The protein families database in 2021*. Nucleic Acids Res, 2021. **49**(D1): p. D412-D419.
227. Delahodde, A., et al., *Pse1/Kap121-dependent nuclear localization of the major yeast multidrug resistance (MDR) transcription factor Pdr1*. Mol Microbiol, 2001. **39**(2): p. 304-12.

228. Ravarani, C.N., et al., *High-throughput discovery of functional disordered regions: investigation of transactivation domains*. Mol Syst Biol, 2018. **14**(5): p. e8190.
229. Vale-Silva, L.A., et al., *Upregulation of the Adhesin Gene EPA1 Mediated by PDR1 in Candida glabrata Leads to Enhanced Host Colonization*. mSphere, 2016. **1**(2).
230. Chaban, B., et al., *Characterization of the vaginal microbiota of healthy Canadian women through the menstrual cycle*. Microbiome, 2014. **2**: p. 23.
231. Ravel, J., et al., *Vaginal microbiome of reproductive-age women*. Proc Natl Acad Sci U S A, 2011. **108** Suppl 1: p. 4680-7.
232. Boskey, E.R., et al., *Acid production by vaginal flora in vitro is consistent with the rate and extent of vaginal acidification*. Infect Immun, 1999. **67**(10): p. 5170-5.
233. Boskey, E.R., et al., *Origins of vaginal acidity: high D/L lactate ratio is consistent with bacteria being the primary source*. Hum Reprod, 2001. **16**(9): p. 1809-13.
234. Owen, D.H. and D.F. Katz, *A vaginal fluid simulant*. Contraception, 1999. **59**(2): p. 91-5.
235. Aldunate, M., et al., *Antimicrobial and immune modulatory effects of lactic acid and short chain fatty acids produced by vaginal microbiota associated with eubiosis and bacterial vaginosis*. Front Physiol, 2015. **6**: p. 164.
236. Chaudry, A.N., et al., *Analysis of vaginal acetic acid in patients undergoing treatment for bacterial vaginosis*. J Clin Microbiol, 2004. **42**(11): p. 5170-5.
237. Lourenco, A., et al., *Effect of Acetic Acid and Lactic Acid at Low pH in Growth and Azole Resistance of Candida albicans and Candida glabrata*. Front Microbiol, 2018. **9**: p. 3265.
238. Krebs, H.A., et al., *Studies on the mechanism of the antifungal action of benzoate*. Biochem J, 1983. **214**(3): p. 657-63.
239. Pampulha, M.E. and M.C. Loureiro-Dias, *Activity of glycolytic enzymes of Saccharomyces cerevisiae in the presence of acetic acid*. Applied Microbiology and Biotechnology, 1990. **34**: p. 375-380.
240. Pampulha, M.E. and M.C. Loureiro-Dias, *Energetics of the effect of acetic acid on growth of Saccharomyces cerevisiae*. FEMS Microbiol Lett, 2000. **184**(1): p. 69-72.
241. Holyoak, C.D., et al., *Activity of the plasma membrane H(+)-ATPase and optimal glycolytic flux are required for rapid adaptation and growth of Saccharomyces cerevisiae in the presence of the weak-acid preservative sorbic acid*. Appl Environ Microbiol, 1996. **62**(9): p. 3158-64.
242. Mira, N.P., M.C. Teixeira, and I. Sa-Correia, *Adaptive response and tolerance to weak acids in Saccharomyces cerevisiae: a genome-wide view*. OMICS, 2010. **14**(5): p. 525-40.
243. Guaragnella, N., et al., *Hydrogen peroxide and superoxide anion production during acetic acid-induced yeast programmed cell death*. Folia Microbiol (Praha), 2007. **52**(3): p. 237-40.
244. Giannattasio, S., et al., *Acid stress adaptation protects Saccharomyces cerevisiae from acetic acid-induced programmed cell death*. Gene, 2005. **354**: p. 93-8.
245. Porter, N.A., S.E. Caldwell, and K.A. Mills, *Mechanisms of free radical oxidation of unsaturated lipids*. Lipids, 1995. **30**(4): p. 277-90.
246. Mollapour, M., A. Shepherd, and P.W. Piper, *Presence of the Fps1p aquaglyceroporin channel is essential for Hog1p activation, but suppresses Slt2(Mpk1)p activation, with acetic acid stress of yeast*. Microbiology, 2009. **155**(Pt 10): p. 3304-11.
247. Kapteyn, J.C., et al., *Low external pH induces HOG1-dependent changes in the organization of the Saccharomyces cerevisiae cell wall*. Mol Microbiol, 2001. **39**(2): p. 469-79.
248. Moosa, M.Y., et al., *Fungicidal activity of fluconazole against Candida albicans in a synthetic vagina-simulative medium*. Antimicrob Agents Chemother, 2004. **48**(1): p. 161-7.
249. Cunha, D.V., Salazar, S. B., Lopes, M. M. and Mira, N. P. , *Mechanistic insights underlying tolerance to acetic acid stress in vaginal Candida glabrata clinical isolates*. Front Microb, 2017. **8**: p. 1-13.
250. Ribeiro, R.A., et al., *Yeast adaptive response to acetic acid stress involves structural alterations and increased stiffness of the cell wall*. Sci Rep, 2021. **11**(1): p. 12652.
251. Childers, D.S., et al., *The Rewiring of Ubiquitination Targets in a Pathogenic Yeast Promotes Metabolic Flexibility, Host Colonization and Virulence*. PLoS Pathog, 2016. **12**(4): p. e1005566.
252. Mira, N.P., J.D. Becker, and I. Sa-Correia, *Genomic expression program involving the Haa1p-regulon in Saccharomyces cerevisiae response to acetic acid*. OMICS, 2010. **14**(5): p. 587-601.
253. Mira, N.P., et al., *Identification of a DNA-binding site for the transcription factor Haa1, required for Saccharomyces cerevisiae response to acetic acid stress*. Nucleic Acids Res, 2011. **39**(16): p. 6896-907.
254. Cunha, J.T., et al., *HAA1 and PRS3 overexpression boosts yeast tolerance towards acetic acid improving xylose or glucose consumption: unravelling the underlying mechanisms*. Appl Microbiol Biotechnol, 2018. **102**(10): p. 4589-4600.

255. Swinnen, S., et al., *Improvement of yeast tolerance to acetic acid through Haa1 transcription factor engineering: towards the underlying mechanisms*. Microb Cell Fact, 2017. **16**(1): p. 7.
256. Fernandes, A.R., et al., *Saccharomyces cerevisiae adaptation to weak acids involves the transcription factor Haa1p and Haa1p-regulated genes*. Biochem Biophys Res Commun, 2005. **337**(1): p. 95-103.
257. Palma, M., J.F. Guerreiro, and I. Sa-Correia, *Adaptive Response and Tolerance to Acetic Acid in Saccharomyces cerevisiae and Zygosaccharomyces bailii: A Physiological Genomics Perspective*. Front Microbiol, 2018. **9**: p. 274.
258. Dong, Y., et al., *RNA-Seq-based transcriptomic and metabolomic analysis reveal stress responses and programmed cell death induced by acetic acid in Saccharomyces cerevisiae*. Sci Rep, 2017. **7**: p. 42659.
259. Semchyshyn, H.M., et al., *Acetate but not propionate induces oxidative stress in bakers' yeast Saccharomyces cerevisiae*. Redox Rep, 2011. **16**(1): p. 15-23.
260. Antunes, M., M. Palma, and I. Sa-Correia, *Transcriptional profiling of Zygosaccharomyces bailii early response to acetic acid or copper stress mediated by ZbHaa1*. Sci Rep, 2018. **8**(1): p. 14122.
261. Guerreiro, J.F., N.P. Mira, and I. Sa-Correia, *Adaptive response to acetic acid in the highly resistant yeast species Zygosaccharomyces bailii revealed by quantitative proteomics*. Proteomics, 2012. **12**(14): p. 2303-18.
262. Bernardo, R.T., et al., *The CgHaa1-Regulon Mediates Response and Tolerance to Acetic Acid Stress in the Human Pathogen Candida glabrata*. G3 (Bethesda), 2017. **7**(1): p. 1-18.
263. Bairwa, G. and R. Kaur, *A novel role for a glycosylphosphatidylinositol-anchored aspartyl protease, CgYps1, in the regulation of pH homeostasis in Candida glabrata*. Mol Microbiol, 2011. **79**(4): p. 900-13.
264. Lelandais, G., et al., *Genome adaptation to chemical stress: clues from comparative transcriptomics in Saccharomyces cerevisiae and Candida glabrata*. Genome Biol, 2008. **9**(11): p. R164.
265. Palma, M., et al., *The Zygosaccharomyces bailii transcription factor Haa1 is required for acetic acid and copper stress responses suggesting subfunctionalization of the ancestral bifunctional protein Haa1/Cup2*. BMC Genomics, 2017. **18**(1): p. 75.
266. Goossens, A., et al., *Regulation of yeast H(+)-ATPase by protein kinases belonging to a family dedicated to activation of plasma membrane transporters*. Mol Cell Biol, 2000. **20**(20): p. 7654-61.
267. Piper, P.W., et al., *Hsp30, the integral plasma membrane heat shock protein of Saccharomyces cerevisiae, is a stress-inducible regulator of plasma membrane H(+)-ATPase*. Cell Stress Chaperones, 1997. **2**(1): p. 12-24.
268. Guerreiro, J.F., et al., *Membrane Phosphoproteomics of Yeast Early Response to Acetic Acid: Role of Hrk1 Kinase and Lipid Biosynthetic Pathways, in Particular Sphingolipids*. Front Microbiol, 2017. **8**: p. 1302.
269. Lindberg, L., et al., *Lipidomic profiling of Saccharomyces cerevisiae and Zygosaccharomyces bailii reveals critical changes in lipid composition in response to acetic acid stress*. PLoS One, 2013. **8**(9): p. e73936.
270. Guerreiro, J.F., et al., *Sphingolipid biosynthesis upregulation by TOR complex 2-Ypk1 signaling during yeast adaptive response to acetic acid stress*. Biochem J, 2016. **473**(23): p. 4311-4325.
271. Godinho, C.P., et al., *Pdr18 is involved in yeast response to acetic acid stress counteracting the decrease of plasma membrane ergosterol content and order*. Sci Rep, 2018. **8**(1): p. 7860.
272. Viegas, C.A., et al., *Regulation of the expression of the H(+)-ATPase genes PMA1 and PMA2 during growth and effects of octanoic acid in Saccharomyces cerevisiae*. Biochim Biophys Acta, 1994. **1217**(1): p. 74-80.
273. Fidel, P.L., Jr., J.A. Vazquez, and J.D. Sobel, *Candida glabrata: review of epidemiology, pathogenesis, and clinical disease with comparison to C. albicans*. Clin Microbiol Rev, 1999. **12**(1): p. 80-96.
274. Borst, A., et al., *Rapid acquisition of stable azole resistance by Candida glabrata isolates obtained before the clinical introduction of fluconazole*. Antimicrob Agents Chemother, 2005. **49**(2): p. 783-7.
275. Pfaller, M.A., et al., *Echinocandin and triazole antifungal susceptibility profiles for clinical opportunistic yeast and mold isolates collected from 2010 to 2011: application of new CLSI clinical breakpoints and epidemiological cutoff values for characterization of geographic and temporal trends of antifungal resistance*. J Clin Microbiol, 2013. **51**(8): p. 2571-81.
276. Kolaczowska, A. and M. Kolaczowski, *Drug resistance mechanisms and their regulation in non-albicans Candida species*. J Antimicrob Chemother, 2016. **71**(6): p. 1438-50.

277. Ueno, K., et al., *Intestinal resident yeast Candida glabrata requires Cyb2p-mediated lactate assimilation to adapt in mouse intestine*. PLoS One, 2011. **6**(9): p. e24759.
278. Subcommittee on Antifungal Susceptibility Testing (AFST) of the ESCMID European Committee for Antimicrobial Susceptibility Testing (EUCAST), R.-T., J. L., Barchiest, F., Bille, J., Chryssanthou, E., Cuenta-Estrella, M., Denning, D., Donnelly, J. P., Dupont, B., Fegeler, W., Moore, C., Richardson, M., Verweij, P.E., *EUCAST discussion document E.Dis 7.1: Method for the determination of minimum inhibitory concentration (MIC) by broth dilution of fermentative yeasts*. Clin Microbiol Infect, 2003**(9)**: p. i–viii.
279. Pfaller, M.A., et al., *Clinical breakpoints for voriconazole and Candida spp. revisited: review of microbiologic, molecular, pharmacodynamic, and clinical data as they pertain to the development of species-specific interpretive criteria*. Diagn Microbiol Infect Dis, 2011. **70**(3): p. 330-43.
280. Riley, M.L., et al., *The PEDANT genome database in 2005*. Nucleic Acids Res, 2005. **33**(Database issue): p. D308-10.
281. Rossignol, T., et al., *Transcriptional response of Candida parapsilosis following exposure to farnesol*. Antimicrob Agents Chemother, 2007. **51**(7): p. 2304-12.
282. Dujon, B., et al., *Genome evolution in yeasts*. Nature, 2004. **430**(6995): p. 35-44.
283. Vale-Silva, L., et al., *Comparative Genomics of Two Sequential Candida glabrata Clinical Isolates*. G3 (Bethesda), 2017.
284. Havelsrud, O.E. and P. Gaustad, *Draft Genome Sequences of Candida glabrata Isolates 1A, 1B, 2A, 2B, 3A, and 3B*. Genome Announc, 2017. **5**(10).
285. Garcia-Effron, G., et al., *Effect of Candida glabrata FKS1 and FKS2 mutations on echinocandin sensitivity and kinetics of 1,3-beta-D-glucan synthase: implication for the existing susceptibility breakpoint*. Antimicrob Agents Chemother, 2009. **53**(9): p. 3690-9.
286. Xu, N., et al., *Genome Sequencing of the Pyruvate-producing Strain Candida glabrata CCTCC M202019 and Genomic Comparison with Strain CBS138*. Sci Rep, 2016. **6**: p. 34893.
287. Helmstetter, N., et al., *Population genetics and microevolution of clinical Candida glabrata reveals recombinant sequence types and hyper-variation within mitochondrial genomes, virulence genes and drug-targets*. Genetics, 2022.
288. Carreté, L., et al., *Patterns of genomic variation in the opportunistic pathogen Candida glabrata suggest the existence of mating and a secondary association to the human host*. bioRxiv, 2017.
289. Vale-Silva, L., et al., *Gain-of-function mutations in PDR1, a regulator of antifungal drug resistance in Candida glabrata, control adherence to host cells*. Infect Immun, 2013. **81**(5): p. 1709-20.
290. Carreté, L., et al., *Patterns of Genomic Variation in the Opportunistic Pathogen Candida glabrata Suggest the Existence of Mating and a Secondary Association with Humans*. Curr Biol, 2018. **28**(1): p. 15-27.e7.
291. Halliwell, S.C., et al., *Heterogeneous expression of the virulence-related adhesin Epa1 between individual cells and strains of the pathogen Candida glabrata*. Eukaryot Cell, 2012. **11**(2): p. 141-50.
292. Nolte, F.S., et al., *Isolation and characterization of fluconazole- and amphotericin B-resistant Candida albicans from blood of two patients with leukemia*. Antimicrob Agents Chemother, 1997. **41**(1): p. 196-9.
293. Alves, R., et al., *Transcriptional responses of Candida glabrata biofilm cells to fluconazole are modulated by the carbon source*. NPJ Biofilms Microbiomes, 2020. **6**: p. 4.
294. Delliere, S., et al., *Fluconazole and Echinocandin Resistance of Candida glabrata Correlates Better with Antifungal Drug Exposure Rather than with MSH2 Mutator Genotype in a French Cohort of Patients Harboring Low Rates of Resistance*. Front Microbiol, 2016. **7**: p. 2038.
295. Gohar, A.A., et al., *Expression Patterns of ABC Transporter Genes in Fluconazole-Resistant Candida glabrata*. Mycopathologia, 2017. **182**(3-4): p. 273-284.
296. Arastehfar, A., et al., *Low Level of Antifungal Resistance in Iranian Isolates of Candida glabrata Recovered from Blood Samples in a Multicenter Study from 2015 to 2018 and Potential Prognostic Values of Genotyping and Sequencing of PDR1*. Antimicrob Agents Chemother, 2019. **63**(7).
297. Merhej, J., et al., *Yap7 is a transcriptional repressor of nitric oxide oxidase in yeasts, which arose from neofunctionalization after whole genome duplication*. Mol Microbiol, 2015. **96**(5): p. 951-72.
298. Subcommittee on Antifungal Susceptibility Testing of the, E.E.C.f.A.S.T., *EUCAST definitive document EDef 7.1: method for the determination of broth dilution MICs of antifungal agents for fermentative yeasts*. Clin Microbiol Infect, 2008. **14**(4): p. 398-405.
299. Simon, R., et al., *Analysis of gene expression data using BRB-ArrayTools*. Cancer Inform, 2007. **3**: p. 11-7.

300. Saeed, A.I., et al., *TM4 microarray software suite*. Methods Enzymol, 2006. **411**: p. 134-93.
301. Romo, J.A. and C.A. Kumamoto, *On Commensalism of Candida*. Journal of Fungi, 2020. **6**(1): p. 16.
302. Dufresne, S.F., et al., *Epidemiology of Candida kefyr in patients with hematologic malignancies*. J Clin Microbiol, 2014. **52**(6): p. 1830-7.
303. Khan, Z., et al., *Candida kefyr as a cause of bloodstream infection and adjunctive role of biomarkers in its diagnosis*. J Mycol Med, 2015. **25**(1): p. 71-5.
304. Tietz, H.J., et al., *Phenotypic and genotypic characterization of unusual vaginal isolates of Candida albicans from Africa*. J Clin Microbiol, 1995. **33**(9): p. 2462-5.
305. Chowdhary, A., et al., *Whole Genome-Based Amplified Fragment Length Polymorphism Analysis Reveals Genetic Diversity in Candida africana*. Front Microbiol, 2017. **8**: p. 556.
306. Miyazaki, T., et al., *Roles of calcineurin and Crz1 in antifungal susceptibility and virulence of Candida glabrata*. Antimicrob Agents Chemother, 2010. **54**(4): p. 1639-43.
307. Lamb, D.C., et al., *Biodiversity of the P450 catalytic cycle: yeast cytochrome b 5/NADH cytochrome b 5 reductase complex efficiently drives the entire sterol 14-demethylation (CYP51) reaction*. FEBS Letters, 1999. **462**(3): p. 283-288.
308. Yu, S.J., Y.L. Chang, and Y.L. Chen, *Calcineurin signaling: lessons from Candida species*. FEMS Yeast Res, 2015. **15**(4): p. fov016.
309. Truan, G., et al., *Cloning and characterization of a yeast cytochrome b5-encoding gene which suppresses ketoconazole hypersensitivity in a NADPH-P-450 reductase-deficient strain*. Gene, 1994. **142**(1): p. 123-7.
310. Rogers, K.M., et al., *Disruption of the Candida albicans CYB5 gene results in increased azole sensitivity*. Antimicrob Agents Chemother, 2004. **48**(9): p. 3425-35.
311. Choudhary, V. and R. Schneiter, *Pathogen-Related Yeast (PRY) proteins and members of the CAP superfamily are secreted sterol-binding proteins*. Proc Natl Acad Sci U S A, 2012. **109**(42): p. 16882-7.
312. Gatta, A.T., et al., *A new family of StART domain proteins at membrane contact sites has a role in ER-PM sterol transport*. Elife, 2015. **4**.
313. Sokolov, S.S., et al., *LAM Genes Contribute to Environmental Stress Tolerance but Sensibilize Yeast Cells to Azoles*. Front Microbiol, 2020. **11**: p. 38.
314. Gangneux, J.P., et al., *Clinical Impact of Antifungal Susceptibility, Biofilm Formation and Mannoside Expression of Candida Yeasts on the Outcome of Invasive Candidiasis in ICU: An Ancillary Study on the Prospective AmarCAND2 Cohort*. Front Microbiol, 2018. **9**: p. 2907.
315. Ishchuk, O.P., et al., *RNAi as a Tool to Study Virulence in the Pathogenic Yeast Candida glabrata*. Front Microbiol, 2019. **10**: p. 1679.
316. Biswas, C., et al., *Whole Genome Sequencing of Candida glabrata for Detection of Markers of Antifungal Drug Resistance*. J Vis Exp, 2017(130).
317. Mansfield, B.E., et al., *Azole drugs are imported by facilitated diffusion in Candida albicans and other pathogenic fungi*. PLoS Pathog, 2010. **6**(9): p. e1001126.
318. Mamelak, M., *Narcolepsy and depression and the neurobiology of gammahydroxybutyrate*. Prog Neurobiol, 2009. **89**(2): p. 193-219.
319. Castano, I., et al., *Telomere length control and transcriptional regulation of subtelomeric adhesins in Candida glabrata*. Mol Microbiol, 2005. **55**(4): p. 1246-58.
320. Lopez-Fuentes, E., et al., *Chromatin Loop Formation Induced by a Subtelomeric Protosilencer Represses EPA Genes in Candida glabrata*. Genetics, 2018. **210**(1): p. 113-128.
321. De Las Penas, A., et al., *Virulence-related surface glycoproteins in the yeast pathogen Candida glabrata are encoded in subtelomeric clusters and subject to RAPI- and SIR-dependent transcriptional silencing*. Genes Dev, 2003. **17**(18): p. 2245-58.
322. Gallegos-Garcia, V., et al., *A novel downstream regulatory element cooperates with the silencing machinery to repress EPA1 expression in Candida glabrata*. Genetics, 2012. **190**(4): p. 1285-97.
323. Jumper, J., et al., *Highly accurate protein structure prediction with AlphaFold*. Nature, 2021. **596**(7873): p. 583-589.
324. Pettersen, E.F., et al., *UCSF Chimera--a visualization system for exploratory research and analysis*. J Comput Chem, 2004. **25**(13): p. 1605-12.
325. Trott, O. and A.J. Olson, *AutoDock Vina: improving the speed and accuracy of docking with a new scoring function, efficient optimization, and multithreading*. J Comput Chem, 2010. **31**(2): p. 455-61.
326. Shapovalov, M.V. and R.L. Dunbrack, Jr., *A smoothed backbone-dependent rotamer library for proteins derived from adaptive kernel density estimates and regressions*. Structure, 2011. **19**(6): p. 844-58.

327. Buchan, D.W., et al., *Scalable web services for the PSIPRED Protein Analysis Workbench*. Nucleic Acids Res, 2013. **41**(Web Server issue): p. W349-57.
328. Peng, Z. and L. Kurgan, *High-throughput prediction of RNA, DNA and protein binding regions mediated by intrinsic disorder*. Nucleic Acids Res, 2015. **43**(18): p. e121.
329. Ritchie, M.E., et al., *limma powers differential expression analyses for RNA-sequencing and microarray studies*. Nucleic Acids Res, 2015. **43**(7): p. e47.
330. Delaveau, T., et al., *Yap5 Competes With Hap4 for the Regulation of Iron Homeostasis Genes in the Human Pathogen Candida glabrata*. Front Cell Infect Microbiol, 2021. **11**: p. 731988.
331. Langmead, B., et al., *Ultrafast and memory-efficient alignment of short DNA sequences to the human genome*. Genome Biol, 2009. **10**(3): p. R25.
332. Li, H., et al., *The Sequence Alignment/Map format and SAMtools*. Bioinformatics, 2009. **25**(16): p. 2078-9.
333. Quinlan, A.R. and I.M. Hall, *BEDTools: a flexible suite of utilities for comparing genomic features*. Bioinformatics, 2010. **26**(6): p. 841-2.
334. Denecker, T. and G. Lelandais, *Empowering the detection of ChIP-seq "basic peaks" (bPeaks) in small eukaryotic genomes with a web user-interactive interface*. BMC Res Notes, 2018. **11**(1): p. 698.
335. Robinson, J.T., et al., *Integrative genomics viewer*. Nat Biotechnol, 2011. **29**(1): p. 24-6.
336. Rafiee, M.R., et al., *Expanding the Circuitry of Pluripotency by Selective Isolation of Chromatin-Associated Proteins*. Mol Cell, 2016. **64**(3): p. 624-635.
337. Wijick, L.V., et al., *ChIP-SICAP: A New Tool to Explore Gene-Regulatory Networks in Candida albicans and other Yeasts*. Methods Mol Biol in press. Methods Mol Biol (in press). 2021.
338. Mellacheruvu, D., et al., *The CRAPome: a contaminant repository for affinity purification-mass spectrometry data*. Nat Methods, 2013. **10**(8): p. 730-6.
339. Jochim, A.L. and P.S. Arora, *Assessment of helical interfaces in protein-protein interactions*. Mol Biosyst, 2009. **5**(9): p. 924-6.
340. Baker, C.M. and G.H. Grant, *Role of aromatic amino acids in protein-nucleic acid recognition*. Biopolymers, 2007. **85**(5-6): p. 456-70.
341. Gopalakrishnan, R., et al., *A conserved genetic interaction between Spt6 and Set2 regulates H3K36 methylation*. Nucleic Acids Res, 2019. **47**(8): p. 3888-3903.
342. Miyake, T., et al., *Genome-wide analysis of ARS (autonomously replicating sequence) binding factor 1 (Abf1p)-mediated transcriptional regulation in Saccharomyces cerevisiae*. J Biol Chem, 2004. **279**(33): p. 34865-72.
343. Martins-Taylor, K., et al., *H2A.Z (Htz1) controls the cell-cycle-dependent establishment of transcriptional silencing at Saccharomyces cerevisiae telomeres*. Genetics, 2011. **187**(1): p. 89-104.
344. Vizoso-Vazquez, A., et al., *Ixr1p and the control of the Saccharomyces cerevisiae hypoxic response*. Appl Microbiol Biotechnol, 2012. **94**(1): p. 173-84.
345. Boyle, E.I., et al., *GO::TermFinder--open source software for accessing Gene Ontology information and finding significantly enriched Gene Ontology terms associated with a list of genes*. Bioinformatics, 2004. **20**(18): p. 3710-5.
346. Gabaldon, T., et al., *Comparative genomics of emerging pathogens in the Candida glabrata clade*. BMC Genomics, 2013. **14**: p. 623.
347. de Groot, P.W., et al., *The cell wall of the human pathogen Candida glabrata: differential incorporation of novel adhesin-like wall proteins*. Eukaryot Cell, 2008. **7**(11): p. 1951-64.
348. Seider, K., et al., *The facultative intracellular pathogen Candida glabrata subverts macrophage cytokine production and phagolysosome maturation*. J Immunol, 2011. **187**(6): p. 3072-86.
349. Brunke, S. and B. Hube, *Two unlike cousins: Candida albicans and C. glabrata infection strategies*. Cell Microbiol, 2013. **15**(5): p. 701-8.
350. Galocha, M., et al., *Divergent Approaches to Virulence in C. albicans and C. glabrata: Two Sides of the Same Coin*. Int J Mol Sci, 2019. **20**(9).
351. Rai, M.N., et al., *Functional genomic analysis of Candida glabrata-macrophage interaction: role of chromatin remodeling in virulence*. PLoS Pathog, 2012. **8**(8): p. e1002863.
352. Kaur, R., B. Ma, and B.P. Cormack, *A family of glycosylphosphatidylinositol-linked aspartyl proteases is required for virulence of Candida glabrata*. Proc Natl Acad Sci U S A, 2007. **104**(18): p. 7628-33.
353. Roetzer, A., et al., *Autophagy supports Candida glabrata survival during phagocytosis*. Cell Microbiol, 2010. **12**(2): p. 199-216.

354. Srivastava, V.K., K.J. Suneetha, and R. Kaur, *A systematic analysis reveals an essential role for high-affinity iron uptake system, haemolysin and CFEM domain-containing protein in iron homeostasis and virulence in Candida glabrata*. *Biochem J*, 2014. **463**(1): p. 103-14.
355. Nevitt, T. and D.J. Thiele, *Host iron withholding demands siderophore utilization for Candida glabrata to survive macrophage killing*. *PLoS Pathog*, 2011. **7**(3): p. e1001322.
356. Kasper, L., et al., *Identification of Candida glabrata genes involved in pH modulation and modification of the phagosomal environment in macrophages*. *PLoS One*, 2014. **9**(5): p. e96015.
357. Seneviratne, C.J., et al., *Architectural analysis, viability assessment and growth kinetics of Candida albicans and Candida glabrata biofilms*. *Arch Oral Biol*, 2009. **54**(11): p. 1052-60.
358. Goncalves, B., et al., *Environmental pH modulates biofilm formation and matrix composition in Candida albicans and Candida glabrata*. *Biofouling*, 2020. **36**(5): p. 621-630.
359. Schmidt, P., et al., *Proteomic analysis of the pH response in the fungal pathogen Candida glabrata*. *Proteomics*, 2008. **8**(3): p. 534-44.
360. De Las Penas, A., et al., *Local and regional chromatin silencing in Candida glabrata: consequences for adhesion and the response to stress*. *FEMS Yeast Res*, 2015. **15**(6).
361. Juarez-Cepeda, J., et al., *The EPA2 adhesin encoding gene is responsive to oxidative stress in the opportunistic fungal pathogen Candida glabrata*. *Curr Genet*, 2015. **61**(4): p. 529-44.
362. Roetzer, A., et al., *Candida glabrata environmental stress response involves Saccharomyces cerevisiae Msn2/4 orthologous transcription factors*. *Mol Microbiol*, 2008. **69**(3): p. 603-20.
363. Weig, M., et al., *Systematic identification in silico of covalently bound cell wall proteins and analysis of protein-polysaccharide linkages of the human pathogen Candida glabrata*. *Microbiology (Reading)*, 2004. **150**(Pt 10): p. 3129-44.
364. Chaudhuri, R., et al., *FungalRV: adhesin prediction and immunoinformatics portal for human fungal pathogens*. *BMC Genomics*, 2011. **12**: p. 192.
365. De Groot, P.W., K.J. Hellingwerf, and F.M. Klis, *Genome-wide identification of fungal GPI proteins*. *Yeast*, 2003. **20**(9): p. 781-96.
366. Pittet, M. and A. Conzelmann, *Biosynthesis and function of GPI proteins in the yeast Saccharomyces cerevisiae*. *Biochim Biophys Acta*, 2007. **1771**(3): p. 405-20.
367. Orlean, P., *Architecture and biosynthesis of the Saccharomyces cerevisiae cell wall*. *Genetics*, 2012. **192**(3): p. 775-818.
368. Xu, Z., et al., *De novo genome assembly of Candida glabrata reveals cell wall protein complement and structure of dispersed tandem repeat arrays*. *Mol Microbiol*, 2020. **113**(6): p. 1209-1224.
369. Goncalves, B., et al., *Revealing Candida glabrata biofilm matrix proteome: global characterization and pH response*. *Biochem J*, 2021. **478**(4): p. 961-974.
370. Zarnowski, R., et al., *Novel entries in a fungal biofilm matrix encyclopedia*. *mBio*, 2014. **5**(4): p. e01333-14.
371. Cavalheiro, M. and M.C. Teixeira, *Candida Biofilms: Threats, Challenges, and Promising Strategies*. *Front Med (Lausanne)*, 2018. **5**: p. 28.
372. Guo, X., et al., *Understand the genomic diversity and evolution of fungal pathogen Candida glabrata by genome-wide analysis of genetic variations*. *Methods*, 2020. **176**: p. 82-90.
373. Barber, A.E., et al., *Comparative Genomics of Serial Candida glabrata Isolates and the Rapid Acquisition of Echinocandin Resistance during Therapy*. *Antimicrob Agents Chemother*, 2019. **63**(2).
374. Thierry, A., et al., *Megasatellites: a peculiar class of giant minisatellites in genes involved in cell adhesion and pathogenicity in Candida glabrata*. *Nucleic Acids Res*, 2008. **36**(18): p. 5970-82.
375. Timmermans, B., et al., *Adhesins in Candida glabrata*. *J Fungi (Basel)*, 2018. **4**(2).
376. Iraqui, I., et al., *The Yak1p kinase controls expression of adhesins and biofilm formation in Candida glabrata in a Sir4p-dependent pathway*. *Mol Microbiol*, 2005. **55**(4): p. 1259-71.
377. Cavalheiro, M., et al., *From the first touch to biofilm establishment by the human pathogen Candida glabrata: a genome-wide to nanoscale view*. *Commun Biol*, 2021. **4**(1): p. 886.
378. Silva, S., et al., *In vitro biofilm activity of non-Candida albicans Candida species*. *Curr Microbiol*, 2010. **61**(6): p. 534-40.
379. Ames, L., et al., *Galleria mellonella as a host model to study Candida glabrata virulence and antifungal efficacy*. *Virulence*, 2017. **8**(8): p. 1909-1917.
380. Roumanie, O., et al., *Functional characterization of the Bag7, Lrg1 and Rgd2 RhoGAP proteins from Saccharomyces cerevisiae*. *FEBS Lett*, 2001. **506**(2): p. 149-56.
381. Pais, P., et al., *Characterization of the Candida glabrata Transcription Factor CgMar1: Role in Azole Susceptibility*. *J Fungi (Basel)*, 2022. **8**(1).
382. Cain, C.W., et al., *A conserved transcriptional regulator governs fungal morphology in widely diverged species*. *Genetics*, 2012. **190**(2): p. 511-21.

383. Malcher, M., S. Schladebeck, and H.U. Mosch, *The Yak1 protein kinase lies at the center of a regulatory cascade affecting adhesive growth and stress resistance in Saccharomyces cerevisiae*. Genetics, 2011. **187**(3): p. 717-30.
384. Gomez-Molero, E., et al., *Proteomic analysis of hyperadhesive Candida glabrata clinical isolates reveals a core wall proteome and differential incorporation of adhesins*. FEMS Yeast Res, 2015. **15**(8).
385. Aperis, G., et al., *Galleria mellonella as a model host to study infection by the Francisella tularensis live vaccine strain*. Microbes Infect, 2007. **9**(6): p. 729-34.
386. Trevijano-Contador, N. and O. Zaragoza, *Immune Response of Galleria mellonella against Human Fungal Pathogens*. J Fungi (Basel), 2018. **5**(1).
387. Tojo, S., et al., *Involvement of both granular cells and plasmatocytes in phagocytic reactions in the greater wax moth, Galleria mellonella*. J Insect Physiol, 2000. **46**(7): p. 1129-1135.
388. Lorenz, M.C. and G.R. Fink, *The glyoxylate cycle is required for fungal virulence*. Nature, 2001. **412**(6842): p. 83-6.
389. Chew, S.Y., et al., *Glyoxylate cycle gene ICL1 is essential for the metabolic flexibility and virulence of Candida glabrata*. Sci Rep, 2019. **9**(1): p. 2843.
390. Kim, M.S., et al., *Activation of Haa1 and War1 transcription factors by differential binding of weak acid anions in Saccharomyces cerevisiae*. Nucleic Acids Res, 2019. **47**(3): p. 1211-1224.
391. Killiny, N., *Generous hosts: Why the larvae of greater wax moth, Galleria mellonella is a perfect infectious host model?* Virulence, 2018. **9**(1): p. 860-865.
392. Romao, D., et al., *A New Determinant of Candida glabrata Virulence: The Acetate Exporter CgDtr1*. Front Cell Infect Microbiol, 2017. **7**: p. 473.
393. Mota, S., et al., *Candida glabrata susceptibility to antifungals and phagocytosis is modulated by acetate*. Front Microbiol, 2015. **6**: p. 919.
394. Danhof, H.A. and M.C. Lorenz, *The Candida albicans ATO Gene Family Promotes Neutralization of the Macrophage Phagolysosome*. Infect Immun, 2015. **83**(11): p. 4416-26.
395. Hassan, Y., S.Y. Chew, and L.T.L. Than, *Candida glabrata: Pathogenicity and Resistance Mechanisms for Adaptation and Survival*. J Fungi (Basel), 2021. **7**(8).
396. Kumar, K., et al., *Candida glabrata: A Lot More Than Meets the Eye*. Microorganisms, 2019. **7**(2).
397. Wray, G.A., et al., *The evolution of transcriptional regulation in eukaryotes*. Mol Biol Evol, 2003. **20**(9): p. 1377-419.
398. Gasch, A.P., et al., *Conservation and evolution of cis-regulatory systems in ascomycete fungi*. PLoS Biol, 2004. **2**(12): p. e398.
399. Kuo, D., et al., *Coevolution within a transcriptional network by compensatory trans and cis mutations*. Genome Res, 2010. **20**(12): p. 1672-8.
400. Longtine, M.S., et al., *Additional modules for versatile and economical PCR-based gene deletion and modification in Saccharomyces cerevisiae*. Yeast, 1998. **14**(10): p. 953-61.
401. Thomas-Chollier, M., et al., *A complete workflow for the analysis of full-size ChIP-seq (and similar) data sets using peak-motifs*. Nat Protoc, 2012. **7**(8): p. 1551-68.
402. Sugiyama, M., et al., *Nuclear localization of Haa1, which is linked to its phosphorylation status, mediates lactic acid tolerance in Saccharomyces cerevisiae*. Appl Environ Microbiol, 2014. **80**(11): p. 3488-95.
403. Collins, M.E., J.J. Black, and Z. Liu, *Casein Kinase I Isoform Hrr25 Is a Negative Regulator of Haa1 in the Weak Acid Stress Response Pathway in Saccharomyces cerevisiae*. Appl Environ Microbiol, 2017. **83**(13).
404. Teytelman, L., et al., *Highly expressed loci are vulnerable to misleading ChIP localization of multiple unrelated proteins*. Proc Natl Acad Sci U S A, 2013. **110**(46): p. 18602-7.
405. Park, D., et al., *Widespread misinterpretable ChIP-seq bias in yeast*. PLoS One, 2013. **8**(12): p. e83506.
406. Amemiya, H.M., A. Kundaje, and A.P. Boyle, *The ENCODE Blacklist: Identification of Problematic Regions of the Genome*. Sci Rep, 2019. **9**(1): p. 9354.
407. Cherry, J.M., et al., *Saccharomyces Genome Database: the genomics resource of budding yeast*. Nucleic Acids Res, 2012. **40**(Database issue): p. D700-5.
408. Mira, N.P., et al., *Genome-wide identification of Saccharomyces cerevisiae genes required for tolerance to acetic acid*. Microb Cell Fact, 2010. **9**: p. 79.
409. Reimand, J., et al., *Comprehensive reanalysis of transcription factor knockout expression data in Saccharomyces cerevisiae reveals many new targets*. Nucleic Acids Res, 2010. **38**(14): p. 4768-77.
410. Keller, G., et al., *Haa1, a protein homologous to the copper-regulated transcription factor Ace1, is a novel transcriptional activator*. J Biol Chem, 2001. **276**(42): p. 38697-702.

411. Hollenhorst, P.C., G. Pietz, and C.A. Fox, *Mechanisms controlling differential promoter-occupancy by the yeast forkhead proteins Fkh1p and Fkh2p: implications for regulating the cell cycle and differentiation*. *Genes Dev*, 2001. **15**(18): p. 2445-56.
412. Hollenhorst, P.C., et al., *Forkhead genes in transcriptional silencing, cell morphology and the cell cycle. Overlapping and distinct functions for FKH1 and FKH2 in Saccharomyces cerevisiae*. *Genetics*, 2000. **154**(4): p. 1533-48.
413. Navarre, C., et al., *Two distinct genes encode small isoproteolipids affecting plasma membrane H(+)-ATPase activity of Saccharomyces cerevisiae*. *J Biol Chem*, 1994. **269**(33): p. 21262-8.
414. Chang, A. and G.R. Fink, *Targeting of the yeast plasma membrane [H+]ATPase: a novel gene AST1 prevents mislocalization of mutant ATPase to the vacuole*. *J Cell Biol*, 1995. **128**(1-2): p. 39-49.
415. Ullah, A., et al., *Intracellular pH homeostasis in Candida glabrata in infection-associated conditions*. *Microbiology (Reading)*, 2013. **159**(Pt 4): p. 803-813.
416. Moreno-Garcia, J., et al., *Differential Proteome Analysis of a Flor Yeast Strain under Biofilm Formation*. *Int J Mol Sci*, 2017. **18**(4).
417. Nguyen, N.T.T., et al., *RSAT 2018: regulatory sequence analysis tools 20th anniversary*. *Nucleic Acids Res*, 2018. **46**(W1): p. W209-W214.
418. Oliveira, J., et al., *From a genome assembly to full regulatory network prediction: the case study of Rhodotorula toruloides putative Haa1-regulon*. *BMC Bioinformatics*, 2021. **22**(1): p. 399.
419. Faria-Ramos, I., et al., *Species distribution and in vitro antifungal susceptibility profiles of yeast isolates from invasive infections during a Portuguese multicenter survey*. *Eur J Clin Microbiol Infect Dis*, 2014. **33**(12): p. 2241-7.
420. Costa-de-Oliveira, S., et al., *A first Portuguese epidemiological survey of fungaemia in a university hospital*. *Eur J Clin Microbiol Infect Dis*, 2008. **27**(5): p. 365-74.
421. Merhej, J., et al., *A Network of Paralogous Stress Response Transcription Factors in the Human Pathogen Candida glabrata*. *Front Microbiol*, 2016. **7**: p. 645.
422. Yao, D., et al., *Mechanisms of azole resistance in clinical isolates of Candida glabrata from two hospitals in China*. *Infect Drug Resist*, 2019. **12**: p. 771-781.

Appendix – Supplementary Data

Annex Table II. 1. Revision of non-synonymous mutation identified in *CgPdr1* clinical isolates and strains [6, 47, 51, 55, 67, 204-206, 295, 296, 316, 422]. Non-synonymous mutations were separate according to the evidence that they result in azole resistance through hyperactivation of *CgPdr1*: -, Non-synonymous mutations found in susceptible and resistant clinical isolates; --, Non-synonymous mutation result in hypersusceptibility to azoles; +, non-synonymous mutation identified in a resistant isolate but not in susceptible isolates; ++, non-synonymous mutation found in a resistant strain evolved by *in vitro* evolution or *in vivo* during infection of a patient; +++, the *CgPDR1* allele of the resistant clinical isolate is responsible for the azole resistance and/or MDR target gene upregulation when transformed in the genomic background of susceptible clinical isolate or laboratorial strain; * *CgPDR1* allele carries more than one mutation only identified in resistant clinical isolates.

https://docs.google.com/spreadsheets/d/1dszJYoyvH9Sjp7AJm72LLqRHtL3KKNvze7H_5iFkqo/edit?usp=sharing

Annex Table III. 1. List of isolates tested and the local where the sample was collected. In some cases a MIC of fluconazole was tested previously on the hospital. The washed sample corresponds to bronchoalveolar lavage fluids. Isolates signalized with an asterisk were isolated from patients with AIDS that followed fluconazole treatment.

<https://docs.google.com/spreadsheets/d/17De0tmtNvlxWwF8MR0Ve-nt4hczYA-v6PTAyZVaDiWk/edit?usp=sharing>

Annex Table III. 2. Proteins previously described to be involved in fluconazole and/or voriconazole resistance in *C. glabrata* and that were found to harbour non-synonymous SNPs in the FFUL887 strain, when compared with their CBS138 counter-partners.

<https://docs.google.com/spreadsheets/d/1TZ7gYZXKQdkJXcXDA77NQMel8mTQovOIQUGeW9Mz0mo/edit?usp=sharing>

Annex Table III. 3. List of the genes found to be up- or down- regulated in *C. glabrata* FFUL887 clinical isolate cells compared to the reference strain CBS138. Genes whose expression increased or decreased (above a 1.5-fold threshold level and under a 0.5-fold threshold) were selected and are here listed. Only genes exhibiting a similar degree of variance in the three replica samples performed were considered to be differently expressed, as detailed in materials and methods. The biological function indicated was based on the information available at Candida Genome Database. Upregulated genes highlighted in grey were previously described to be regulated by *CgPdr1*, according to the information available in the PathoYeast database.

<https://docs.google.com/spreadsheets/d/1-eBWZzjObs9WeQ1M3aIBWxcoul8gGjXhtO2soVwNpWk/edit?usp=sharing>

Annex Table III. 4. Search within the predicted FFUL887 ORFeome and within the CBS138 genome of genes orthologous to those described to mediate glucose repression in *Saccharomyces cerevisiae*.

<i>S. cerevisiae</i> gene	Function in glucose-repression pathway	<i>C. glabrata</i> CBS138 orthologue	Identity/similarity/gaps between the Sc and the CgCBS138 orthologues*	<i>C. glabrata</i> FFUL orthologue	Identity/similarity/gaps between the CgCBS138 and CgFFUL887 orthologues
SNF1 PATHWAY					
SAKI	Activates Snf1 kinase by phosphorylation in glucose starvation or non-fermentable carbon sources	CAGL0K02167g	45.2%/57.5%/19.7%	CGFF_03844	98.7%/98.9%/0.9%
SNF1	Kinase that is activated in response to low glucose concentrations or the presence of non-fermentable carbon; inactivates Mig1 by phosphorylation	CAGL0M08910g	83.0%/89.9%/2.6%	CGFF_00630	100%/100%/0
SIP1	Regulatory subunit of Snf1 involved in response to low and high external glucose concentrations	CAGL0F03047g	38.7%/52.4%/21.1%	CGFF_01044	99.9%/99.9%/0
SIP2	Regulatory subunits of Snf1 that are required for activation of the kinase in response to non-fermentable carbon sources	CAGL0K09350g	46.1%/59.6%/15.8%	CGFF_00076	99.8%/100%/0
GAL83		CAGL0A03696g	65.4%/74.4%/7.3%	CGFF_04391	100%/100%/0
SNF4	Activating subunit of Snf1; activates glucose-repressed genes and represses glucose-induced genes	CAGL0K07161g	58.9%/79.3%/0.3%	CGFF_01898	99.7%/100%/0
MIG1	Transcriptional repressor of low-affinity hexose transporters and of transcription factors Cat8, Hap4 and Adr1 involved in response to non-fermentable carbon sources	CAGL0A01628g	37.0%/45.7%/29.7%	CGFF_04479	100%/100%/0
MIG2	Cooperates with Mig1 in glucose repression	CAGL0A01628g	27.1%/38.7%/28.6%	CGFF_04479	100%/100%/0
MIG3	Transcriptional regulator required for glucose repression in wild-type <i>S. cerevisiae</i> isolates; inactivated in the lab strain S288c	CAGL0C02519g	29.5%/42.0%/35.7%	CGFF_02798	100%/100%/0
RGT1 PATHWAY					
SNF3	Plasma membrane low glucose sensor	CAGL0J09020g	54.1%/67.6%/10.5%	CGFF_00241	99.9%/100%/0
RGT2		CAGL0J09020g	52.0%/66.5%/15.0%	CGFF_00241	99.9%/100%/0
RGT1	Represses expression of HXT1-4 genes in the absence of glucose; activates expression of HXT1 in response to high glucose concentrations	CAGL0L01903g	41.9%/53.6%/21.3%	CGFF_02434	98.4%/98.6%/0
MTH1	Negative regulator of the glucose-sensing signal transduction pathway; required for repression of transcription by Rgt1p; interacts with Rgt1p and the Snf3p and Rgt2p glucose sensors	-	-	-	-
CAT8	Transcriptional activator of genes required for metabolism of non-fermentable carbon sources	CAGL0M03025g	36.5%/49.7%/22.8%	CGFF_00559	99.6%/99.8%/0

Annex Table IV. 1. *Set of clinical Candida strains used in our study including both the lab strains and the clinical isolates.* For the lab strains we indicate the corresponding genotype while for the clinical strains we include the description of their name, the species identification and the niche where they were isolated from. Clinical strains considered resistant to FLZ and/or VZ are highlighted in grey.

https://docs.google.com/spreadsheets/d/1qkIv4QJcWBDHrOAbR_8asDG-DG7hJT_cM4HpmvKsXiQ/edit?usp=sharing

Annex Table IV. 2. Modifications found in the sequences of *CgPdr1* transcription factor (at the nucleotide and amino acid level) encoded by the azole-resistant *Candida glabrata* isolates identified in this study or the study of Salazar, B. S. et al., 2018 [7]. As a point of comparison, the *CgPdr1* sequence of the susceptible reference strain CBS138 was used. Nucleotide modifications leading to non-synonymous SNPs are marked in orange.

Strain	<i>CgPDR1</i> coding sequence coordinates																				
	162	226	271	293	427	705	727	765	820	837	871	1126	1176	1663	1672	1749	2319	2408	2587	2994	3156
CBS138	C	T	G	T	A	C	G	C	A	C	T	C	T	A	G	C	A	T	T	T	G
FFUL412/FFUL443	T	C	A	C	C	T		T		T	C		G			T	T		C	C	A
FFUL674			A	C			A											C			
FFUL830/FFUL866			A	C			A							G							
FFUL878/FFUL887			A	C			A		C												
ISTA56			A	C			A								T						
ISTB556/ISTB607			A	C			A					T									
ISTB218			A	C			A														

Annex Table IV. 3. *Comparative transcriptomic profiling of Candida glabrata FFUL443 isolate, in comparison with the reference strain CBS138.* Cells of both strains were cultivated as detailed in materials and methods. Documented targets of CgPdr1 are highlighted in grey (for this it was selected among the activated genes those in which documented positive influence of CgPdr1 has been described, while in the down-regulated genes we have only considered those in which inhibitory effect of CgPdr1 has been described). Regulatory associations between CgPdr1 and its target genes were taken from the PathoYeast database.

https://docs.google.com/spreadsheets/d/1urc6T3D_fBvjclwSPFyRZVh8ccYv-eQzs5rk_qYVKus/edit?usp=sharing

Annex Table IV. 4. *Comparative transcriptomic profiling of Candida glabrata FFUL674 isolate, in comparison with the reference strain CBS138.* Cells of both strains were cultivated as detailed in materials and methods. Documented targets of CgPdr1 are highlighted in grey (for this it was selected among the activated genes those in which documented positive influence of CgPdr1 has been described, while in the down-regulated genes we have only considered those in which inhibitory effect of CgPdr1 has been described). Regulatory associations between CgPdr1 and its target genes were taken from the PathoYeast database.

<https://docs.google.com/spreadsheets/d/11U2DbeMTvREsRCbiPoywVSQZY1c2ly7iWbIVrZZQuys/edit?usp=sharing>

Annex Table IV. 5. *Comparative transcriptomic profiling of Candida glabrata ISTB218 isolate, in comparison with the reference strain CBS138.* Cells of both strains were cultivated as detailed in materials and methods and in this table are shown genes exhibiting a differential expression in the two strains above 2-fold. The effect of gene deletion in *C. glabrata* tolerance to azoles is also indicated based on previously published reports. Genes up-regulated in ISTB218 documented to provide protection against azoles or genes down-regulated in ISTB218 isolate whose inactivation was described to improve tolerance to azoles are shaded in grey.

https://docs.google.com/spreadsheets/d/1yaiytFYRbTOv46sn0XVBQwQUAghc4oZMgjKje49_7vk/edit?usp=sharing

Annex Table IV. 6. *Results from detection of SNPs that were found in the genome of the azole-resistant strain ISTB218 (but not in the genome of the azole susceptible strain ISTA29) when compared with the genome of the reference strain CBS138.* Cells of both strains were cultivated as detailed in materials and methods and in this table are shown genes that harbour non-synonymous SNPs in the ISTB218 strain, when compared with their CBS138 and in their azole susceptible strain ISTA29 counter-partners. Genes documented to influence azole resistance are shaded in grey. SNPs leading to frame-shifts are shaded in yellow.

<https://docs.google.com/spreadsheets/d/1AmVk3UYWPnyjT5-8M2ouY0vl-iYv5H7b1JjBIwl8dx0/edit?usp=sharing>

Annex Table V. 1. *List of primers used in this work*

Primers	Sequence	Application
PrCg <i>YHB1</i> -F	GGGGGTTTTCTCGAAGAG	qPCR of Cg <i>YHB1</i> promoter sequence in ChIP-seq samples
PrCg <i>YHB1</i> -R	GGTTGGTCTAGGAAAAGCA	qPCR of Cg <i>YHB1</i> promoter sequence in ChIP-seq samples
Prom <i>PDR1</i> _REV	CTTCCACGGAATAGGAGGCTC	qPCR of Cg <i>PDR1</i> promoter sequence in ChIP-seq samples
Prom <i>PDR1</i> _FW	GTAGACTCATTCCACGGAGC	qPCR of Cg <i>PDR1</i> promoter sequence in ChIP-seq samples
Prom <i>CDR1</i> _FW	GCAAGTCCACGGAATATTTCC	qPCR of Cg <i>CDR1</i> promoter sequence in ChIP-seq samples
Prom <i>CDR1</i> _REV	CATCGTTGCTCCTCGCTCC	qPCR of Cg <i>CDR1</i> promoter sequence in ChIP-seq samples

Annex Table V. 2. *CgPdr1^{WT}* and *CgPdr1^{K274Q}* ChIP-seq peaks calling analysis. A peak was considered valid if detected by bPeaks peak calling in at least two replicates and does not overlap ORF regions or a tRNA locus. Information herein detailed includes the location of the peak detected in the chromosome of *C. glabrata*, the flanking ORFs (no farther than 2.5kb), and its fold change (SKY107_ pYR29.MycHIS_CgPdr1^{K274Q} vs SKY107_ pYR29.MycHIS_CgPdr1^{WT}), and the distance of the peak to a flanking ORF (rounded in 0.5 increments). If peaks were found in an intergenic region, both genes are assumed to be potential direct regulated targets of CgPdr1, with the exception if only one of the genes is upregulated. In this case, the gene with unchanged expression (marked in red) and is excluded from further analysis. The presence of a potential PDRE motif identified in the peak sequences is also summarized. The peaks identified in both transformed strains were the same.

Chr	Peak position (nt)		Gene 1				Gene 2				PDRE
			<i>C. glabrata</i> ORF/ Standard Name	<i>S. cerevisiae</i> Ortholog	Log2 Fold	Distance to promoter (kb)	<i>C. glabrata</i> ORF/ Standard Name	<i>S. cerevisiae</i> Ortholog	Log2 Fold	Distance to promoter (kb)	
A	46651	47601	CAGL0A00451g/ <i>CgPDR1</i>	<i>PDR1</i>	-0.105	0.4					+
C	328101	328601	CAGL0C03289g/ <i>CgYBT1</i>	<i>YBT1</i>	0.325	0.4					+
D	562551	562951	CAGL0D05918g/ <i>CgATF2</i>	<i>ATF2</i>	0.515	0.7					+
F	260501	261301	CAGL0F02717g/ <i>CgPDH1</i>	<i>PDH1</i>	0.87	0.4	<i>CAGL0F02673g</i>	<i>RPB7</i>	0.045	0.6	+
G	25201	25801	CAGL0G00242g/ <i>CgYOR1</i>	<i>YOR1</i>	0.545	0.6	<i>CAGL0G00264g</i>	<i>PXR1</i>	-0,02	0.6	+
I	442901	443301	CAGL0I04862g/ <i>CgSNQ2</i>	<i>SNQ2</i>	0.195	0.1					+
I	700451	700801	CAGL0I07249g	<i>BAG7</i>	0.03	0.1					+
K	154951	155551	CAGL0K01727g/ <i>CgRPN4</i>	<i>RPN4</i>	0.295	0.4					+
L	1094601	1095201	CAGL0L10142g/ <i>CgRSB1</i>	<i>RSB1</i>	0.135	0.6	<i>CAGL0L10120g</i>	<i>RTA1</i>	0.05	2.3	+
M	202001	204501	CAGL0M01760g/ <i>CgCDR1</i>	<i>CDR1</i>	1.26	0.1					+
M	964051	965201	CAGL0M09713g	<i>YIM1</i>	1.085	0.1	<i>CAGL0M09735g/ CgMEC3</i>	<i>MEC3</i>	0,175	0,1	+
M	1277051	1277551	CAGL0M12947g/ <i>CgPUP1</i>	<i>PUP1</i>	1.44	0.4	<i>CAGL0M12969g</i>	<i>YIL077C</i>	-0,1	1	+

Annex Table VII. 1. *Acetic acid stress CgHaa1 regulated genes.* Comparative transcriptome analysis of the wild-type KUE100 wild-type strains vs the KUE100 Δ Cg*haa1* strain was obtained in the same experimental growth conditions used for ChIP-seq analysis in materials and methods. A gene was considered differentially expressed if its mean absolute Log₂ fold change value of two independent biological experiments was higher than 0.5 with a cut-off p-value of 0.05. The possible involvement of transcriptional regulators, whose genes were found upregulated, in the regulation of CgHaa1 indirect targets was assessed by comparing homologous networks in *S. cerevisiae* using Yeastract+.

<https://docs.google.com/spreadsheets/d/1CJgvGUibRVw-eFOv5sbIV08hVmYJwwFIhE9CYkPM7Bk/edit?usp=sharing>

Annex Table VII. 2. CgHaa1 ChIP-seq peaks calling analysis. A peak was considered valid if detected by bPeaks peak calling in at least two replicates and does not overlap ORF regions or a tRNA locus. Information herein detailed includes the location of the peak detected in the chromosome of *C. glabrata*, the flanking ORFs (no farther than 2kb), and its fold change (KUE100_chr606 vs KUE100ΔCghaa1), and the distance of the peak to a flanking ORF (rounded in 0.5 increments). If peaks are found in an intergenic region both genes are assumed to be potential direct regulated targets of CgHaa1, with the exception if only one of the genes is upregulated. In this case, the gene with unchanged expression (marked in red) is excluded from further analysis. The second set of genes, in grey lines, represents a set of possible direct targets that interaction of CgHaa1 to the promotor needs to be confirmed since the peaks observed in the ChIP-seq experiments have often low intensities and were not detected by bPeaks, at least not in all replicates.

Chr	Peak position		Gene 1				Gene 2			
			<i>C. glabrata</i> ORF/ Standard Name	<i>S. cerevisiae</i> Ortholog	Log2 Fold	Distance to promoter (kb)	<i>C. glabrata</i> ORF/ Standard Name	<i>S. cerevisiae</i> Ortholog	Log2 Fold	Distance to promoter (Kb)
A	178551	179201	CAGL0A01782g/ CgHXT4	HXT4	0.64	1.5 to 2				
D	648151	648701	CAGL0D06732g/ CgEPA21	no ortholog	-	1 to 1.5				
G	266001	266251	CAGL0G02893g	POS5	0.47	< 0.5				
G	311601	312151	CAGL0G03289g/ CgSSA3	SSA3	0.57	0.5 to 1	CAGL0G03267g	AST2	0.93	1.5 to 2
G	849901	850551	CAGL0G08866g	FKH1	1.33	0.5 to 1	CAGL0G08844g	ZCF17	0.25	1 to 1.5
H	982251	982451	CAGL0H10076g	YRO2	2.49	< 0.5	CAGL0H10054g	YBR053C	0.06	1.5 to 2
	981351	981551				0.5 to 1				< 0.5
I	1025951	1026501	CAGL0I10384g/ CgTPO3	TPO3	1.86	1.5 to 2				
	1026501	1026950				1 to 1.5				
	1026950	1027200				0.5 to 1				
J	573366	573751	CAGL0J06050g	YGP1	1.2	1 to 1.5				
J	828451	828601	CAGL0J08316g	MET2	0.36	< 0.5				
K	523651	524401	CAGL0K05357g/ CgGLN1	GLN1	0.01	1 to 1.5				
K	874551	874951	CAGL0L08008g	PMP1	1.19	1 to 1.5				
L	876001	876151	CAGL0L08030g	SLM5	1.14	1 to 1.5				
	876351	876851				0.5 to 1				
L	773901	774401	CAGL0L06864g	SIP5	0.79	0.5 to 1				
M	1181101	1181501	CAGL0M11902g	FUN19	-0.11	< 0.5				

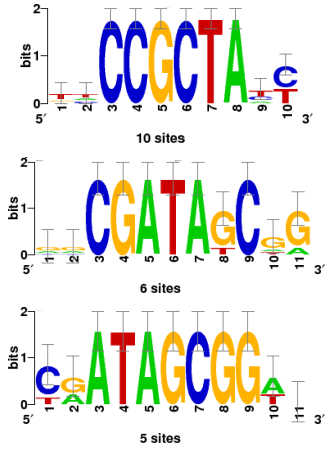
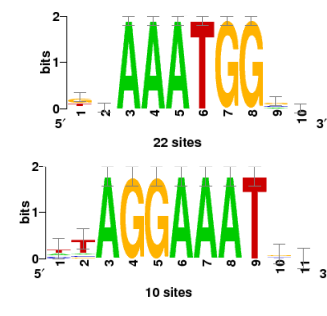
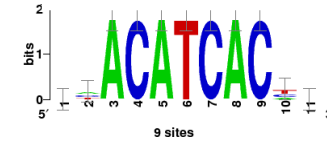
Annex Table VII. 2 (Part II)

Chr	Peak position		Gene 1				Gene 2			
			<i>C. glabrata</i> ORF/ Standard Name	<i>S. cerevisiae</i> Ortholog	Log2 Fold	Distance to promoter (kb)	<i>C. glabrata</i> ORF/ Standard Name	<i>S. cerevisiae</i> Ortholog	Log2 Fold	Distance to promoter (Kb)
A	57850	58300	CAGL0A00495g/ CgPMA1	PMA1	0.62	< 0.5	CAGL0A00517g	PMCI	0.04	0.5 to 1
	58300	58650				0.5 to 1				< 0.5
C	289500	290000	CAGL0C02893g	HKR1	0.99	0.5 to 1	CAGL0C02937g	PAC1	-0.09	0.5 to 1
C	373250	373750	CAGL0C03740g	-	1.21	1 to 1.5	CAGL0C03762g	-	0.03	0.5 to 1
E	549300	551500	CAGL0E05566g	TYE7	1.17	< 0.5	CAGL0E05588g	REV1	0.29	< 0.5
G	534500	536500	CAGL0G05632g	YDL218W	2.16	< 0.5				
I	373500	377200	CAGL0I04246g/ CgSUT1	SUT1	1.55	< 0.5	CAGL0I04224g	RAD54	0.11	0.5 to 1
L	1012500	1013500	CAGL0L09339g/ CgHAA1	HAA1	3.155	0.5 to 1				

Annex Table VII. 3. *CgHaa1* ChIP-seq peaks detected that require further analysis. These more dubious peaks include: low intensity reads when compared to the MOCK sample detected by the bPeaks software that were not always reproducible in the three biological replicates; possible peaks that are visible in the promoters of chipable ORFs found in the conditions of study when compared to the MOCK. The subset of peaks can be visualized in the Annex Figure VII. 1. Information herein detailed includes the location of the peak detected in the chromosome of *C. glabrata*, the flanking ORFs (no farther than 2kb), and its fold change (KUE100_chr606 vs KUE100Δ*CgHaa1*), and the distance of the peak to a flanking ORF (rounded in 0.5 increments). If peaks are found in an intergenic region both genes are assumed to be potential direct regulated targets of *CgHaa1*, with the exception if only one of the genes is upregulated. In this case, the gene with unchanged expression (marked in red) is excluded from further analysis.

Chr	Peak position		Gene 1				Gene 2			
			<i>C. glabrata</i> ORF/ Standard Name	<i>S. cerevisiae</i> Ortholog	Log2 Fold	Distance to promoter (kb)	<i>C. glabrata</i> ORF/ Standard Name	<i>S. cerevisiae</i> Ortholog	Log2 Fold	Distance to promoter (Kb)
A	63251	64101	CAGL0A00539g	<i>COG7</i>	0.41	< 0.5				
E	180200	181100	CAGL0E01793g/ <i>CgYPS6</i>	-	-0.05	< 0.5				
E	185000	185700	CAGL0E01837g/ <i>CgYPS9</i>	-	0.135	< 0.5				
E	187300	188200	CAGL0E01859g/ <i>CgYPS10</i>	-	0.25	< 0.5	CAGL0E01881g/ <i>CgYPS11</i>	-	-0.09	< 0.5
H	342300	342700	CAGL0H03707g	<i>SIS1</i>	0.135	< 0.5				
H	70000	71500	CAGL0H00704g	<i>ATG41</i>	0.295	< 0.5				
K	523651	524501	CAGL0K05357g	<i>GLN1</i>	0.01	< 0.5				

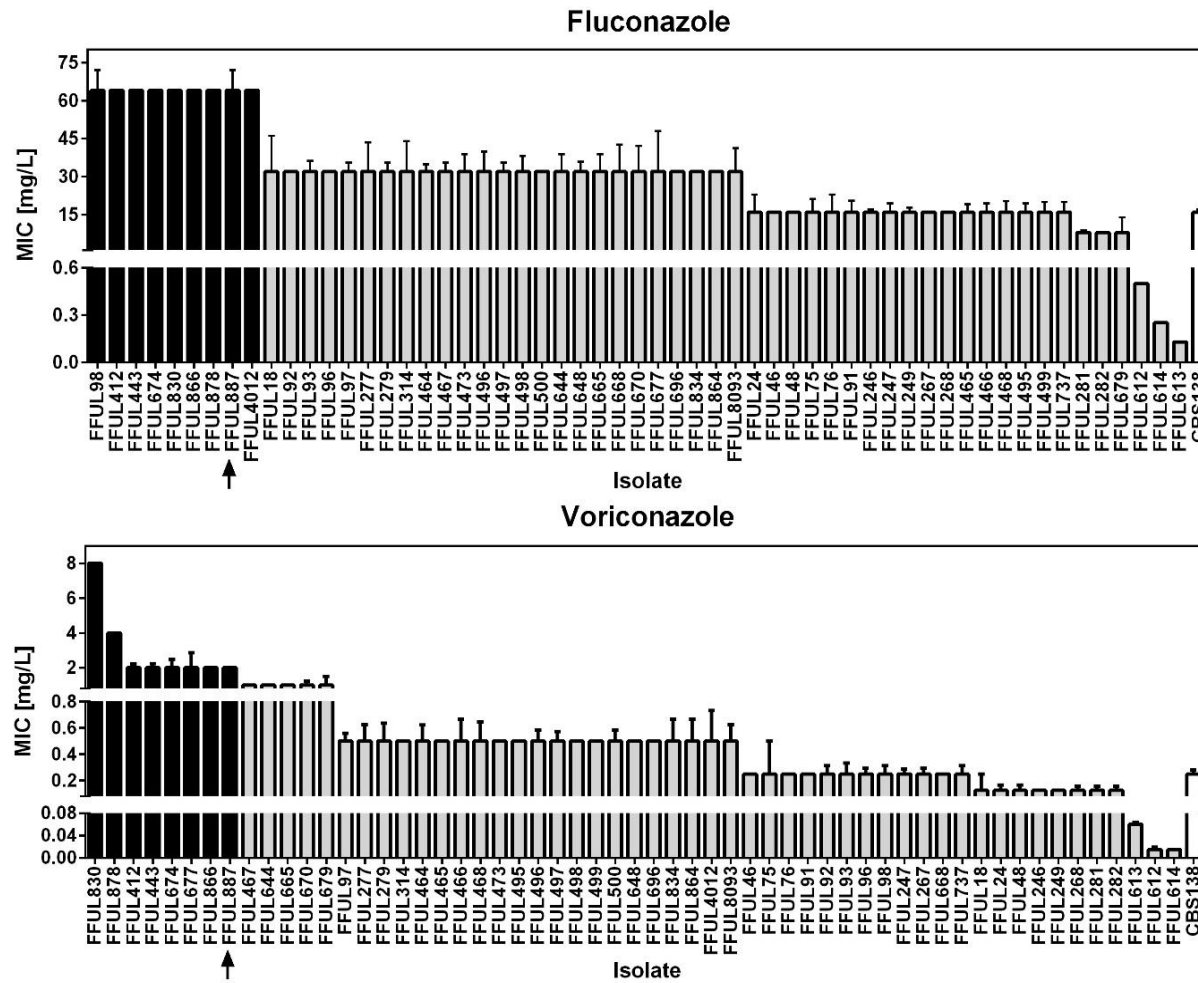
Annex Table VII. 4. *De novo* potential binding motif of CgHaa1 during acetic acid stress found in the ChIP-seq peaks sequences using the RSAT tools.

Motifs in <i>C. glabrata</i> (total of motifs found)	Motif type	% of ChIP peaks in motif (number per motif)	Maximum number of motifs per peak	Total peaks with motif
	HRE-like	27.78 (5)	3	9
	Motif 1 RSAT	61.11 (11)	5	13
	Motif 2 RSAT	27.78 (5)	2	4

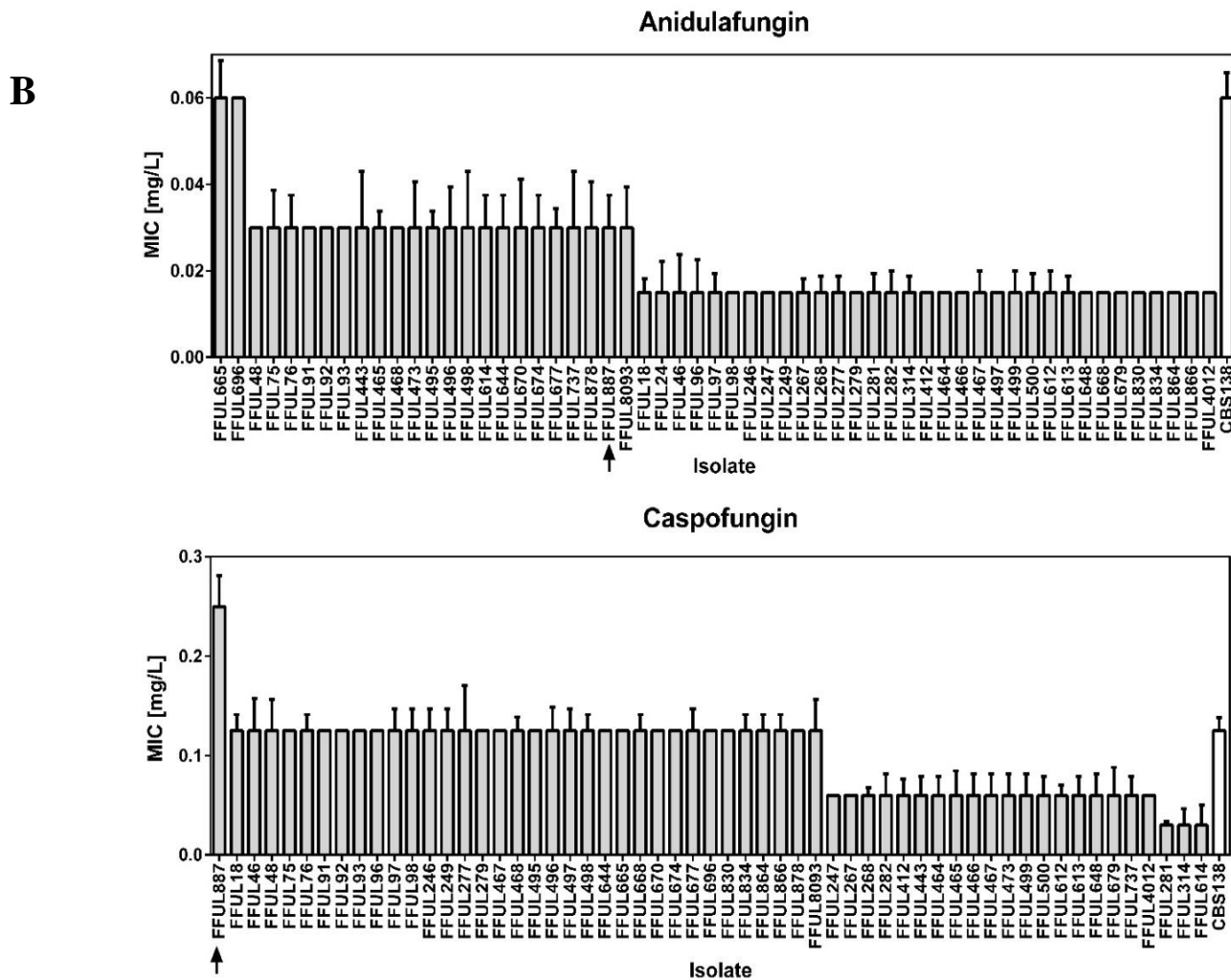
ScPdr3	-----MKVVKSTRSKVSTACVNCRRKIKCTGRV	29	
CgPdr1	MQTL-----ETTSKNPGEVKAQKPFSTRRTKVGKACDSCRRIKCKNGLK	45	
ScPdr1	MRGLTFKNGVHIETGPDTSESSADSNFSTFGSGKIRKPRSKVSKACDNCRRRIKCKNGKF	60	
ScPdr3	PCFNCSYDCTCVFLKHLKLPQKEDSSQ---SLPTTAVAPPSSHANVEASADVQHLD---	82	DBD
CgPdr1	PCPSCCTIYGCECTYTDAKSTRKLNKSNDAKSKMPTGRVSKNKETTRV---DKDIRKLEQQYV	103	
ScPdr1	PCASCEIYSCECTFSTRQGGARIKNLHKTS---LEGTIVQVKEETD-----S-----	104	
ScPdr3	---TAI-----KLDNQYFFK-L	95	
CgPdr1	PINANIHVGRFRFSENILNGYPCGAPQNNVVGNIPLAVNTQCHRGLSETPMSSTFKESNL	163	
ScPdr1	-----SSTSFSPQRCITDGPQAVEQPTKFFEN--	131	
ScPdr3	MND-LIQ-----IFVSPSATHAFD-----TSNNFTNDNNILFKDDSKYQNLVTVQN	141	
CgPdr1	RDRRLQSSDTRDMRNGDSEERDLKGSSENKSKDNKSDPLIYKDDTHIESTVNLTKQ	223	
ScPdr1	-----FKLGGRSSGSDNGSDGK-----NDDVNRNGFYEDDESQATLSTLQT	174	
ScPdr3	ILTNLYALPPCD-DTQLLIDKTKSQLNLLINSWNPEINYPKLSFSFRPQRSIETIYLLTN	200	
CgPdr1	AVNELKSLQNAFSSIKSSIDAIELQLRNILDNWKEVDFEKAKINESAATKSLNLLRN	283	
ScPdr1	TLKLNKEMAHLGTHVTSIAIESIELQISDLLKWEKVRITKELATTKFYFNKSIETQLMKN	234	
ScPdr3	KYRNKIHMTFRSFWIDQMVKSQS-----PDSLEATTEFLVDEVFGLFSPIQAFS	248	ID
CgPdr1	KYTNHVHLTRFRIWIDYKNANKNNHFMGECGFLAESFHSANQPLVDELFGLYSQVEAFS	343	
ScPdr1	KYCDVHLTRYAASNNKDKQ-----ITSSQPLIDEIFGLYSPFQFS	277	
ScPdr3	LRGIGYLKKNIENTGSS-MLIDTKETIYILRLFDLCYEHLIQGCISISNPLENVLQKI	307	
CgPdr1	LQGLGCVHLYEFPYKTEAIAKLMKETLYILRFIDICVHINEESISIANPLETVLRKK	403	
ScPdr1	LQGIKCFQNYRSKSKCEIFPRTAKETIYMLRFFDVCFHINQGCVSIANPLENVLQRM	337	
ScPdr3	KQTPTTASASLFTSPAPL-SNDLVISVIHQLPQFFIQSITGFTTTQLIENLHDSFSMFR	366	
CgPdr1	HLMPMTFTPRSSYSSPQASATKSLVSKIIEIRIPQFFIESVTNVSSQLLDRDDESKMFG	463	
ScPdr1	NLLPSTPSSISSGSPNHTAKSHVALVINHLQPFVRNITGISNSELLEMNDISMFG	397	
ScPdr3	IVTQMYAQRKRFAEFLNQAFSLPH-----QEKSVLFSFCSSEYLLSTLCYAY	416	XDB
CgPdr1	TLNMCKSIRKFDVSMVDYDSIVTEKSEGEQNDGKVTVAEFTSLCEAEMLLALCYNY	523	
ScPdr1	ILLKMLDMHNSYQNFLEITS---NPSVAKNTQSIDVLQEFIHQCAGEALIALCYSY	454	
ScPdr3	NVTLYHMLDIN-TLDYLELTVSLEIQNEIDERGFEMKLEVAVTCSTKMGLSRWEYVVG	475	
CgPdr1	NLTLYSFFFGTINIEYMEHLLLEEQALDEYGFVKLVNVAANAKMGFRHREFYVVG	583	
ScPdr1	NSTLYNVVDFTCDIITHEQLYFLDLLFWLSEIYGFVKLVNVAHVFSRGLSRWEYVVG	514	MHR
ScPdr3	IDENTAERRRKIWKIYSLKRFITDGLDSLINHQMNCLLTKDFRDMGFINHKEFLTK	535	
CgPdr1	YEESTAERKRLWKLNYEKASTMKGGFVSIDDATVNCLLPKIFRNFGYLDRAVEFLEN	643	
ScPdr1	LDFNFAERRRNLWKAIFYEFTLASKLGYPSNIDDSKINCLLTKNFRDVGFLDNRDFIEN	574	
ScPdr3	IGTSSLSPSSPKLNLSRLIEYELALAIQIVGDFSETLYNEKFTSLEVSVKPTIIRQ	595	CRD
CgPdr1	IQKP---MDLSVFSDDVPIVSLCKYGEALITVTSFEHFKFLYADRYTSIRNSAKPPTLKN	700	
ScPdr1	VHLV---RRSEAFDNMCISDLKYGELAVLQIVSHFSSSVLFNEKFTSIRNTPKPSVVR	631	
ScPdr3	KLLEKVFEDIESFRLKLAIKLHTSRVQVACHKYP---EYPRNDLIEAAKVFVSYHKNTW	652	
CgPdr1	QLIKEIVDGIAYTETSVEAIRKQAKLWDIALGKVT-KDKINKEDTAAASKFTLSVEYHR	759	
ScPdr1	KLLFEVLEIFNETEMKYDAIKEQTGKLFDAFASKDSTELKVSREDKIMASKFVLFYEHF	691	
ScPdr3	FSILGAVNNLIARLSEDF---EVITGQSMKYANEMFQEWREINQFLIQVDTFIVWACLDF	710	NLS
CgPdr1	FRLINMADNLIARLMVFKPSDWLISVMKGLNRLYEHKVMNIEIISMDNDYSIATTFEY	819	
ScPdr1	CRMVNESDNIVARLCVHRRPSILLENKLYLHKIYKSWTDMNKILLDFDNDYSVYRFAH	751	
ScPdr3	YELIFFVMAKFFVEDPHITLEDVINILKVFKRITNIIISFFNNLDEKDYDCQTFREFSR	770	
CgPdr1	YAPSCCLATQTLIVRNEMDDVQKMMVAVYKFRNLGMFLQSAKCVSLADSHTRDFDSR	879	
ScPdr1	YSISCIILVSQAFSVAEFIKVNDVNNMIRVFRFLDIKIFSENETNEHFVNSQSFQDYTR	811	
ScPdr3	SSSLVAISIRIIFLKCYAEQIDRAEFIERLKEVEPGLSDDLREFFDTRSFIRYMLKSV	830	
CgPdr1	SFSFTIISRMIIEFMQIKELTKVEFIEKFSVCPDLADLPMLLDPNCLYFSLQQI	939	
ScPdr1	AFSFLTIVTRIMLAYGESSTNLDVISKYIDENAPDLKGIIEVLVDTNSCAYRFLLEPV	871	
ScPdr3	EKSGFHLIIRKMLESDYK---FLYRDKLATGNIPDQGNSSQISQLYDSTAPSYNN----	882	
CgPdr1	KKSGFTLSFKKILEDARMDDFNYDRNLDSEAIKCKNG-----EFSKMPFCIN----	987	
ScPdr1	QKSGFHLTVSQMLKNRKQPELMSN-EDNKQMKHNSG-----KNLNPDLPSLKTGTSCLL	925	
ScPdr3	-----ASAS---AANSPLKL-----SLL-----NSGEESYIQ--	907	TAD
CgPdr1	VSD-----TTAVSDNSAKKASMGARSVNSTDT---LTASPLSGLRNQTLQD	1032	
ScPdr1	NGIESPQLPFNGRSAPFVRNNSLPEFAQLPSFRSLSVSDMINPDYAQPTNGQN-NTQ--	982	
ScPdr3	-----DASENVPCN-----LRHQ---D---RSLQQTQRKHSAPSQISAN	940	
CgPdr1	SKDSVPSLEAYTIPDSVSDVPTGEINVPFPVY-----NQNGLD	1071	
ScPdr1	-----VQSNKFINAQQQIPTS-VQVFPMTNIEINNNNNNNNNNNNNNNNNNNNNNF	1034	
ScPdr3	ENNIYNLGTLEEFVSSGDLTDLHTLWNDNTSYFPL*	976	
CgPdr1	QQTTYNLGTLDEFVNGDLENYLNSLWGDLSFSDVYL*	1107	
ScPdr1	SATSFNLGTLDEFVNGDLEDLYSILMSDVYFDS*--	1068	

Annex Figure II. 1. Alignment of the Pleiotropic Drug Resistance transcription factor in *Saccharomyces cerevisiae* (*ScPdr1* and *ScPdr3*) and *Candida glabrata* (*CgPdr1*). The DBD, CRD, and TAD domains were defined in Simonicova, L. and Moye-Rowley, W.S. 2020 [181]. Minimum ID, MHR, XDB and NLS were defined by sequence homology to these domains identified in *S. cerevisiae* [6, 27, 47, 50, 51, 53, 67, 105, 207, 225, 227].

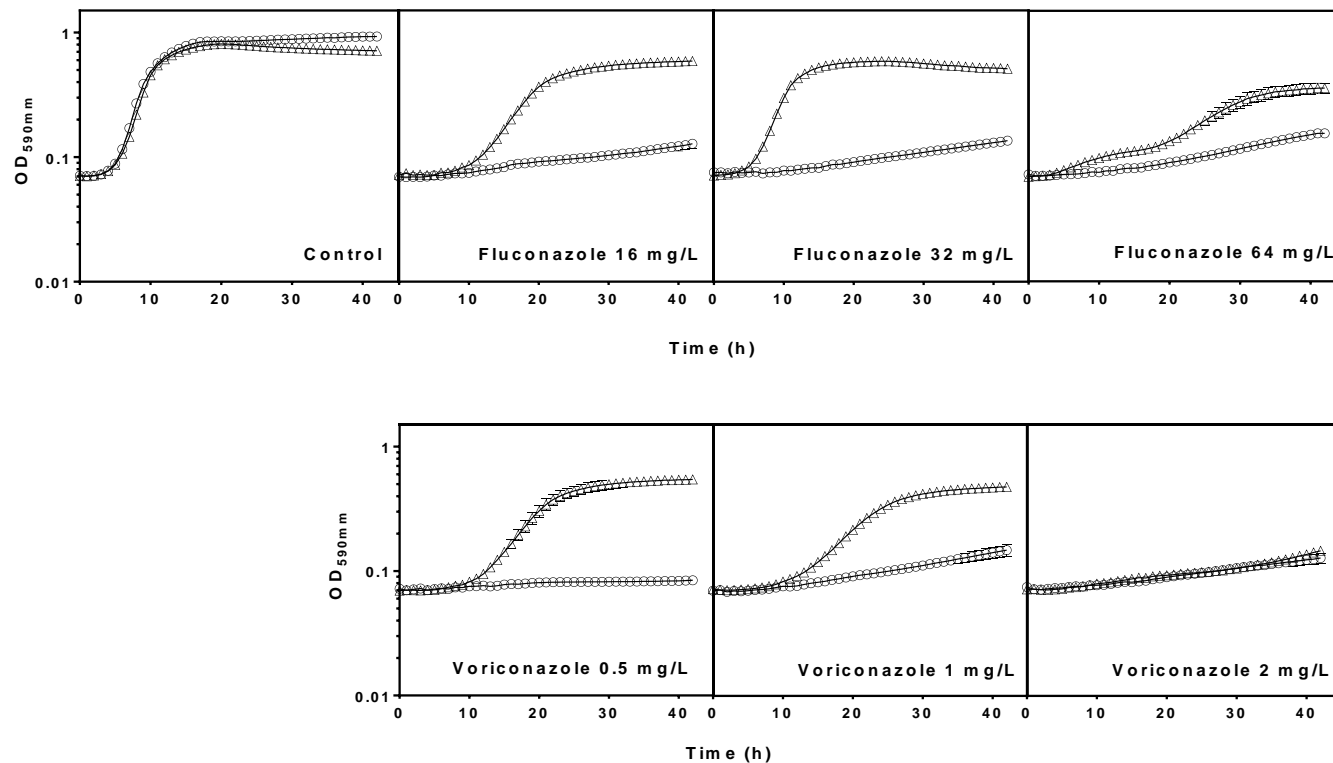
A



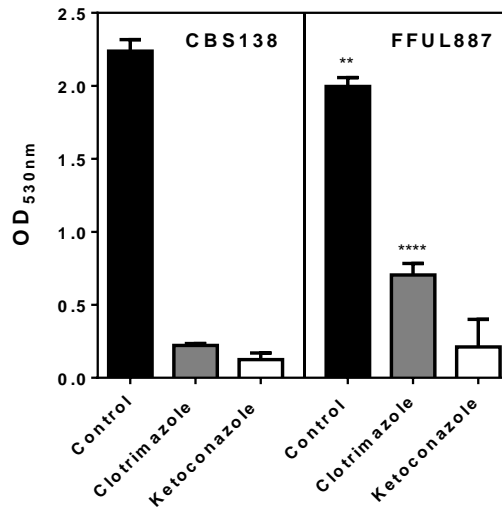
Annex Figure III. 1. Panel A



Annex Figure III. 1. MIC of fluconazole, voriconazole (panel A), anidulafungin and caspofungin (panel B) obtained for the cohort of clinical isolates used in this study and for the reference strain CBS138 (white bar). Resistant isolates are highlighted in black bars, while isolates classified as being susceptible or intermediately resistant are shown in gray bars. The FFUL887 strain, analysed in further detail in this study, is highlighted with an arrow.

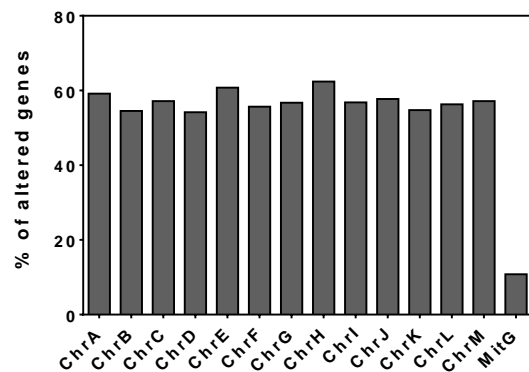


Annex Figure III. 2. Growth curves of CBS138 (○) and FFUL887 (Δ) strains in RPMI growth medium (Control) or in this same medium supplemented with inhibitory concentrations of fluconazole and voriconazole. The experimental setup used was the same as the one used to assess the MIC value. Growth of the strains was followed based on the increase in OD_{590nm} of the cultures along 40h. The growth curves shown are representative of four independent replicas that gave rise to the same growth patterns.

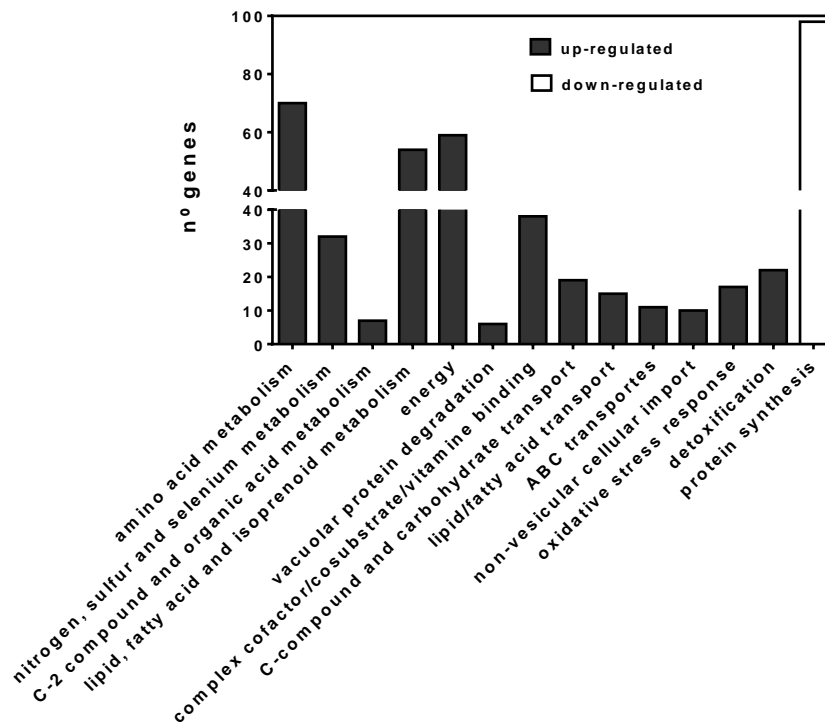


Annex Figure III. 3. Comparison of growth of CBS138 and FFUL887 strains in the presence of the imidazoles ketoconazole and clotrimazole. The strains were cultivated in RPMI growth medium or in this same medium supplemented with 1 mg/L clotrimazole and 4 mg/L ketoconazole, these concentrations representing the resistance breakpoints defined by EUCAST. The results shown are representative of four independent replicas. In each case the statistical analysis was performed using the CBS138 strain as a reference. * *p*-value below 0.01; ** *p*-value below 0.001; **** *p*-value below 0.0001.

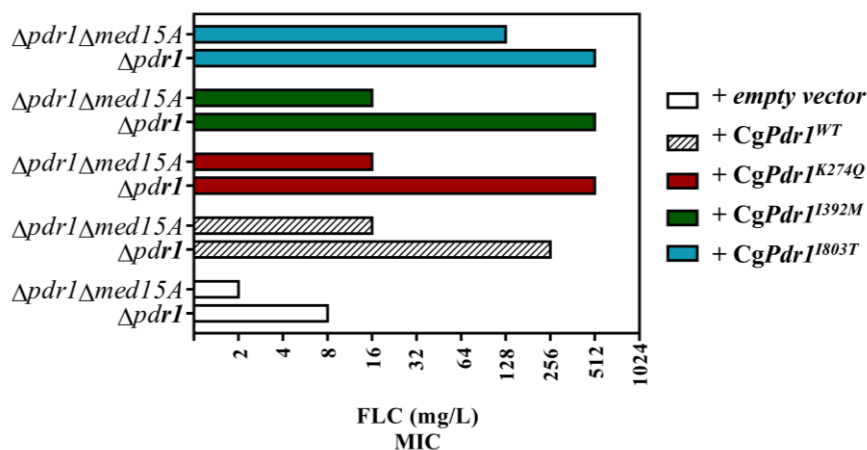
SNP calling between FFUL887 vs CBS138	
Total	77 749
Synonymous SNPs	25 432
Non-synonymous SNPs	9 466
In non-coding regions	42 851



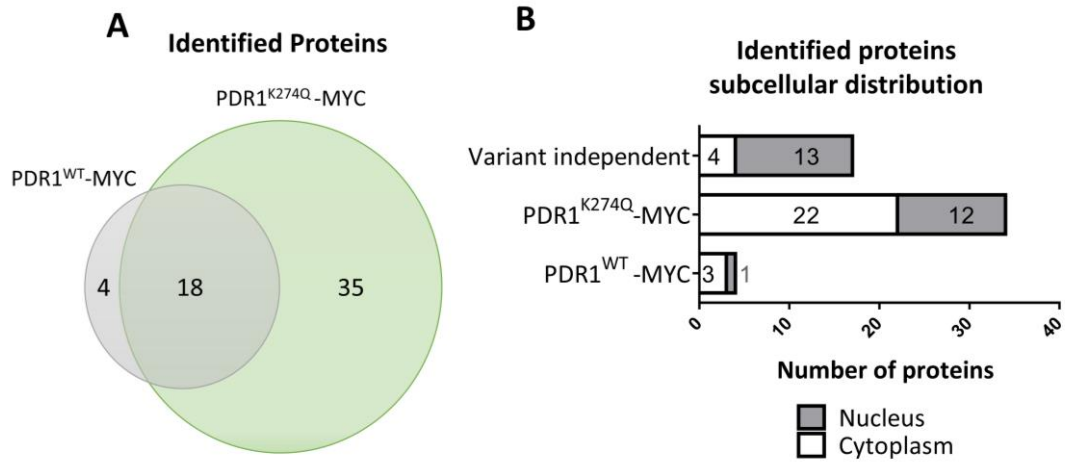
Annex Figure III. 4. The table shows the results of the SNP calling performed after having mapped the reads of FFUL887 genome against the genome of the CBS138 strain. On the right, it is shown the percentage of genes harbouring non-synonymous SNPs in the FFUL887 distributed by the nine nuclear and one mitochondrial chromosome of the CBS138 strain.



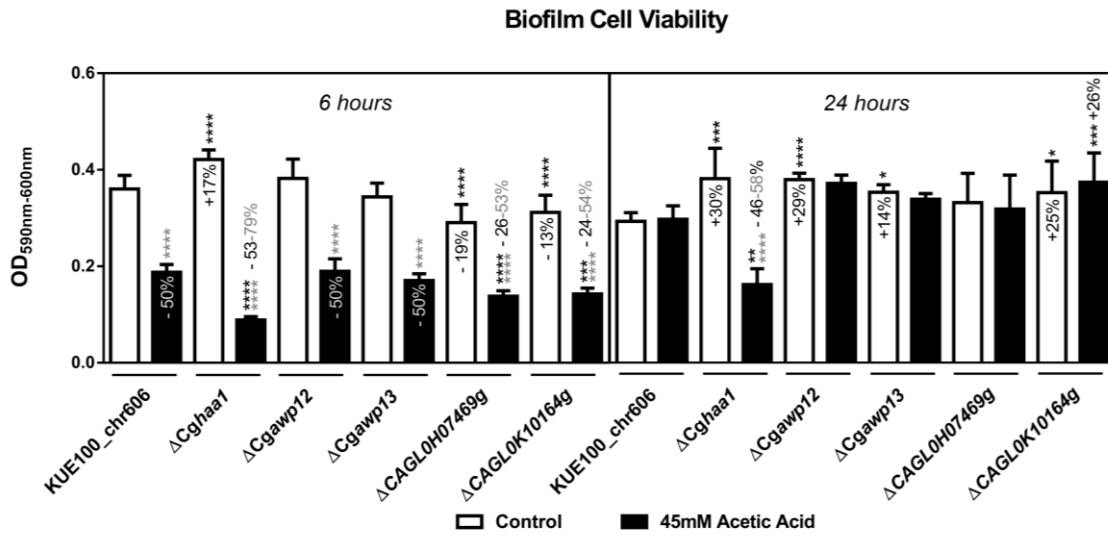
Annex Figure III. 5. Functional clustering of the genes found to be up- (black bars) or down- (white bars) regulated in the FFUL887 strain, compared with CBS138, according to the MIPS functional catalogue. Only those functional classes considered to be enriched (p -value below 0.001) in the dataset are shown.



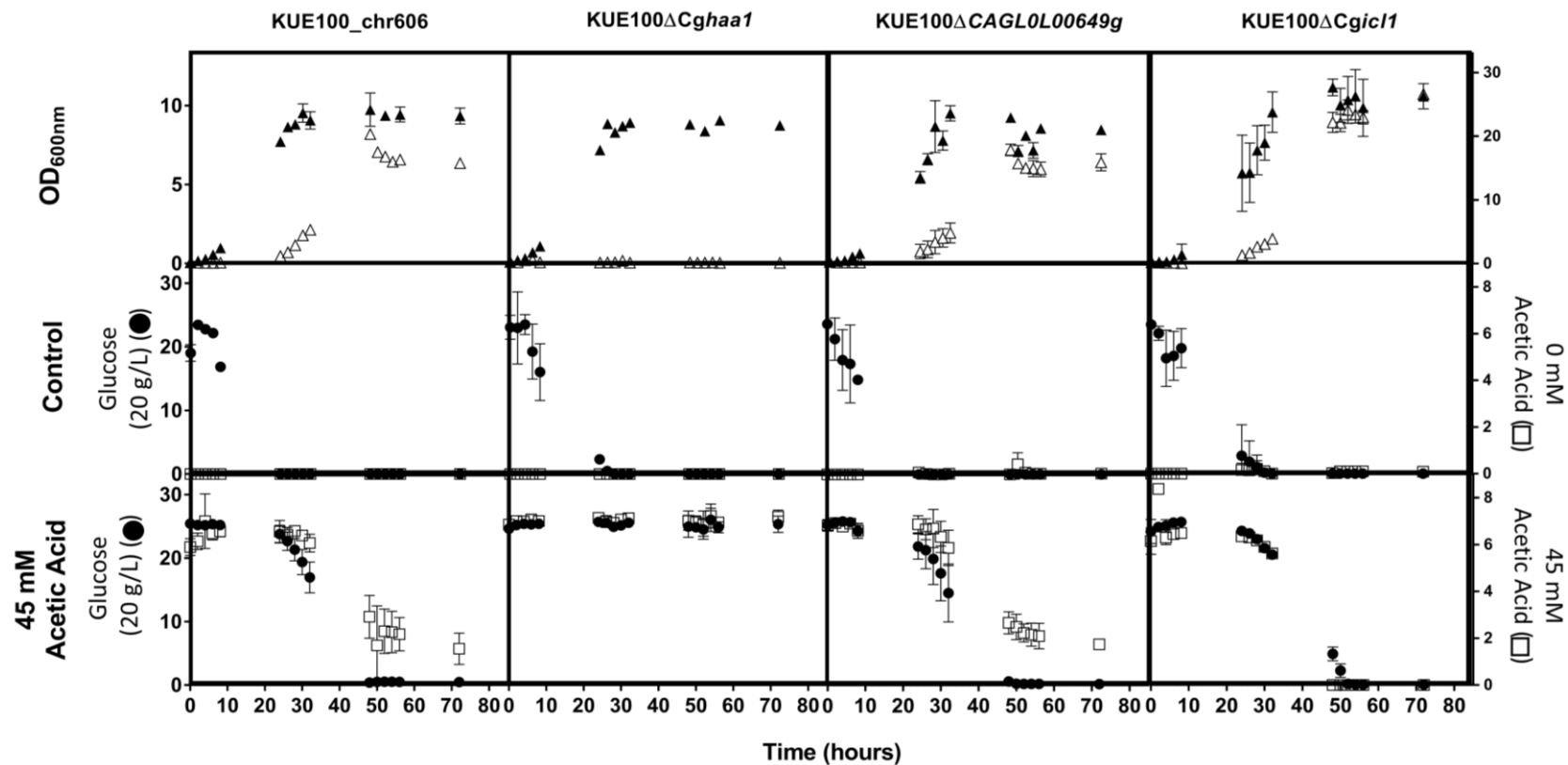
Annex Figure IV. 1. Influence of the *CgGal11A* mediator subunit in tolerance to fluconazole of *Candida glabrata* cells expressing wild-type or the *CgPdr1* GOF variants K274Q, I392M and I803T. $\Delta Cgpd1$ or $\Delta Cgpd1 \Delta CgGal11a$ cells were transformed with the pYR29_MycHis_CgPDR1 plasmid (which drives expression of *CgPDR1* from its natural terminator and promoter) or with the derived plasmids pYR29_MycHis_CgPDR1^{A820C}, pYR29_MycHis_CgPDR1^{T1176G} or pYR29_MycHis_CgPDR1^{T2408C} which encode of the corresponding GOF variants K270Q, I392M and I803T and where used to compare the MICs values to fluconazole, as detailed in materials and methods.



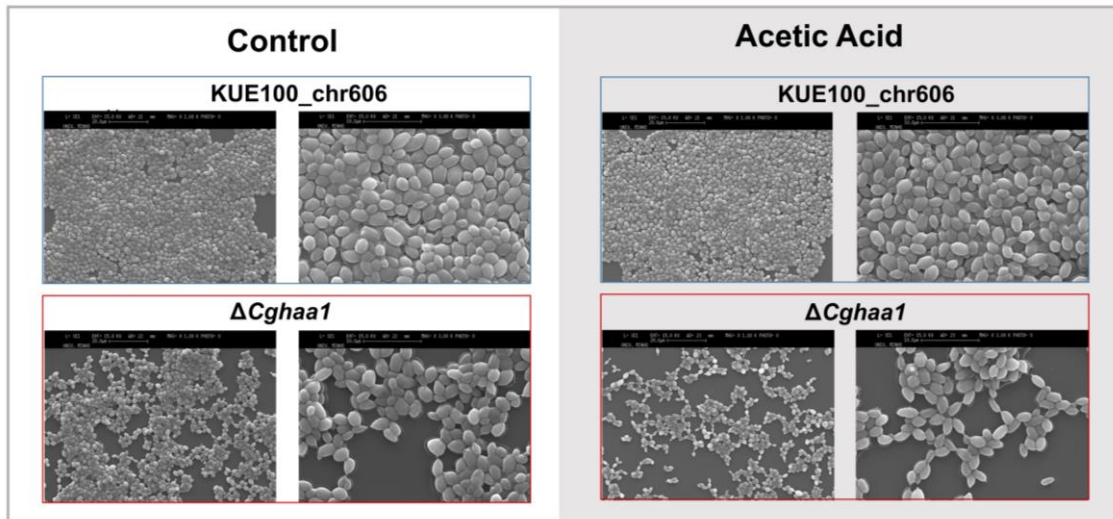
Annex Figure V. 1. MS identification of the proteins immunoprecipitated with the Myc-tag CgPdr1 wild-type variant and/or K274Q gain-of-function variant using ChIP-SICAP methodology. For ChIP-SICAP and MS analysis, CgPdr1 Myc-tagged versions were expressed in the SKY107 strain and immunoprecipitated in mid-exponential growth in RPMI medium at pH7. (A) Representation of the number of proteins identified to interact with one or to CgPdr1 variants. (B) Number of proteins identified with subcellular localization in the nucleus or the cytoplasm.



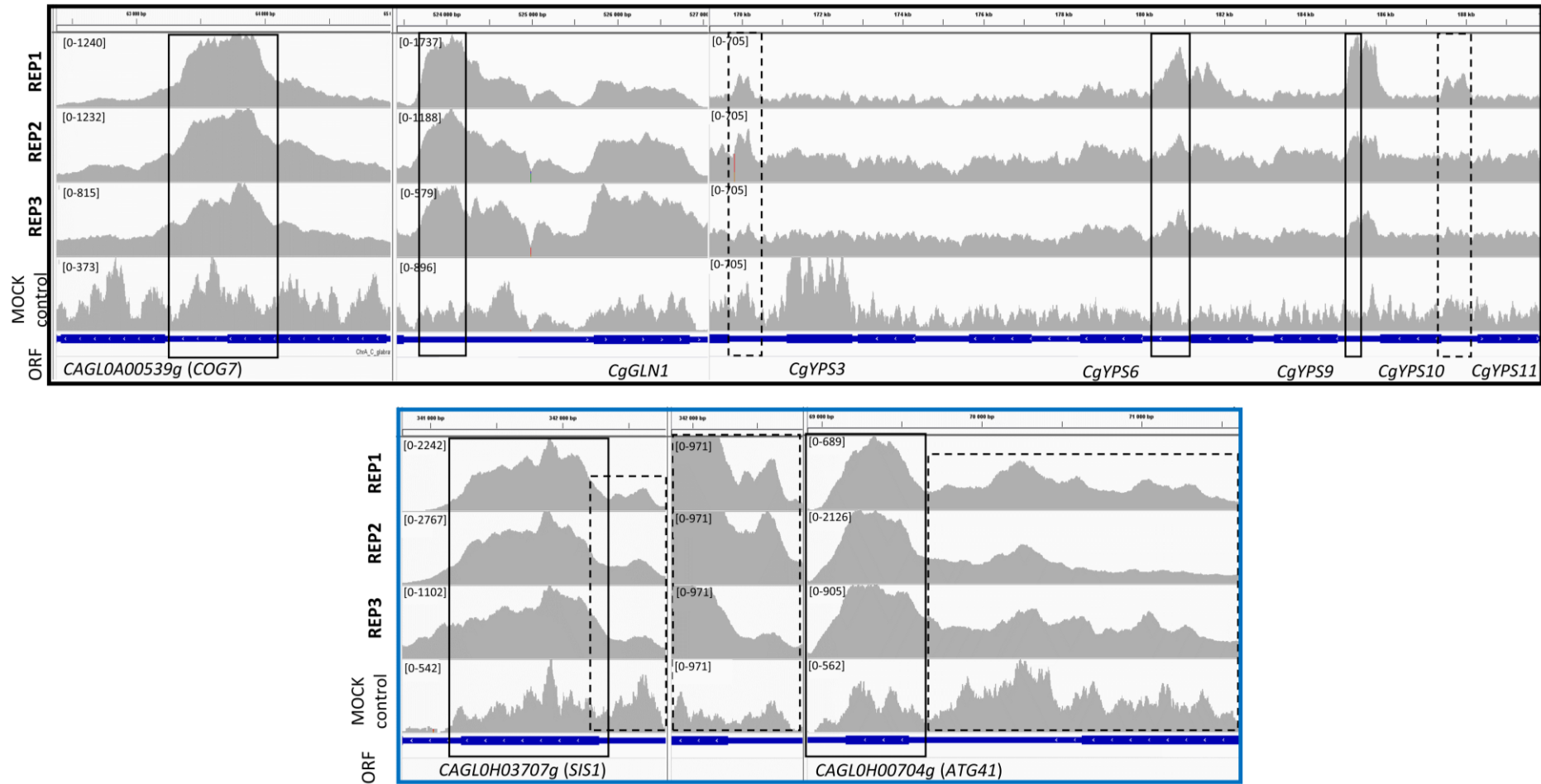
Annex Figure VI. 1. Cell viability in biofilm was measured using PrestoBlue after 24 h growth in RPMI at pH4, with or without 45mM acetic acid. Results represent the means of ten independent experiments. Statistical significance was assessed using ANOVA considering different replicas performed (* p > 0.05, *** p ≤ 0.001, **** p ≤ 0.0001).



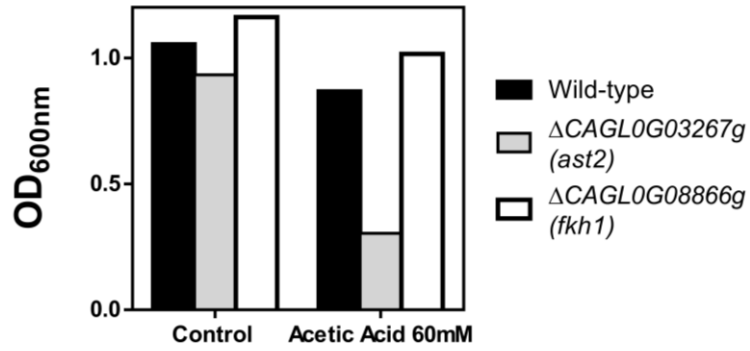
Annex Figure VI. 2. Consumption of acetic acid and glucose, the control *KUE100_chr606* strain, and the deletion mutant strains $\Delta CAGL0L00649g$ and $\Delta Cgic11$ were cultivated in liquid MM medium at pH 4.0 either or not supplemented with acetic acid. Growth was followed for approximately 72 h during which samples of culture supernatants were harvested and used for the quantification of acetic acid and glucose concentrations by HPLC. The results shown are means of the results obtained in three independent experiments.



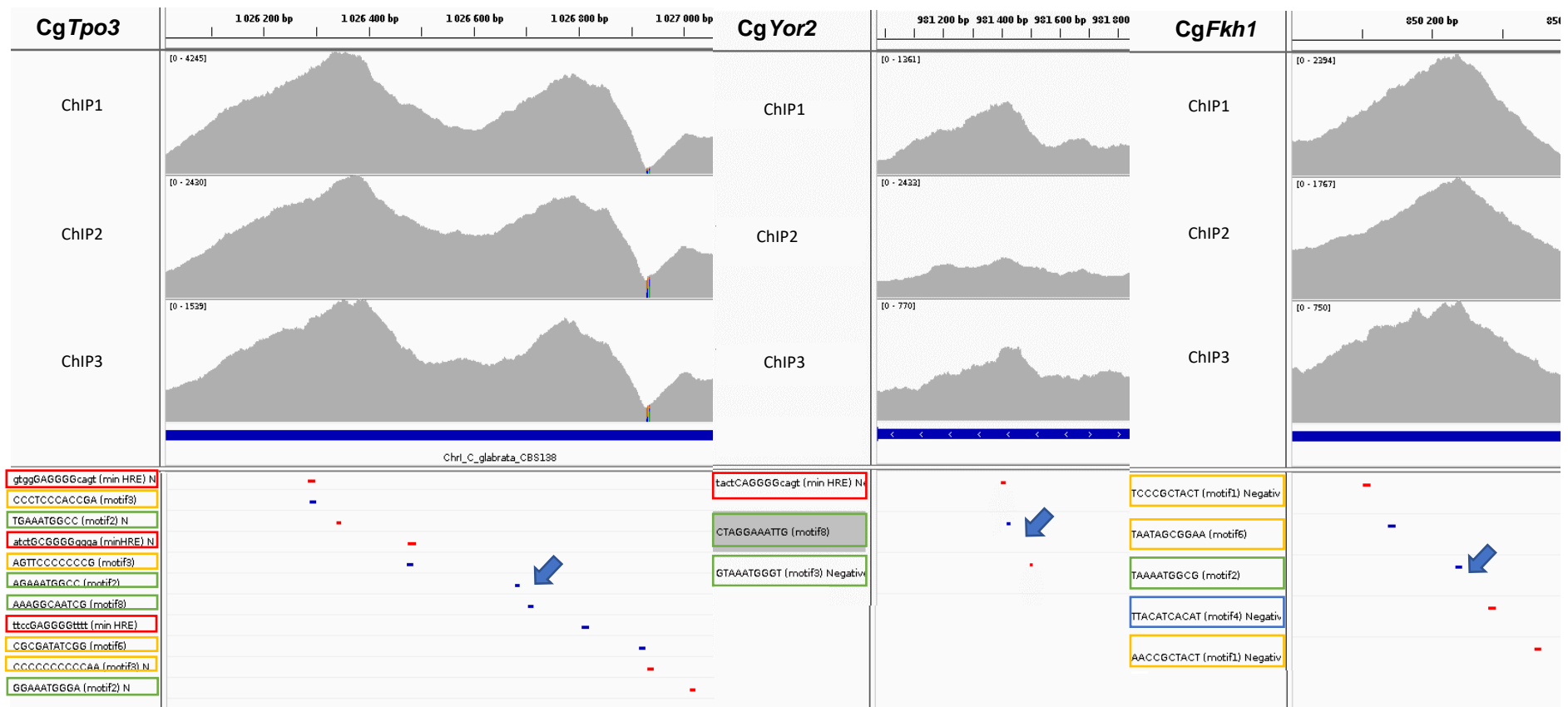
Annex Figure VI. 3. Importance of *CgHaa1* in biofilm structure *in vitro*. Scanning electron microscopy of *C. glabrata* control KUE100_chr606 strain and the mutant $\Delta Cghaa1$ biofilms formed in RPMI at 24h, with or without 30mM acetic acid.



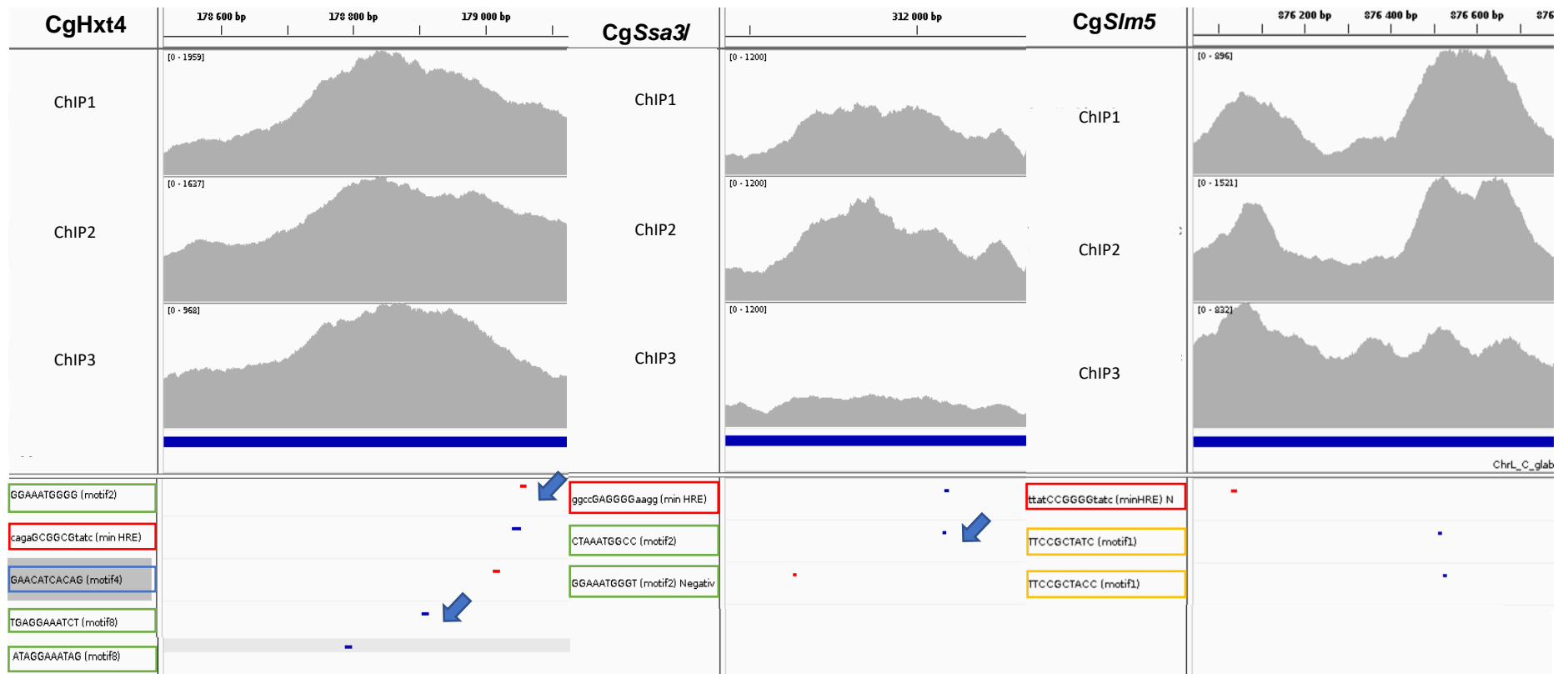
Annex Figure VII. 1. Representation of peaks identified by bPeaks that require further confirmation that they correspond to CgHaa1 interactions. These interactions require further confirmation, since they are low in intensity and were not always identified by bPeaks in all replicates or that might have missed bPeaks dependence due to the enriched reads in ChIPable ORFs (blue boxed). The peaks highlighted in dashed boxed were not confirmed by bPeaks software analysis.



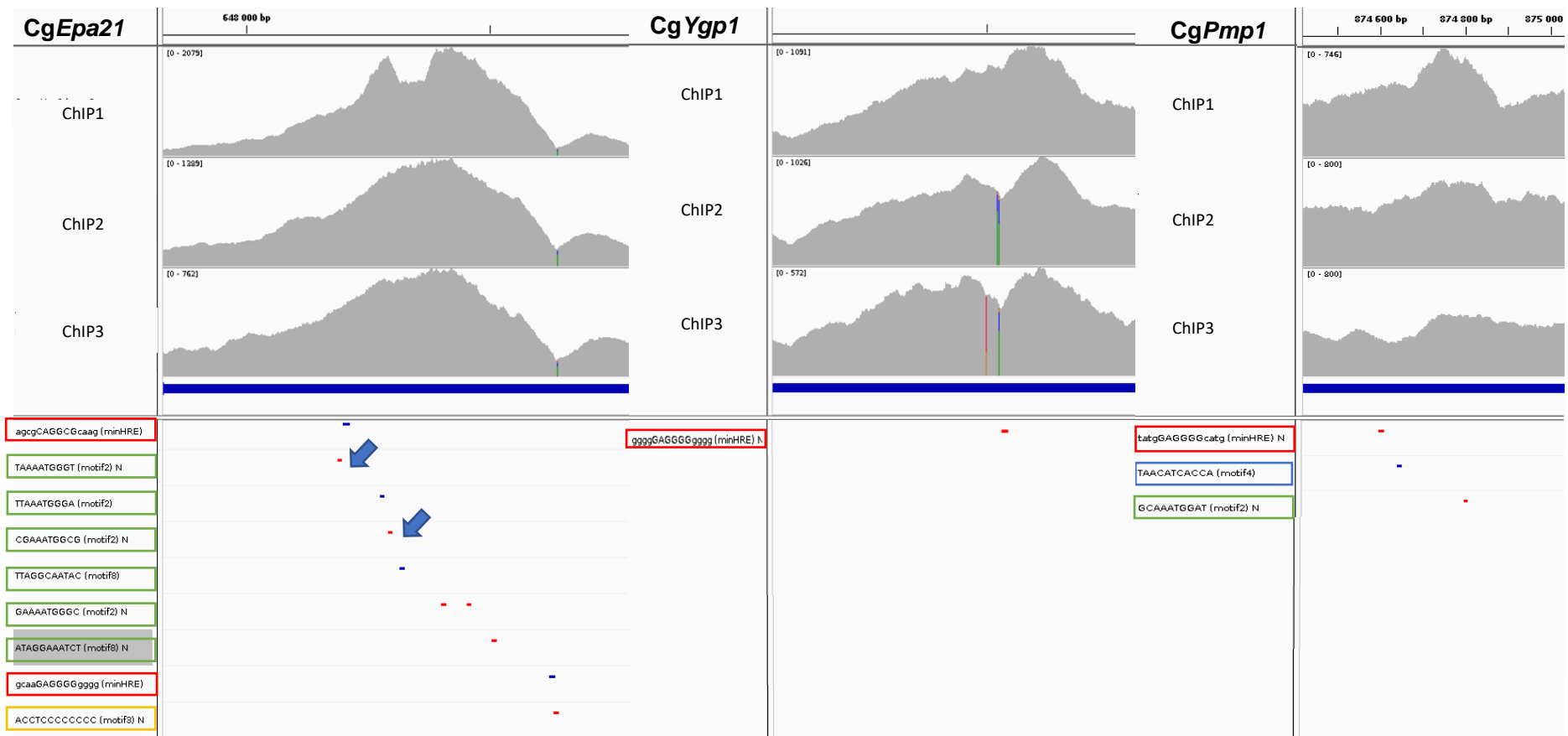
Annex Figure VII. 2. Effect of the *CAGL0G03267g* and *CAGL0G08866g* gene deletion in *C. glabrata* cell resilience to acetic acid. The ATCC2001 Δ *his3* Δ *leu2* Δ *trp1* wildtype strain and the Δ *CAGL0G03267g::Nat1* and Δ *CAGL0G08866g::Nat1* deletion strains [57] were cultured with an initial OD₆₀₀ of ~0.0125 in 200 μ l minimal medium at pH4 supplemented with histidine, leucine, and tryptophan in 96-wells. Resilience to acetic acid was measured with supplementation of the medium with 60 mM acetic acid at pH 4. The OD_{600nm} was measured after 24h. The results herein represented are preliminary results, that are part of a unpublished work involving the screening of a large collection of deletion mutants for acetic acid susceptibility [57].



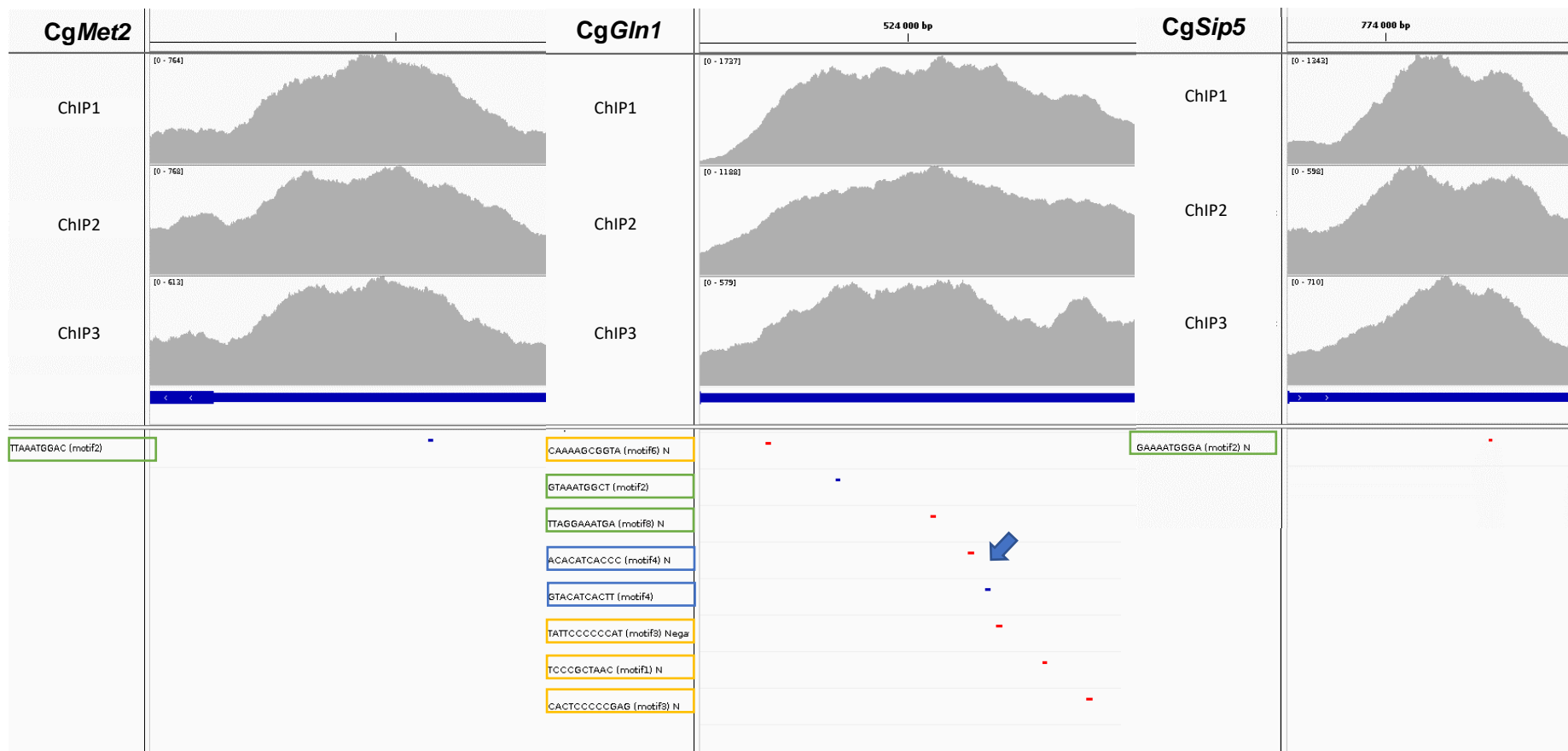
Annex Figure VII. 3. (Part1).



Annex Figure VII. 3. (Part2).



Annex Figure VII. 3. (Part3).



Annex Figure VII. 3 (Part4). Representation of the motifs found using the RSAT-tools in the peak sequences identified by ChIP-seq analysis. The three main identified motifs characterized in this study are highlighted as followed: in red the minimum HRE motif of *S. cerevisiae*, in yellow the HRE-like motif, in green the RSTA tools identified motif 1, and in blue the RSTA tools identified motif 1. The arrows signalize a motif 1 adjacent to a minimum HRE motif or a HRE-like motif.